Author:
Veldenz, Laura

Title:
Automated Dry Fibre Placement and Infusion Process Development for Complex Geometries

Automated Dry Fibre Placement and Infusion Process Development for Complex Geometries

Laura Veldenz

A dissertation submitted to the University of Bristol in accordance with the requirements for award of the degree of Doctor of Engineering in the Faculty of Aerospace Engineering

January 2019

Word count: 53 850

Abstract

Composite manufacture in the aerospace industry increasingly requires high production rate, increased part quality and simplification of manufacture. Current processes such as Automated Fibre Placement (AFP) in conjunction with an autoclave cure only partially satisfy these requirements. In order to address industry needs, the potential of the Automated Dry Fibre Placement (ADFP) process in combination with a high temperature infusion process using an oven was investigated as an alternative future manufacturing route. It reduces frozen storage requirements and the need for autoclave cure as well as potentially providing increased capability of tapes conforming to steered fibre paths. However, manufacturing using ADFP is a complex process chain and the laminate quality is affected by a multitude of material and process variables. The main challenge in using this novel process is the lack of detailed understanding of the influence and interaction of raw materials with the processing steps.

The aim of this research is to study the effect of various materials as well as process parameters in the ADFP process on the deposition and infusion process of complex composite parts. The process was investigated from the individual raw materials, through simple coupon manufacture to a highly complex component. A knowledge-based approach avoids costly trial and error for process optimisation, as shown on a demonstrator component. A multi-criteria selection tool is proposed as a material selection methodology for novel dry fibre tape materials. Coupon level deposition trials were carried out to understand the material behaviour under different processing conditions and its impact on the quality of the preform. A topography-based surface scan method was used to assess such impact on deposition quantitatively. The impact of laminate design and part geometry on infusion characteristics and laminate quality was determined. The applicability of the results obtained through coupon level testing to real parts was assessed and evaluated using an industrially relevant demonstrator.

The guidelines developed within this work enabled rapid decision making in defining manufacturing process conditions to facilitate industrial implementation of a novel manufacturing process and reduce the barrier to entry. Investigating the scalability of the process with scientific methods to an industrially relevant level responds to requirements of the aerospace industry.

Previous Publications

Journals

L. Veldenz, M. Di Francesco, P. Giddings, B. C. Kim, K. Potter, *Material Selection for Automated Dry Fibre Placement using the Analytical Hierarchy Process,* Advanced Manufacturing: Polymer and Composites Science, 2018 *(accepted manuscript)*

M. Di Francesco, L. Veldenz, G. Dell'Anno, and K. Potter, *Heater power control for multi-material, variable speed Automated Fibre Placement*, Composites Part A: Applied Science and Manufacturing, vol. 101, pp. 408–421, Oct. 2017.

Conferences

L. Veldenz, M. Di Francesco, *Enabling the exploitation of automated composite manufacturing through data-driven process definition*, The Fourth International Symposium on Automated Composites Manufacturing, 2019

L. Veldenz, L. Carter, P. Giddings, B. C. Kim, K. Potter, *A metrology-based technique for Automated Fibre Placement programming strategy optimisation*, 8th Internation Symposium on Composites Manufacturing for High Performance Applications, 2018.

L. Veldenz, M. Di Francesco, P. Giddings, B. C. Kim, and K. Potter, *Overcoming Challenges in Manufacturing Complex Structures with Automated Dry Fibre Placement*, 11th International Conference on Manufacturing of Advanced Composites, 2018.

M. Di Francesco, C. Hopcraft, L. Veldenz, P. Giddings, *Preforming Large Composite Aerostructures: A Unique UK Capability*, SAMPE Europe Conference 2018 Southampton, 2018

M. Davies, L. Veldenz, *Manufacturing High-Performance and Complex Geometry Sandwich Structures by Additive Manufacturing Methods*, Composites UK Annual Conference, 2018

M. Di Francesco, L. Veldenz, S. Astwood, P. Giddings, G. Dell'Anno, and K. Potter, *Feature-Based Design for Manufacturing Guidelines for Dry Fibre AFP*, The Third International Symposium on Automated Composites Manufacturing, 2017.

Y. Bauswein, L. Veldenz, and C. Ward, *Developing a cost comparison technique for hand lay-up versus automated fibre placement and infusion versus out-of-autoclave*, SAMPE Europe Conference 2017 Stuttgart, 2017.

L. Veldenz, S. Astwood, P. Giddings, B. C. Kim, and K. Potter, *Infusion characteristics of preforms manufactured by automated dry fibre placement*, SAMPE Europe Conference 2017 Stuttgart, 2017.

L. Veldenz, M. Di Francesco, S. Astwood, P. Giddings, B. C. Kim, and K. D. Potter, *Assessment of Steering Capability of Automated Dry Fibre Placement through a Quantitative Methodology*, The Third International Symposium on Automated Composites Manufacturing, 2017.

L. Veldenz, M. Di Francesco, S. Astwood, G. Dell'Anno, B. C. Kim and K. Potter, *Characteristics and Processability of Bindered Dry Fibre Material for Automated Fibre Placement*, 17th European Conference on Composite Materials, 2016.

Di Francesco, L. Veldenz, A. Koutsomitopoulou, G. Dell'Anno, and K. Potter, *On the development of multi-material Automated Fibre Placement technology*, International Conference on Manufacturing Advanced Composites, 2015.

Dedication and Acknowledgements

I would like to express my appreciation to Ivana Partridge and Kevin Potter for setting up the Industrial Doctorate Centre in Composites Manufacture. Between the academic staff, university staff and my fellow doctorate candidates, they have created an exciting, interesting and inspiring four-year programme enabling me to develop the skills and competencies needed to complete a thesis and enable a successful start into my career.

My gratitude goes towards my academic supervisors Byung Chul Kim and Kevin Potter for their guidance, support and advice that empowered me to complete this thesis. Thank you for many interesting discussions and debates that have helped me shape this work. The same goes for my industrial supervisor Peter Giddings, who has been an invaluable mentor alongside supporting me as a supervisor with indispensable advice and support.

I would like to thank the National Composites Centre and sponsoring members (Airbus, BAE Systems, General Electric, GKN Aerospace, Leonardo Helicopters, QinetiQ, and Rolls-Royce) for funding my research and providing industrial insights through the 2014-2018 National Composites Centre Core Research and Technology Programme. Thank you to the many colleagues who have supported me throughout my work. In particular to Giuseppe Dell'Anno and Simon Astwood for sharing their knowledge and given me many opportunities to grow.

Many others that have contributed in various ways, thanks to the individuals of the different teams at the NCC supporting this work. Particular thanks to Matt Scott, Max Sasnauskas, Luke Martin, Lorna Carter, Michael Petty, Philippe Monnot, Steve Boulter, Chris Payne and Chris Young. The entire Automated Deposition team has made the time at the NCC a cherished memory. Special thanks go to Mattia Di Francesco; thank you for many inspiring discussions and conversations, as colleague and friend, supporting me to achieve my best.

Last but not least, thank you to my family for always being there in support, shaping the person I am today and taking my mind off composites every once in a while. Vielen Dank für eure bedingungslose Unterstützung. Matthew Tolladay, my eternal gratitude for teaching me how to code even though I was resistant first, thank you for continued encouragement and inspiration.

Author’s Declaration

I declare that the work in this dissertation was carried out in accordance with the requirements of the University's *Regulations and Code of Practice for Research Degree Programmes* and that it has not been submitted for any other academic award. Except where indicated by specific reference in the text, the work is the candidate's own work. Work done in collaboration with, or with the assistance of, others, is indicated as such. Any views expressed in the dissertation are those of the author.

SIGNED: ..... DATE: .....

Table of Contents

Table of Figures

Table of Tables

Symbols

C	Criteria score
c	Sub-criteria score
i	Integer counter
j	Integer counter
K	Permeability, m^2
K_{LSF}	Permeability by least square fit method, m^2
K_{SFF}	Permeability based on squared flow front method, m^2
l	Arc length, mm
n	Number of plies
R	Radius, mm
t	Thickness, mm
T	Time, s
T_g	Midpoint glass transition temperature
T_m	Peak melt temperature
U	Normalised weight
u	Normalised sub-criteria weight
V_f	Fibre volume fraction, %
V_p	Peak volume, ml/mm^2
V_v	Valley volume, ml/mm^2
W	Weight, g/m^2
w	Course width, mm
α	Angle, rad
Θ	Deposition end effector tilt
λ	Wavelength, µm
μ	Viscosity, Pa·s
ρ	Density, g/m^2

Abbreviations

ADFP	Automated Dry Fibre Placement
AFP	Automated Fibre Placement
AHP	Analytical Hierarchy Process
ATL	Automated Tape Layers
BF	Bulk factor
CF	Carbon fibre
CoI	Chain of Interactions
COTS	Commercial-of-the-shelf
DIC	Digital Image Correlation
DSC	Differential Scanning Calorimetry
ELECTRE	Elimination and Choice Expressing Reality
EP	Epoxy based
FEM	Finite Element Model
FOD	Foreign object damage
HGT	Hot gas torch
ID	Identification
IDC	Industrial Doctorate Centre
ILSS	Inter-laminar shear strength
IR	Infrared
LWIR	Long wave infrared
MDSC	Modulated Differential Scanning Calorimetry
NCC	National Composites Centre
NCF	Non-crimp fabric
NDT	Non-destructive testing
QI	Quasi-isotropic
R&D	Research and development
Sa	3D surface parameter - average roughness
SAW	Simple Additive Weighting Method
SD	Standard deviation
Sp	3D surface parameter - maximum peak height
Sq	3D surface parameter - root mean square roughness

Sv	3D surface parameter - maximum valley depth
Sz	3D surface parameter - maximum height
TGA	Thermo-gravimetric analysis
TOPSIS	Technique for Order of Preference by Similarity to Ideal Solution
TP	Thermoplastic based
UD	Unidirectional
UNDET	Ultrasonic non-destructive evaluation technique
X-CT	X-ray computerized tomography

Chapter 1

Introduction

This first chapter gives an overview of the main drivers towards automated manufacturing processes in general and outlines the motivation behind the development of Automated Dry Fibre Placement in particular. The collaborative research environment in which this work was carried out is described. This chapter concludes with an overview of the structure of the following thesis.

1.1 Success and Challenges of Automated Composite Manufacture

A drastic increase in the manufacturing of aircrafts is forecasted, which implies an unprecedented surge in production volume of composite components [1], [2]. In the forecast of Airbus alone, a demand of 24 827 single-aisle aircrafts is predicted until 2036. This equates to an average of 103 aircrafts per month, but as of July 2018, the rate for the A320 and A220 families is just below 54 per month [3]. Similar numbers are reported by Boeing [4]. This shows clearly that linearly scaling the production will not be successful and innovative solutions are needed to increase the production volume, such as automating processes [5].

In response to the need for a change in manufacturing, Automated Tape Layers (ATL) and Automated Fibre Placement (AFP) have become the most common automated solution for deposition of pre-impregnated (prepreg) materials. Automated technologies are known for repeatability and can manufacture at high quality parts, where ATL is the more frequently used technology [6]. These are both manufacturing processes for continuous fibre reinforced epoxy-based composites suitable for convex and concave geometries. The process entails placing fibres onto a mould without tension, circumventing any textile processes such as non-crimp fabric (NCF) production. ATL is used for very large and simple structures such as empennages, wings or wind turbine blades. AFP is well suited for intricate shapes, such as double curvature and smaller parts, due to the deposition of a series of

parallel narrow tapes as opposed to a single, wide tape as in ATL; AFP is the focus of this work. Especially AFP has seen a steep rise in production applications since the late 1980s, as shown in Figure 1-1.

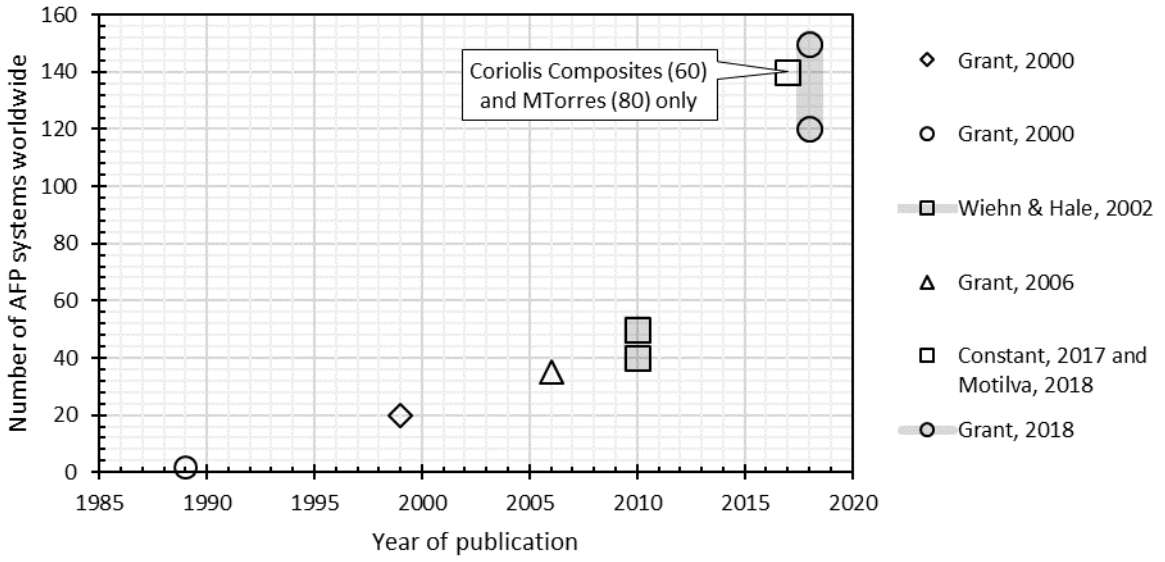

Figure 1-1: Estimated number of AFP systems in production worldwide [7]–[11] *and Grant (personal communication 06. September 2018)*

In comparison to the 35 AFP systems in 2006, approximately 60 large ATL systems were in operation [8]. The estimate of 120 – 150 AFP systems existing worldwide made by Grant in 2018 is likely to be conservative, given that two machine manufacturers (Coriolis Composites and MTorres) alone are reporting to have a total of 140 machines in operation in 2017 [10], [11]. However, the usage of automated composite manufacturing processes still has a relatively small share of all available processes [12]. Nevertheless, the rapid increase in interest around the AFP technology, indicated by the number of machines sold as well as papers published is indicative of the high potential and a promising future.

The AFP process was patented in the 1970s (US patent [13]), and has since reached a high maturity [13]–[15]. The promise of high deposition rates and therefore high productivity as well as low material waste were drivers for the development [14]. The first publications were made in the time frame 1990-1994; tens of papers published per year 1995-2009 and hundreds of papers 2010-2014 show a steep rise consistent with the rise in machines in operation [16]. However, the aim of reaching a high deposition rate, such as 45 $^{kg}/_{h}$ set out by Spirit in 2008, is still a challenge [17]. A variety of estimations has been made, often without sufficient details to assure comparability, but a general trend of rising deposition rates emerges, see Figure 1-2. It must be noted that deposition rate is a mixture of actual

machine program run, set-up of the machine, maintenance and trouble shooting. Only very limited reports of actual deposition rates as opposed to anticipated deposition rates are accessible.

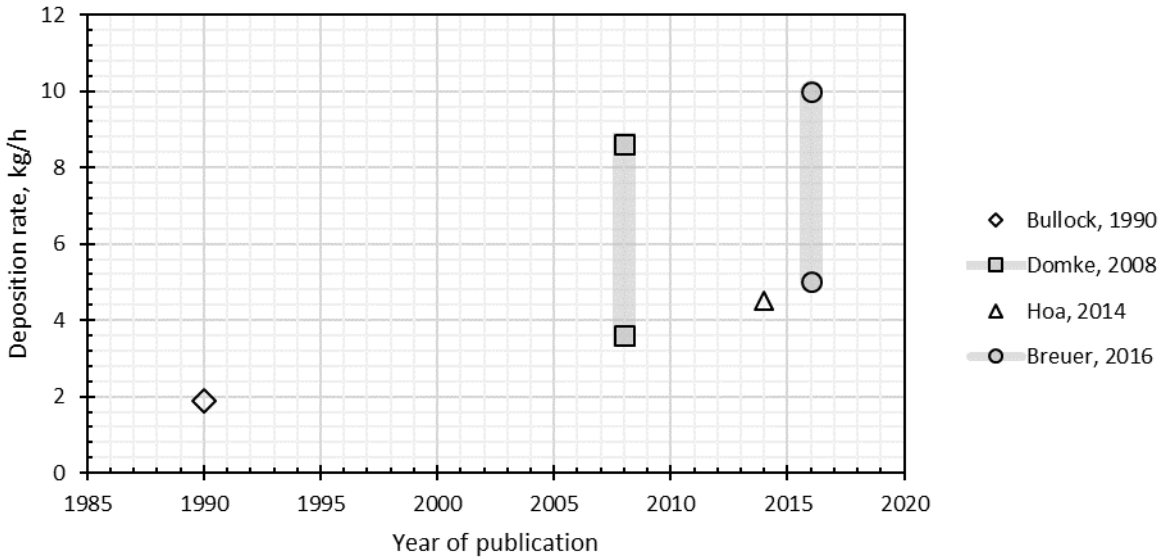

Figure 1-2: Deposition rates of the AFP process quoted in literature and open source documents [17]–[20]

Various research was conducted to compare manual solutions with AFP, a summary by Croft *et al.* shows that AFP parts perform similar or better in terms of mechanical properties than the manually produced equivalent [21]. But there is room for improvement, prepreg materials come at high cost due to their extensive manufacturing requirements, including tow spreading, resin application and slitting [18], [22]. As the material is B-staged (partially cured), it requires logistically demanding frozen storage, which is especially challenging in transport and out-life management [18]. The need for autoclave consolidation limits the scalability of the process as autoclaves come in finite sizes, have high running expenditures (time and resources) and pose a high upfront investment [23], [24]. The advantages and drawbacks of the prepreg AFP technology are summarised in Table 1-1 (a).

In contrast, other industries such as automotive, wind energy or marine industry predominantly use textile precursors for large scale, continuous fibre reinforced composites, combined with epoxy based resin infusion [25]–[27]. The initial investment is usually lower than in the aerospace industry, but the textile production and preform preparation is labour intensive and creates a significant amount of waste. The advantages and disadvantages of the infusion process are also summarised in Table 1-1 (b).

Table 1-1: Advantages and disadvantages of prepreg AFP and infusion of textiles [14], [23], [28], [29]

	(a) Prepreg AFP	(b) Infusion of textiles
Advantages	Automated process	Low initial investment and tooling costs
	High quality laminate	Out-of-autoclave process
	High repeatability	Can achieve complex geometries
Disadvantages	Requires autoclave	Disposable consumables
	Limited geometrical flexibility	Labour intensive process
	Limited shelf life and frozen storage	High precursor material waste

Despite the disadvantages, prepreg AFP as a manufacturing technology was adopted in the aerospace industry, a technology currently used for parts used in aircrafts such as Boeing 787 and 777 as well as various Airbus models (A320, A350, A380), replacing hand lay-up of prepreg [23]. To mitigate the limitations of the prepreg manufacturing route and to gain the advantages of the infusion process, an interest in a combination of the two technologies arose [30]. Using an AFP machine to deposit dry carbon fibre tapes into a preform and subsequent infusion followed by curing in an oven has the potential to combine the advantages of both processes. The aim is to increase the output while remaining cost competitive, and therefore prevent offshoring by automating a process to decrease the need for manual labour. The adoption of such a novel manufacturing process presents a high risk due to the high investments into industrial research and development (R&D) programmes. These efforts can be reduced by providing tools to facilitate implementation and enable first-time-right production, decreasing the need for extensive development.

The aim of this work is to investigate if the ADFP technology is a feasible technology and to determine the outcome of the process, in terms of manufacturing quality, repeatability and productivity. The knowledge gained through this initial, generic technology assessment must be transferable to specific components to be applicable to industrial components. This will reduce the need for development processes to an industrial scale production. In order to achieve this, the effect of material as well as process parameters in the ADFP process on the deposition and infusion process has to be understood.

1.2 Research Environment

A largely manual labour driven industry in need of upscaling production risks relocation of the production to a low salary country, as it happened for example in the garment industry [31]. As the composites manufacturing industry provides a large number of jobs in the UK, the government has a significant interest in preventing offshoring [32]. The governmental support to retain a strong national aerospace industry manifests itself, amongst other policy leavers, in funding research centres such as the National Composites Centre (NCC) part of the catapult network, which partially funded this work.

Providing the facilities and the infrastructure is a significant effort towards fostering national R&D. The NCC runs the Core Research and Technology Programme (Core Programme) sponsored by industry members as a consortium project. The Core Programme consist of four independent projects, this work is based on the ADFP Project. Industry members of the NCC, in this instance Airbus, BAE Systems, General Electric, GKN Aerospace, Leonardo Helicopters, QinetiQ, and Rolls-Royce act as steering board and advisors. This is a practical example of collaborative efforts investigating a novel manufacturing technology to address topics such as high efficiency, increased production volume and low manual labour. These somewhat conflicting requirements need a significant amount of R&D to fulfil the objective to remain competitive.

The collaboratively financed project had a total budget in the order of hundreds of thousands of pounds across four years, which is required for a relatively high cost technology and enables synergy effects. Over the course of this time, numerous NCC staff members contributed to this work, recognised in the acknowledgement section. On an annual basis, the industry members and the NCC scope the content of the work for the year to ensure all participants can steer the project. The overarching aim is to investigate if the technology is viable, what quality can be expected and to enable each member an assessment of the ADFP technology against their respective manufacturing requirements.

If research is needed for a high maturity technology that is not yet ready for industrialisation, the use of industry scale equipment ensures direct transferability into a production environment. Often, companies do not have the capacity to reserve one of the machines for R&D purposes only without affecting the production rate, which makes it difficult to improve manufacturing with a step-change rather than incremental changes in parallel to daily business. The industrially sized R&D environment at the NCC enables the development of improvements for users, but also enable a test bed for new adopters.

While the content of this work was sponsored by industrial members, this thesis was written under the umbrella of the Engineering Doctorate Programme (Industrial Doctorate Centre (IDC) in Composites Manufacture) at the University of Bristol sponsored by the Engineering and Physical Sciences Research Council through the EPSRC Centre for Doctoral Training in Composites Manufacture [EP/K50323X/1].

1.3 Thesis Outline

This work investigates the manufacturing process systematically, from the raw material to the manufactured laminate and from simple coupons to a complex geometry. The multifaceted manufacturing process calls for a structured approach investigating the connections across the full

manufacturing chain. Inspired by the concept of the pyramid of testing, a similar approach was used for this work, shown in Figure 1-3. The materials are investigated first, then a manufacturing test campaign increases complexity incrementally up to an industrially relevant demonstrator component.

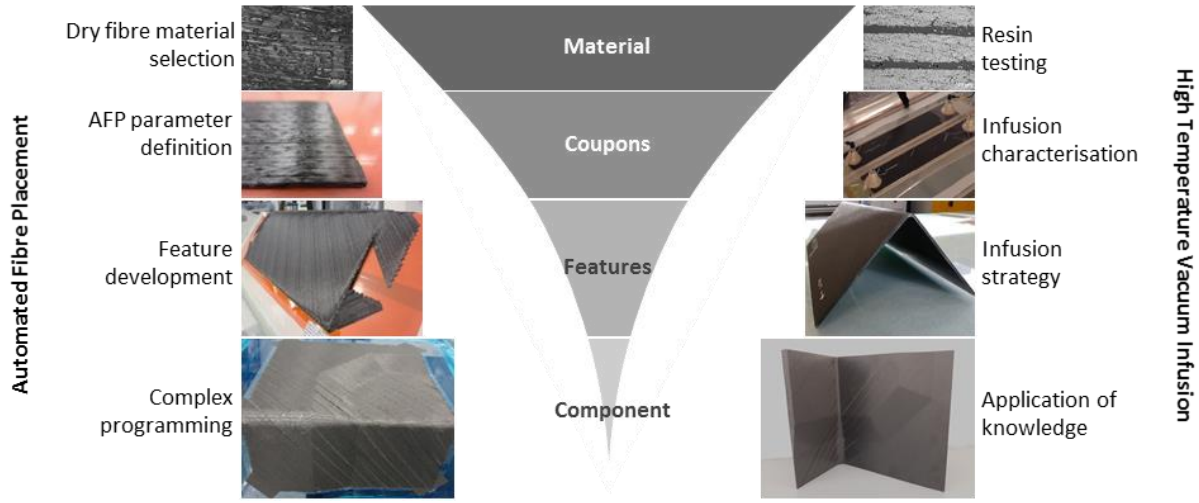

Figure 1-3: Pyramid of testing inspired visual representation of the research approach

As ADFP is intended to be flexible enough to manufacture a wide variety of parts, particular care is taken to ensure transferability of the findings across tool geometries and AFP machines. This is achieved for example by using standard units rather than machine specific inputs as well as equipment independent and comparable outputs. This work is focused on the manufacturing process and investigating the impact of the process on mechanical properties of the laminates is out of scope. The present work is divided into the following sub-sections:

Chapter 2 reviews the ADFP manufacturing process to date. Prior research primarily focused on ADFP as well as relevant and related research is presented, outlining the current knowledge gaps to be addressed in this thesis.

Chapter 3 characterises dry fibre materials to enable a link between material constituents and the preform as well as the impact on the infusion process. To select a suitable material, criteria that assess the manufacturability are established. Qualitative and quantitative material assessments enable an evidence based and transferable material selection.

Chapter 4 establishes the methods to document processing parameters of AFP in a comprehensive and comparable manner. The impact of the different parameters on the fibre volume fraction of a simple preform is quantified, enabling process optimisation. Furthermore, a measurement method enabling the quality of steered paths quantitatively is defined and assessed. Then the method is applied to determine the impact of process parameters on steering path quality. This method can

replace the current, visual and highly subjective measurement method, and enables AFP parameter optimisation for steered laminates.

Chapter 5 determines to what extent the design decisions for the laminate fibre paths influence a high temperature infusion process. The significance of the level of intervention achieved by laminate design is compared to the impact of the infusion strategy. Furthermore, the link between preform and laminate quality will be established in terms of fibre volume fraction, tracing the impact of multiple manufacturing processes.

Chapter 6 demonstrates the feasibility of the dry fibre ADFP process in an industrial environment, assessing the scalability, variability and economic aspects of the entire process on a complex demonstrator. In addition, as a complex component requires extensive fibre path planning, the quality prediction capability of the AFP programming software is investigated. This address the need for a better link between the AFP programming and deposition stage.

Chapter 2

State-of-the-Art of ADFP and Infusion

This chapter outlines the key concepts as well as the most recent stage in the development of the ADFP technology. Prior knowledge and published research regarding ADFP as well as prepreg AFP and carbon fibre-based fabrics containing binder is reviewed. This defines the areas in which further research is needed and guides the focus of this thesis.

2.1 Automated Dry Fibre Placement Process

2.1.1 Mechanisms of the AFP Process

Automated Fibre Placement (AFP) is a technology developed to replace the manual lamination process. The basic principle of AFP is to apply individual tapes, side-by-side and layer-by-layer to a mould by automated means. The layers are not interlaced like a woven material but adhered by non-mechanical means, by the tack of the resin in the case of prepreg and by the tack of the binder in the case of dry fibres. In order to activate this adhesion, pressure by a roller is applied. Elevated temperature often aids the process, depending on the material requirement. The system movements are pre-programmed using bespoke software and the computer-controlled deposition system then builds up the preform according to the design in a mould. The machine articulations are dependent on the type of machine used, robotic or gantry style. The machine type dictates the degrees of freedom for the machine movement. Greater flexibility and a larger working envelope are associated with robotic systems; higher accuracy at increased payloads can be achieved with gantry systems [33]. These systems are often a commercial-of-the-shelf (COTS) robot or gantry with a bespoke creel system and end effector. The creel system stores the fibres and the end effector is a proprietary system to apply them. The end effector commonly comprises a tape feeding system, including clamps and

cutters, a compaction device, most commonly a roller, a heater and in some cases also the creel [6]. While in principle, the combination of temperature, pressure and time can be re-created in any machine, some hardware components are significantly different and may cause challenges in the transferability of results; especially the tape guiding systems is a hardware configuration that can vary notably between machines. Different machine configurations are shown in Figure 2-1 to Figure 2-3.

Figure 2-1: AFP system with detached creel and continuous guiding system [34]

Figure 2-2: AFP system with detached creel and free hanging tapes [35]

Figure 2-3: AFP system with end effector mounted creel [36]

2.1.2 Challenges of AFP Programming

Programming plays a significant role in preparing manufacturing; it is part of developing the manufacturing process. A virtual product is created based on the design such as the basic part dimensions, the ply book and ply dimensions. The transfer of the part into an AFP programming software includes selecting programming strategies to achieve as many of the sometimes-conflicting requirements as possible. Complex parts require complex programs, which rely on software predictions for optimisation. It is not possible to test every iterative improvement of the program physically, so an inbuilt prediction feature is used for optimisation. The optimised program then has to be tested on an AFP machine and can trigger further iterations if the software predictions are not adequate.

During the machine program development, every ply, every roller pass applying multiple tapes (referred to as course) and even individual tapes are carefully planned. This includes not only position but also their direction and location in respect to other tapes and plies. The individual ply can be checked for specific characteristics such as steering radii and angle deviation based on the idealised programmed paths. Subsequently, the machine motion to action the desired courses is programmed. Most machine suppliers provide a proprietary programming software to do this complex task, which is linked to the machine system. Few suppliers of machine independent software exist, but this is a field forecasted to grow [37].

As the programming stage is very important for a successful and high-quality manufacturing process, it has become a research field in its own right. Research is conducted on topics such as path

optimisation for improved mechanical behaviours [38], [39] by using specific programming strategies [40] especially for variable stiffness composite laminates [41] as well as optimisation of robotic movements leading to improvement of productivity [42], [43]. Many different optimisation routines are suggested; however, these are rarely implemented in COTS programming software. Often the manufacturability of parts is not necessarily a focal point of such optimisations, and some results may not be transferable to reality. Gonzalez Lozano *et al.* state, *"The subjects of optimisation of structural performance objectives and manufacturing objectives simultaneously have not been found"* [41]. The performance of different materials during the deposition process does not currently inform optimisation algorithms. A significant knowledge gap lies in the correlation between the software output and real the observed deposition quality. A discrepancy between those can lead to an overly conservative program (e.g. a higher minimum steering radius than necessary to achieve desired quality) and to a costly series of iterations between deposition and programming, as shown in Figure 2-4. This process can be manual, lengthy and highly dependent on the programmers' experience and expertise. Instead of the current practice of iterations between the steps, a direct first-time-right program could be achieved if the current knowledge gaps are closed. An improved process simulation capability in critical areas could eventually make it possible to skip the iterative cycles.

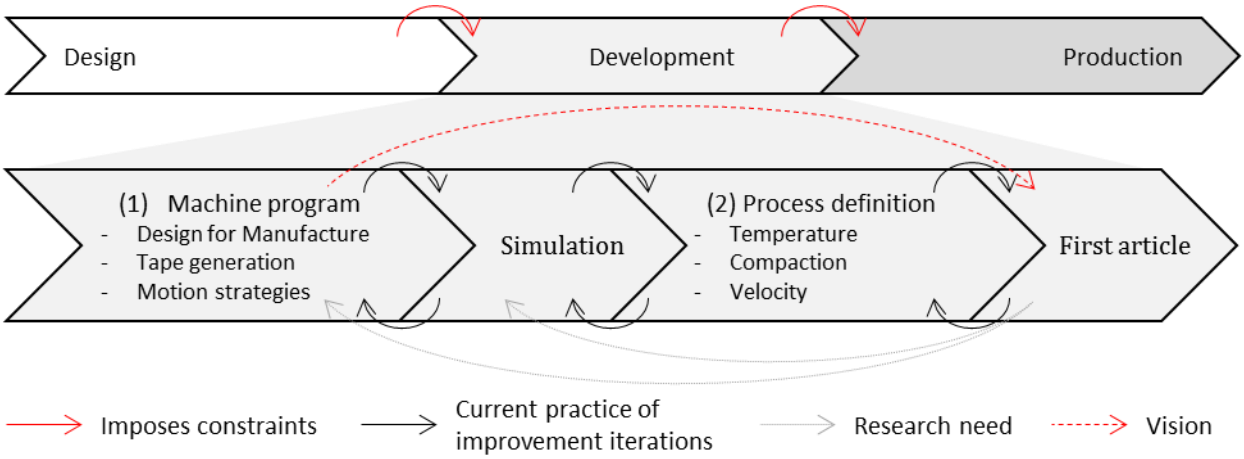

Figure 2-4: Conceptual route from design to production

A programming software package is a useful tool to predict the manufacturing process, but only if the program gives an accurate and reliable indication of the quality resulting from its deposition. The capabilities of programming software to identify areas of potentially low deposition quality reliably, has not yet been investigated. One reason could be that there are very few methodologies available to inspect plies to the degree of detail required to make this comparison. Most work has focused on defect detection for in process monitoring [44], which is designed to flag up inconsistencies, but does not capture the deposition quality for the purpose of comparison to the software predictions.

2.1.3 Process Parameters

The AFP process is governed by time, temperature and pressure. Therefore, it should be possible to re-create the same conditions on every machine. However, this can pose a challenge in practice, as machines are usually controlled by inputs such as heater power, programmed speed and compaction force. These parameters describe the machine performance but are not transferable to any other machine with differences in set-up or technical specifications. Transferable parameters, measured at specified locations, are deposition temperature and compaction pressure varied in response to deposition speed and component geometry. These transferable parameters are often not measured as part of the commercial AFP process and external measurements are required to determine these parameters. Publications investigating dry fibre material deposited by AFP experimentally often do not cite either of these parameters sufficiently in order to replicate the conditions of the test set up. Table 2-1 gives an overview of the parameters given in the methodology section of different publications regarding ADFP. This overview is comprehensive to the author's best knowledge at the time of writing.

Table 2-1: Deposition process details given in various publications including selected values if applicable

Heat source	**Heater power, W**	**Temperature at nip-point, °C**	**Compaction force, N**	**Compaction pressure, N/mm²**	**Deposition speed, m/s**	**Source**
Laser	800	200-320	200	n/a	0.4-0.8	[28]
n/a	n/a	n/a	n/a	n/a	n/a	[29]
Laser	no	n/a	n/a	n/a	n/a	[45]
Laser	n/a	n/a	n/a	n/a	n/a	[46]
Laser	800	250	200	n/a	1	[47]
Hot Gas Torch	n/a	n/a	n/a	n/a	n/a	[48]
n/a	n/a	n/a	n/a	n/a	n/a	[49]
n/a	n/a	n/a	n/a	n/a	n/a	[50]
n/a	n/a	n/a	n/a	n/a	0.02	[51]
Two IR lamps	n/a	n/a	n/a	n/a	n/a	[52]
Laser	800	200-320	200	n/a	0.4-0.8	[53]

While some of these sources are focusing on permeability, the measurement method or simulation thereof, the results are not reproducible with the lack of information given about the preform. This information is necessary, as the connection between process parameters and process output is not fully understood yet and therefore the relevance of the process parameters in regard to the preform is not well defined.

Thermal Process Aspects

A variety of heating sources are available for AFP, in particular the high temperature requirements of thermoplastic prepreg (up to 400 ˚C deposition temperature [54]) have triggered the development of a wide array of heating solutions. For thermoset material, a slight elevation between 25-35 ˚C and up to 40 ˚C is sufficient for deposition, which can easily be achieved with a relatively simple Infrared (IR) heater, such as a 550W IR emitter achieving up to 50°C [55]–[58]. Using multiple IR emitters is suitable for dry fibre placement, where a temperature of around 200 ˚C is required [59]. The challenge with an IR heater is its reaction time, which generally has a reaction delay of multiple seconds. This leads to low controllability of the heating source, which is problematic with parts requiring a wide range of speeds during deposition. Further heating devices for high temperature deposition are the hot gas torch (HGT) and diode lasers (typically 3 or 6 kW, for ≤ 50 mm course width) [28], [48], [54].

In order to describe the heating source sufficiently to replicate experiments, many details of the set-up are required. A summary of the details needed to define heating sources are outlined in Table 2-2, but often these details are not exhaustively provided.

Table 2-2: Descriptors of various heating mechanisms required to ensure reproducibility

Diode laser [28], [54], [60]	**Hot Gas Torch** [48]	**IR lamp** [61]
Laser power input as a function of speed	Nozzle exit temperature	Lamp power
Length, width and location of heating zone	Gas flow rate	Lamp distance from nip point
Angle of incidence of the beam in respect to the substrate	Nozzle dimensions (height, width)	Dimensions of heated area
	Nozzle location (angle and distance)	Angle of IR lamp

Other heating sources have been proposed, such as a Xenon flash lamp (Humm3) or resistance heating (CoRe HeaT), but will not be considered in this work [62]–[64].

As an alternative to a detailed description of the set-up to allow repeatability, a reliable method for temperature monitoring during the deposition process is required. Common measurement techniques in AFP deposition are a LWIR camera, thermocouples or pyrometers [47], [60], [65]. In order to employ a LWIR camera, the material specific emissivity is required, which has to be obtained experimentally following ASTM E1933-14. Thermocouples require good thermal contact and need to be thin in order not to disrupt the deposition process, which is challenging to achieve in a loose fibre bed. Using the thermal measurements, a relationship between required heater power and output

temperature can be established over the full range of deposition speeds. The relationship between increasing deposition speed and required heater power for constant temperature processing using a laser follows a power law and is a requirement as machine input for variable speed deposition [54].

For thermoset materials the prepreg preform quality (voidage and compression strength) is driven by temperature, it is also well known that the AFP process using thermoplastic material is thermally driven [58], [66]. Despite the acknowledged importance of processing temperature in the context of other materials classes, a relationship between deposition temperature and the preform as output of the ADFP deposition process has not yet been established. A large variety of heat transfer models is available, but the direct transferability of these models to dry fibre materials is not straightforward for a number of reasons. Figure 2-5 gives an overview of the different mechanisms during AFP processing with thermoplastic material, which many of the available heat transfer models have in common [67].

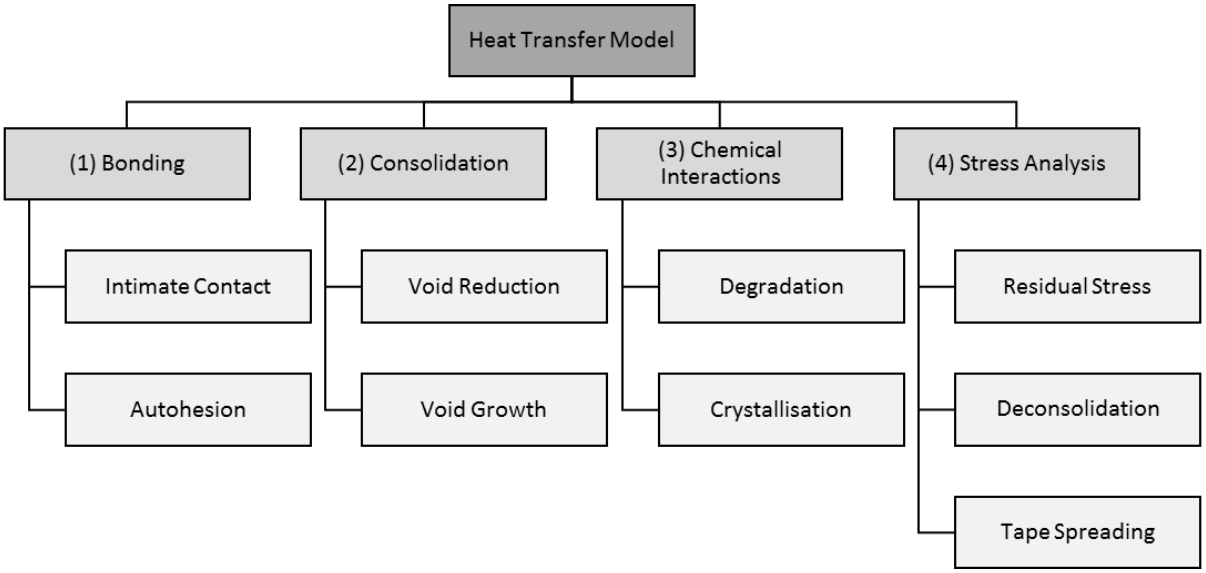

Figure 2-5: AFP process mechanisms relevant for a heat transfer model for thermoplastic processing, adapted from [66], [67]

Bonding (1) does not occur for dry fibre material in the same manner as with thermoplastic materials; intimate contact and autohesion occur only for the binder particles (5-10 wt. %) if at all, instead only binder adhesion and potentially binder diffusion from the surface into the centre of the tape can occur. The same applies to consolidation (2), because the material contains 40-50% interconnected voids, the issue of trapped voids between deposited layers is not present in the deposition stage. The only metric for bonding is the bulk factor a material exhibits, or in other words, how close the fibre volume fraction (V_f) of the preform is to the V_f of the laminate. Regarding the chemical interaction (3), crystallization can only occur on the binder particles, but due to the small quantity do not form a significant energy transfer pathway. Degradation of the binder may happen during the deposition

process at excessive deposition temperatures. The stress state (4) within the preform may also lead to residual stresses due to constrained deformation [66], [67]. Due to these numerous differences, a model to describe the ADFP process mechanism cannot easily be defined based on pre-existing models. The underlying mechanisms occurring during the deposition of dry fibres are still undefined.

Compaction pressure

The deposition on concave surfaces is one of the main features that distinguishes AFP from filament winding. For concave surfaces, compaction is necessary to enable the depositioned tapes to adhere to the tool, as opposed to utilise tension. The material is not fed actively but pulled out of the deposition end effector by the motion of the deposition roller against the tool.

Most AFP systems use a roller as compaction device, moving over the preform with variable speed. Less common, but also reported is the use of an air-jet compaction system for the consolidation in the automated manufacture of composite components, but these systems have not gained much attention recently [55], [68].

Roller material and make is often poorly described; terms such as “rigid material” [69], “soft roller” [53], “compressive roller” [70] or even simply “compaction roller” [48] are used for flexible rollers, which are commonplace in thermoset deposition. This is insufficiently describing the process if the compaction pressure is not used as a process descriptor. One of the few very detailed descriptions is by Lichtinger *et al.* including roller dimensions as well as pressure distribution, as they developed an Finite Element Model (FEM) of the roller [71]. This work exhibits a non-uniform distribution under the roller, shown in Figure 2-6.

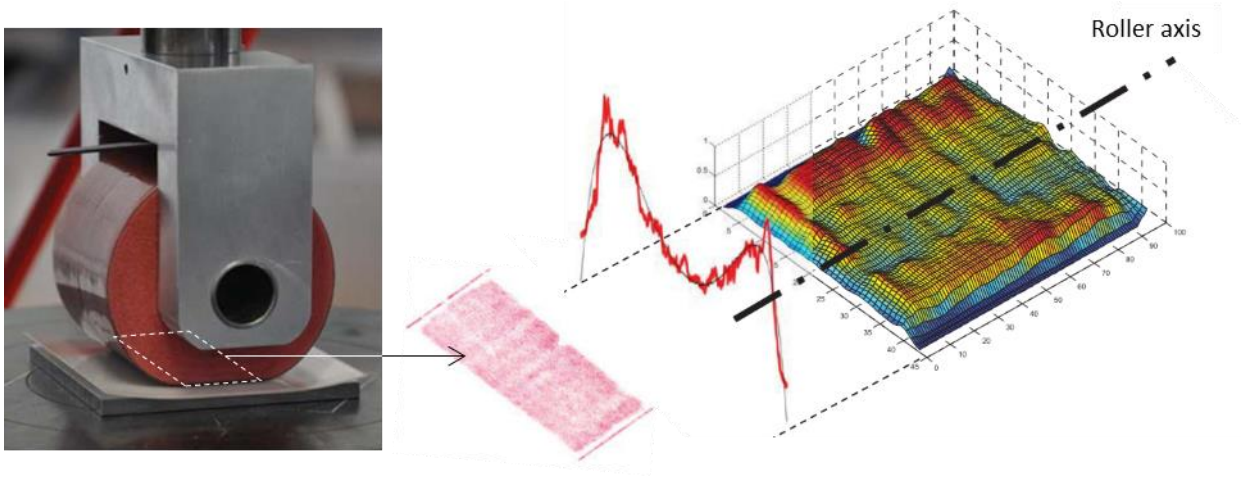

Figure 2-6: Normal pressure evaluation procedure and result for static compaction roller testing, modified from [71]

Metallic rollers are quite common in thermoplastic deposition, such as steel, which can be heated [55], [72]. Quite rarely the diameter of the roller is given (e.g. 30 mm [69]). Acknowledging the

importance of an accurate process description, some work was conducted to describe the roller and its compaction behaviour numerically [73]. This useful tool determines the number of tapes that can be applied on a convex geometry simultaneously. However, this is not yet linked to a material model to predict a material state.

The level of compaction can commonly be selected in an AFP system, but this process parameter is frequently determined by trial and error. Lukaszewicz determined the relationship between pressure and temperature and their impact on void content for thermoset material in the AFP process [58], similar to Han *et al.* showing a decrease of void content with increasing compaction force [69]. There are a number compaction models available for pre-impregnated materials like thermoset and thermoplastic prepreg, often exploring the conditions required to manufacture in-situ consolidated laminates [74]. These existing models are often based on flow or flow-compaction (squeezing and bleeding flow) modelling, none of which applies to dry fibres due to the lack of resin [75], [76].

Many investigations on the compaction of textiles have been carried out, which could potentially be adapted to ADFP due to the similarities in material constituents. An exponential correlation between V_f and compaction pressure was established for textiles, showing a similar effect with and without binder, schematically shown in Figure 2-7 [77], [78].

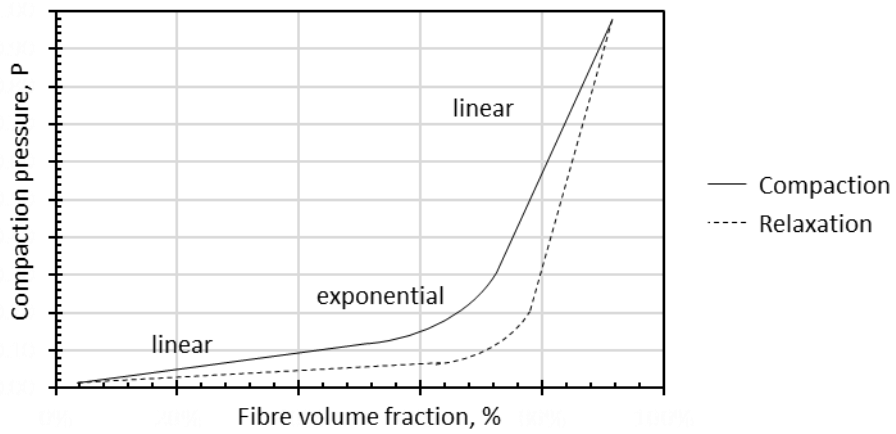

Figure 2-7: Typical compaction pressure versus V_f curve exhibiting a hysteresis effect [77], [78]

According to Aranda *et al.* most compaction models fail to take effects such as permanent deformation remaining after compression, hysteresis or the effects of cyclic loading into account [79], which is highly relevant for the AFP process. Velocities tested in compaction experiments are often orders of magnitude below speed of the compaction within an AFP system because the research is aimed at characterising closed mould processes. The compaction speed influences the preform V_f of conventional materials, which means that the established models for textiles are unlikely to be transferable to the ADFP process [80]. The compaction of tows was explored in its raw state without

any binder, showing an experimentally determined exponential compaction behaviour, consistent with previous findings on broad good with binder [80].

Compaction of ADFP preforms were investigated by Deléglise and Binétruy, showing an exponential behaviour of the preform V_f and the applied force [70]. The preforms were tested between two flat plates mounted on a Zwick compression test unit. Three configurations with different gap and overlap were tested up to 90 kN. As the size of the plates is not reported, the results cannot be converted into pressure and are therefore not directly comparable, only the general trend can be compared [70]. The force in this study appears rather high, while other similar studies report applied forces of 200 - 850 N [53], [69], [81]. One of these studies by Han *et al.* reports an applied pressure in deposition trials, which can be used for comparison with other machines, however no impact of compaction on either preform thickness or resulting mechanical properties were reported [69]. With all of these findings established around quasi-static compaction testing, the question that remains unanswered is if the results are transferable to a highly dynamic process. The presented research of compaction behaviour of textiles has demonstrated that the material constituents are highly affecting the compaction behaviour. Due to the many differences of the previously studied materials to dry fibre materials for AFP, transferability of previous findings to ADFP could not be established. The relationship between the compaction in the AFP process and resulting material behaviour needs to be established.

Deposition Speed

The deposition speed can have a high impact on deposition quality and preform and laminate properties. The deposition speed can depend on the articulation capability of the deposition system as well as the geometry of the component on which tapes are applied. Reported deposition velocities are often as low as 10; 15 and 20 mm/s [69]; 100, 200 and 300 mm/s [82] or 25 and 80 mm/s [81] for thermoset or thermoplastic material. For thermoplastic materials, speed is a crucial factor for high quality laminates, especially when attempting an in-situ consolidated lay-up, deposition velocities as low as 100 mm/s are reported [83], [84]. In contrast to that, industrial machines are often capable of a speed up to or in excess of 1000 mm/s [54]. Dry fibre material was reportedly deposited at 400 - 800 mm/s, but the influence of speed on the preform quality has not yet been established for ADFP [53].

Deposition speed may have an impact on the quality of the laminate, but also leads to a trade off on productivity. Manufacturing is the second largest contributor to the cost of a laminate component after raw material cost [85]. The deposition phase is a relatively small part in the production process, however the need for high speed deposition is recognised [86]–[88]. The aspect of productivity in the context of ADFP has not yet been established.

2.2 Constituents of Dry Fibre based Composites

2.2.1 Dry Fibre Material

Dry fibre materials for AFP have in common that they are made up from continuous carbon filaments. Tows are a bundle of filaments, typically carbon fibre tows contain 3k, 6k, 12k, 24k or 48k filaments [89]. These tows are processed (e.g. in a spreading process) and a binder is applied to ensure coherence of the tape, usually ~5-10 wt. %. The binder material can be epoxy or thermoplastic based [90]. The absence of B-staged resin eliminates the need for frozen storage, facilitating the logistics in material supply chain significantly. Introducing the resin at a later stage is not only cost effective; it also provides the opportunity for out-of-autoclave processing. Figure 2-8 gives an overview of the different dry fibre materials that can be processed using ADFP, the various manufacturing routes are described, as they have a significant influence on the dry fibre tape constituents. The most common tape width for ADFP dry fibre tapes is ¼", less commonly ½" or ⅛" are available.

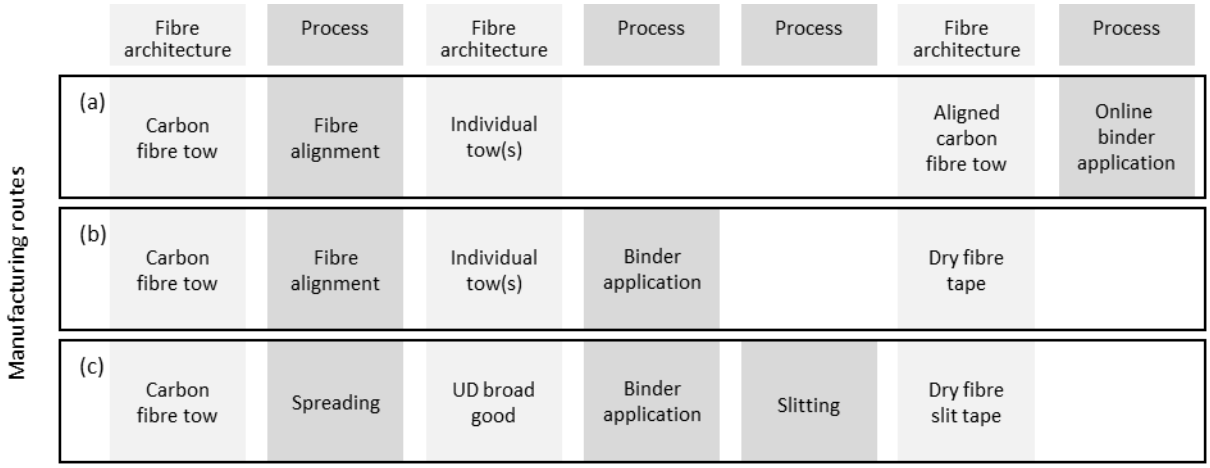

Figure 2-8: Classification of AFP dry fibre materials by manufacturing route and fibre architecture, online binder application (a), tape with previously applied binder (b) and slit tape process (c)

The slit tape process starts with spreading tows, which are then processed into a binder stabilised, uni-directional (UD) sheet and subsequently slit into tapes. This method is similar to prepreg production, whereby resin is applied to spread carbon fibres which is subsequently slit [37]. The advantage is that there are no constraints in manufacturing a specific areal weight or tape width; however, the process creates open edges that may fray. Another option for tape manufacture is to keep the original architecture of a tow and apply binder directly to it. Dry fibres are commonly based on 24 k tows or multiple lower count tows (e.g. combining three 6 k tows). While this option does not result in potentially fraying edges, the width variation and fibre misalignment are often higher, and the areal weight is dictated by the filaments present in the precursor. The availability of specific areal weight tapes is only relevant when a direct replacement of a pre-existing design using prepreg is envisioned, which is not considered a constraint in this work. The limitations for the scope of this work

is that materials and machines are commercially available as of 2015. Therefore, online binder application systems are out of scope, as commonly online binder application mechanisms are bespoke machine developments or developed for glass fibres using low temperature binders [29], [51], [91]–[93]. The online binder application route requires a bespoke hardware [92] while the other materials can be processes with a conventional AFP system. Furthermore, it was out of scope to modify a machine or to develop a new tape material.

When excluding development material that is not commercially available, the most mentioned and used materials in literature are available under trade names HiTape® (Hexcel Corporation, US) and TX1100 (Solvay Group, Cytec, US) [28], [45], [46], [48]–[50]. TX1100 is available at least since 2014 [94], related patents were filed from 2012 onwards [95]–[97]. TX1100 was originally developed for the Russian MS-21 programme where a dry fibre solution was selected over a conventional prepreg solution [98], [99]. HiTape® is available since 2013 [100] as a COTS alternative. However, one of the earliest mention of tapes containing a binder to avoid mechanical interlocking and instead placing tapes is by Tenax Fibers (2005) but this first publication was not followed by a commercial product [101], [102]. A further provider of a dry fibre tapes suitable for AFP deposition is Porcher Industries [30], [103]. In 2018, new tape manufacturers entered the market, Cevotec with the product CevoTape [104], [105] and MTorres with dry carbon fibre material [106], but these products were not considered within this work due to late market entry. These tape materials are considered raw materials in the context of this work.

There is currently no dominant design of the tape material on the market; the different suppliers provide substantially different products. Often suppliers provide a variety of dry fibre tape products, varying in fibre material, binder quantity, material width, areal weight or even provide materials bespoke to customer requests. The specific composition and manufacturing processes of the different materials is proprietary information of the suppliers. Five different materials from four suppliers were obtained as part of this market analysis; Porcher provided a range of materials, while the other suppliers provided either their only available product (in the case of TX1100) or a selected product (in the case of HiTape and Toho Tenax products). Some basic information on structure and constituents was provided by each respective supplier, shown in Table 2-3. The material identification (ID) in the left column will be used for the remainder of the document to describe the materials.

Table 2-3: Different material trade names and provided information (CF = carbon fibre; EP = epoxy based; TP = thermoplastic based), all with a nominal tape width of 6.35 mm (¼ inch)

Material ID	Supplier	Product Name	Nominal fibre density, g/cm³	Nominal areal weight, g/m²	Binder type	Binder application	Tape type
A	Solvay Group, Cytec, US	TX1100 IMS65	1.78	196	EP	CF veil & EP powder	Slit tape
B	Toho Tenax Europe GmbH, Japan	TENAX-E HTS40 X030	1.76	126	EP	EP powder	Tow based
C	Porcher Industries, France	TP binder yarn	1.77	126	TP	TP powder	Tow based
D	Hexcel Corporation, US	HiTape®	1.79	210	TP	TP veil	Tow based
E	Porcher Industries, France	TP binder yarn	1.78	261	TP	TP powder	Tow based

A detailed description of the dry fibre tapes is not available in literature. The different types of dry fibre tapes were compared by Agogue *et al.* for comparison of permeability, with a focus on the measurement method, but the influence of the different material constituents was not discussed [50]. This is a significant gap as the differences and similarities between available dry fibre materials for AFP are not known, even though the details of the constituents may drive material behaviour during the manufacturing process.

2.2.2 Binder and Resin

Dry fibre tapes contain different binder types, but also vary in binder quantity and distribution. The majority of work that has been carried out to investigate the influence of binder using an on-line binder application route (refer to Figure 2-8), where the binder and the application parameters can be changed directly. Rimmel *et al.* concluded that a higher binder content leads to a slightly higher permeability, however their data shows a high error bar and therefore low statistical significance [107]. The binder size was also investigated, and a coarser binder size lead to a lower permeability than a finer version, but again exhibiting a large coefficient of variation. The binder size influences the permeability more than the binder quantity [51]. Other authors using similar online-binder application techniques did not investigate the binder quantity as part of their ADFP studies [29], [91]. However, the influence of binder on NCF or woven preforms (in this context also referred to as tackifier) has been studied more widely [108]–[111].

The importance of the binder location on NCF or woven material (within the fibre bundle or on the outside of the tows) as well as uniform distribution, binder particle size and density is highlighted [108], [109]. The binder material make-up (fleece/veil or powder) has an impact on the compaction behaviour, attributed to the binder diffusion into the tape and the lubrication effect due to this permeation [79]. The initial binder location is influenced by the manufacturing parameters of the tapes, the binder penetration depth into the tape can be affected by the manufacturing temperature [108]. Inter-ply binder has a significant effect on the compaction behaviour of NCF and woven materials, but the effect may be different as ADFP does not have a through thickness mechanical intra-ply locking mechanism as conventional fabrics. The activation parameters during preform manufacture can influence the permeability, likely by influencing the diffusion and distribution of the binder within the textile [112], [113]. Binder on the surface as opposed to the centre of the tow leads to a lower permeability for two material combinations [111], [114]. Shih *et al.* additionally conclude that a surface dominated binder application yields a better inter-ply adhesion and spring back control, but also show inhibited resin flow [110].

Even though there are differences in nature of the constituents, these findings allow the hypothesis that the binder type, application method, distribution, location and activation parameters are of relevance to the preform compaction and permeability. This supports the importance of characterising the different materials in depth with an emphasis on the binder location. It is currently unclear which of the available ADFP materials are best suited for the process, and which elements in the composition causes their behaviour. Without this information, linking material constituents and its behaviour in the manufacturing process is not possible.

In order to avoid any potential issues of the compatibility of binder to resin, the use of the same chemistry is recommended to avoid an effect [110]. Solubility of the binder in the matrix material has also been investigated as a proxy for likelihood of binder wash out, which would lead to a non-uniform distribution of binder in the laminate [92]. However, epoxy resins used in the aerospace industry often require a binder phase of different chemistry. These materials are known as toughened resin systems, containing a thermoplastic phase as pure epoxy is inherently brittle. The technology to include toughening agents in the prepreg production is mature and is applied to many conventional aerospace grade prepreg materials [18], [115]. For dry fibre tapes, there are two convenient options to introduce toughening agents, either as part of the fibre and binder combination or as part of the resin. Blend thermoplastic toughening particles into resin improves the resistance to fracture of the resin system, the underlying principle is that more energy is required to create cracks perpendicular to laminate surface. Transverse crack growth is not affected and the matrix based composite properties can be compromised [116]. This is likely to be the case for Material A, as the binder material is epoxy based

and the recommended resin (PRISM™ EP2400 (Solvay Group, Cytec, US)) is marketed as a toughened resin [117].

The second mechanism is the use of a discrete interlayer, either as a film, a porous membrane or coated particles, which were originally developed for prepreg [116], [118], [119]. The interlayer acts as a mechanical toughener by locally deflecting crack direction to require more energy to extent per unit area of crack growth [116]. As some of the dry fibre materials contain such a discrete layer of thermoplastic particles this might be the intended mechanism for toughness increase. For example, the use of Material D is recommended in conjunction with HexFlow® RTM6 or RTM6 (Hexcel Corporation, US), a resin system that is not marketed as toughened system [120]. This shows that different mechanisms can be present to obtain certain mechanical properties and compatibility between binder particles and resin system are important. As the resin, binder and fibre interaction results in a variety of different mechanism affecting mechanical properties, it is not possible to use fibre and resin systems interchangeably.

2.3 High Temperature Infusion Process

The conventional manufacturing route using prepreg tapes and an autoclave cure has a significant drawback, which is the scalability of the process. The outlined rise in demand for advanced composite components requires a manufacturing process where capacity can be increased more easily than the current autoclave process, such as an oven infusion. This will drastically decrease the required upfront investment for manufacturing companies when trying to achieve lower tact times by acquiring more equipment. An advantage of the autoclave process is that the curing cycle might be mitigating AFP defects [58], [121]. Therefore, the challenge with an infusion process is the higher emphasis on the quality of the preform, as potentially an oven infusion has less impact on defect mitigation due to the lack of application of external pressure during the consolidation process.

A challenge in assessing infusion processes is their wide variability, as reported in many studies. The investigation of permeability of broad goods such as NCF and woven material has a long history, and the differences in results of in-plane permeability measurement across institutions and measurement instruments have a variability of up to ± 20 % (standard deviation, SD). A round robin established that permeability measurements are highly dependent on the set up, the preform preparation and the calculation of the permeability K(based on interpolation of the flow front position K_{SFF}, used in Figure 2-9, or applying a least square fit K_{LSF}) [122]. The compaction force, binder activation temperature and their duration can have a significant effect on the fibre volume content of NCF preforms, which impacts transversal permeability significantly [123]. Studies regarding permeability of ADFP preforms

are relatively scarce in comparison to materials that are more conventional, but the values found are shown in Figure 2-9.

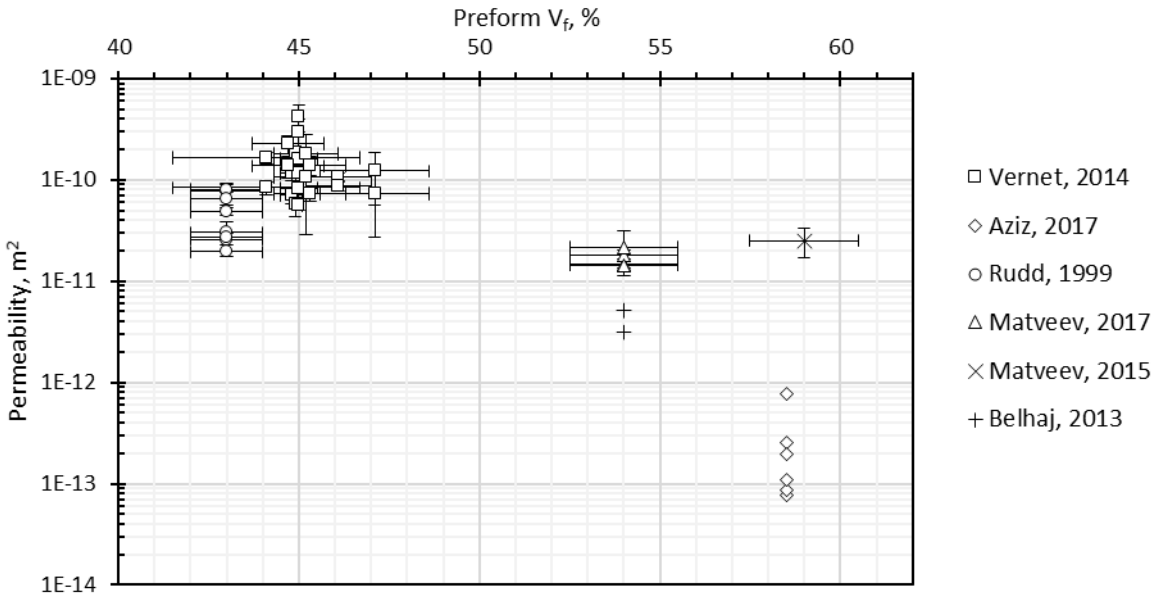

Figure 2-9: Various permeability values (K_{SFF}) of ADFP preforms reported in literature in in-plane direction [28], [29], [45], [53], [91] *as well as values obtained in a round robin with conventional textiles* [122]

In addition to the inherent, demonstrated variability of the measurement itself, it must be noted that the dimensions of the test instruments can be very small when considering the repeating patterns of ADFP preforms (dimensions of 100 × 400 mm are common [122]). The repeating patterns of ADFP preforms are significantly larger than for woven or NCF preforms, and therefore tests conducted with current practice require a large number of repeats to be reliable.

A small number of papers have investigated the infusion behaviour of ADFP preforms, and the comparison between them shows the challenge in determining the permeability reliably and as a true material parameter of the reinforcement. Aziz *et al.* report that the permeability can vary a factor of five, depending on the design of the preform, and is highly susceptible to AFP placement accuracy [45]. However, their model of permeability on the basis of tape gaps and overlaps does not take into account the compaction of the preform prior to infusion by means of the applied vacuum at temperature during the heating cycle, which may mitigate some of those inconsistencies. In addition, this work is relying on X-ray computerized tomography (X-CT), which is a non-destructive test method but is constrained by specimen size. The high variability of the infusion is also supported by Matveev *et al.*, where difference between the actual geometry and the designed geometry can result in 50 % reduction of the permeability. The stochastic geometry model predicts results within 20 % of the

experimental values [28], [53]. The use of the nominal gap width between the individual courses of multiple tapes for modelling the infusion is not sufficient [28].

Belhaj *et al.* investigate in-plane water permeability of preforms made of a dry fibre tape material with a thermoplastic binder, with the conclusion that gaps do not have an effect on in-plane permeability [29]. They hypothesize that the effect is due to gaps closing due to compaction. Graupner regarded pure through-thickness permeability for biaxial preforms made with a similar dry fibre tape material and a test fluid, which derived the conclusion that the gap configuration significantly affects the through-thickness permeability without a compaction step in the preform preparation [124]. The deliberate use of gaps between courses or tapes in order to enhance the resin flow in the infusion process has been investigated showing a high impact on out-of-plane permeability [51], [107], [124]. Even though laboratory scale research around the impact of gap width on permeability has been investigated, it is still unknown if the resin flow is influenced by the infusion set-up, and therefore flow direction, or by the design of the preform (gap with and frequency).

2.4 Manufacturing Quality Assurance

Monitoring the manufacturing quality throughout the process enables linking up processing conditions with the quality of the resulting preform. Even though ADFP is derived from mature technologies, significant differences to conventional prepreg materials inhibit the use of common quality metrics in the preforming stage. In the first part of this section, assessment methods for conventional AFP are reviewed and applicability to ADFP is considered. Once a preform is infused, the laminate has many similarities to laminates manufactured with other technologies, and conventional assessment methods can be used to measure various established metrics.

2.4.1 Preform Assessment

Even though AFP is an advanced, automated manufacturing process, a large proportion of the inspection work is still done manually. Automated online assessment of the deposited material in the context of AFP is still relatively rare and predominantly researched for monitoring the industrial production process, not necessarily as research tool. The tool used for this purpose is commonly a laser line scanner, which then is utilised to detect manufacturing defects during the production process [44], [125]. Defect detection is an important aspect of AFP deposition; however, it does not assess the general impact of processing parameters on the preform.

Conventionally, the quality parameters assessed of consolidated or un-consolidated parts are bond strength, void and resin content, material degradation, degree of crystallinity (thermoplastic only), residual stresses and mechanical characterisation [58], [67], [126]. All of these metrics not only rely on the presence of resin, these methods are destructive. This shows a clear gap for an assessment

method that enables a meaningful, quantitative assessment of the preform that is non-destructive. The advantage of a non-destructive method is that a part can be assessed during and after the preforming stage. Furthermore, the preform is still suitable for infusion after the measurement, making non-destructive test (NDT) methods more economical.

Defects

Even though automated manufacturing processes are utilised for the purpose of high repeatability, it is well known that defects can occur in the AFP process. Detecting and avoiding these defects is very important; a variety of research has found negative effects of defects on mechanical properties, most studies are focused on the influence of gaps and overlaps, but also twists and wrinkles have been studied [21], [127]–[130].

Different types of defects are not clearly defined in literature so far. There are two types of defects identified as part of this work: random defects and systematic defects.

Systematic defects are introduced during the design stage of the laminate. Systematic defects are often required in order to achieve a specific design, e.g. ply drops in a structure with variable part thickness. Significant efforts can be made to avoid this type of defects, but they may be necessary to make a part. These defects are repeatable, as they will occur in every part in the predefined location and conscious decisions regarding their severity, location and acceptable limits are made during the design process in order to ensure the compliance of the finished part with the performance requirements. For the purpose of this work, this defect category will be referred to as manufacturing features, as their existence is unrelated to the material used and they are repeatable [131].

Random defects occur during the manufacturing process and are not part of the design. These defects are not repeatable but can be minimised by the choice of processing parameters and must be monitored in order to be detected. Random defects can also be described as non-compliances. In practice, some of the random defects can be corrected by an operator, such as placement inaccuracies can be corrected by tape removal, however the dry fibre material can be more fragile than prepreg [48]. Table 2-4 shows a collation of different defect types reported in literature on the AFP process and a classification thereof.

Table 2-4: Classification of identified defects on AFP manufactured preforms from literature on prepreg and dry fibre materials incl. reference

#	Tape based defects	#	Course and ply based defects
1.	Blisters [132]	15.	Angle deviation [133]
2.	Fold [133]–[136]	16.	Bridging [133], [137], [138]

#	Tape based defects	#	Course and ply based defects
3.	Horizontally split tapes [48]	17.	Gap/overlap between courses [21], [53], [125], [127], [128], [133], [135], [137], [139]–[141]
4.	Loose tape [133]	18.	Gap/overlap within courses [28], [53]
5.	Missing tape [133], [137]	19.	Part edge (boundary coverage) [133]
6.	Puckers [133], [142]	20.	Position defects [125], [133], [135]
7.	Resin deposits [137]	21.	Wandering tow [133]
8.	Sheared fibres/ buckling [132], [136]	22.	Ply edge lifting [48]
9.	Splice[1] [133], [135], [143]	23.	Preform relaxation [144]
10.	Tow pull up[2] [81], [132], [145]	24.	Foreign body/object (FOD) [90], [125], [133], [137]
11.	Twist [21], [82], [90], [125], [133], [135], [137]		
12.	Vertically split tapes [143]		
13.	Waviness [134], [135]		
14.	Wrinkles [81], [125], [132], [133], [135], [136], [146]		

A lack of a detailed dry fibre material description inhibits tracing the defect origin, which would be the first step towards preventing them. The majority of the listed defects are observed in prepreg manufacturing, very few of the identified defects are based on dry fibre materials and the list potentially needs to be expanded for the particularities of dry fibres.

Tape steering

Steering of fibres is required in almost every composite part produced by AFP, whereby the deposition path follows a specific radius instead of the geodesic path. Conforming a relatively stiff, resin saturated prepreg tape is challenging, but dry fibre materials are closer to a flexible textile material in their composition and therefore have the potential to conform better to steered paths. Steering may be used deliberately where fibres are aligned to the load path to increase mechanical properties, see Figure 2-10 (a) [147]. However, steering occurs more often when a fibre path follows a non-geodesic path on complex geometries, which is often the case in aerospace structures to maintain 0°, 90° and ±45° fibre angles on curved surfaces as highlighted in Figure 2-10 (b) [71].

[1] A splice is acceptable at a width of up to 75 mm if the splice is ≤ 12% of the total width. The splice may not be thicker than double the tape thickness. A maximum of three splices on 8 m is permissible, there has to be 1 m space between each splice.

[2] Please note: Smith *et al.* refer to their observed defect as “tow fold-over” [145], which is consistent with the tow pull up observed by Bakhshi [132] instead of what is referred to as fold by others [125–127, 129]. Zhao *et al.* refer to this effect as “tow warpage” [81]

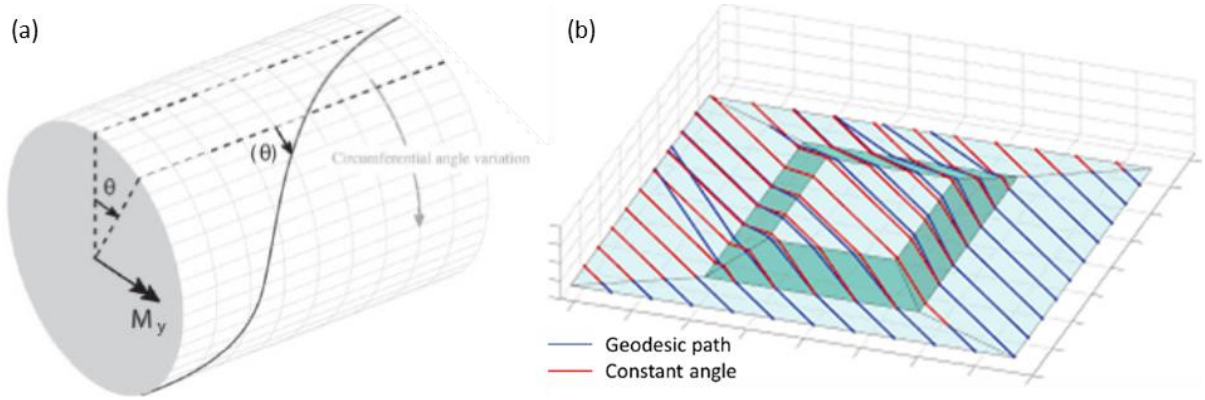

Figure 2-10: Fibre path in load direction for cylinder in bending (a) [147]*; tapered structure on a flat surface with constant angle paths (red) and geodesic paths (blue) (b)* [71]

Wrinkles and waviness are two different terms often used interchangeably in the context of fibre steering. The common term is fibre misalignment, defined as the deviation from the nominal fibre path. To distinct these terms, out-of-plane misalignment is defined as wrinkling and in-plane misalignment as waviness [61], [148]. Fibre misalignment can be regarded as features or defects, depending on their origin. A misalignment induced by steering is a direct effect of the manufacturing method, and is therefore considered a feature, while misalignment occurring randomly within a nominally straight path would be considered a defect [131]. Typical characteristics for AFP material associated with steering are grouped as seen in Figure 2-11, refer to Table 2-4 defect 1, 2, 8, 13 and 14 [134].

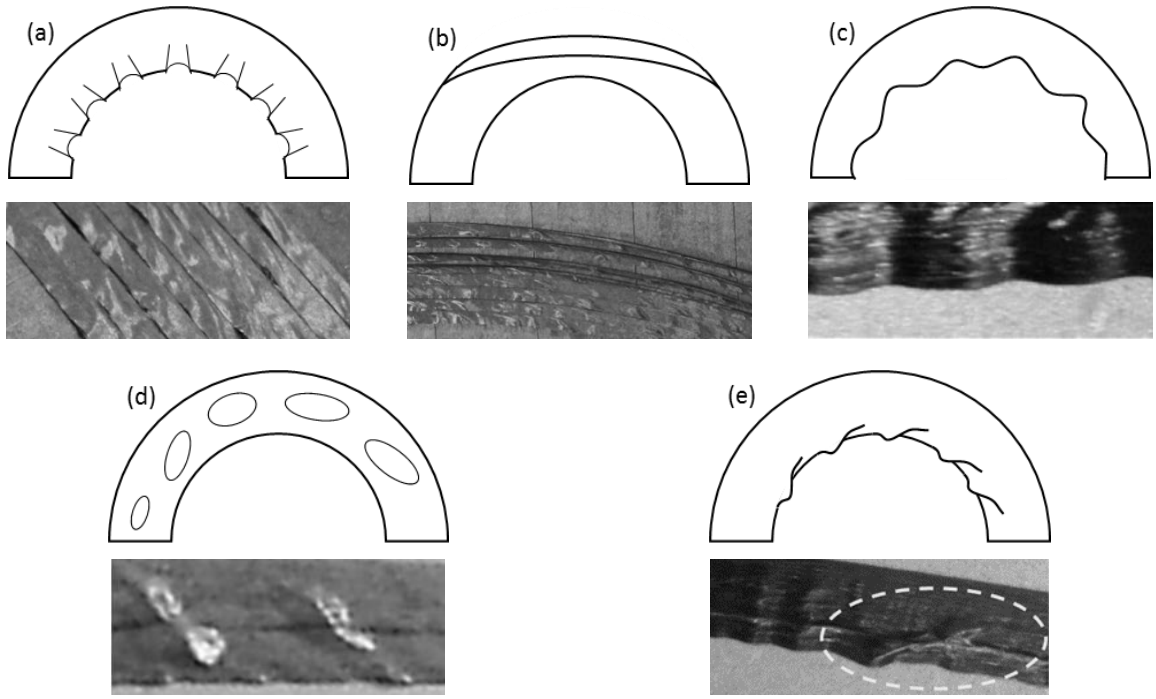

Figure 2-11: Typical defects/features associated with steered tapes (sketch and photo): wrinkling on the inner side of a tape (a) [134]*, fold-over on the outer side of a tape (b)* [134]*, in-plane waviness (c)* [132]*, blisters (d)* [132]*, tape shearing/buckling (e)* [132], [136]

Visual inspection has widely been accepted to be sufficient for prepreg material to determine the 'minimum steering radius', considered to be the minimum radius acceptable in the machine program to manufacture an satisfactory part [9], [132], [145], [149]–[153]. The drawback of subjective visual assessments is the wide variety of minimum steering radii reported, as shown in Figure 2-12. The wide range shows the lack of reliable assessment method and common quality standard.

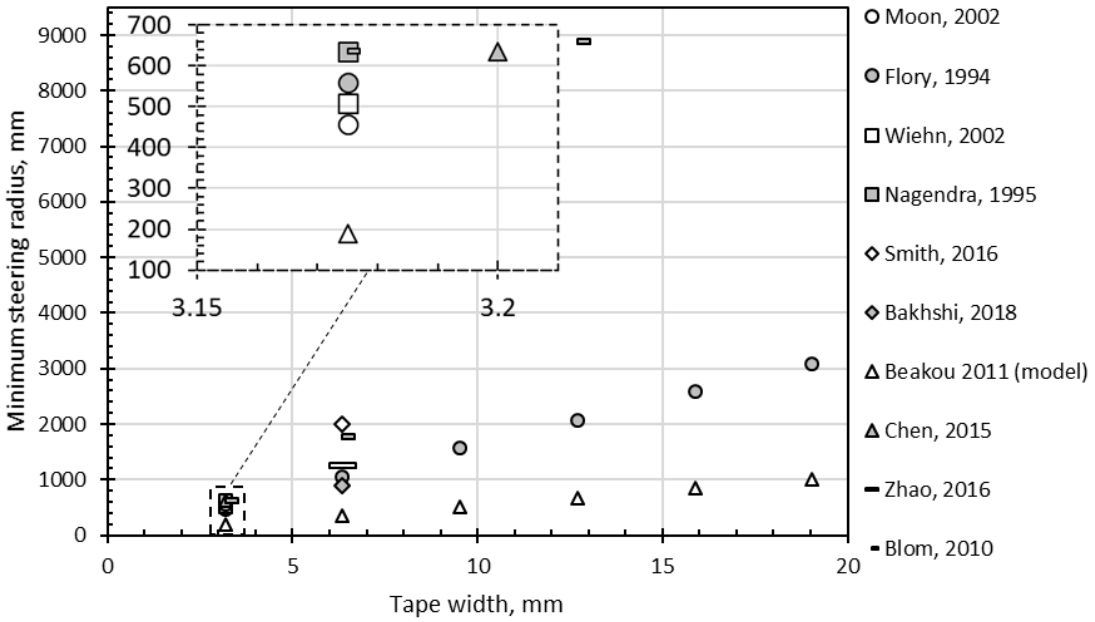

Figure 2-12: Minimum steering radii reported in literature for various tape widths for thermoset prepreg tapes [9], [81], [132], [145], [149]–[153]

The steering radius is decreased by more than 50% when the tape width is decreased from 6.35 mm (¼ inch) to 3.2 mm (⅛ inch) [145], [151]. Zhao *et al.* acknowledge that steering radii determine the wrinkle severity and that steering quality is depending on the material characteristics, such as fibre grade, width and thickness, as well as AFP process parameters. Their suggestion is to experimentally determine the minimal steering radius using deposition experiments with a single tape and calculate a wrinkle ratio (height versus length), whereby 0.1 is considered wrinkle free. The authors hypothesize that these results could be used to adjust deposition process parameters to counteract the wrinkle formation based on the material state [81]. The assessment method of Zhao *et al.* as well as Clancy *et al.* is a caliper, which is more objective than a visual assessment but also very tedious and time consuming [81], [154]. In addition, dry fibre material is compressible due to its textile characteristics, which may have an impact on the results of the measurements using a caliper.

In contrast to the sharply defined wrinkles in prepreg deposition that can be counted and measured, dry fibre materials can have a more subtle wrinkling pattern without distinct, countable wrinkles. Due to the absence of resin, dry fibres are likely to overcome internal friction forces and fibre re-

arrangement can occur more easily than in prepreg materials [155]. In order to determine the steering quality without operator dependent visual observation and judgment, a reliable metric is needed.

Due to the lack of available objective methods for measuring steering quality in AFP, methods in other areas of composites manufacture were considered. Wrinkle measurement is more common in draping and forming of dry broad goods, such as NCFs or woven materials. The majority of the effort is targeted at obtaining measurements for reliable simulations of draping. A brief literature survey summarised in Table 2-5 shows some methods used for wrinkle detection, as well as the material configuration and the scale of the method. Methods that are targeted at detecting defects in general and not specifically wrinkles are disregarded in this review.

Table 2-5: Available wrinkle measurement methods

Method	**Material**	**Scale**	**Source**
Digital image correlation	Broad good, fabric	Specimen in picture frame ~200 x 200 mm	[156]
Shape-from-focus analysis of a stack of photographs	Broad good, fabric	Specimen Ø = 300 mm	[157]
Scan with a robot-guided high-frequency eddy current sensor for yarn orientation	Broad good, fabric	Specimen, test rig	[158]
Scanner and image analysis Matlab routine	Fabric	Specimen from wrinkle simulator	[159]
Vernier caliper for thickness comparison of straight and steered tapes	Thermoplastic AFP tape	Tape level	[136]
Optical Microscopy	Laminate	Specimen	[160]
Optical Microscopy	Laminate	Suitable for fibre misalignment	[161]
Ultrasonic Non-destructive Evaluation Technique (UNDET)	Laminate	Full part	[150]
Digital Image Correlation (DIC) to measure the strains of deformation on the material	Uncured prepreg AFP tape	Individual or multiple tapes	[135], [162]
3D Non-destructive Testing (NDT)	Laminate	Small parts	[163], [164]

A requirement for the wrinkle measurement is that it is non-destructive and can be carried out fast. The only listed method that would be suitable for full parts is the UNDET. This method was utilised for

laminates but is not suitable for preforms as it relies on the absorption of the echo pulse by the entrapped air. Overall, this list shows a clear lack of a measurement methodology for steering quality assessment of dry fibre materials used in ADFP.

Various efforts in terms of modelling steering behaviour have been made, both for prepreg [135], [148], [149] as well as dry fibre [47], but manufacturability and the required parameters to achieve a specific quality is rarely taken into account. The first step towards establishing a threshold of what is acceptable is to quantify wrinkling. Only then a preform with wrinkles can be infused and the laminate used as an input to mechanical tests to create transferable results. Furthermore, none of the reviewed work has been carried out or transferred to a geometry, but it cannot be assumed that there is no influence of the tool geometry on the material behaviour. It remains to be verified if in-plane steering on a flat surface is a suitable representation of in plane steering on a geometry.

2.4.2 Laminate Assessment

As the laminates produced with ADFP are relatively similar to conventionally used materials, the majority of the common quality indicators for composite materials are applicable. As the ADFP process is still relatively immature, only relatively few datasets for comparison are available.

One of the more widely used assessment methods in literature is microscopic imaging. Microscopy is a widely accepted and used method for the assessment of composite materials, whereby a composite material is cut into a small piece, potted polished and microscopic images can be taken of the cross section [154], [165], [166]. The sample size is typically no larger than ~ 50 mm length. Obtaining a representative sample for laminates manufactured with AFP can require quite a significant effort due to its large repeating pattern.

Nevertheless, some numbers were reported using dry fibre material (HiTape®) manufactured into preforms using a COTS machine (Automated Dynamics) and infused with high temperature resin (EP2400) resulted in a laminate V_f of 51.5 ± 1.5% (2 SD) across five samples of different ply sequences and a void content of < 1%, evaluated by microscopy [48]. Other laminates manufactured with a bespoke ADFP system resulted in reportedly 25 – 30% laminate V_f, but no measurement method was reported [55]. In comparison, prepreg material deposited at different AFP parameters but identical cure, resulting in laminates containing a range of void content from 3.5 % to 0.4 %, also determined by microscopy [69].

Other relevant inspection methods that are directly applicable to laminates manufactured using the ADFP and infusion route include a variety of methods ranging from very simple equipment to cost intensive methods. Visual inspection is a simplistic method, but it can be useful for an immediate indication of laminate quality. A part can be inspected in respect to colour, thickness, defect detection

such as cracks and surface quality [167]. Another simple tool to obtain the weight W of a preform, resin consumption and/or laminate is a conventional scale. If the density ρ of both is known and express fibre volume fraction V_f of the laminate as [167]

$$laminate\ V_{\mathrm{f}} = \frac{W_{\mathrm{fibre}}\ \rho_{\mathrm{fibre}}}{W_{\mathrm{fibre}}\ \rho_{\mathrm{fibre}} + W_{\mathrm{matrix}}\ \rho_{\mathrm{matrix}}} \qquad \textit{Equation 2-1}$$

The weight of the preform can be substituted with the areal weight of the dry fibres, the number of plies and dimension of the part. Calipers are frequently used to obtain the thickness t of a laminate at discrete locations of the part. The fibre volume fraction V_f of the laminate can also be calculated using

$$laminate\ V_{\mathrm{f}} = \frac{W_{\mathrm{ply}}\ n}{\rho_{\mathrm{fibre}}\ t_{\mathrm{laminate}}} \qquad \textit{Equation 2-2}$$

Where W indicates areal weight of a single ply of the fibre material and n is the number of plies and ρ is the fibre density. Furthermore, the conformity to the anticipated thickness can be evaluated, but also the variability of the measurements can give a quality indication.

Ultrasonic C-scan is a widely used non-destructive test method in the aerospace industry, often affiliated with a pass/fail criterion [127], [168]. The attenuation loss of ultrasonic waves is measured as voids will absorb the waves and a high loss in signal indicates porosity. A laser line scanner is a measurement method using a two dimensional line projection on a surface to generate a digital counterpart of a surface by moving the scanner laterally. This 3D point cloud can be used for further processing in the COTS metrology software, conventionally to compare a part to its CAD model [44].

2.5 Productivity and Scalability

For each part manufactured using AFP, an optimum compromise between deposition speed, preform quality and productivity can be found. Figure 2-13 highlights the relationship between these objectives, whereby the maximum deposition rate an AFP machine can deliver is only achievable for very simple parts. At a high deposition speed, the machine and material experience higher stress, and the maintenance requirement may increase. Especially for complex parts, a high deposition speed is limited by the frequent acceleration and deceleration areas that geometrical features required. While a lower speed often leads to higher part quality, the productivity will decrease. At the sweet spot in the centre, the optimum compromise between the competing requirements is found, but this may be different for different materials.

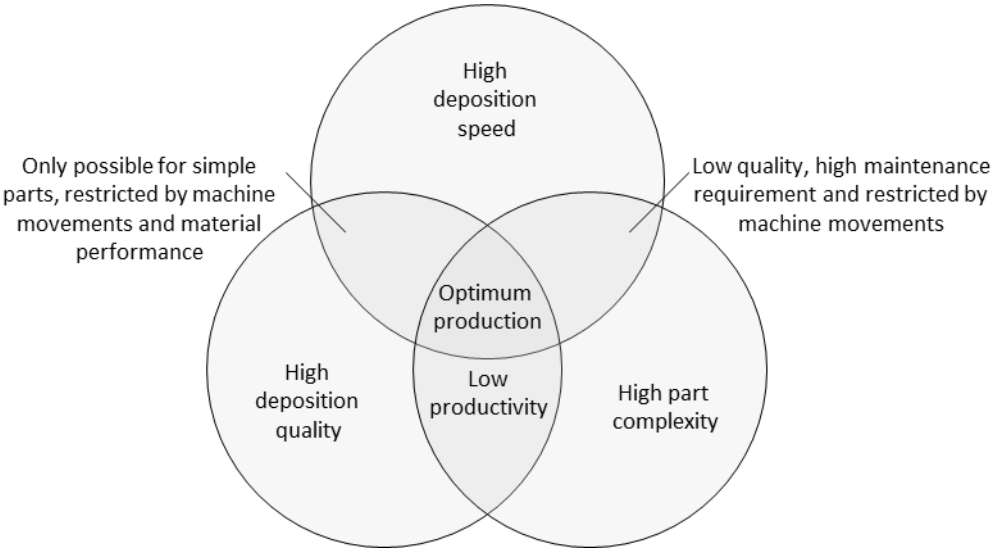

Figure 2-13: Competing objectives and resulting effect of optimising deposition speed, part quality and part complexity

A manufacturing time split during manufacture can give some indication how close to the optimum a deposition is. In lean manufacturing, value added and non-value added time are differentiated, where the non-value added time (any activity that does not change the product or assembly) has the potential to be reduced, and is considered waste [169]. Winter furthermore distinguishes 'non-value added' and 'non-value added but necessary' and presents a detailed list of all activities in the AFP process [170]. If assuming acceptable quality, a high proportion of time spend on maintenance (non-value-added time) may indicate that the production is not in the area of optimum production. Even though counterintuitive, a high proportion of time spend of deposition (value added time) can also indicate low productivity, as low deposition speed will take more time for deposition, so this is only a positive indicator if maximum deposition speed is achieved.

Few publications are available detailing the split between different activities in AFP manufacturing, but Rudberg *et al.* as well as Halbritter *et al.* provide some data [171], [172], see Figure 2-14. Both take into account 'inspection and repair' and 'program layup'. In both examples, the deposition phase only takes up around a quarter of the time. As other metrics differ slightly, a direct comparison is challenging. Relevant details such as part size, type of AFP machine (robotic or gantry style, tape width, number of tapes) are not reported. There is no published time split for ADFP available for direct comparison. Evidence that ADFP has similar or better efficiency in comparison to AFP would significantly increase industrial interest.

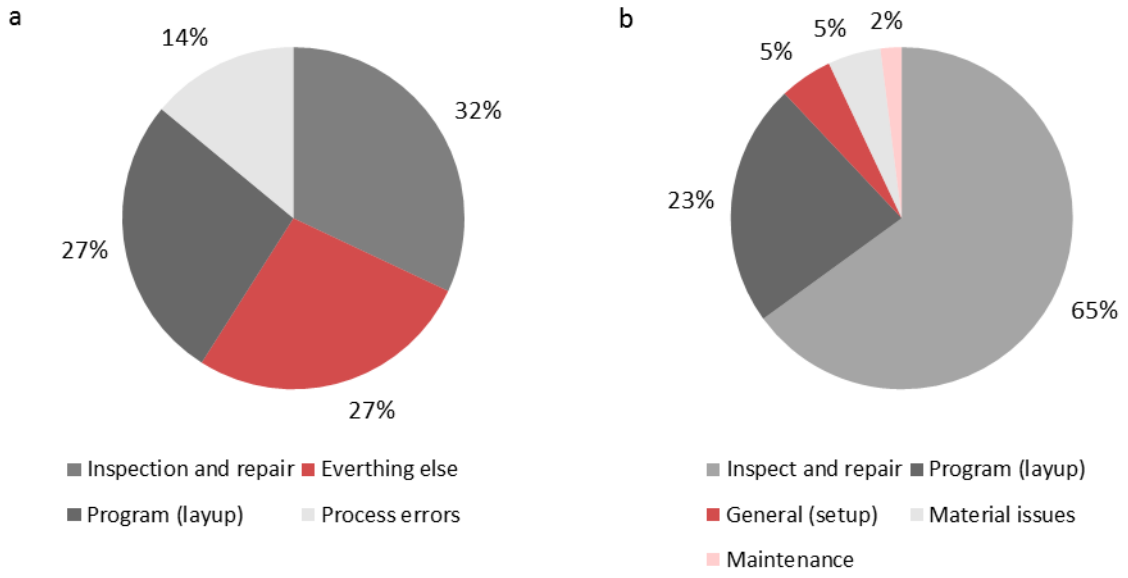

Figure 2-14: Distribution of time spend in AFP manufacturing as reported by Rudberg et al. (a) [171] *and by Halbritter and Harper (b)* [172]

A further metric that is often used in industrial environments is the deposition rate in kilogram per hour [87]. This metric is problematic to be used in the context of ADFP for comparability to conventional AFP processes. If regarding the deposition process only, the rate of ADFP is much lower than conventional as the weight only includes fibres but not the resin; or the duration of the infusion process would have to be added to the time component, if the weight should include fibres and resin. Commonly reported values for prepreg AFP are between 1.9 and 13.6 $^{kg}/_{h}$ [17]–[20].

A variety of projects have investigated the scalability of the ADFP process. One of the first European projects was PreCarBi, developing the underlying materials and supporting technologies for the ADFP process [173], with a potential application in a rotor blade pitch horn [174]. Later projects include ADVITAC, which aims to lower production cost and develop novel composite architecture [175], AUTOW aiming to reduce weight and cost supported by novel design and manufacturing approaches [120] and PRESCHE aiming to develop a rapid, automated manufacturing process for electric vehicles [176]. Other projects are ECOMISE which aims to develop monitoring systems, probabilistic process simulation methods as well as a new method for in-situ structural evaluation [177] and GroFi, which is a German project focused on the research of high productivity on an industrial scale using various and combined deposition mechanisms for dry fibres [59]. These research programmes are funded by large consortiums of industry leaders and research centers, hence detailed works and publications are very limited. The ADFP process development often not the focus of these projects, and even though large structures are manufactured, the underlying interconnections between the materials used, the processes employed and the resulting structural properties are not yet fully understood.

2.6 Conclusions and Research Needs

Previous work addressing ADFP directly as well as relevant work from related fields, was reviewed and has shown that the current research on ADFP is relatively fragmented and not yet comprehensive. Overall, an overview of the full manufacturing chain is needed in order to determine the relevance of the various manufacturing process steps towards the resulting laminate. This will enable more detailed research work in the context of a full manufacturing chain.

A variety of dry fibre materials are on the market, but an assessment of the behaviour of these materials in the manufacturing process has not yet been made. A selection process for dry fibre that enables a structured and evidence-based a selection is needed. This will require criteria that describe indicators for well performing materials.

Processing parameters reported in the context of ADFP in literature are often specified in non-comparable metrics, which makes it impossible to compare the impact of AFP processing parameters across different machines. A non-destructive method to assess ADFP preforms directly after the deposition process is needed, to enable an assessment prior to infusion to avoid assessing the combined influence of the deposition and the infusion process. This also would make it possible to isolate the process parameters that have the highest impact on the preform. A measurement method and metric to quantify the quality of courses with a steered fibre path is needed to replace the currently predominantly used visual assessment.

Every AFP deposition is preceded by a programming phase, which often requires many manual iterations to improve a program. It is industrial practice to use software outputs to optimise the program for multiple criteria, but it has not yet been verified that the software output accurately represents the ADFP preform quality. An assessment method to verify the accuracy of predictive capabilities of AFP programming software is needed.

A high temperature infusion step follows the deposition, converting the preform into a laminate. Some permeability values were found in literature; however a wide spread of values is reported. The records of the manufacturing process of the preform is often poor, so it remains unclear if the results are representative of real processing conditions. The majority of the research conducted investigates the impact of the laminate design (gap width and frequency). The significance of the level of intervention achieved by laminate design compared to the impact of the infusion strategy allows for an informed process optimisation but has not yet been investigated.

Finally, the scalability of the process has not yet been investigated systematically. Some examples of large-scale demonstrators are available, but a thorough assessment if findings obtained on coupon

level can inform and predict large-scale manufacture has not yet been made. Productivity assessments of the ADFP process are not yet available.

In spite of the many obstacles outlined preventing the technology to be used in an industrial environment, it is a promising technology. Overcoming the outlined challenges would unlock the potential of the ADFP process; the use of material with much less demanding logistics as the frozen storage of materials unnecessary, the potential of the material conforming to low radii to expand the flexibility of the technology and the use of a low upfront investment out-of-autoclave process. This work will not only investigate the fundamental mechanisms in the process but also establish the necessary background to understand if this manufacturing process provides the advantages that it promises.

Chapter 3

Material Selection

This chapter provides a detailed description of the available dry fibre materials. Furthermore, the initial material selection based on a multi-criteria selection tool focused on manufacturability is outlined. This selection process identifies the materials suitable for further investigations, but more importantly outlines the criteria and their significance for the decision. The decision-making tool was critically assessed and the applicability of the result was checked against a complex part.

3.1 Background and Aim

ADFP is in its early stages of development and material suppliers are entering the market with a range of different dry fibre materials. Due to the novelty of the process, very limited research has been conducted and published, which makes it challenging to select the most suitable material for a specific application. Particularly in the AFP process, material and manufacturing equipment are strongly linked and cannot be assessed separately. Material driven manufacturing issues can increase the production cost (e.g. due to machine stoppage), and can have a significant effect on the properties of the laminate (e.g. due to defects). Therefore, the early stage of product development requires a significant budget and time commitment. A reliable method for material suitability assessment is essential to minimise iterative manufacturing trials, which are currently commonplace in industrial development.

Multi-criteria decision-making tools are suitable for such material selection to enable objective, structured, transparent and cost effective decision making [178]. It is advised to use such tools as guidance only in an engineering context, as the choice of a decision making tool (decision making paradox) and the considered criteria may have an impact on the result [179]. Nevertheless, the benefits outweigh the drawbacks: in addition to guiding material selection, the assessment process

can build up a re-usable database when the same materials are the candidates to be used for different applications.

The material selection methods most frequently used feature the same three basic steps: (1) criteria and alternatives are established; (2) numerical measures are determined to the relative importance of the criteria and alternatives are assessed and (3) an overall ranking is calculated [180]. One of the main differences among decision-making tools is whether the weightings for the criteria can be determined as part of the process or not. Commonly used examples are 'Technique for Order of Preference by Similarity to Ideal Solution' (TOPSIS), 'ELimination Et Choix Traduisant la REalité (ELimination and Choice Expressing REality)' (ELECTRE) and 'Simple Additive Weighting Method' (SAW). These methods require weighting factors as an input, but do not offer a method to determine the weighting, or are unable to handle objective and subjective criteria at the same time [181]–[183].

In the case of a less mature and therefore only partially characterised manufacturing process, the weighting factors of different criteria cannot easily be predefined. Therefore, a systematic approach to defining the weighting factors is needed. A method that offers a way to define criteria weight as part of the process is the Analytical Hierarchy Process (AHP) and derivatives thereof [184], [185]. The AHP allows the use of qualitative and quantitative criteria in the same model. Furthermore, this method has been applied in a wide range of context. However, only limited examples on composite materials and manufacture thereof are available. While the AHP is the most suitable selection method in this instance, Adhikari and Mirshams found that it is beneficial to interrogate materials using multiple selection tools to gain confidence in the result [186]. Therefore, as a second method a variation of the AHP will be used for comparison. This less frequently used selection method in the area of material selection is the AHP extension Chain of Interactions (CoI), as a way of weighting criteria [187]. While the weighting of each criterion is reliant on experts' judgements in the AHP, the CoI method uses the number of interactions between criteria to calculate the weighting of a criterion instead. The AHP extended by CoI (AHP + CoI) could minimise the subjective influence of the decision makers, which has proven to be successful and less costly in the context of supplier selection [187].

The AHP process has been successfully applied to identify a design concept of a composite bumper beam [188], to select a fibre material for an automotive brake lever [189], to select a matrix for an automotive armrest [190] and to determine the most suitable composites manufacturing method for a bicycle crank arm [191]. In the case of the material selection for the automotive brake lever, only the four criteria weight (density), cost (raw material cost) and performance (strength and stiffness) were considered, the manufacturing process of the composite material was excluded. Often, a sensitivity analysis verified the robustness of the decision against various scenarios. The process selection by Luqman et. al took into account a wider range of criteria, such as production

characteristic, the design, cost, material and ease of maintenance [191]. While these works indicate that the use of AHP was suitable for composite materials, parts had not been manufactured to verify the selection made through AHP.

In related areas, such as Additive Manufacturing, material selection processes are also frequently used. Zaman et. al use a detailed list of criteria for both, material and machine, however the performance of a material on a particular machine is not considered [192]. In this and similar work, the material selection often depends on Ashby charts or other material property data as input to the process, assuming that the material performance is independent of the machine and manufacturing process [186], [192]–[194]. While this may be the case for manufacturing processes using isotropic, single-phased materials, this assumption does not apply to composite material manufacture. The influence of manufacturing defects on a wide range of material properties is widely recognized [195]–[198]. Defects induced by the AFP and subsequent infusion process have a significant effect on the performance of the material during the manufacturing process and therefore must be included [21], [127], [133], [199], [200]. In summary, this chapter aims to:

(1) Identify sophisticated material selection criteria for AHP based on industrial scale AFP manufacturing trials and in-depth knowledge of different dry tape materials.
(2) Apply the AHP to select a dry fibre material for ADFP based on small-scale manufacturing trials and build up a database with material and machine specific test results.
(3) Compare two different weighting methods used in AHP (weightings established through experts' judgement compared to using CoI) to address the the dependence of the approach on the criteria weighting.
(4) Identify the most suitable material for the presented case out of the available options based on qualitative and quantitative metrics, and verify the selection method through manufacturing trials of an industrially representative L-shaped part.

3.2 Materials and Methods

3.2.1 Dry Fibre Material

The variation in the constituents and manufacturing process of the dry fibre materials results in significant differences in their processability on an AFP machine. The differences originate in their dissimilar manufacturing methods. To shape the raw material into tapes, either a binder stabilized broad good is produced and slit into tapes (as Material A), referred to as slit tapes; or a raw carbon tow (or roving) is transformed into a tape form, and then stabilized with a binder (Material B-E). A further difference in dry fibre materials is caused by different binder application techniques. The

binder used in the different tapes is either epoxy or thermoplastic based and was applied using different methods, which is part of the proprietary information from the suppliers.

Table 3-1 shows the different resulting surface morphology of available materials by microscopic and high resolution scan images, exhibiting different surface characteristics due to different binder application methods [90]. Most materials have the same finish on both sides, except Material A, which has distinct features on either side of the tape. Material A has a carbon fibre veil on the top side and epoxy-based binder spots on the bottom side. Material B, C and E have binder spots evenly distributed on both sides, where B exhibits a lower density of spots than C and E. Material D has a thermoplastic fibre veil on both sides.

Table 3-1: Micrographs (a) and high-resolution scans (b) of Material A (top) to E (bottom)

Material	(a) Micrograph	(b) High-resolution scan
A	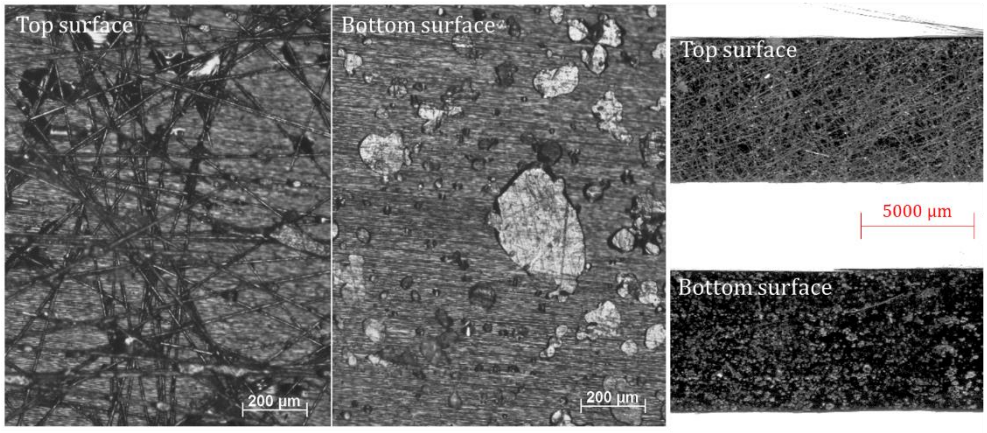	
B	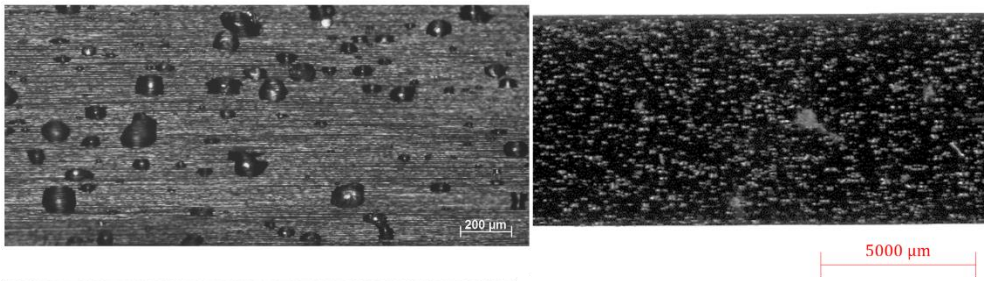	
C	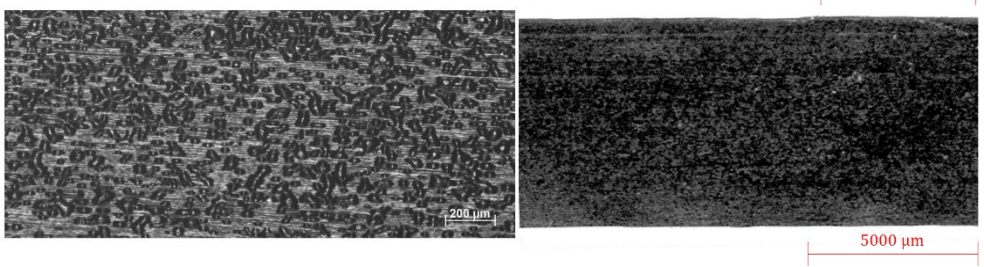	

Material	(a) Micrograph	(b) High-resolution scan
D	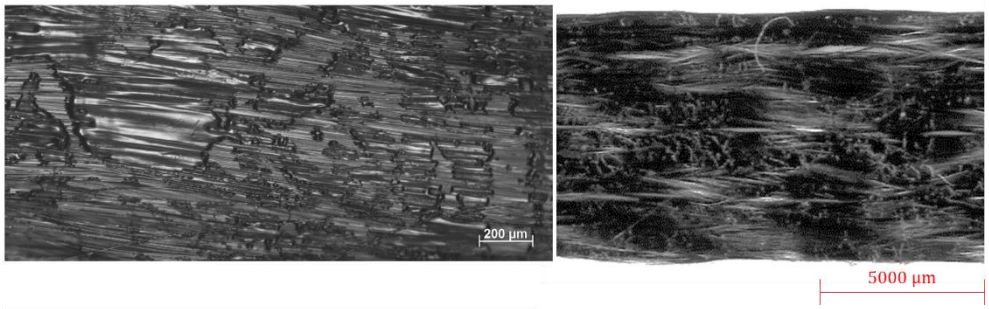	
E	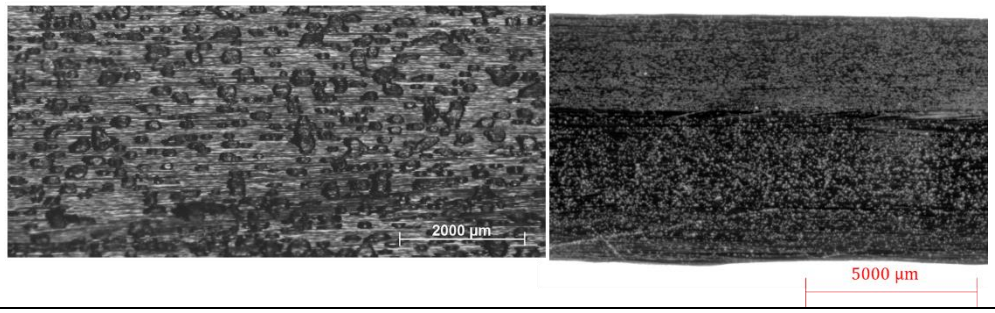	

The available materials were assessed in terms of width and compared to the nominal value (6.35 mm). Furthermore, the binder quantity was determined. For the width measurements, 80 samples (10 per bobbin) of approximately 200 mm length each were measured. These 80 samples were taken throughout trials when possible; during those trials, a length of approximately 500 m was used for each material. A high-resolution scanner (2400 dpi, 0.01 mm per pixel) and a subsequent image analysis (Matlab, US) was used to assess the width of each sample. The areal weight of the material was assessed using the same scanned images and the weight measurement from a high precision scale (XSE105, Mettler Toledo, US). All 80 samples per material were used to calculate the average areal weight and were considered representative for this material batch. The binder quantity (wt. %) was investigated using thermogravimetric analysis following ASTM E1131 on one sample per bobbin (eight samples per material). The weight of the binder can then be subtracted from the measured sample areal weight [90].

3.2.2 Automated Dry Fibre Placement

In order to assess the characteristics of different dry tape materials and their processability on an AFP machine, a series of deposition tests were carried out. These tests investigated the quantitative and some qualitative sub-criteria required as input to the AHP.

The process parameters were established within a day of trial and error and visual assessment, where possible in collaboration with the respective material supplier. The deposition speed, compaction pressure and machine hardware were kept constant. The use of a single deposition speed eliminates the need to establish a function to control laser power and deposition speed, only one laser power is

required [54]. The chosen temperature for deposition delivered a preform V_f within 95% of the maximum achievable V_f achievable on the used system. A high preform V_f was considered favourable over lower values to mitigate potential defect generation during consolidation similar to prepreg material processing (see Figure 3-1). While this was a quick way of determining the processing parameters, the drawback to this approach is that the ideal conditions may not have been used for deposition.

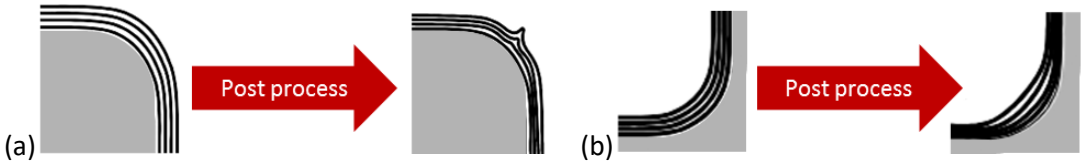

Figure 3-1: Schematic wrinkle on a convex corner (a), schematic bridging on concave corner (b) [201]

The AFP system used for this work is supplied by Coriolis Composites Technologies S.A.S (Queven, France) and equipped with a bespoke laser-heating system (Laserline, Mülheim-Kärlich, Germany) see Figure 3-2. The machine deposits eight 6.35 mm wide tapes. The bobbins of dry fibre material were mounted in an environment-controlled creel and guided through individual channels to the deposition end effector. At the outlet of the deposition end effector, the material was heated by a 3 kW diode laser with a wavelength of 1025 ± 10 nm, which was collated into a rectangular beam in the laser homogeniser optics. The laser operates in a different spectrum from the diode laser (λ = 0.9 - 1.0 µm). Therefore, the risk of the laser beam reflection in the nip-point region affecting the measurements was minimised. The laser beam size in this instance had a focal point of 8 x 57 mm to activate the binder. The laser optics were positioned to deliver the rectangular laser beam 50% at the roller and 50 % at the substrate for this laser beam size. The tilt of the deposition end effector was set at a constant value of Θ = - 7° normal to the surface throughout the entire work. The processing temperature was measured at visible the nip-point, where the incoming material meets the substrate (see Figure 3-2 (c)) and Figure 3-3. The materials were deposited at a constant speed of 400 mm/s. The flexible roller (Silicone, Shore 40A hardness, 60 mm wide, Ø = 70 mm) applies a compaction force of 446 ± 23 N (2 SD), to promote adhesion of the incoming tapes to the substrate.

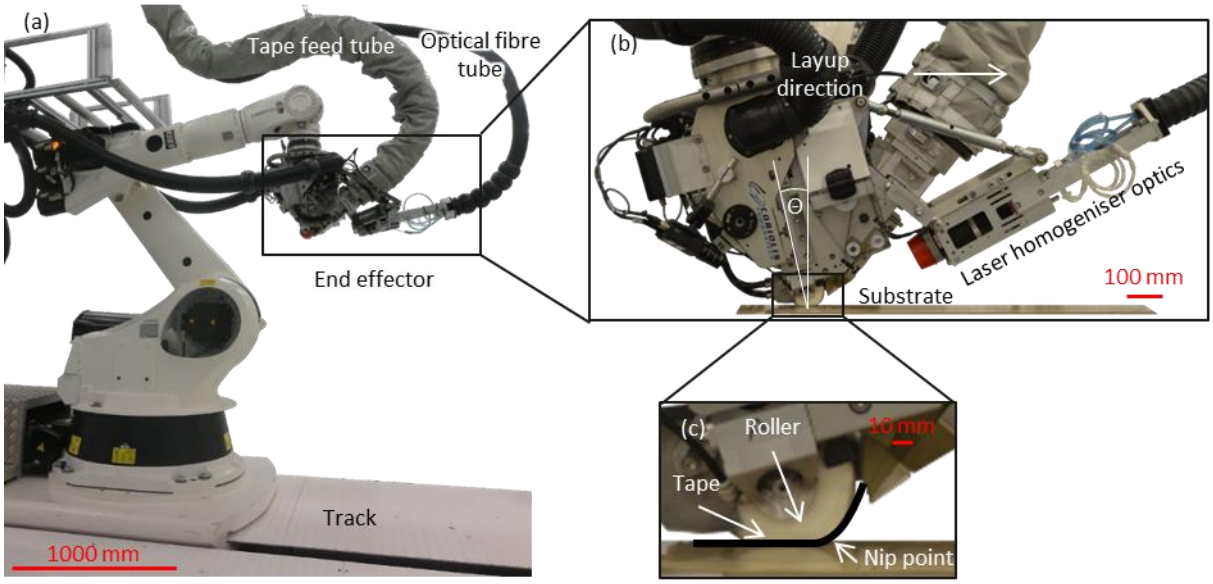

Figure 3-2: AFP machine at the National Composites Centre, UK (a), details of the deposition end effector (b) and roller and nip-point of the deposition end effector (c)

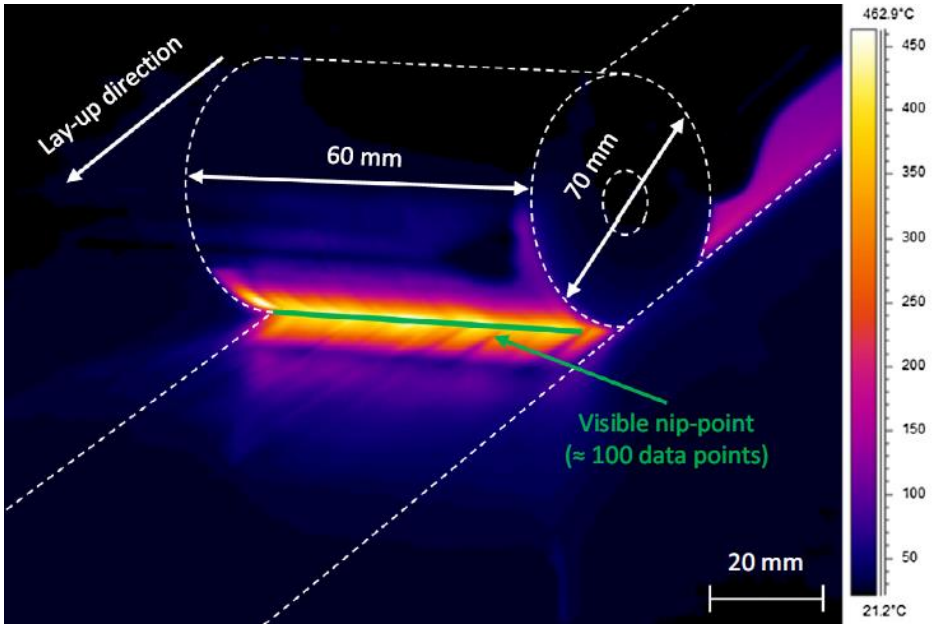

Figure 3-3: Thermal camera view of the visible nip-point during material deposition [54]

The LWIR camera had a resolution of 320 x 240 pixels (≈ 0.5 mm/pixel). It is calibrated in the 0 to 700 °C range to within ± 2 °C or ± 2%, whichever is greater; all recordings were made at 30 Hz. The LWIR camera was mounted on the deposition head, to the side of the laser optical unit. Using the software provided by the camera manufacturer (ThermaCAM Researcher Pro 2.10), the images were recorded (refer to Figure 3-3). Using a line tool provides the temperature in close vicinity of the nip-point on the substrate. Only the visible nip-point can be measured, as a LWIR camera cannot capture the process nip-point temperature, see **Error! Reference source not found.**. Due to this geometric constraint, the temperature is decreasing while passing the shaded zone and the temperature under

pressure is lower than the visible nip-point temperature. The shaded zone length is dependent on the exact configuration but was measured to be approximately 2 mm long in the described configuration [202].

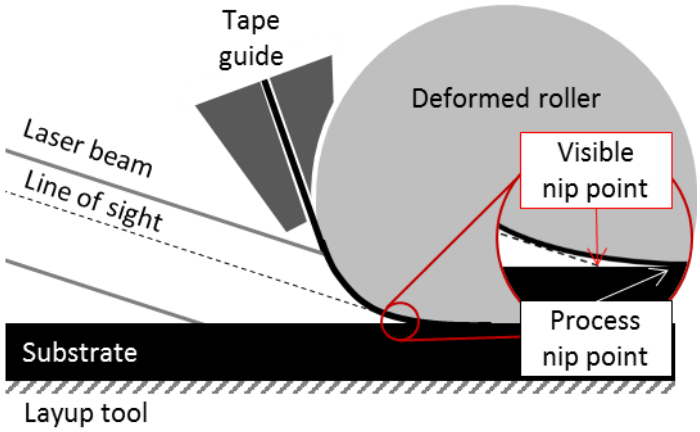

Figure 3-4: Explanatory sketch for visible and process nip point (not to scale)

The approximately 100 data-points located along this straight line set to be parallel to the roller axis (i.e. perpendicular to the travel direction) were averaged, sampled from at least 15 frames, excluding the feeding and cutting operation at the beginning and end of deposition of a course. In order to obtain accurate temperature measurements, the LWIR camera requires the distance from the target, the ambient temperature, the relative humidity and the material emissivity to be known, which were consistently 0.3 m, 20 °C and 40 % respectively. The apparent emissivity of the materials in the relevant temperature range was experimentally determined in accordance to ASTM E 1933. The angle of the LWIR camera was placed in the same distance and tilt as on the machine (20° to the surface). As prescribed by the standard, the temperature measured by the LWIR camera was corrected by the reading of thermocouples placed in intimate contact with the material surface. As the emissivity is a function of temperature, the apparent emissivity ε was specified for all materials within a range spanning 60 °C, shown in Table 3-2. in **Error! Reference source not found.**

Table 3-2: Apparent emissivity as determined for all materials used

Material ID	Temperature range, °C	Apparent emissivity, ε	2 SD
A	170 – 230	0.81	±0.01
B	165 – 225	0.71	±0.01
C	170 – 230	0.65	±0.06
D	180 – 240	0.79	±0.03
E	280 – 340	0.70	±0.09

Heat radiation from the incoming tapes may be reflected by the substrate. Therefore, the radiation detected by the camera at the visible nip-point may be a combination of radiation from the substrate

and the incoming tapes and the apparent emissivity would be higher than experimentally determined on flat laminates. The impact of radiation on emissivity was not quantified as part of this work; it was part of the experimental uncertainty. Monnot *et al.* have demonstrated that if the roller is part of the test set up, the shadow it casts is increasing the emissivity to 0.85 for Material D [203]. This difference of 0.06 is equivalent to ~12°C increase in the temperature reading, showing the sensitivity of the resulting temperature measurement to changes in emissivity.

The as-supplied material samples for the previously described material tests were taken after it passed the tape feeding system of the machine to capture possible distortions caused by the feeding process (e.g. contact with rollers and guiding elements). A flat preform with a stacking sequence of $[0/90]_{ns}$ was manufactured with each material using the same machine program defining the fibre paths and identical processing parameters apart from deposition temperature, as discussed. The number of plies was flexibly chosen to fill the 3 mm deep cavity of the mould used for the subsequent infusion, which led to a laminate V_f as close to 55 % as possible. The preforms were infused with an epoxy resin in a closed mould (500 x 500 x 3 mm). The epoxy resin used was Epikote RM135/H137 (Hexcel Corporation, US) and the preform was infused under vacuum pressure only keeping the tool temperature at 30 °C [90].

3.2.3 Preform Assessment Methods

An important quality metric for material and processing using prepreg is the evaluation of resin and void content of the laminate [138], [204]–[206], this also extends to AFP processing [58], [207], [208]. However, while void content is a useful quality metric for the raw material as well as the assessment of as-laid thermoplastic or thermoset prepreg, the quality metric does not apply to dry fibre preforms. Using the same assessment methods for the dry fibre materials would require testing and analysing the material after the infusion stage, which does not allow tracing the impact of the deposition process directly, as it will always be an interaction between deposition, infusion and cure. Laminate-based assessment is not a quality indicator that can be used during the manufacturing process to verify the preform is of a quality that is suitable for the post-processing step.

The use of a preform thickness measurement gives a direct indicative measure of preform quality. The measurement system must be non-destructive to further process it and without contact due to the textile character of the dry fibre preform. An advantage of non-contact measurement system is that it is not dependent on the preform geometry. A disadvantage is the dependency on averaged or nominal values such as the areal weight or the fibre density. The fibre volume fraction V_f of a measured preform can be calculated using Equation 3-1:

$$preform\ V_{\mathrm{f}} = \frac{W_{\mathrm{ply}} \cdot n}{\rho_{\mathrm{fibre}} \cdot t_{\mathrm{preform}}} \qquad \textit{Equation 3-1}$$

using the areal weight W of a single ply, the number of plies n, the nominal fibre density ρ and the measured preform thickness t. The measurement method chosen was an articulated arm with an integrated laser line scanner (ModelMaker MMDx 100 digital laser scanner and MCAx35+ Manual Coordinate measuring Arm, Nikon, Japan). The measured point cloud was cropped to only evaluate the central area of the preform in a metrology software (PolyWorks® IMInspect™, InnovMetric, Canada), the average distance of the individual measurement points determines the preform thickness against the tool. The measurement was taken immediately after the deposition was completed. Converting the thickness into preform V_f provided a comparable metric.

3.2.4 Analytical Hierarchy Process

The first step in the AHP is the determination of criteria. In addition to the author, staff at the National Composites Centre considered experts in fields closely related to ADFP were consulted to list relevant criteria and sub-criteria (a total of six experts were asked). The identified criteria were procurement, manufacturing processes and the assessment of the resulting laminate. The sub-criteria break down each criterion into assessable components, and their definitions are shown in Table 3-3.

Table 3-3: Criteria and sub-criteria used in the AHP (Notes: if no unit is given, the criterion was assessed qualitatively by pairwise comparison; uniformity was considered a positive feature)

Criteria	Sub-criteria	Assessment	Impact
Procurement	Lead time, weeks	Number of weeks between order and arrival on site.	Can be a critical factor for completing a project on time and budget.
	Risk	Likelihood of receiving false information from the supplier (e.g. wrong lead-time, wrong technical information) and the risk of a supplier terminating production.	
	Customer service	Answering questions about procurement satisfactorily (e.g. prompt response to inquiries and its validity, etc.).	
	Technical support	Answering questions about manufacturing satisfactorily (e.g. recommendation of processing parameters).	
	Material cost, £/kg	Obtained through quotes from the suppliers.	Can be prohibitive to the usage of a material.

Criteria	Sub-criteria	Assessment	Impact
	Procurement conditions	Restrictions on material usage (e.g. use of specific resins or any other formal constraints).	Relevant for the R&D environment in which a project was completed.
Raw material characteristics	Width deviation, mm	2 SD of the tape width, indicating its consistency.	Random width deviation may cause unintended gaps and overlaps in the preform [128], [209].
	Width compliance, mm	Width deviation from nominal width (in this case 6.35 mm), indicating compliance to product specification [90], [206].	Material consistently too wide or too narrow for the machine may cause distortion of the tapes or gaps.
	Material complexity	Number of constituents within the material (reflecting the material and production costs)	Taken as a proxy of the potential for raw material cost to decrease in the future.
	Binder quantity deviation, wt. %	No binder quantity target is available, only the consistency of the binder application is used (2 SD of binder quantity) [90].	May cause local inconsistencies in the preform quality and affect the infusion behaviour.
AFP deposition process	Defect occurrence, $^{count}/_{100m}$	The number of defects (defined in Table 2-4) per 100 meters counted by visual inspection without accounting for severity.	Defects have a negative effect on ultimate strength of the laminate (up to 13% difference to material without defects) [21].
	Preform V_f, %	Calculated using nominal fibre density, nominal areal weight, number of plies and measured preform thickness.	A high preform V_f is a positive indicator for high V_f in the part. A preform V_f should be between 50 – 55% [90].
	Areal weight, g/m^2	Measured by weighing a known length of material on a scale [90].	A high fibre areal weight is a positive indicator for high deposition rate.
	Steering capability	Visual assessment of the equality of the steered tapes by trained technician.	Indicates the suitability of the material for deposition of complex structures [145].
	Preform integrity	Preform integrity is the perceived stiffness and coherence assessed by the technician handling the preform.	A stiff preform is a positive indicator for ease of handling.
Infusion process	Infusion time, min	Measured between opening the resin valve and the completion of infusion when resin appears at the outlet.	A faster fill of the preform indicates a higher production rate.

Criteria	Sub-criteria	Assessment	Impact
	Bulk factor (BF) of preform	Ratio of the measured preform thickness to the measured thickness of the consolidated laminate.	A low bulk factor is a positive indicator to avoid wrinkles when closing the tool in complex geometries [131], [201], [210]. Common values are 1.1 to 1.5 for prepreg materials [211].
Laminate characteristics	Void content, %	Percentage of air trapped in the laminate measured using microscopy, three cut samples, and ten images per cross section.	A low void content is a positive indicator for a high-quality laminate [212]–[214].
	Laminate V_f, %	Calculated based on nominal fibre density, nominal areal weight, number of plies and measured total thickness.	A high laminate V_f is a positive indicator for a high-quality laminate [215]. The target value is 55%.
	Geometrical tolerance, mm	Deviation of the thickness against the nominal tool cavity of 3 mm.	Predictability of the outcome of the process is considered positive.
	Ply areal weight, g/m^2	Measured by weighing a known length of material on a scale [90].	Thinner plies are considered positive for high mechanical performance of the laminate [216].

All materials were assessed with the methods outlined in Table 3-3 and detailed in section 3.2.1 and 3.2.3 as quantitative assessment where possible. Qualitative assessments were made using pairwise comparison, where two criteria at a time are compared to judge which of each entity is preferred. Not all materials were assessed through to the end of the process, materials were excluded from further experimental work, if

i. The preform manufacturing has > 200 defined (refer to Table 2-4) and observable defects per 100 m and/or
ii. The preform was not fully infused whereby the flow front is stagnant for 20 min.

The second step was to determine the relative importance of the different criteria as a set of normalised weights, U_i. The same principle was applied to the sub-criteria yielding the weights $u_{i,j}$. The scores for all the sub-criteria $c_{i,j}$ were determined and then combined using

$$C = \sum_{i,j} U_i u_{i,j} c_{i,j} \qquad \textit{Equation 3-2}$$

where C is the overall and comparable score. The concept of the hierarchy is shown in Figure 3-5.

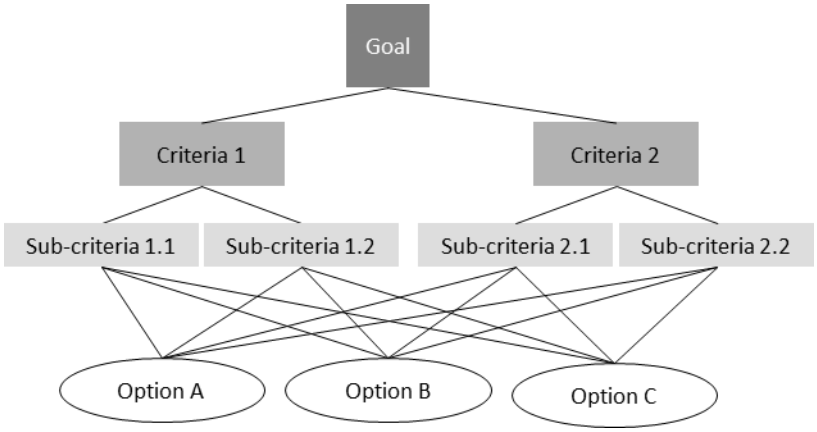

Figure 3-5: Simplified structure of the hierarchy used in the AHP, adapted from [187]

Two different approaches to determine the relative importance of the criteria weights were used in this work. In the first approach, the established AHP, the criteria weights U_i and $u_{i,j}$ were determined by pairwise comparison. Two criteria were compared at a time using a scale of 1-9, followed by a consistency check[3] [184], [185]. Weightings were derived from experience and therefore potentially incomplete knowledge. In this case, all experts gathered most of their knowledge and experience in related fields as the ADFP technology is still immature. If the consistency check failed, it indicated that the experts were unable to agree, and the respective options were given equal weighting. The experts were asked to base their decisions on a specific application; a small-scale but representative thin L-shaped section described in section 3.2.5.

A second approach to determine the weighting of the criteria is CoI, which was initially developed to cut the cost of gathering the expert's judgement. CoI reduces the reliance on subjective estimates and perceptions [187]. This method gives a higher weight to a criterion dependent on the number of other criteria with which it interacts (i.e. a direct relationship: influence each other or are dependent on each other). This approach simplifies the nine-step scale in a pairwise comparison to a binary condition describing if two criteria interact (1-state) or were independent (0-state). The sum of the total interactions of a criterion were normalised and used as $u_{i,j}$. The concept is shown in Figure 3-6.

[3] "The procedure requires calculating the "inconsistency index", that is, the difference between the largest eigenvalue and the number of elements of the matrix, divided by the number of elements minus one. The largest eigenvalue of a matrix of perfectly consistent comparisons equals the number of elements. The higher the eigenvalue is, compared to the number of elements, the more inconsistent the pairwise comparisons are. By dividing the inconsistency index by a similar index based on randomly chosen pairwise comparisons, the "inconsistency ratio" is obtained: Saaty suggests that acceptable values for this ratio should not exceed 0.1." [33, pg. 119]

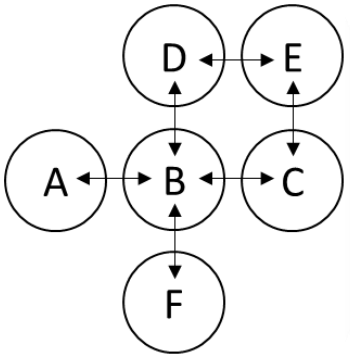

	A	B	C	D	E	F
A	-	1	0	0	0	0
B	1	-	1	1	0	1
C	0	1	-	1	1	0
D	0	1	0	-	1	0
E	0	0	1	1	-	0
F	0	1	0	0	0	-
Total	1	4	2	2	2	1

	Factors
A	1/12 = 0.08
B	4/12 = 0.3
C	2/12 = 0.17
D	2/12 = 0.17
E	2/12 = 0.17
F	1/12 = 0.08
Total	12/12 = 1

Figure 3-6: Exemplary process of CoI (left to right): diagrammatic representation of CoI; CoI responses for the given example; resulting elative weightings of criteria (factors), adapted from [187]

The CoI approach resulted in weighting a criterion based on interactions with other the criteria listed, while the experts may consider wider ranging implications when assigning a ranking on a numerical scale. A direct comparison of the approaches highlighted the differences in material selection outcome due to the method rather than due to the actual material suitability.

3.2.5 Manufacturing of L-shaped Laminate Component

In order to make the proposed material selection an industrially viable process, the selected materials were applied to a part that had a higher complexity than the individual material characterisation tests conducted in the sub-criteria assessment stage. The part was a small-scale representative of geometries common in the aerospace industry, which was a symmetrical L-shaped geometry with 600 mm length and 225 mm flange height, with a 10 mm inner corner radius (see Figure 3-7). The panels had 26 plies and were as close to quasi-isotropic as possible while achieving a thickness of 5 mm. The laminate design was as close to being balanced and symmetrical as possible within the constraints of the required ply number; the stacking sequence was $[(45, -45, 0, 90)_s, 0, (45, -45, 0, 90)]_s$. Panels with this stacking sequence will be referred to as quasi-isotropic (QI) preforms or laminates for simplicity in the remainder of the document. The deposition speed was limited by the complex machine kinematics and was as low as 5 mm/s in the corner region and up to 200 mm/s in the flange region. Due to the variable deposition speed, the laser power was adjusted accordingly. The relationship between deposition speed and required power to achieve a constant temperature was derived using the process proposed by Di Francesco *et al.* [54]. The resin used was RTM6, and the preforms were infused at supplier recommended set-up and parameters [217], [218].

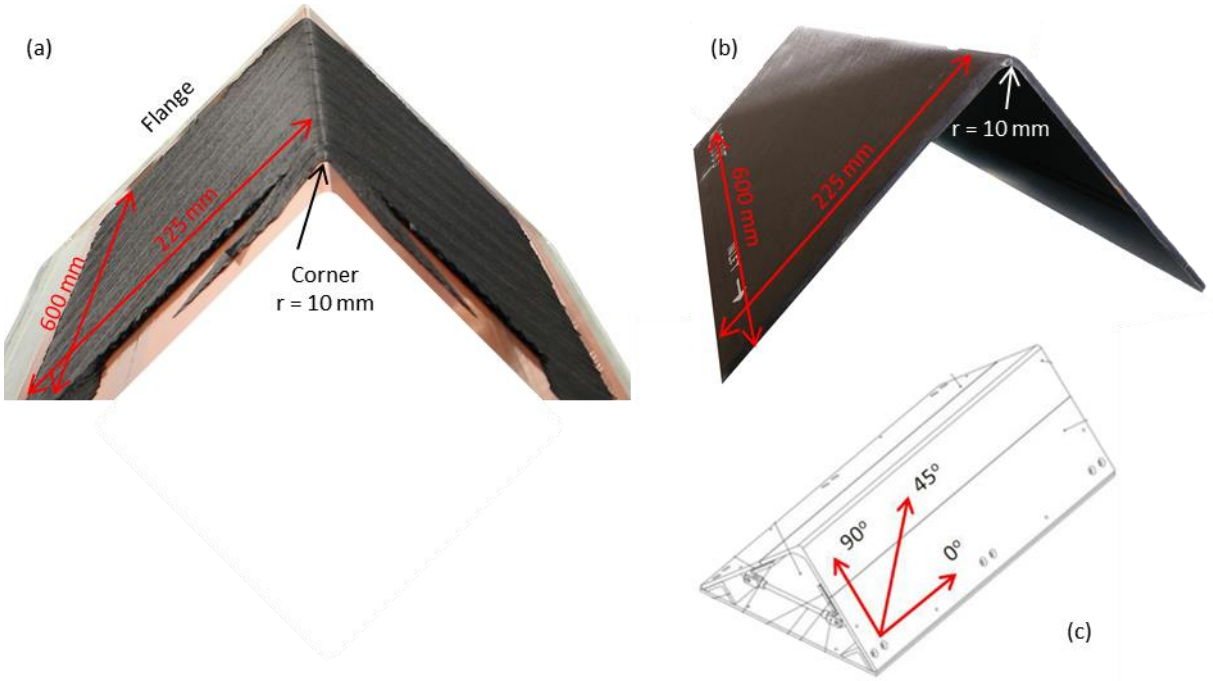

Figure 3-7: Dimensions of L-shaped panels used to support the material choice as preform (a) and infused laminate (b); whereby (c) indicates the ply directions

The quality of the L-shaped laminates was assessed against key quality factors: preform and laminate V_f as well as the resulting bulk factor, in addition to void content. A portable ultrasonic C-scanner (Olympus Omniscan MX2 with a 5MHz 64 El Array) was used to check imperfections and voids within the laminates [219]. The part thickness was converted into preform or laminate V_f based on nominal areal weight, fibre density and number of plies. To capture any influence of the increase in geometry, two distinct areas of an L-shaped geometry (flanges and the corner) were assessed and compared. The dimensions of the measurement area and the definition of the apex measurement area is shown in Figure 3-8.

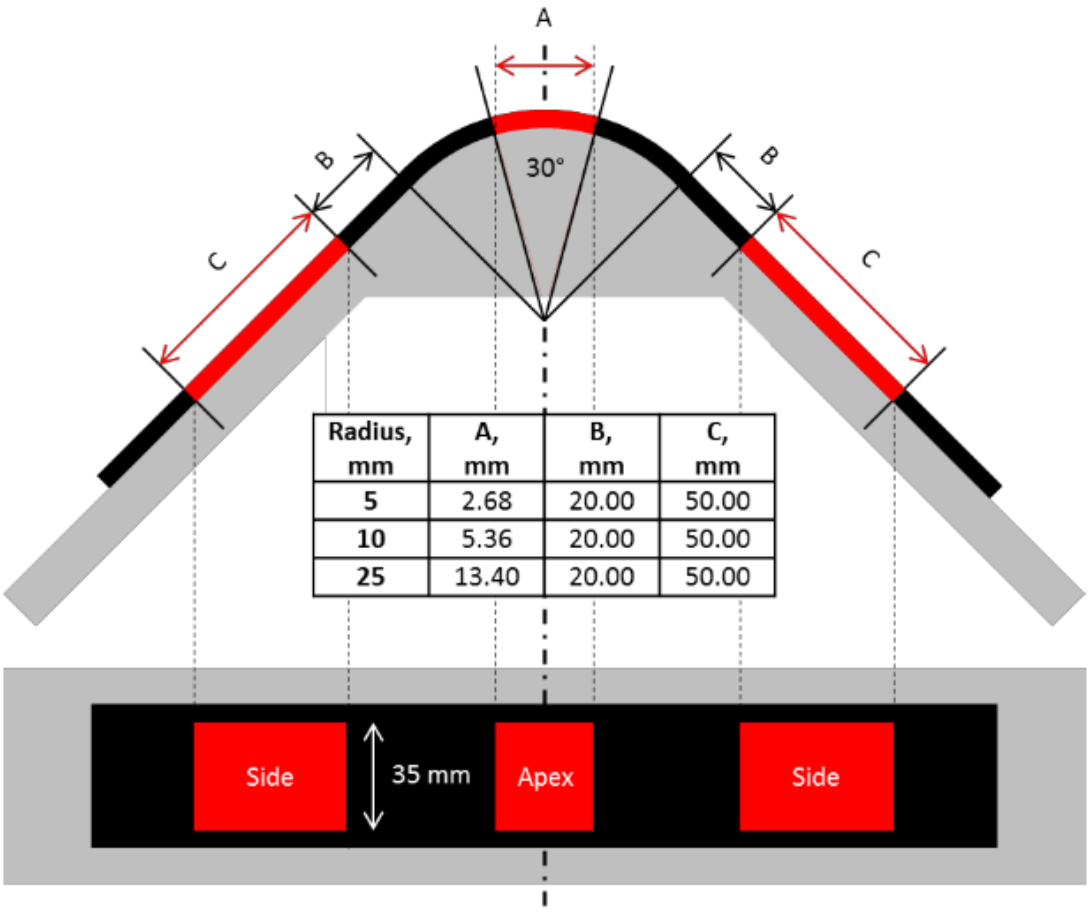

Figure 3-8: Thickness measurement locations, defined by [202]

3.3 Results and Discussion

3.3.1 Material and Manufacturing Process Assessment

A summary of the results of the various quantitative tests of Material A to E are shown in Table 3-4. The bold values are the highest scoring values of the criterion, showing that each material had at least one criterion that scores highest.

Table 3-4: Results of all quantitative material test results (bold: best value achieved)

Sub-criteria name	**Unit**	**Results**				
		A	B	C	D	E
Lead time	weeks	52	**3**	**3**	**3**	**3**
Material cost	£/kg	223	**80**	**80**	114	100
2 SD of width	mm	**0.2**	0.8	0.6	0.4	0.4
Deviation from nominal width	mm	0.2	0.4	**0.0**	0.5	0.3
Material complexity	n/a	8	**4**	**4**	5	**4**
2 SD of binder quantity	wt. %	**0.79**	1.73	2.05	1.15	2.0*
Defect occurrence	$^{count}/_{100m}$	24	195	244	84	**19**
Preform V_f	%	54.2	**55.8**	-***	43.9	33.8
Measured ply areal weight	g/m^2	211	128	139	203	268

Sub-criteria name	Unit	Results				
		A	B	C	D	E
Infusion time	hours	**1**	-**	-***	2.5	2
Bulk factor		**1.0**	**1.0**	-***	1.2	1.6
Void content	%	1.7	-**	-***	**0.5**	0.8
Laminate V_f	%	**50.2**	-**	-***	43.8	47.5
Ply areal weight	g/m^2	211	-**	-***	**203**	268
Geometrical tolerance	mm	**0.0**	**0.0**	-***	0.2	0.1

*data provided by supplier
**did not fully infuse
***fault count higher than permitted

Tape material manufactured by a slitting process had the lowest variability in width, but at the same time creates edges that might exhibit loose fibres, leading to an increase in fibre residue on the substrate.

A trained operator inspected each ply of the 3 mm thick $[0/90]_{ns}$ preform during the deposition trials. A defect library was generated and seven different types of the 24 previously identified defects were observed during the trials. These defects were logged (see Table 3-5); an additional defect (loose fibres on surface) was identified.

Table 3-5: List of different defect types observed during AFP deposition

Observed defects types	*Sketch*	*Example*
1. Binder accumulation		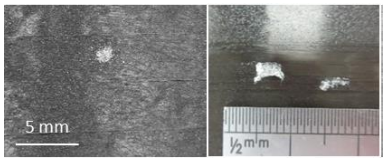
2. Foreign material inclusion	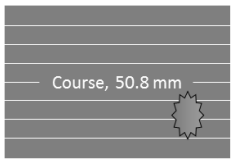	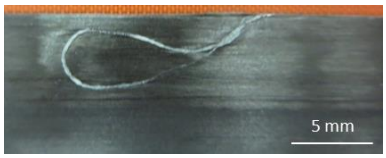
3. Loose fibres on surface		
4. Tape folding		

Observed defects types	*Sketch*	*Example*
5. Tape overlap	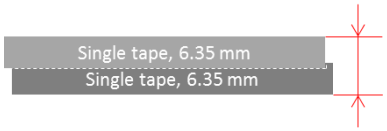	
6. Tape shearing		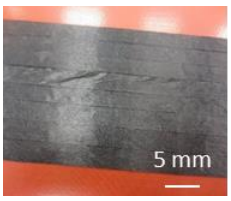
7. Twisted tape		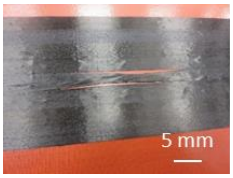
8. Unintended Gap (>2 mm)		

The two materials with the lowest areal weight (B and C) showed a very high fault count, as the thin tapes were not as rigid as the other materials and hence prone to twisting or folding. For these thinner materials, a high count of twists and folds (Table 3-5; defect type 4 and 7) were induced by contact with guiding elements such as the inner ducts in the tape feed tubes, refer to Figure 3-2 (a), as they shifted due to the robotic motions during the deposition. The distribution of the defects across the materials tested can be seen in Figure 3-9. Material A had the highest count of loose fibres on the surface, likely due to its manufacturing process including a slitting process of a broad good that promoted fraying edges.

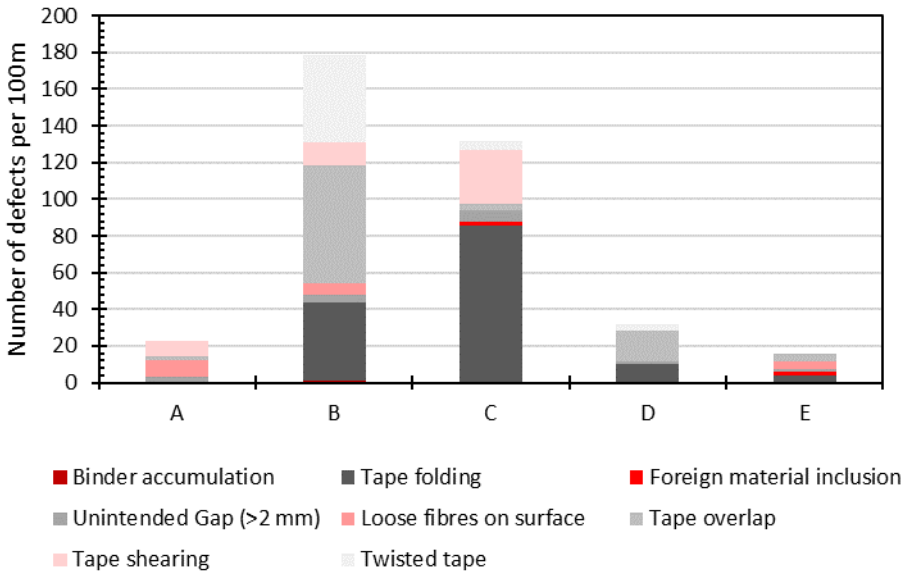

Figure 3-9: Distribution of eight identified defect types per material

Material B was the only material not to infuse fully during the vacuum infusion. It was visible from the micrographs that the binder quantity on its surface was lower than all other materials, while the overall binder quantity by weight was close to the quantity in other materials. This indicates that the binder was present within the material rather than on the surface, which could be the reason for its low bulk factor as well as a low permeability. Rimmel et al. have already reported an influence of binder distribution on permeability (in this instance binder content and binder particle size), whereby the latter has greater influence [51]. The material that infused the preform fastest was Material A, which has the distinctive feature of a carbon fibre veil. It can be inferred that the veil acted as a highly permeable resin distribution layer between the plies and provides additional flow channels.

3.3.2 Analytical Hierarchy Process Results

Two different methods were used to determine the weighting of the criteria and compared, as shown in Figure 3-10 and Figure 3-11.

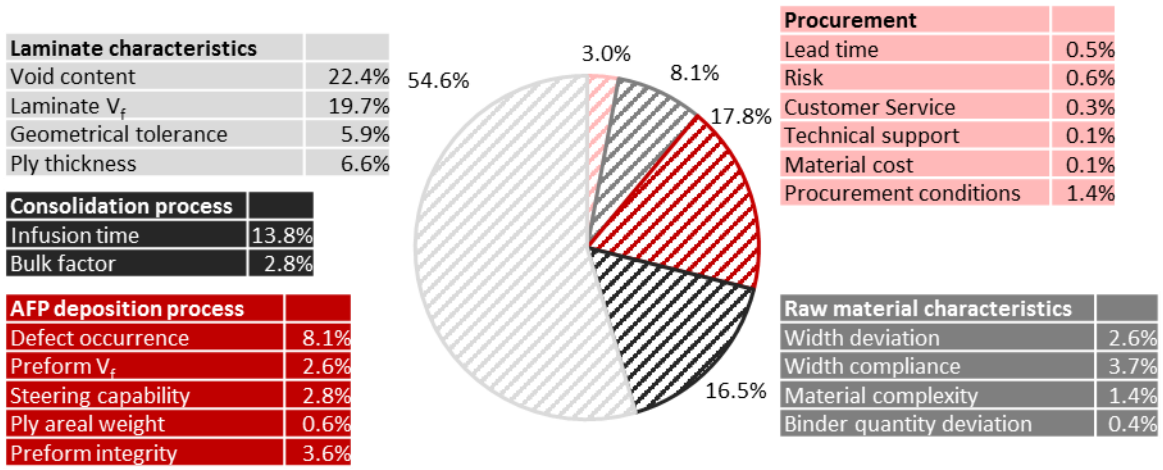

Figure 3-10: Weightings determined by the established AHP based on the experts' judgement

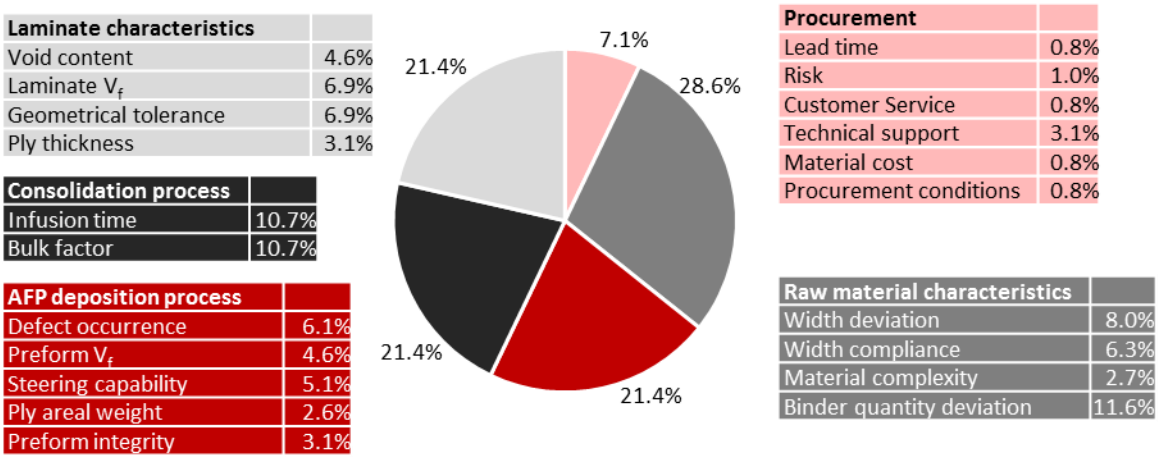

Figure 3-11: Weightings determined by AHP in conjunction with CoI

As shown in Figure 3-10 the experts' judgement indicates the highest priority for the laminate characteristics, and therefore a lower importance to the remaining criteria. Experts were more focused on laminate quality of the manufactured part rather than the manufacturing aspects. The part quality is a metric often used in the aerospace industry when buying or selling parts, something that is known by the experts. Commonly, materials are selected based on their laminate characteristics only as it is assumed any manufacturing challenges are eliminated prior to start production. This, however, may not be the case in this instance of a novel material, which is in the product development phase. The AHP + CoI, as shown in Figure 3-11, shows overall more balanced weighting factors, disregarding external factors such as industrial influence, but only capable of taking the defined criteria into account.

The experts chosen and the way the experts were briefed prior to providing their opinion may have had a significant impact on the results. It is important to interrogate experts from a variety of fields relevant to the selection. This is strength and weakness of the established AHP at the same time, the

experts were able to tailor the results to the specific case queried and therefore make the result more relevant to the case considered, but is relying on the surrounding factors that were intangible and cannot be captured within the framework. In order to mitigate this, a large pool of people may need to be asked for their opinion. The result of the CoI on the other hand is less dependent on such external factors, but at the same time may neglect relevant industrial influences and the choice of criteria had a more significant impact. The selection of the method used becomes engineering judgement, leading to a decision-making paradox.

The results of two different weighting methods for each material are shown in Figure 3-12, which were obtained by the material assessment results (shown in Table 3-4) multiplied with their respective weightings (Figure 3-10 and Figure 3-11) and summarised as described in section 3.2.1 using Equation 3-2.

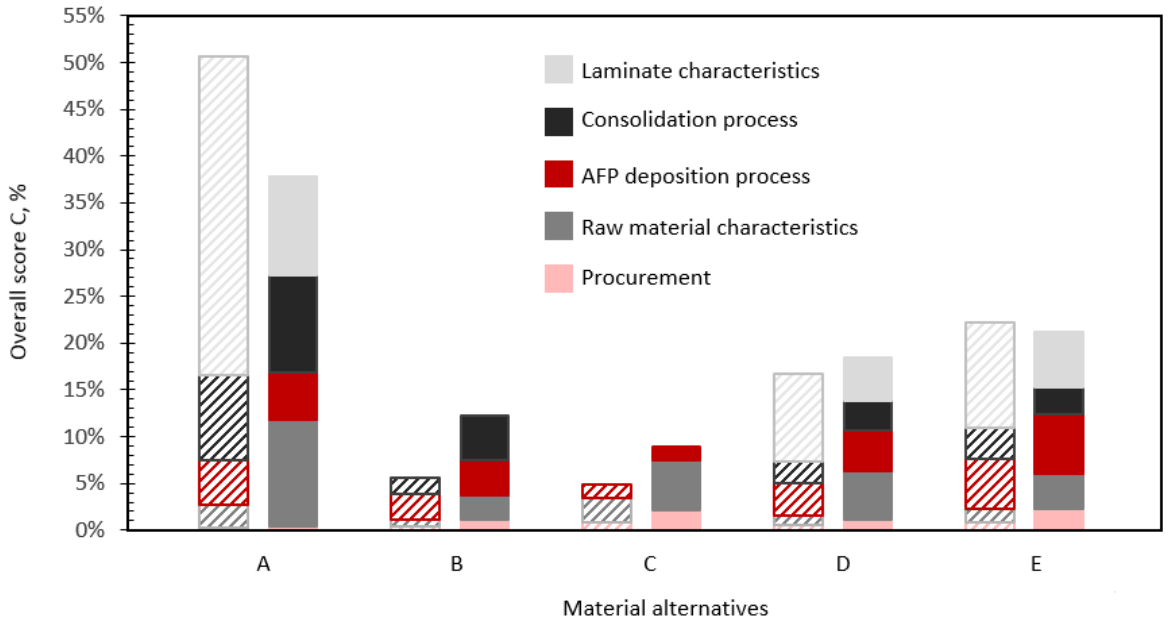

Figure 3-12: Result of the AHP using different weighting methods for materials A to E; shaded: established AHP, solid: AHP with CoI

Material A was ranked clearly favourable by both methods. Material D and E show similar results; a decision between D and E should not be made with confidence due to their close results. Materials B and C were only partially tested, as Material B did not fully infuse and material C exhibited a high defect count; therefore, these materials received the lowest scores. Both methods overall recommend the same material. The manufacturing process had a higher priority within the AHP + CoI method and was well suited to objectively assess a material for manufacturability, while the experts give a higher weight to the laminate and take into account the wider industrial impact. A hybrid method could be

explored in the future where main criteria could be assessed by experts to capture the industry needs and the more tangible sub-criteria could be assessed using CoI to provide impartial weighting of the aspects within a criterion. This would keep the effort associated with the opinion gathering at a minimum but enable the capture of a wider industrial focus.

3.3.3 Demonstration of Material Selection in Laminate Manufacture

Material characterisation data used in the material selection processes was gathered through manufacturing tests of flat panels. In order to demonstrate the applicability of the material selection processes as well as their suitability for predicting the manufacturing quality of non-flat component, two L-shaped laminates were manufactured using Material A (highest priority) and Material D (low priority) and their manufacturing quality was assessed. The quality difference between the corner and flanges on the L-shaped parts was of particular interest to check the influence of increased geometrical complexity on the material selection. The key criteria assessed and their results for the two L-shaped laminates are shown in Table 3-6.

Table 3-6: Three selected criteria for comparison of two L-shaped parts and their results (error indicates 2 SD)

	Material A	**Material D**
Sound loss in C-scan	3-6db	3-6db
Average preform V_f		
Corner	56.4±1.7%	58.5±1.7%
Flange	50.2±0.8%	46.2±2.3%
Difference	6.2%	12.3%
Average laminate V_f		
Corner	56.7±0.8%	58.5±0.6%
Flange	57.2±0.8%	53.4±2.0%
Difference	0.5%	5.1%
Bulk factor		
Corner	1.0	1.0
Flange	1.1	1.2
Difference	0.1	0.2

Figure 3-13 (a) shows the top view of the L-shaped preform and the areas used for thickness measurements to calculate the V_f before and after resin infusion and cure. Figure 3-13 (b) shows an exemplary result of the C-scan of the flat flange area where red indicates a very low loss of the back wall echo and therefore signifies a low void content. The green areas show a slightly higher loss of the echo, indicating the potential presence of voids; however, this loss was below the allowable limit of 12 dB for a laminate with less than 5 mm thickness [220]. Both materials showed a void content within the acceptable limits.

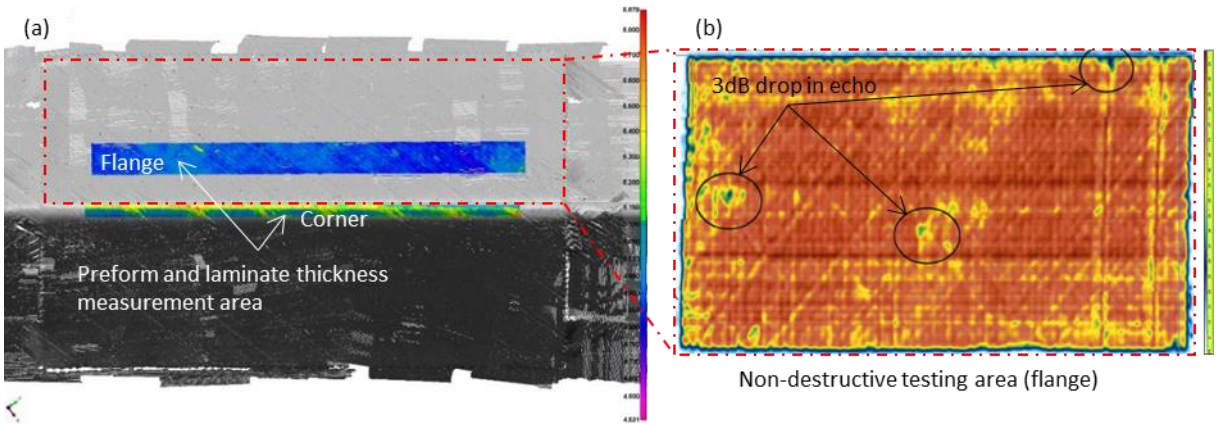

Figure 3-13: Exemplary measurement results for Material D laser line scan with height colour plot (a); ultrasonic scan of flange (b)

In the laminates manufactured with Material A and D, the bulk factor on the corner was lower than that on the flanges, indicating a higher compaction of the material on the corner. The bulk factors of the flat areas were close to the target (1.1), with a lower bulk factor for Material A which indicated higher laminate quality in comparison to Material D. These results were consistent with the flat preform trials.

Material A resulted in a higher average laminate V_f overall, with both corner and flange regions having a laminate V_f above the target of 55%. The difference between corner and flanges was minimal, which was considered a positive indicator for high consistency and quality. Material D resulted in a lower laminate V_f below the target laminate V_f and a higher difference between the corner and the flanges, both indicators for lower laminate quality.

Overall, the higher quality laminate was manufactured with Material A, which was consistent with the recommendations by the AHP. The detailed comparison between the flat area and the corner area suggests that Material D results in a more variable laminate induced by geometrical complexity, which was not specifically captured by the small-scale material characterisation tests. In order to account for this, the material selection process could be expanded by assessing the material behaviour under different process conditions, which vary depending on the geometry of the component, i.e. high deposition pressure or low deposition speed, which would give a higher confidence in the material selection at the penalty of a more extensive test campaign. Despite such a limitation, it was found that the selected criteria were sufficient to suggest the best candidate materials for achieving high manufacturing quality.

3.4 Conclusion

A knowledge-based material selection process of dry fibre materials for the use in ADFP was proposed based on the Analytical Hierarchy Process. Most of material selection methods for metals, plastics and

sometimes well-characterised composite materials are based on the material properties readily available from literatures or suppliers' catalogues. However, most of the dry fibre tape materials used in the AFP process were relatively new and had not been well characterised. Additionally, the processability of the dry fibre tapes in the ADFP process should be taken into account in the material selection process, which is critical to the final production quality.

Selection criteria were established for commercially available dry fibre materials, the production process and the manufacturing quality by industry experts. Five major criteria (procurement, raw material, AFP deposition process, infusion process, laminate characteristics) and 22 sub-criteria defining these criteria were outlined. Five different materials available on the market at the time were compared against these criteria. To assess the materials against these criteria, an experimental programme based on small scale testing was devised. A combination of measurements in manufacturing trials and pairwise comparisons was used to generate the material specific scores for each criterion used in the AHP, resulting in a re-usable database.

Two different criteria weighting methods were compared; the established AHP that has been used in similar contexts and the Chain of Interactions method that was developed to decrease the cost of using the AHP in supplier selection. Both weighting methods recommend the same material but with some difference in scores between materials. Experts' judgement resulted in a higher emphasis on the laminate characteristics than AHP + CoI. The experts were able to tailor their responses to a particular part geometry for the application in the aerospace industry resulting in a focus on laminate quality. CoI exclusively takes into account the selected criteria, resulting in a focus on the manufacturing aspects. The choice of method may alter the result in other cases, a hybrid method to capture both aspects was proposed.

The selected materials were used to manufacture a representative part geometry, and the quality aspects influenced by the increased geometrical complexity were examined. It was found that the results of a material selection based on flat samples recommends the same material as a direct comparison of a more complex L-shaped part. The proposed method can prevent industrial users selecting suitable materials by spending time and effort with a trial and error approach during the production process. Using AHP as a knowledge based decision-making tool could provide a framework for an extendable database to account for future findings and insights. A more extensive material test campaign could increase certainty for selecting a suitable material for AFP production of highly complex geometries at the penalty of increased cost to gather data. For instance, scaling the process up to larger components can require investigating material behaviour at high deposition rate, repeatability or robustness of the process.

Chapter 4

Process Optimisation of ADFP

This chapter determines the impact of various process parameters of the AFP process on the preform quality, using preform V_f as a metric and applies them to a more complex preform. This was achieved with experimental measurement of preform response to variation in pressure, temperature and speed, derived from the machine parameters laser power, laser optics, applied force and deposition speed. The impact of steering on the preform quality was assessed by preform V_f as well as a newly introduced measurement method and metric to quantify wrinkles in more detail.

4.1 Background and Aim

The review of the state-of-the-art (Chapter 2) revealed common poor practice in the ADFP community, with authors often opting not to disclose and report processing parameters. Causal links between process parameters and preform quality are not available, in part due to lack of metrics to quantify preform quality. This chapter aims to provide methods to determine these links and applies these methods to quantify manufacturing variation in three important situations. The first section identifies variability in straight fibre paths across a range of three key manufacturing parameters. The additional manufacturing variabilities introduced by repetitive deposition to create a thick preform and steered fibre path are assessed individually in the second and third sections. Each topic is addressed individually, and specific aims are defined in the respective sections. Overall, this chapter aids understanding of the different factors influencing the variability of the ADFP process and assesses the viability of applying these finding to efficient development of industrially relevant laminates.

4.2 Manufacturing Variability Induced by Process Parameters

The main process parameters in the AFP process are time, temperature and pressure. More specifically, the defining relationship is the duration and intensity of positive compaction pressure and elevated deposition temperature simultaneously. Deposition temperature and temperature history are a direct result of the heat source, its set-up and operation of the system. Compaction pressure is defined by the contact area between the compliant compaction device and the substrate well as the applied force resulting in a specific pressure profile.

It became evident that process models developed based on thermoplastic or thermoset prepreg materials are not directly transferable based on the discussion in section 2.1.3. Therefore, it was necessary to establish the contribution of the process parameters to the preform output experimentally. In this section, the impact of the processing parameters was measured by capturing the preform thickness. The thickness measurement was converted into preform V_f for comparability across materials, as described in section 3.2.2. In summary, this sub-chapter aims to:

(1) Assess the feasibility of defining the ADFP deposition temperature requirement by thermal characterisation of dry fibre material.
(2) Determine the sensitivity of the dry fibre materials to changes in deposition temperature, heat zone size and speed as well as compaction pressure.
(3) Establish which material can achieve the target preform V_f and determine the range of process parameters required.
(4) Verify that the process parameter definition based on UD strips is valid for bi- and multi-axial preforms.
(5) Provide insights into the response behaviour of the different dry fibre materials based on the material constituents caused by process variables.

4.2.1 Materials and Experimental Method

Flat, UD test strips made up of eight tapes (each 6.35 mm wide) were deposited in a single 50.8 mm wide course to test the impact of deposition temperature, compaction pressure, speed and heat zone length. Heat zone length was varied by using different sized laser optics, collating the beam into different shapes, which will be described in more detail in the next section. These strips were laid up for each set of machine process parameters; the number of repeats varied between the tests and was indicated in the relevant section. The number of plies was adjusted depending on the material areal weight to obtain a cured thickness of nominally 2 mm at 55% V_f (Material A and D: 10 plies; Material B and C: 16 plies; Material E: 8 plies). Temperature measurements were taken at the top plies at least 1 mm from the tool surface to avoid any influences of the tool acting as a heat sink and influencing

the result. The strips were deposited over a Nylon film (Wrightlon® 7400, Airtech International Inc., Huntington Beach, US) vacuumed to the surface of a granite metrology table (Mitutoyo Graplate[4]) with a coated nylon peel ply (Nylon woven peel ply 60BR, Tygavac, Oldham, UK) in between. This set-up ensured a good adhesion between the preform and the granite table. The length of the strips was 500 mm unless stated otherwise. The thickness of the scanned strips was measured against a datum plane, which was generated based on the area in close vicinity of the relevant strip; the use of the granite table was ensuring a flat surface that allows for this procedure.

All strips were measured using the laser line scanner as described in section 3.2.2 immediately after the deposition was finished. The measured area was limited to the central 300 mm long and 35 mm wide region of the UD strips, excluding edge effects. The measurement repeatability and reproducibility for a series of strips with the same equipment as used in this chapter was established by Di Francesco for Material D [202], with the data used to construct the confidence interval shown in Table 4-1. The appropriate uncertainty will be applied to all measured samples to ensure comparability, and the data gathered with Material D on UD strips is assumed to be representative for all other materials.

Table 4-1: Measurement and manufacturing repeatability and reproducibility of Material D (confidence interval 95%) [202]

Description	**Uncertainty (± 2 SD), µm**
Measurement system repeatability *Sample description: One UD strip* *Measurements: Ten times the same strip, operator is insignificant* *Time frame: within 1 h of deposition*	± 6
Manufacturing system repeatability *Calculated using the sum in quadrature for uncertainty* [221]	± 34
Combined measurement and manufacturing system repeatability *Sample description: Eight nominally identical UD strips* *Measurements: One time per strip* *Time frame: within 1 h of deposition*	± 36
Measurement system reproducibility *Sample description: One metallic gage block* *Measurements: Eight times, moved between scans* *Time frame: Repeated three times over three months*	± 54
Manufacturing system reproducibility *Calculated using the sum in quadrature for uncertainty* [221]	± 70
Combined measurement and manufacturing system reproducibility *Sample description: 15 nominally identical UD strips*	± 88

[4] Code No.: 517-917 0UK; Grade: 0; Size: 2000 x 1200 mm; Weight: 1080 kg; Serial No. 20120005; Flatness: ~10 µm

Description	Uncertainty (± 2 SD), µm
Measurements: 1 time per every strip measured *Time frame: 5 UD strips per set over 3 months*	
Combined measurement and manufacturing system repeatability and reproducibility *Calculated using the sum in quadrature for uncertainty* [221]	± 96

The resulting preform V_f calculated using Equation 3-1 can be compared to the initial fibre volume fraction V_f of the as-supplied tapes, which was calculated similarly to Equation 3-1, where

$$tape\ V_{\mathrm{f}} = \frac{W_{\mathrm{ply}} - W_{\mathrm{binder}}}{\rho_{\mathrm{fibre}} \cdot t_{\mathrm{tape}}} \qquad \textit{Equation 4-1}$$

with weight W of the measured areal weight and the measured binder weight, ρ the nominal fibre density according to the data sheet provided by the respective manufacturer and measured tape thickness t. The binder weight was determined in accordance with ASTM D 3529 by removing the binder of a sample with known weight. The binder quantity was determined following ASTM E 1131 - 08, using a thermogravimetric analyser (TGA) (Q500 V20, TA Instruments, US). The measurement was carried out with one sample per bobbin (eight samples per material), taken at the end of the deposition trials, roughly in the middle of the bobbins. The material thickness was measured using a 3D micro coordinate measurement machine (InfiniteFocus, Alicona, Austria) on three samples per material. The cross-sectional profile on three discrete locations of each scanned sample was taken and the area measuring the surface of the tape referenced against the sample holder, these distance measurements were averaged. The carbon fibre veil that is present on Material A was neglected, as it was not possible to measure its weight independently and therefore had to be considered part of the continuous fibres.

A selected set of machine variables was applied to manufacture preforms of 600 × 600 mm for Material A and D with the previously described QI preform configuration (refer to section 3.2.5). Data of the bi-axial panels manufactured as part of section 3.2.2 was also be used for comparison.

4.2.2 Deposition Variables

Temperature

Using the material characteristics to develop the target input temperature by testing the binder activation temperature is a quick, low cost and convenient way to define the process. This approach has been used when defining the AFP process parameters for thermoplastic and thermoset prepreg deposition [71], [202]. To determine if the activation temperature of the binder is linked to the deposition temperature, the activation temperature was measured using a Modulated Differential Scanning Calorimetry (MDSC) for the thermoset-based binders (Material A and B). The activation

temperature was defined as the temperature at which crosslinking begins to occur, as indicated by the exothermic heat flow versus temperature plot. The ramp rate was set to 3 °C/min up to 350 °C with a modulation of ± 1 °C once every minute. Two samples were tested for each material. For one thermoplastic binder-based material (Material D), Differential Scanning Calorimetry (DSC) was used to determine the transition temperatures midpoint glass transition temperature (T_g) and peak melt temperature (T_m). Following ASTM D3418, the ramp rate was set to 10 °C/min up to 300 °C; three samples of the material were tested.

To determine temperature during AFP deposition, in-process temperature measurements during the process was required. A minimum of 1 mm thickness was deposited on top of each other to minimise the effect of the heat sink into the metallic tool. The use of thermocouples (25 µm diameter K-type, at 90 Hz logging rage) verified the insulating characteristic of the ply stack [222]. Even after the second ply, no significant influence of the tool acting as a heat sink was observable. The preform was allowed to cool down to ambient temperature before laying up subsequent plies to ensure the same initial conditions for each test run.

In these trials, two different laser optics were tested, the laser optics delivering a rectangular laser beam of 8 × 57 mm (beam aimed 50% on the roller, 50% on the substrate) was used as default unless otherwise stated. The variation was a laser optic delivering a rectangular laser beam of 28 × 57 mm (beam aimed 30% on the roller, 70% on the substrate), this results in a heated length of 18.1 mm and 69.6 mm respectively, valid for a compaction pressure of 0.47 N/mm^2 [54]. The shorter heat zone length had a significant advantage over the longer heat zone length when considering the deposition over convex corner. While the deposition head is slowly turning over a convex shape, the area behind the convex shape may already be subjected to the large heat zone area projected by the laser beam, which can cause over-heating. All tests taken into account for the effect of temperature on the preform V_f are summarised in Table 4-2.

Table 4-2: Laser power, compaction pressure (2 SD) and resulting temperatures (2 SD) used for the tested configurations, all carried out at 400 mm/s deposition speed, a pressure of 0.47 ± 0.14 N/mm^2 and with the laser optics delivering a 8 x 57 mm beam

Material	Laser power, W	Temperature, °C	Number of repeats
A	450	172 ± 15	1
A	627	223 ± 22	5
A	550	204 ± 17	1
A	650	232 ± 16	1
A	850	283 ± 18	1
A	750	258 ± 18	1
A	950	309 ± 19	1
A	1050	334 ± 24	1

Material	Laser power, W	Temperature, °C	Number of repeats
B	750	230 ± 15	1
B	450	157 ± 9	1
B	350	131 ± 8	1
B	650	206 ± 16	1
B	850	256 ± 15	1
B	550	186 ± 10	1
B	609	196 ± 12	8
C	871	355 ± 30	1
C	529	241 ± 21	1
C	1100	433 ± 33	1
C	757	312 ± 28	1
C	986	397 ± 36	1
C	300	156 ± 17	1
C	643	286 ± 25	1
C	738	307 ± 27	8
D	557	259 ± 13	1
D	343	179 ± 10	1
D	271	150 ± 8	1
D	700	307 ± 17	1
D	486	231 ± 12	1
D	629	283 ± 15	1
D	200	121 ± 7	1
D	414	207 ± 11	1
D	549	248 ± 13	8
D	549	280 ± 20	3
D	549	276 ± 16	5
E	679	354 ± 35	1
E	421	249 ± 24	1
E	336	212 ± 22	1
E	850	430 ± 41	1
E	593	325 ± 32	1
E	764	389 ± 36	1
E	507	290 ± 29	1
E	668	348 ± 34	7

Pressure

Polymeric rollers are recommended for the deposition of dry fibre material by the machine supplier and was also the material of choice for previous work on ADFP [28], [47], [53], [132]. Two different rollers were used as part of this work, a Shore 40A hardness silicone roller (8F14-S40SH-BL) which is recommended for use with a laser as well as a foam roller (8F14-M510) recommended for use with an IR lamp, provided by Coriolis Composites.

These two rollers had a different compliance at the same force, resulting in different pressure applied to the material during deposition. Apart from impact of the roller material on compaction pressure, the change of exposed area due to a change in roller geometry can cause a change in measured temperature at identical laser power input. For the purpose of this work, the area exposed to the heater on the incoming tapes was assumed consistent across various applied pressures, even though a slight variation will be present in reality. Consequently, all measured temperatures were treated as apparent temperatures and the nip-point temperature as well as the laser power will be used as process descriptors. Hence, it was either possible to achieve the same temperature by adjusting the laser power and hence altering the power input into the system, or to keep the power constant and achieve a slight difference in apparent temperature, this cannot be decoupled. This means that critical process parameters are not adjustable independently in modern AFP machines. This had a significant influence on the experimental procedure, making it impossible to conduct a full Design of Experiments.

The compaction pressure was derived by converting the nominal compaction force (machine input) into actual compaction force (machine output) and the respective area of roller contact (measured contact length and nominal 50.8 mm material width). The roller contact area was established by Di Francesco for the silicone and foam roller in a static test fixture and a pressure map to determine contact length [202]. Similarly, Lichtinger *et al.* determined the contact length for the foam roller by using a similar test fixture and analysing an image taken of the roller in the test set-up [71]. Furthermore, Lichtinger *et al.* show that the assumption of uniform pressure delivery is not accurate (compare Figure 2-6); however, for the purpose of this work this will be neglected. Kok determined the contact length for the silicone roller using the machine directly and also used image analysis [208].

Intermediate values of contact length for both rollers were approximated by inter- and extrapolation of the experimental points obtained by Di Francesco using a second order polynomial function (silicone: R^2 = 99.3; foam: R^2 = 99.7), instead of the assumption made by Lichtinger *et al.* and Kok that the relationship is linear. The last point at 1206 N was too far from the dataset for extrapolation and was therefore approximated as the same contact length as the previous point at 1017 N; shown in Figure 4-1. For conversion to compaction pressure, the error in contact length measurement as well as the error in force measurement was taken into account by calculating the combined standard uncertainty by the fractional uncertainties of quadrature [221]. The data obtained by Kok shows that the machine induced variability is relatively high which is reflected in the relatively high error for compaction pressures. The actual compaction pressure cannot be measured during deposition, so the same calculated nominal values were applied to the tests.

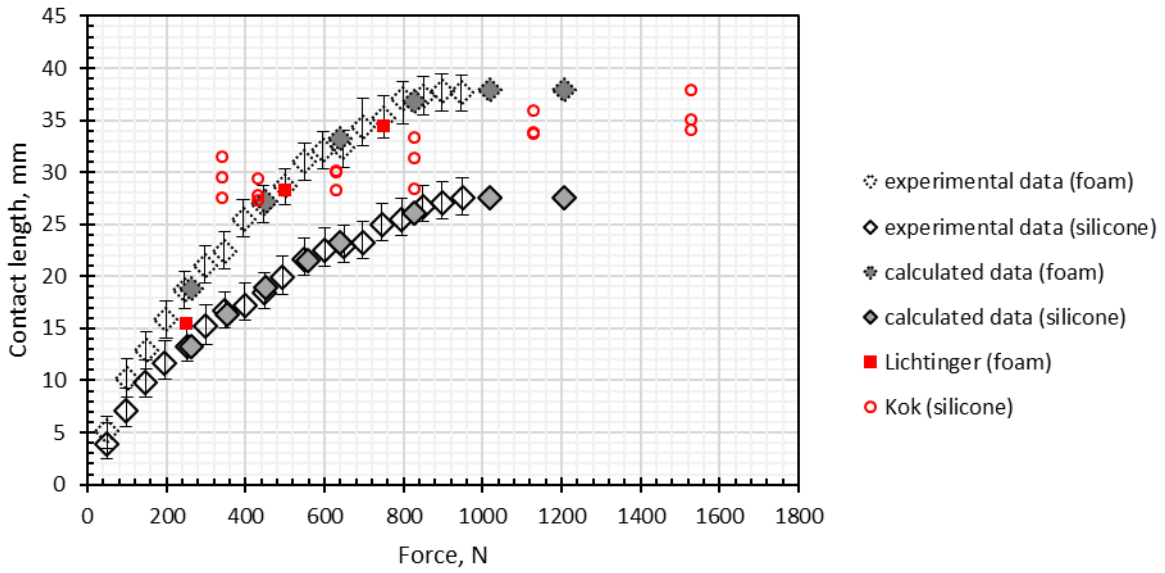

Figure 4-1: Values of roller contact area used to approximate applied pressure during deposition; the error bars indicate the measurement uncertainty associated with the resolution of the sensor; experimental data [202]*, Lichtinger* [71] *and Kok* [208]

The deposition temperature for the tests investigating compaction was selected based on the data gathered in the trials determining the impact of deposition temperature. The chosen temperature for deposition delivered a preform V_f within 95% of the maximum achievable V_f achievable on the used system. All tests taken into account for the effect of pressure on the preform V_f are summarised in Table 4-3.

Table 4-3: Laser power, nip-point temperature (2 SD) and nominal compaction pressure (2 SD) used for the tested configurations, all carried out at 400 mm/s deposition speed and with the laser optics delivering a nominal 8 x 57 mm beam

Material	Laser power, W	Temperature, °C	Nominal compaction pressure, N/mm²	Number of repeats
A	627	223 ± 15	0.47 ± 0.14	8
A	627	223 ± 22	0.47 ± 0.14	5
A	609	217 ± 18	0.86 ± 0.08	5
A	697	214 ± 15	0.47 ± 0.14	5
B	609	196 ± 12	0.47 ± 0.14	8
B	522	199 ± 20	0.86 ± 0.08	7
B	712	195 ± 21	0.47 ± 0.14	5
B	669	191 ± 24	0.86 ± 0.08	5
C	738	307 ± 27	0.47 ± 0.14	8
C	649	341 ± 38	0.86 ± 0.08	5
D	549	248 ± 13	0.47 ± 0.14	8
D	549	296 ± 17	0.86 ± 0.08	8
D	549	280 ± 20	0.47 ± 0.14	3

Material	Laser power, W	Temperature, °C	Nominal compaction pressure, N/mm^2	Number of repeats
D	549	290 ± 18	0.39 ± 0.15	5
D	549	276 ± 16	0.47 ± 0.14	5
D	549	294 ± 19	0.70 ± 0.10	5
D	549	284 ± 19	0.58 ± 0.09	8
D	549	277 ± 17	0.73 ± 0.11	8
D	549	282 ± 19	0.27 ± 0.15	5
D	549	300 ± 19	0.32 ± 0.14	5
D	549	312 ± 21	0.38 ± 0.09	5
D	549	320 ± 23	0.44 ± 0.10	5
D	549	326 ± 27	0.53 ± 0.07	5
D	549	332 ± 25	0.63 ± 0.08	5
E	668	329 ± 34	0.47 ± 0.14	7
E	559	348 ± 33	0.86 ± 0.08	8
E	668	348 ± 36	0.86 ± 0.08	8
E	668	273 ± 36	0.47 ± 0.14	3

Speed

The impact of deposition speed was determined by varying the speed of the programmed path. Because of the wide range of potential velocities (theoretically 1 mm/s up to 1000 mm/s), keeping the laser power constant was not possible across different trials. Instead, the laser power was varied to adjust for constant temperature at constant compaction force of 0.47 N/mm^2. The relationship of the required laser power for variable speed follows a power law; a semi-empirical procedure was established and provides the necessary machine input at variable speed to adjust the laser power [54]. This may introduce an additional source of error, as the machine input was a piecewise linear approximation of the power curve. In order to have a sufficiently high frame rate of the LWIR camera at high velocities the length of the path was adjusted. The strips manufactured at a deposition speed greater than 400 mm/s were longer (800 mm) which was a sufficiently long section of constant deposition speed in the central region of the strip. Strips manufactured at considerably lower speeds were shorter (300 mm) to reduce the deposition time. Three nominal velocities were tested, 32 mm/s, 400 mm/s and 1000 mm/s. The accuracy of the speed is governed by the robot capability; for the purpose of this work, the nominal value was assumed representative of the actual value. All tests taken into account for the effect of temperature on the preform V_f are summarised in Table 4-4.

Table 4-4: Laser power and nip-point temperature (2 SD) used for deposition trials, all trials were carried out at a compaction pressure of 0.47 N/mm^2 and with the laser optics delivering an 8 x 57 mm beam

Material	Laser power, W	Temperature, °C	Speed, mm/s	Number of repeats
A	122	225 ± 32	32	2

Material	Laser power, W	Temperature, °C	Speed, mm/s	Number of repeats
A	627	223 ± 22	400	5
A	1056	228 ± 21	1000	5
A	627	223 ± 15	400	8
D	102	n/a	32	3
D	549	n/a	100	5
D	938	n/a	200	5
D	549	283 ± 31	300	5
D	549	248 ± 13	400	8
D	549	276 ± 16	400	5
D	938	262 ± 15	1000	5
E	668	329 ± 34	400	7
E	108	297 ± 39	32	3
E	668	273 ± 36	400	3
E	1103	297 ± 62	1000	3

4.2.3 Results and Discussion

Dry Fibre Material Testing

The recommendation for deposition temperature given by the material supplier often appears to be based on material properties alone. The transferability of the approach to dry fibre materials was investigated, however this simple approach of using the material-based binder activation temperature to define the deposition quality was not successful. As shown in Figure 4-2, the curve describing the thermal behaviour of the binder material was not a good indicator of the temperature needed during deposition to achieve a preform V_f of 50 - 55% (the temperatures of deposition trials at which preforms reach the preform V_f value is highlighted in the graphs). The two materials with epoxy-based binder do not show consistency between them. Material A achieves the desired preform V_f across two exothermic peaks, which indicates the presence of two different materials; see Figure 4-2 (a). Material B was processed well ahead of the peak, Figure 4-2 (b). Material D had an average T_m of 156 ± 1.4 °C (2 SD), which could be used as deposition temperature in theory, but the preform V_f was far below the desired value, see Figure 4-2 (c).

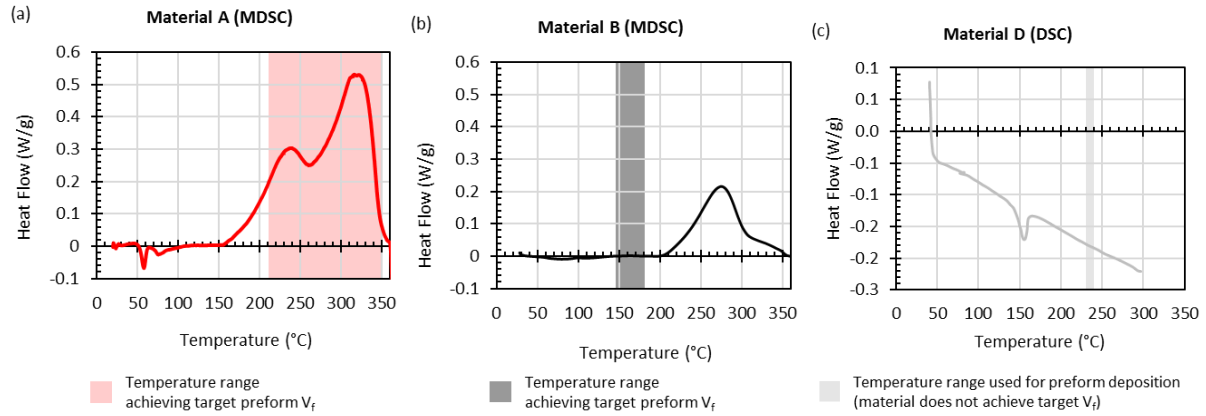

Figure 4-2: Results of MDSC and DSC superimposed with temperature used to achieve 50 - 55% or highest value of preform V_f in deposition trials for Material A (a), Material B (b) and Material D (c)

As an elaborate and reliable model was not available, a different approach was needed. A more practical way to deposition temperature definition was to use the machine directly, which was material and machine specific and would need to be repeated if either were varied.

The test results of the areal weight measurements are shown in Table 4-5. The results were relatively close to the nominal values in the case of Material B – E. A difference of 1 – 4 g/m^2 could be a result of measurement inaccuracies. The high difference for Material A is due to the carbon fibre veil. The supplier does not disclose the areal weight of the carbon fibre veil, but the measurement data suggests that the veil accounts for up to 12 g/m^2 of the areal weight.

Table 4-5: Measured areal weight and binder quantity, absolute difference between the nominal value and the measured areal weight without binder (errors indicate 2 SD)

Material	Areal weight, g/m^2	Binder quantity, wt.%	Difference, g/m^2
A	218 ± 17	4.5 ± 0.8	12
B	136 ±6	5.5 ± 1.7	2
C	139 ± 9	6.9 ± 2.1	3
D	219 ±3	3.8 ± 1.1	1
E	282 ±9	5.7 ±3.8	4

As the measurement of the actual areal weight was not possible for Material A because the veil cannot be measured separately, the collected data was inaccurate. For consistency, the nominal values will be used for all materials for the remainder of the work.

Material Robustness and Variable Influence

A material that is robust to processing parameters enables a more repeatable manufacturing process. In order to assess this, the variables temperature, deposition speed and heat zone length at two

compaction pressure levels were tested. The highest and the lowest achieved preform V_f was used to define the range possible for each material. Variables were kept within the same range across materials where possible for comparability. This applies to compaction pressure (min: 0.47 ± 0.14 N/mm^2; max: 0.86 ± 0.08 N/mm^2), heat zone length (8 mm and 28 mm) and speed (32-1000 mm/s). Only temperature had a variable range, depending on the material. The upper end of the range is defined as the power when smoke was visible during deposition; the lower end was defined as the power where the material does not adhere to the previous ply, determined by trial and error. Table 4-6 shows the various ranges resulting from deposition trials.

Table 4-6: Range of preform V_f upon changing the variables (temperature, error indicates 2 SD and laser power refers to the variations within each material, the other variables refer to all materials at the same time), variables are underlined

Variable		**Details of parameters**				
Test case		#1	#2	#3	#4	#5
		Apparent nip-point temperature	Deposition velocity	Compaction pressure	Heat zone length at high pressure	Heat zone length at low pressure
Temperature, °C	*A*	172-334	225±4	223-239	221±7	220±10
	D	121-307	267±31	248-332	266±29	259±7
	E	212-430	338±56	248-394	351±13	n/a
Laser power, W	*A*	450-1050	122-1056	627	627, 890	609, 851
	D	200-700	102-938	549	606, 549	467-562
	E	336-850	108-1103	668	756, 668	n/a
Pressure, N/mm^2		0.47	0.47	0.47 - 0.86	0.47	0.86
Nom. heat zone length, mm		8	8	8	8, 28	8, 28
Speed, mm/s		400	32-1000	400	400	400
Material		**Resulting range of preform V_f obtained, %**				
A		6.2	1.2	1.2	0.2	1.0
D		13.6	7.1	6.0	1.6	0.0
E		9.5	3.5	2.9	2.4	n/a

Material B and C were not fully examined, as these materials did not fulfil the requirements outlined in Chapter 3. For all tested materials, the variable temperature had the most significant influence on preform V_f, followed by deposition speed and compaction pressure. Heat zone length did not have a

high impact either combined with high or low compaction pressure. Material D and E respond more to the process parameters than A in all instances; these two materials were relatively similar in composition. Both contain a thermoplastic binder that is predominantly located on the outside of the tapes. It becomes clear in the Table 4-6 that Material A was less variable than the other materials. This result confirms the result of Chapter 3, Material A was more favourable than the other materials investigated and Material D and E behaved similarly. The robustness could be an additional criterion for the selection process, at the expense of an increased test campaign.

Achievement of Target Preform Fibre Volume Fraction

Not every material achieved the target V_f (50-55%) during the trials, the desired range of preform V_f was achieved using Material A and B only. For Material A, this was possible within a wide temperature range of 204 – 334 °C. The speed range to achieve the target was 32-400 mm/s, with the high deposition speed of 1000 mm/s yielding 49.9% preform V_f. High compaction pressure (0.86 N/mm^2) only yielded target values in combination with the long heating zone (28 × 57 mm) but lower compaction pressure was suitable to reach the target with both laser optics. Material B was the only material, which achieved a higher preform V_f than intended (> 55%) frequently, the process parameter range to achieve the desired preform V_f (52.2 – 53.1%) was relatively small (temperature: 157 – 199 °C). Overall, a smaller range was tested as the material failed to comply with the selection criteria.

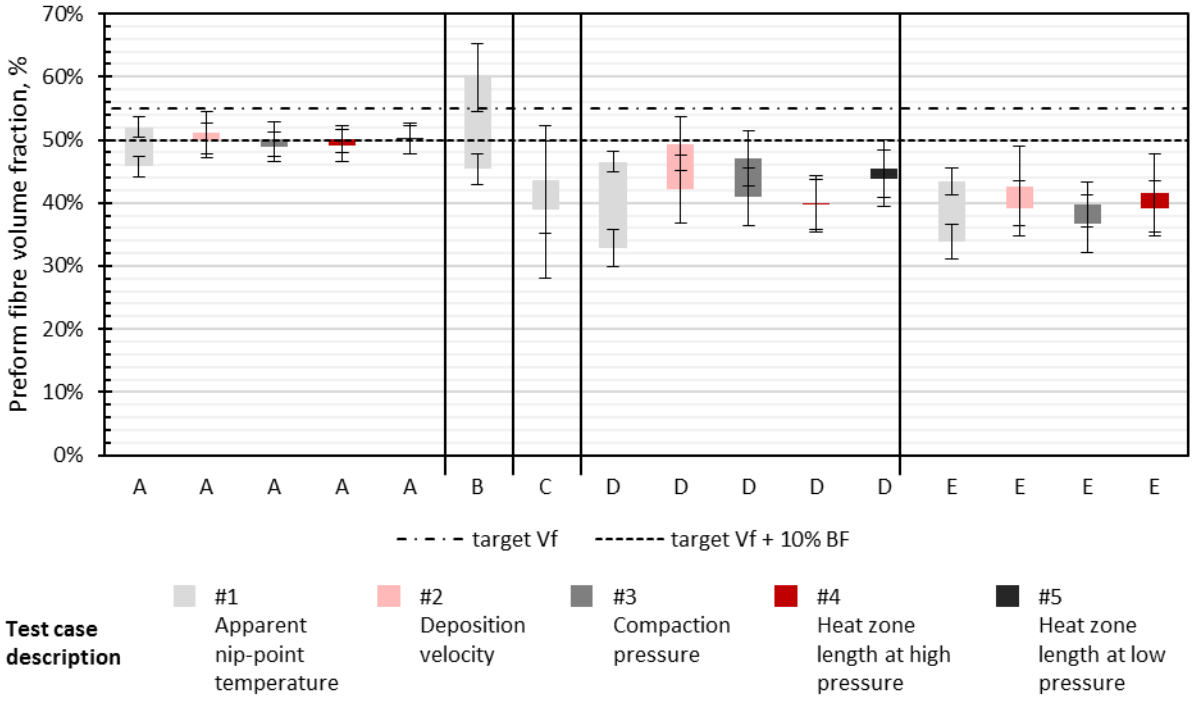

Figure 4-3: All materials showing the ranges of preform V_f reached within the test matrix, the error bars indicate 2 SD, preform V_f variability is determined across samples and the combined measurement and manufacturing system reproducibility is added, describing the variability of the minimum or maximum value of the shown test case (refer to Table 4-1)

For the processing parameters that lead to the target preform V_f using Material A in Figure 4-3, refer to Table 4-7. These combinations are all suitable for applications to larger scale trials.

Table 4-7: All parameter combinations yielding 50 - 55% preform V_f with Material A; the error bars indicate 2 SD, preform V_f variability is determined within and across samples, calculated using the sum in quadrature for uncertainty [221]

Laser power, W	Laser optics	Temperature, °C	Deposition speed, mm/s	Pressure, N/mm²	Preform V_f, %	Number of repeats
850	8x57	283 ± 18	400	0.47 ± 0.14	51.4 ± 1.7	1
550	8x57	204 ± 17	400	0.47 ± 0.14	50.4 ± 1.4	1
1050	8x57	334 ± 24	400	0.47 ± 0.14	52.0 ± 1.6	1
750	8x57	258 ± 18	400	0.47 ± 0.14	51.5 ± 1.7	1
950	8x57	309 ± 19	400	0.47 ± 0.14	51.5 ± 1.5	1
650	8x57	232 ± 16	400	0.47 ± 0.14	51.1 ± 1.5	1
851	28x57	222 ± 18	400	0.86 ± 0.08	54.1 ± 6.5	5
890	28x57	223 ± 13	400	0.47 ± 0.14	54.1 ± 5.4	5
851	28x57	224 ± 16	400	0.86 ± 0.08	50.2 ± 4.9	5
890	28x57	219 ± 15	400	0.47 ± 0.14	50.2 ± 5.0	5
652	8x57	206 ± 16	400	0.47 ± 0.14	50.7 ± 5.4	4
697	8x57	214 ± 15	400	0.47 ± 0.14	50.7 ± 5.4	5
886	28x57	221 ± 16	400	0.47 ± 0.14	50.7 ± 7.0	8

Laser power, W	Laser optics	Temperature, °C	Deposition speed, mm/s	Pressure, N/mm²	Preform V_f, %	Number of repeats
122	8x57	225 ± 32	32	0.47 ± 0.14	51.1 ± 9.5	2
627	8x57	223 ± 22	400	0.47 ± 0.14	50.0 ± 7.8	5
652	8x57	240 ± 15	400	0.47 ± 0.14	54.2 ± 2.1	1

Validity of Scalability of Results

For the manufacture of industrial parts, a specific laser power is not sufficient, as the deposition speed varies. The method to establish the relationship between selected power and achieved temperature at variable speed was developed using Material D, but was successfully applied to Material A within this work [54]. Material A achieved a measured temperature of 215 ± 7 °C at a target temperature of 220 °C, and Material D achieved 259 ± 4 °C at a target temperature of 260 °C (2 SD course to course variability, eleven courses analysed in each case).

To check if the results obtained using the UD strips are consistent with the results for panels, preforms manufactured using the same processing parameters for both formats (UD strips and panels) were compared. Figure 4-4 shows the preform V_f for bi-axial (Material B) or QI preforms (Material A and D) and the corresponding UD strips. The data within each material compared had similar deposition temperature and identical deposition speed, compaction pressure and heat zone length.

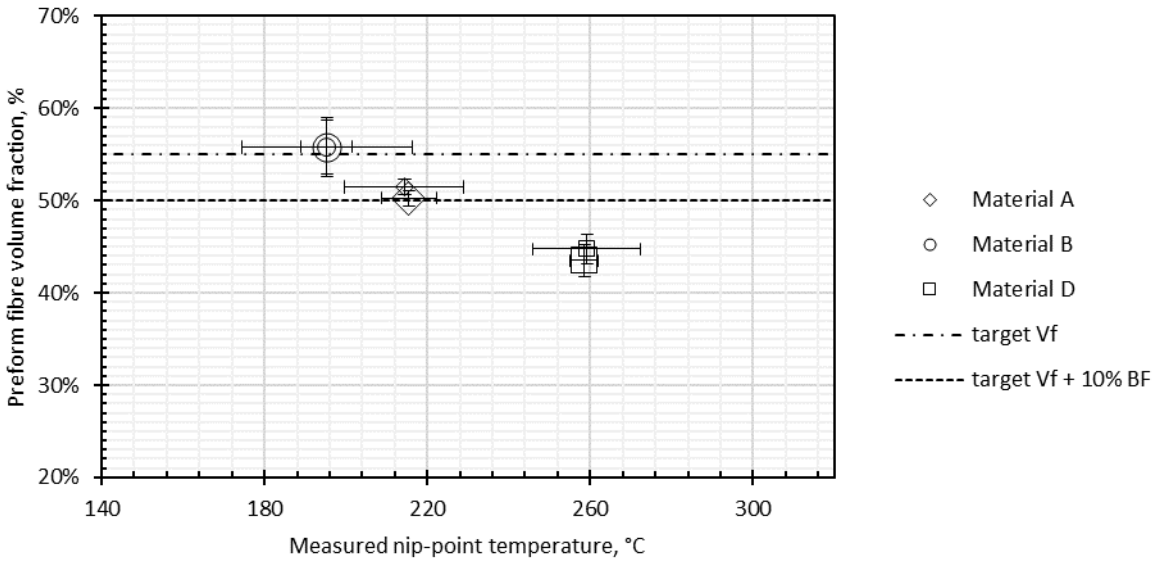

Figure 4-4: Comparison of UD strip (small shapes) and 600 x 600 mm panel (large shapes) preform V_f for three materials; the error bars indicate 2 SD, the variability across samples was taken where possible with the added manufacturing system reproducibility, where only one sample is available the combined measurement and manufacturing system reproducibility and repeatability is added (refer to Table 4-1)

Three different materials all showed good agreement between preform V_f of different preforms manufactured with similar process parameters. Overall, the findings generated using UD strips were scalable and were suitable to guide manufacturing parameter selection of flat panels with multi-axial ply directions.

Preform Behaviour in Response to Process Parameters

Querying the data for similarities across all dry fibre materials could enable links between material constituents and the material responses to the manufacturing process. It was not possible to vary the material constituents directly. However, some insights into the differences across the materials can provide some insights: Increasing the temperature while all other parameters remain constant exhibits a similar trend across the different materials, which was an increase of preform V_f. For all materials, except Material A, an approximation with a quadratic function was a good fit (R^2 = 0.96 – 0.98). In addition, Materials C – E exhibit a very similar curve. As these three materials all contain a surface concentrated thermoplastic binder, a similar behaviour is expected. Without further investigation, a generalisation of the curve description was not possible, but the results show that materials with comparable composition react similarly. A summary of the quadratic functions can be seen in Figure 4-5.

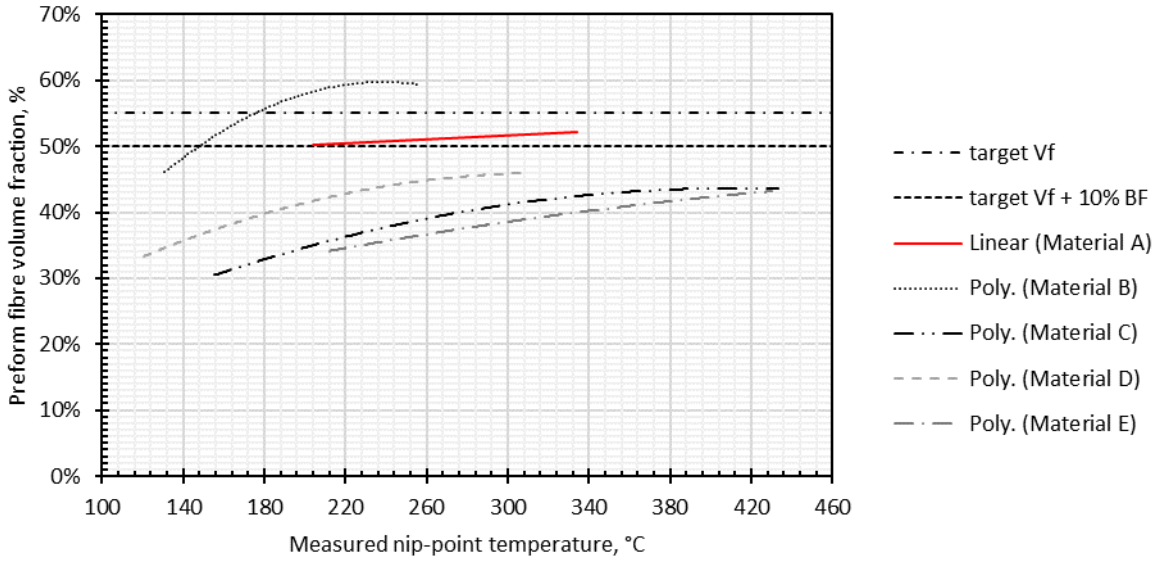

Figure 4-5: Approximations of the dry fibre material behaviour at increasing temperature, all other variables were constant.

The curve describing the behaviour of Material B is a higher and compressed curve than those describing Material C – E, which may be rooted in the different binder composition (epoxy based instead of thermoplastic based), or the location of the binder (distributed within the tape instead of on the surface only). Material A can be described with a linear function with a slight upwards slant, when excluding the first data point below the lower target preform V_f. The detailed test results of

Material A can be found in Figure 4-6. The details of the different data sets of the other materials and their fitted function can be found in Figure 4-7 to Figure 4-10. Even though the function fits well to Material C and E, these materials could also be described using a linear function, given their high variability.

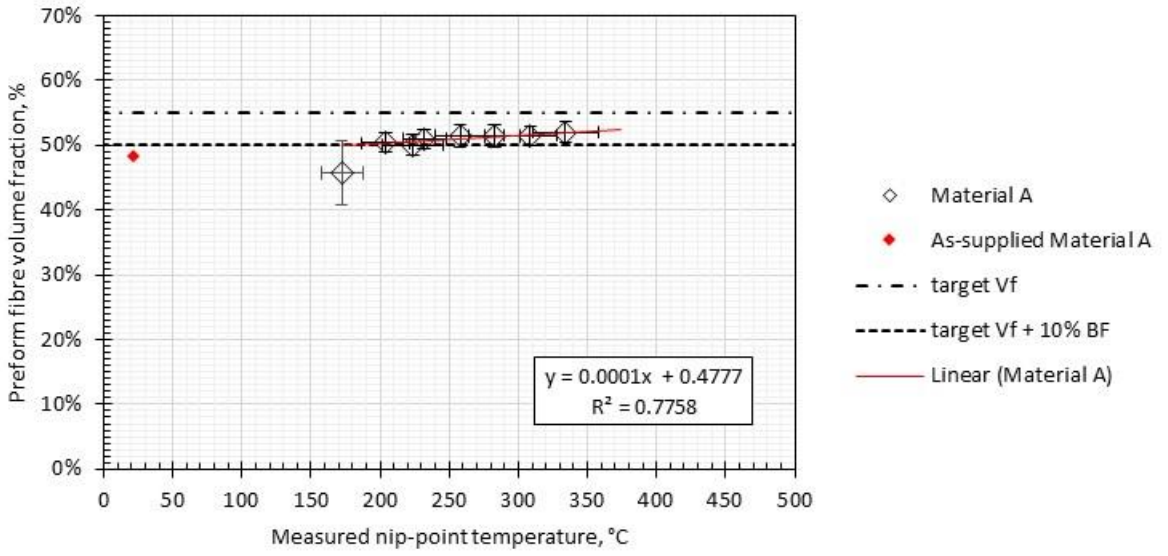

Figure 4-6: Behaviour of preform V_f at increasing temperature (all other variables were constant) for Material A, the error bars indicate 2 SD for preform V_f of variability within one UD strip

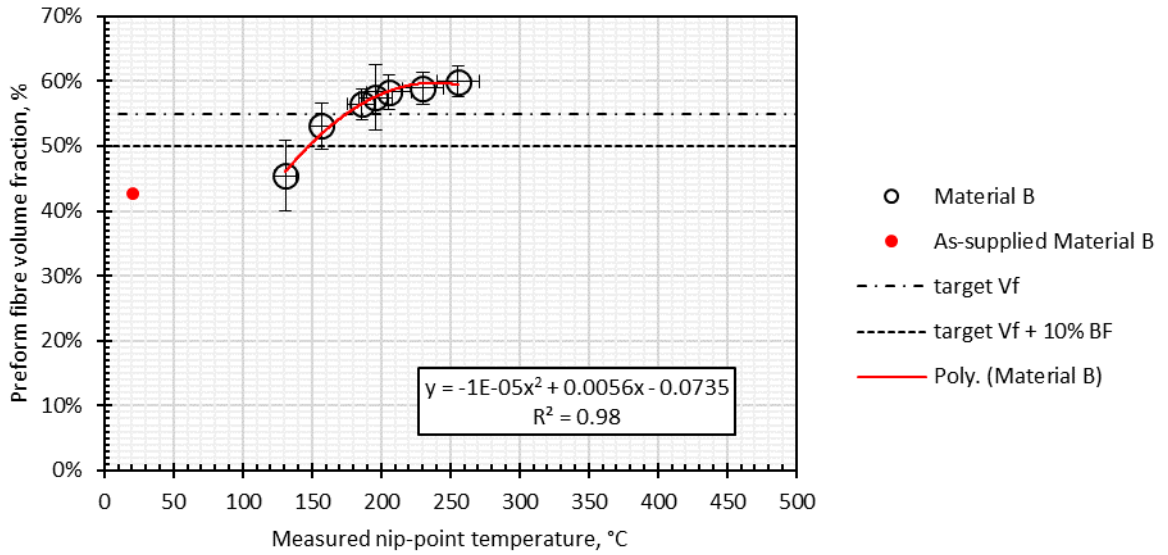

Figure 4-7: Behaviour of preform V_f at increasing temperature (all other variables were constant) for Material B, the error bars indicate 2 SD for preform V_f of variability within one UD strip

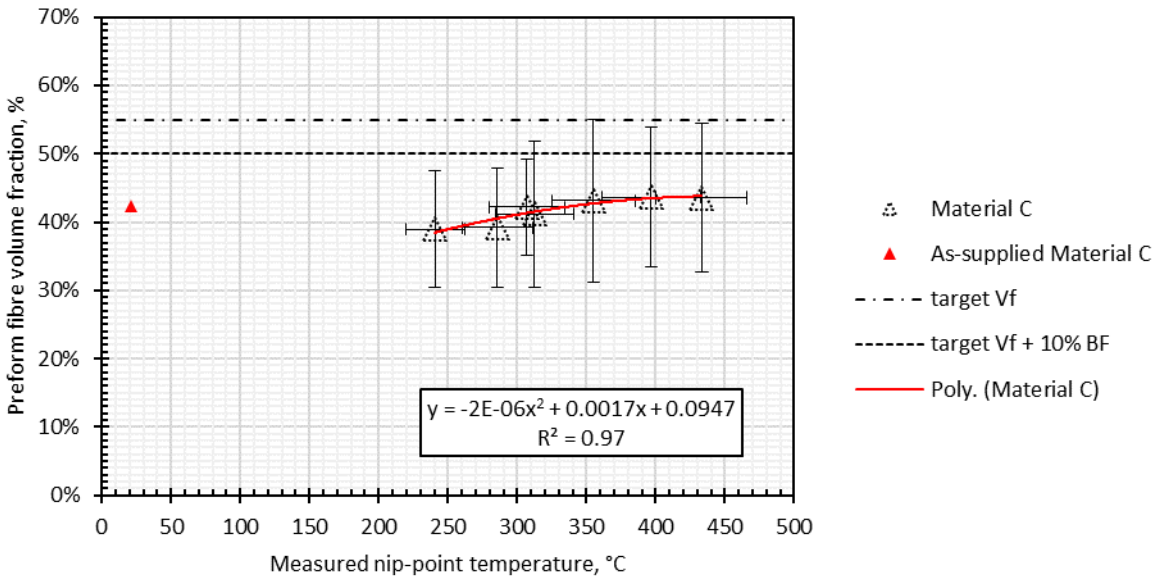

Figure 4-8: Behaviour of preform V_f at increasing temperature (all other variables were constant) for material C, the error bars indicate 2 SD for preform V_f of variability within one UD strip

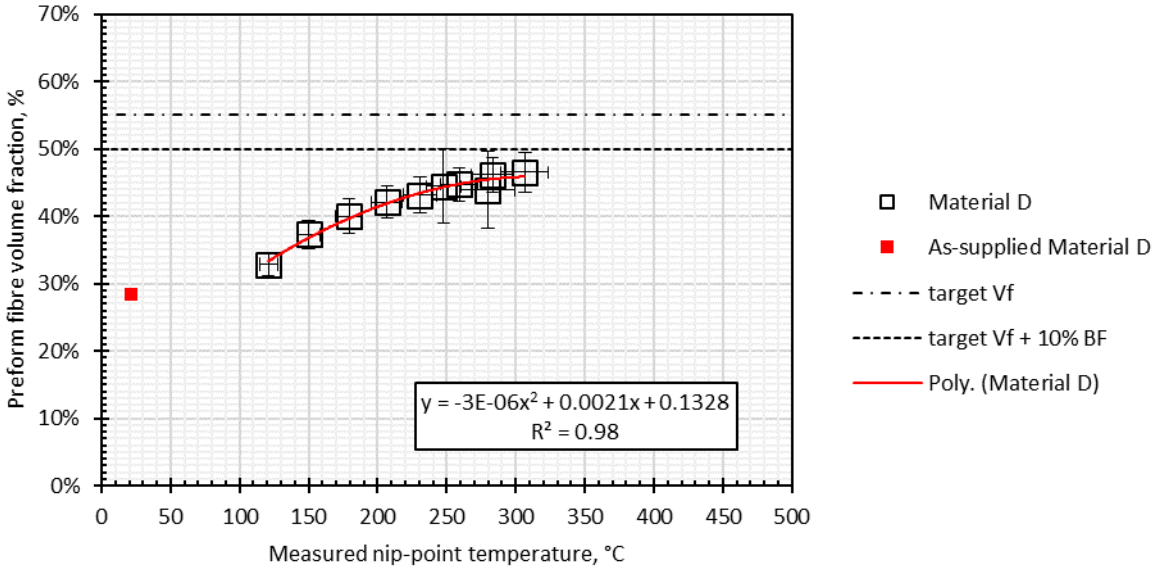

Figure 4-9: Behaviour of preform V_f at increasing temperature (all other variables were constant) for Material D, the error bars indicate 2 SD for preform V_f of variability within one UD strip

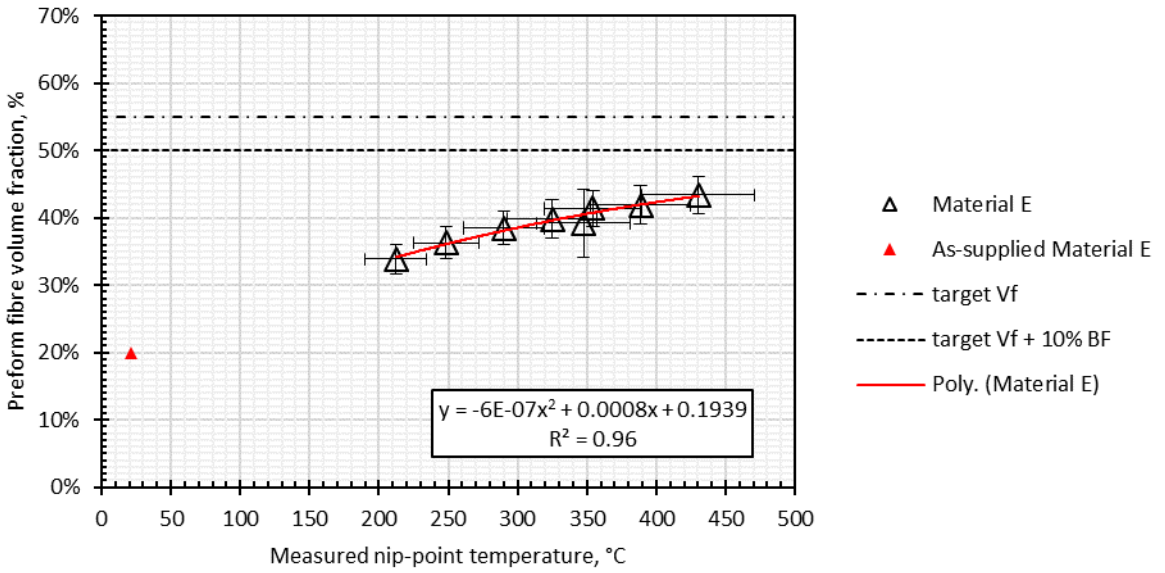

Figure 4-10: Behaviour of preform V_f at increasing temperature (all other variables were constant) for Material E, the error bars indicate 2 SD for preform V_f of variability within one UD strip

The presented data can be used to determine the process window width and allows the choice of deposition temperature dependent on the desired preform V_f. The initial tape V_f shown did not appear to be a good indicator of preform V_f, not in all cases was the initial tape V_f at ambient temperature lower than the preform V_f.

The behaviour of preform V_f at multiple deposition velocities was assessed for Material D by Di Francesco [202]. The relationship between deposition speed and preform V_f at otherwise constant parameters can be described by a power law. The same applies to Material A and E (R^2 = 0.91 – 0.92), where it was less pronounced. Especially for Material A the behaviour was within error, see Figure 4-11.

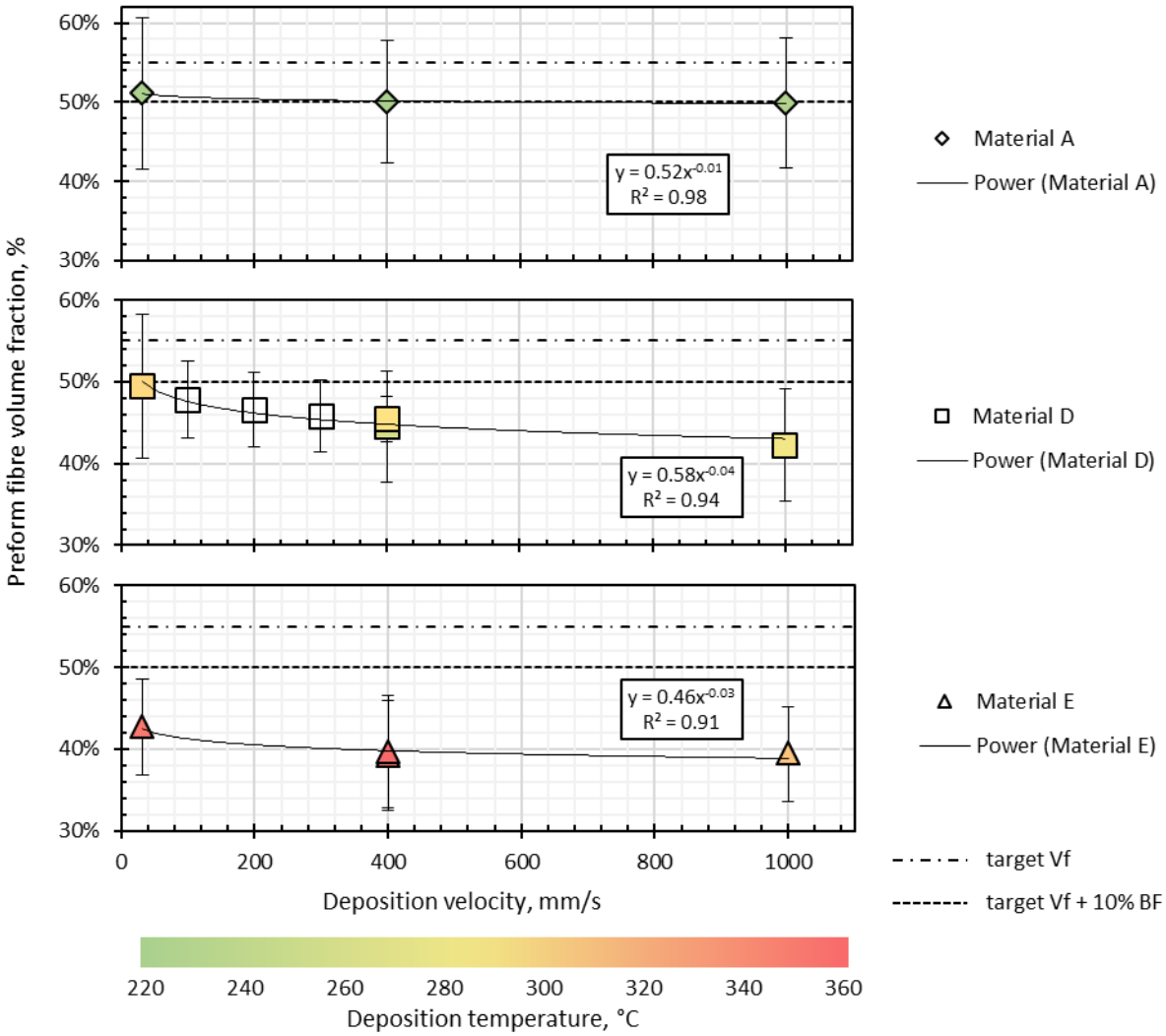

Figure 4-11: Effect of deposition speed on preform V_f (all other variables were constant), (not all thermal measurements for Material D were available), the error bars indicate 2 SD, preform V_f variability is determined across samples with the combined measurement and manufacturing system reproducibility (Table 4-1)

The residence time of the material at the exposure of the heating zone alters the temperature history. Adjusting the laser power to keep the nip-point temperature constant to account for variable speed does not suffice in the case of Material D to obtain consistent preform V_f. However, it was sufficient to keep the outcome constant in the case of Material A. In conclusion, Material A was least influenced by the intensity of the heater as well as the duration of exposure, this applies to the narrow laser spot size (8 × 57 mm).

Already established by Di Francesco for Material D, the increase of compaction force leads to a decrease in preform V_f for both roller types [202]. Only two configurations were tested for Material A and E to verify this trend. In both instances, while the absolute preform V_f was significantly different, a trend of decreasing preform V_f at increasing pressure at constant laser power can be shown, see

Figure 4-12. For the purpose of visualisation, only the upper and lower boundaries (2 SD) of Material D were plotted, the average deposition temperature was 294 ± 45 °C.

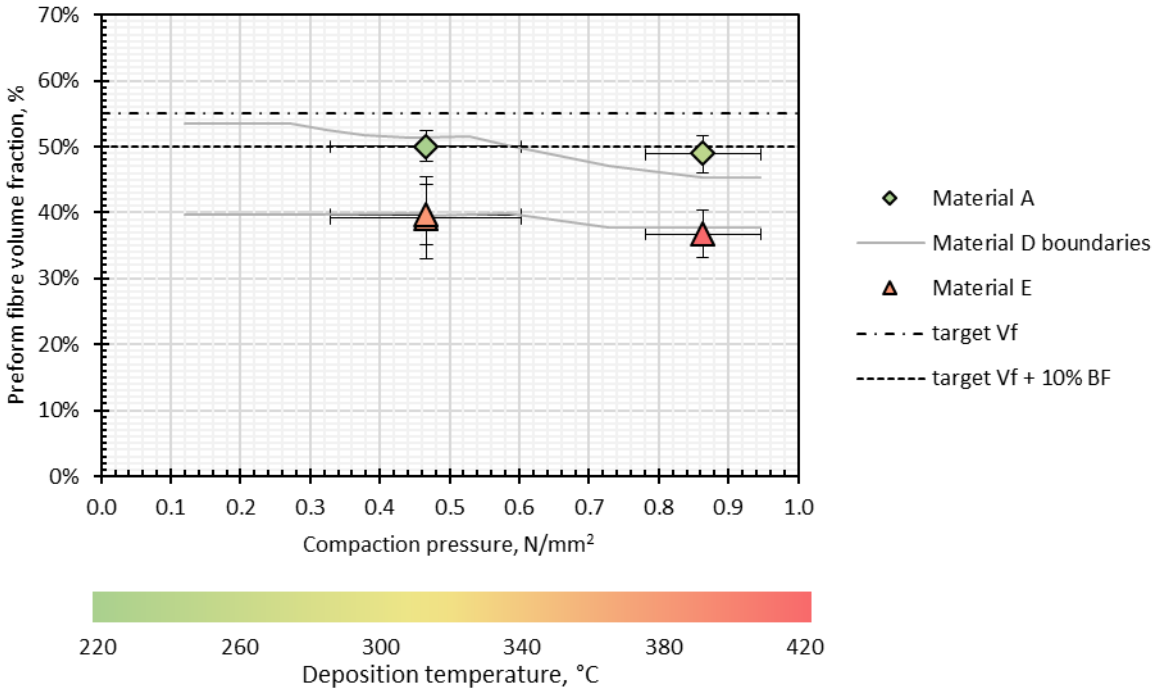

Figure 4-12: Effect of compaction pressure on preform V_f at constant laser power (all other variables were constant), the error bars indicate 2 SD, preform V_f variability is determined across samples and the combined measurement and manufacturing system reproducibility is added (refer to Table 4-1)

The preform V_f decrease at high compaction pressure could be a result of competing through thickness compression and tensile stress imposed by the roller. Directly under the roller, a compression stress compacts the materials, immediately before and after the roller, a counteracting tensile stress causes the material to bulk upwards. This tensile stress is exceeding the binder adhesion strength and can cause deconsolidation, the higher the compaction force, the higher the counteracting tensile force and therefore increased deconsolidation [202], [223].

Even though the laser power and deposition speed were kept constant within each material across all trials, a significant variation of the temperature occurs under varying compaction pressure. This shows the limitations of using temperature as a processing parameter. The energy put into the system remains the same, but the apparent temperature increases at increased compaction pressure. This supports that the thermal measurement does not fully characterise the process and comparisons of apparent temperature were only valid for consistent machine settings and variables.

Recommendations for AFP Process Parameters

In the following chapters, the knowledge of the materials response to the process will be used to define the process for more complex geometries. The significance of the effect incurred by the

different parameters will be informing the level of monitoring that was required for future trials. As the results of the material selection and the robustness assessment agree that Material A was the most suitable material for manufacturing complex parts, the remainder of this work will focus on Material A.

An increased temperature does not significantly contribute to a high preform V_f for Material A, so the temperature can be kept at the lower end in order to avoid binder degradation, it is recommended to use temperatures between 200 °C and 330 °C. Material A can cope with any deposition speed, and no constraints were inflicted on the program of complex parts. A low compaction pressure appears to be beneficial but had a low impact; compaction pressure of < 0.47 N/mm^2 is recommended. Should it be necessary to correct for increasing bulk factor, the compaction pressure should be decreased. The laser optics did not have a significant effect on the preform V_f and can therefore be chosen based on other constraints, due to the advantages of the narrow spot size on geometrically complex parts, the 8 x 57 mm laser optic is recommended. While this was only the immediate and practical use of the findings, in the future these insights may facilitate a practical focus in process models, which would be a useful tool to capture the interactions of the various process parameters, an aspect that was not possible to investigate within the constraints of this work.

4.2.4 Concluding Remarks

The use of thermal characterisation methods such as DSC or MDSC was not sufficient to define the temperature required for the AFP deposition process. Characteristics such as T_g and T_m were not suitable to inform the temperature requirement directly. The definition of process parameters had to be defined experimentally for reliable results.

Material A reached the target V_f with a broad spectrum of parameters, making it the most robust material out of the options. This confirmed the selection of the material based on manufacturability, determined in Chapter 3. Changes in deposition temperature caused the widest spread of preform V_f results for all materials, followed by speed and compaction pressure, which affected the preform V_f less. Changes in thermal history due to heat zone length did not have a significant effect. A limitation of the conducted testing is the effect of interactions of the variables, which is partially limited by the coupling of variables.

Only two materials achieved the target preform V_f of 50-55% during the conducted tests. The range each process parameter in which the goal was achieved was outlined for these materials. These two materials (A and B) had a high degree of similarity; both materials contained epoxy-based binder distributed within the tape. This differed significantly from the other tested materials with

thermoplastic-based binder on the tape surface. Binder type and distribution are likely determining the material performance.

Comparing the resulting preform V_f of UD strips with the preform V_f of available bi- and multiaxial preform panels confirmed that the results were transferable. The strips and panels were selected for comparison if deposition temperature was similar and showed a good agreement across all materials. The result showed that UD strips enabled testing with low material consumption and relatively short timeframes. Small-scale tests reliably informed the process definition for expensive and large parts, reducing lengthy trial and error efforts significantly.

The in-depth comparison of the response behaviour of the different dry fibre materials towards process parameter changes showed some trends. A parabolic function was a good fit to describe material behaviour towards increase of laser power of most materials. The turning point at which the preform V_f increasing effect of laser power begins decrease was not determined due to experimental constraints. Material A was the only material that follows a linear trend within the range of 50-55% preform V_f. The effect of deposition speed on preform V_f can be described with a decreasing power law across all tested materials but the effect of Material A was not significant as the preform V_f showed minimal responsiveness to speed. The counter-intuitive trend of preform V_f decrease at increasing compaction pressure as described in previous work for Material D was confirmed for all tested dry fibre materials. This knowledge could be used to improve the process definition in the future based on desired preform V_f.

This section successfully applied a rapid process definition method based on small scale testing suitable to inform process parameters for larger components. A set of material specific parameters was defined for optimised preform manufacture using the most suitable Material A.

4.3 Manufacturing Variability Induced by Thickness

The process was scaled up to determine the preform variability in parts more complex as well as the applicability of the found parameters (section 4.2) to a manufacturing environment. In order to do so, flat, quasi-isotropic preforms were manufactured with a high ply number, one of which was including a thickness change. This sub-chapter aims to:

(1) Evaluate the applicability of AFP process parameters defined on a coupon level to preforms with high material thickness and a thickness change within the preform by comparing the resulting preform V_f.
(2) Identify aspects preventing direct transferability and propose adjustments of process parameters to achieve the target preform V_f.

(3) Determine the impact of the starting location for the end effector movement to deposit tapes on the preform quality by assessing the impact on preform V_f.

4.3.1 Materials and Experimental Method

Material A was used as recommended in Chapter 3 for the assessment of scalability. The recommended AFP machine parameters determined in the previous section were followed. The deposition temperature was above 200 °C (initially at 220 °C), the compaction pressure was kept at the lower level with 0.47 N/mm^2 achieved using the silicone roller. The laser optics chosen had a nominal spot size of 8 × 57 mm and the deposition speed was set to the maximum achievable speed within the constraints of the machine movement.

The ply book for the thick preform was set out to be as close as possible to QI, with $[[(45, 135, 0, 90)_{12}$ 45, 135]$_s$]$_4$, leading to a nominal thickness of 800 mm. Due to experimental constraints, the first 133 plies of this ply book constitute the first trial and plies 134 to 400 constitute the second trial. This split results in some differences of the ply book between these trials, but the ply direction did not affect the preform V_f as long as the process parameters were constant, refer back to Figure 4-4. The deposition of thick parts required a support structure around the preform for the approaching roller. Self-adhesive cork with a 2 mm thickness (AK Rubber & Industrial Supplies Ltd, Bishop's Stortford, UK) was added around the perimeter of the preform every 19 plies or when needed.

An effect of the feeding mechanism on the preform quality has already been reported by Di Francesco [202]. Material D exhibits in-plane waviness in the area of the feeding operation as shown in Figure 4-13 (a). This occurs likely due to the material approaching the substrate perpendicularly, and buckling when hitting the surface of the tool; see Figure 4-13 (b). This was not observed at the end of a ply during the cutting operation.

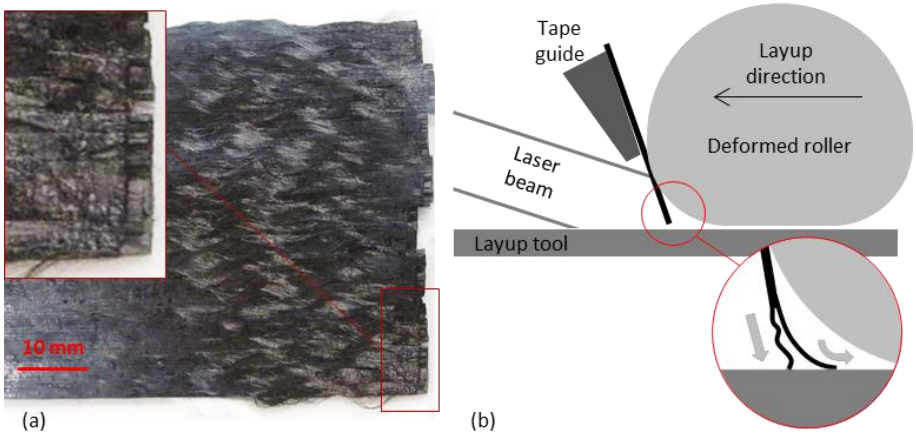

Figure 4-13: Wrinkled underside surface of a single course of eight tapes manufactured using Material D with detail image (a) and hypothesised wrinkles formation mechanism (b) [202]

Material A did not exhibit any visible in-plane fibre distortion as Material D. To assess the potential impact of the tape feeding operation on Material A, two preforms were manufactured using different fibre path programs. The difference in the two preforms was the feed direction, as outlined in Figure 4-14. The machine program for the first preform had one deposition direction for the 45 °, 90 ° and 135 ° plies and two deposition directions for the 0 ° plies. The second machine program doubles each deposition direction for each ply, increasing the number of edges on which fibre feeding occurs, and decreasing the number of repeated machine movements.

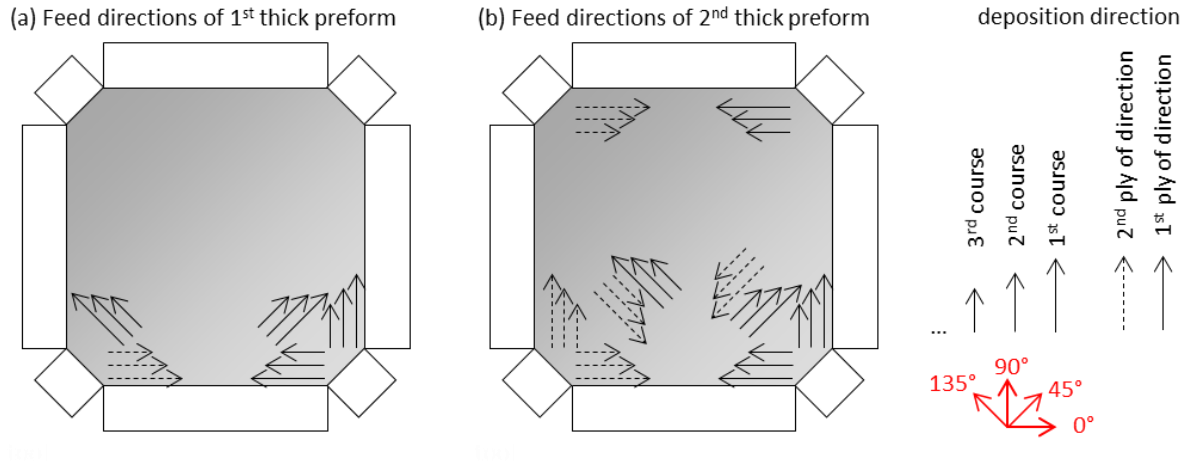

Figure 4-14: Feed direction of the different fibre path program used for the manufacture of the first preform (a) and the second preform (b)

The preform containing the ramp was manufactured on a flat tool, building up a thicker area on one-half and a thinner area on the other. The first ply was flat and the top ply results in a 1:5 ramp. The ply book contains three sections with continuous plies over the entire preform area (skin plies) and two distinct wedge packs (wedge pack plies) that were gradually shorter to create a ramp as shown in Figure 4-15.

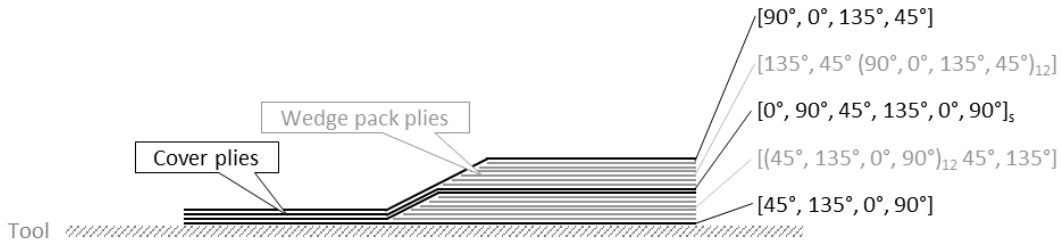

Figure 4-15: Laminate design of ramp panel (cross sectional view, not to scale) including ply book

The thickness was measured using the laser line scanner and the measurements were converted into preform V_f using Equation 3-1. Surface topography mapping was completed in the previously mentioned metrology software PolyWorks, using an in-built colour-mapping tool, which indicates height from a specified reference by colour. Only the relevant areas were regarded, e.g. edge effects

were not captured. All areas were at least 25 mm from a feature (e.g. beginning of a ramp) or the outer edge. The same approach was taken for the thick section, only the central area of the part was measured, 25 mm on each edge were disregarded.

4.3.2 Results and Discussion

Two attempts of the thick section and the ramp section were documented, a first trial failed to deliver uniform preform V_f, but the second trial was successful. In the first attempt of the thick section, ply 1-133 was deposited. In the second attempt, the deposition was continued from ply 134 to 400 on a new tool, making ply 134 the first ply of the second attempt. This solution was chosen as it provided the option to stack the two panels on top of each other to a full 400-ply panel, time constraints and material availability did not allow starting at the first ply for the second attempt.

The preform thickness was measured at least every 19 plies (3.8 mm) throughout the deposition in order to determine the preform V_f at stages throughout the manufacture of the preform. The first trial shows a gradual decline of preform V_f below the target preform V_f and was aborted after 26.6 mm (nominal thickness), Figure 4-16 (a). This gradual decline suggests that a slight initial distortion led to a slightly more compliant preform, which then can lead to slight excess length in a ply, which continues to get worse with every additional ply. This is an effect previously observed on prepreg materials [128]. During the deposition of the first trial, the increase of temperature was beneficial for a higher quality result based on visual assessment of incremental change during the trial, and the power curve for a nominal 260 °C on the intermediate range of the tested temperatures was applied for the remaining tests, see Figure 4-16 (b). The second attempt at elevated temperature throughout showed a consistent preform V_f of 51.4 ± 0.7 % (2 SD).

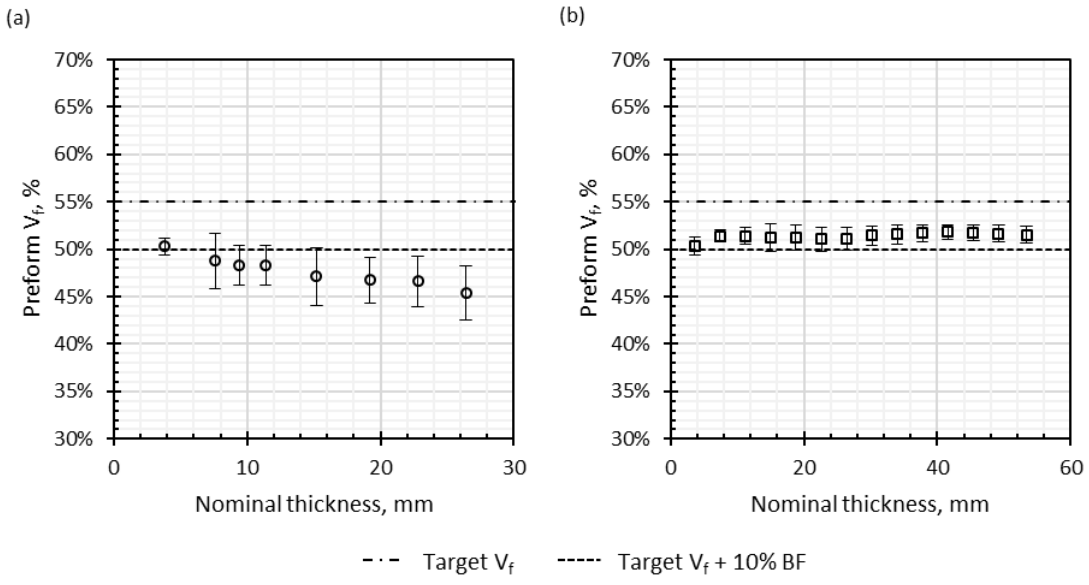

Figure 4-16: Preform V_f through the thickness for thick panels at target temperature 220 °C (a) and target temperature 260 °C (b)

The reduction of preform V_f caused by lifting of the plies from the bulk and the distortion on the surface (leading to a larger error bar) was visible in the photographs. The thickness measurements were used to generate a colour plot to indicate the height distribution to amplify the visually visible distortion on the surface as shown in Figure 4-17 (a). The metrology software has an in-built colour-plotting tool, which uses the height information of the gathered data against a reference, in this instance flat tool; see Figure 4-17 (b).

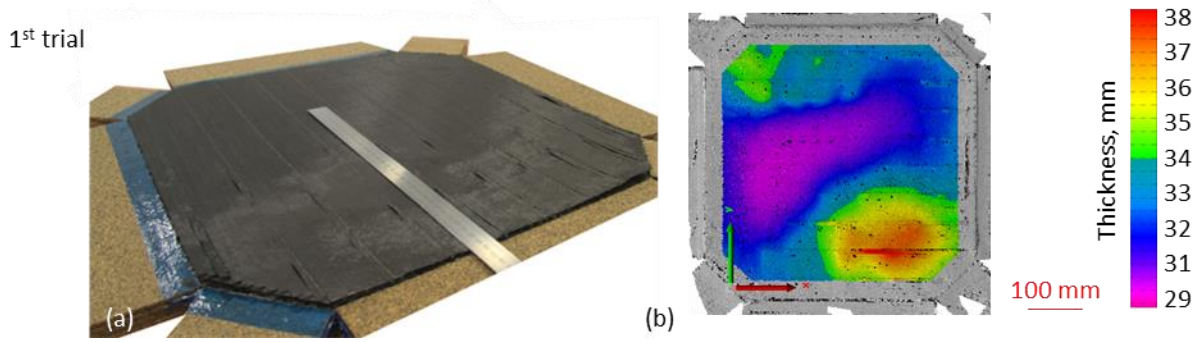

Figure 4-17: Nominally 26.6 mm with visible distortion on the surface of the 1st trial (a); colour plot generated in metrology software of the panel in the photo above (b)

The successful second trial can be seen in Figure 4-18 (a). These coloured height plots furthermore support this improvement (b). The second trial with an increase of feed direction and an increased temperature was stable at 51.4 ± 0.7 % (2 SD) preform V_f throughout the deposition of a panel of 53.4 mm thickness, see Figure 4-16, squares and Figure 4-18 (a) and (b).

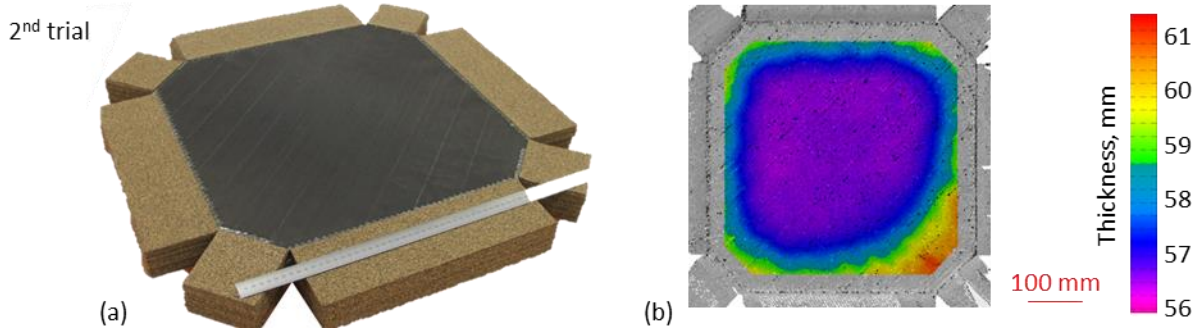

Figure 4-18: Nominally 53.4 mm with visible distortion on the surface of the 2nd trial (a); colour plot generated in metrology software of the panel in the photo above (b)

To introduce further complexity, a panel with variable thickness was manufactured twice. In both cases of the thick ramp panel, all 120 plies were deposited at 260 °C. The first trial (Figure 4-19 (1)) resulted in a highly variable preform with visible distortions. In order to mitigate this issue, the deposition pressure was reduced from nominally 0.47 N/mm^2 to 0.43 N/mm^2 (355 N), resulting in a uniform preform (see Figure 4-19), within the target preform V_f.

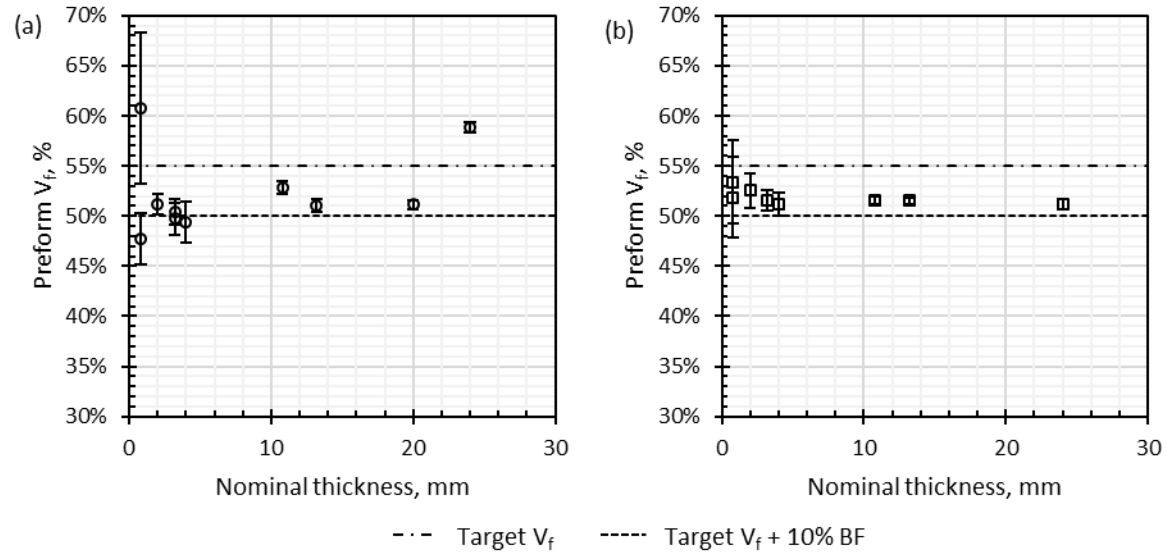

Figure 4-19: Preform V_f through the thickness for thick ramp panels at 0.47 N/mm^2 (a) and at 0.43 N/mm^2 (b)

This result indicates that with increasing complexity, the AFP processing parameters require additional fine-tuning. The coupon level trials were suitable for some scaling (e.g. thin L-shaped part), but do not capture all requirements for the definition of processing parameters for complex parts with consistently high preform V_f. Potential reasons for the differences between simple and complex parts could be the repetitive movements and therefore continuous mechanical strain on the preform, for example an in-plane shear due to a slight mismatch in the timing between material feed and robotic movement. As the temperature did not penetrate far through the ply stack, there is no opportunity to resurrect plies detached due to the movements. Especially on the part with the thickness change, the heating area may be changed due to the out-of-plane movement, affecting the consistency of the processing condition. The interaction between the timing of the incoming tape feed, the moment the laser switches on, the feed speed and acceleration of the end effector, the repetitive movement and the height of the surrounding support material are unknown. In addition, the interaction of compaction pressure and nip-point temperature require better definition in order to understand the different process parameter requirements of simple and complex parts.

4.3.3 Concluding Remarks

The applicability of the previously defined parameters was tested by increasing the complexity of the manufactured part. Firstly, the thickness was increased to investigate any potential influence of repetition. Secondly, thickness change within the part was introduced. The applicability of the previously found parameters was limited, and the preform V_f decreased when using the previously defined AFP parameters.

Knowledge about the impact of AFP parameter change on preform V_f gathered in the previous section informed the adjustment of the parameters to achieve the target preform V_f of 50 – 55 %. The apparent deposition temperature was increased by 40° C and the compaction pressure was decreased by 0.04 N/mm^2 to achieve a preform V_f of 51.4 ± 0.7 % (thick) and 51.9 ± 1.5 % (thickness change). Laser spot size and deposition speed were verified to be transferable without adjustments. The main distortion of the preform occurred around the edge where the feeding operation took place. The coupon testing did not capture the behaviour of the preform during the feeding operation.

This highlighted the importance of the program strategy to mitigate the effect of feeding edge distortion. The distribution of tape feeding operations around the preform resulted in fewer feeding operations per edge and was beneficial to preform quality. This indicates that a high number of repetitions of the machine movement had a negative effect on the preform quality than fewer repeats. The root cause of the interaction between the various named factors during the feeding operation requires better understanding to mitigate the effect.

4.4 Manufacturing Variability Induced by Steered Fibre Paths

The main challenge of steering any ribbon in plane, is that additional length on the inner and outer edge of the ribbon has to be accommodated. This is the case regardless of the width and composition of a ribbon, it applies to a single tape as well as a full course of 8 tapes. For the purpose of this work, steered fibre paths contain eight parallel tapes The reason they must be treated like one wide tape is that all tapes are deposited using one roller with a continuous width, causing the same length to be dispensed for all tapes across the width of the roller. This results in a length discrepancy between the inner and outer edges of the course when steering. Within each tape, there is also a discrepancy between inner and outer edge. The inner edge has a shorter and the outer edge a longer length in comparison to the centre radius, which is compensated by wrinkles and tape pull up. The arc length l is defined as $l = R\,\alpha$, with the radius R and the angle in radians α. A schematic of the steered course is shown in Figure 4-20.

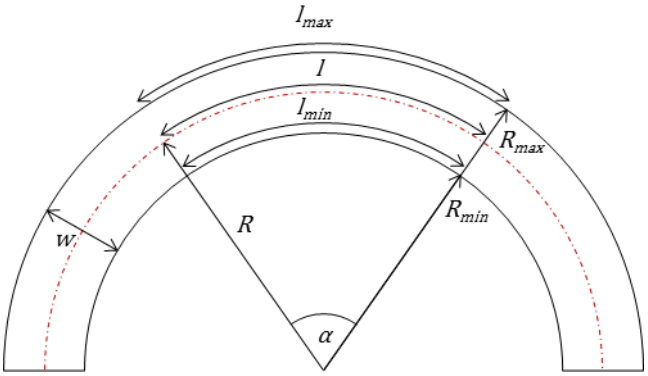

Figure 4-20: Schematic of a course with a steered fibre path

Therefore, the absolute arc length of the inner and outer course edge are defined as $l_{min} = (R - {}^{w}/_{2})\,\alpha$ and $l_{max} = (R + {}^{w}/_{2})\,\alpha$, respectively, using the course width w_c. The length difference between the inner or outer radius and the centre radius $\Delta l = |l - l_{min}|$ can be expressed as

$$\frac{\Delta l}{l} = \frac{R\alpha - \left(R - \frac{w}{2}\right)\alpha}{R\alpha} \qquad \textit{Equation 4-2}$$

and then simplified to

$$\frac{\Delta l}{l} = \frac{w}{2R} \qquad \textit{Equation 4-3}$$

This equation describes the additional length of material that has to be accommodated within the steered path independent of steered path length. This relationship gives an indication of wrinkle severity, as a higher length difference leads to larger or more frequent wrinkles.

The determination of a minimum steering radius is an important input to the design process; however, it is not a fully defined term. According to [224], it is defined as "*(…) a lower limit to the radius that it [the tape] can be persuaded to follow, without causing wrinkles or puckers*". This needs to be redefined, as any radius will cause a fibre distortion leading to wrinkles, dictated by the length differential between inner and outer edge of the tape in regards to its radius [135]. For the purpose of this work, it shall be redefined as *"lower limit radius at which a tape of specified width and material generates wrinkles small enough to be negligible or acceptable for the purpose of its application"*. In other words, the minimum steering radius is a parameter that either does not create features large enough that they need to be accounted for in the design of the part or has a known impact that has been accounted for.

The need for an understanding of the correlation between steering radius and laminate quality was established in section 2.4.1. In particular, to exploit the full potential of the ability to tailor fibre paths to the component requirements, a minimum steering radius is an important input to AFP fibre paths programming software. Visual inspection is accepted to be sufficient for prepreg material to

determine the minimum steering radius, but some dry fibre materials cause a gradual change in wrinkling without a distinct transition to clearly indicate failure to pass visual inspection [134], [145], [153]. In order to determine the minimum steering radius without reliable visual observation and judgment, a metric is needed. Therefore, the first challenge was to establish a reliable measurement method of wrinkles as an output of the AFP deposition. A quality metric does not only aid in determining a minimum steering radius, it also enables the optimisation of the AFP parameters to achieve the best possible preform quality. A quality metric not only quantifies the output of the AFP process, but also the input to the subsequent infusion process. Only then, deriving rules or recommendations for the programming phase is possible. Available models do not yet capture the complex outcome of the production process [47], [149]. A large variety of prepreg AFP studies have been conducted to model, test and optimise laminates containing steered fibre paths, but these works rarely considering manufacturing aspects of the parts [136], [142], [225]. As neither, an experimental or modelling approach was available, this work was focused only on the development of a quality metric to define the input to establish a relationship between steering and laminate quality, as well as assessing some AFP deposition variables.

Different methods for the quantification of steering quality were considered and compared. The three methods investigated, the first method (preform V_f) was used as part of this work for preform characterisation (refer to section 4.1), the other two proposed methods were based on 3D surface roughness. These metrics were well established in the field of surface metrology [226]–[229]. Generally, some form of digital surface representation was needed, and a variety of metrics can be derived from this data, for example following ISO 25178 [230], [231]. The limitation of this approach was that only out-of-place wrinkles were captured, however the use of a visual assessment for wrinkle observation was suggesting that it is sufficient to do so. In summary, this chapter aims to:

(1) Assess the wrinkle mitigation of the infusion process to determine the relevance of wrinkle measurement on a preform.
(2) Identify available methods to quantify wrinkle severity and assess methods suitable for the application in the context of ADFP.
(3) Apply the identified method to investigate the impact of ADFP processing parameters and steering radii on the preform using the developed metric.
(4) Assess the potential of lower minimum steering radii fibre path of ADFP in comparison to prepreg based AFP.

4.4.1 Materials and Experimental Method

Preforms with in-plane steering were manufactured and compared to preforms with straight fibre paths but with otherwise identical stacking sequence and ADFP process parameters. This aims to define the difference in preform and laminate V_f between different materials by using global preform thickness, as a way to gage the impact of steering on the laminate. Newly introduced methods were used for the comparison of individual steered paths with variable AFP parameters; to identify the AFP parameters influencing out-of-plane wrinkles the most. One of those methods was also used to compare two different material dry fibre material grades and different steering radii.

Out of five available materials, three were identified as possible materials for AFP manufacture in [90] and Chapter 3, and two out of those were chosen to study in this section. The first material was Material A (Figure 4-21 (a)) which complies with the preform quality requirements. Material D (Figure 4-21 (b)) was chosen as a second material due to its significantly different surface topography. The majority of the tests was carried out using Material D due to material availability at the time. Material A is a slit tape that contains an epoxy binder and a carbon fibre veil on one surface and Material D has a thermoplastic veil on both sides of a tow to act as a binder. The as-supplied tapes exhibit inherent waviness and wrinkles due to their manufacturing process. Even after the deposition, the inherent wrinkles may not be relieved, as shown in Figure 4-21 (a). Internal waviness has been reported for prepreg [148], [232]. Even though prepreg is a different class of material and not all findings are directly transferable, at least partial internal waviness was attributed to storage of the materials on bobbins, which was the case for both material classes. The path difference between the inner and outer surface of the material when wound on a spool or bobbin can create waviness and wrinkles. Therefore, the wrinkles in Material A were likely to be induced by winding the material on a bobbin.

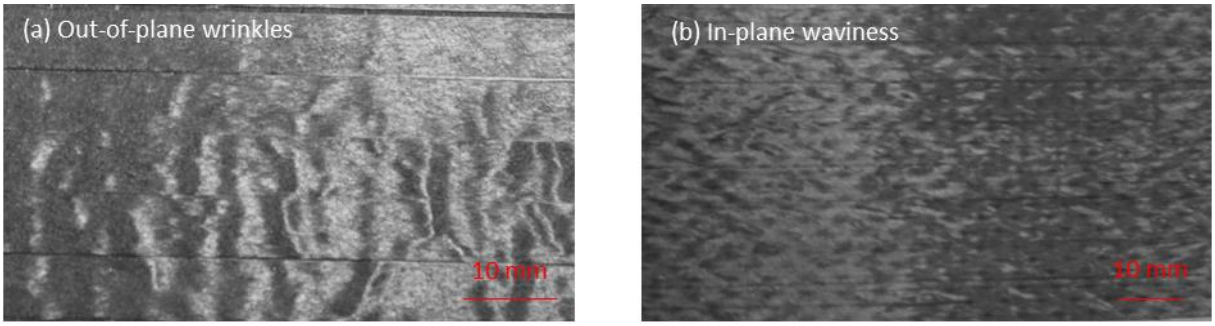

Figure 4-21: Photograph of an as laid nominally straight course with Material A (a); photograph of an as laid nominally straight course with Material D (b)

The structure of a single tape of Material D as supplied with a significant degree of in-plane waviness, in plane between 5° and 15°, some of which may be occurring due to a perforation process that is part

of its production process, see Figure 4-21 (b). The reason for this characteristic manufacturing step is possibly to enhance the material integrity or to improve the through thickness permeability.

The impact of fibre misalignment in composite materials has been studied widely on a macroscopic level, where mostly wrinkles are introduced in a post process, such as forming or curing [233]. The wrinkles often propagate through the thickness of the laminate and the detrimental effect on mechanical properties was quantified [234], [235]. The impact of internal fibre waviness also suggest a large impact on the mechanical properties [148], [236], [237].

Three different types of manufacturing trials were used to capture a variety of cases and enable the investigation of transferability across the different levels of specimen size. Full QI preforms were the largest specimen size, single strips with multiple plies and single ply trials were the smaller specimen sizes tested. This approach was taken in an attempt to cover a range of specimen size possible and to confirm or disprove the applicability of single ply trials to full parts.

Deposition Trials

Four identical steered panels using Material D and one repeat using Material A were manufactured, using variable machine speed, which was set to its maximum capacity. The 600 x 600 mm, 26 plies thick, QI preforms with steered plies were deposited and measured with a laser line scanner (as shown in Figure 4-22). Every ply has the same steering path concept, the fibres were programmed around a central circular cut-out (90 mm diameter) with a fibre path radius of 400 mm in the centre area, fading out towards the edge of the panel to an 800 mm radius. Preforms with identical stacking sequence were deposited with straight courses for comparison for both materials. The centre of the laminate was filled with straight fibres. The machine was programmed to feed and cut the material at 200 mm/s for improved feed and cut accuracy and to accelerate during the deposition to the maximum achievable speed. The maximum gap allowance was 2.5 mm, which has been reported as maximum allowable gap width in the aerospace industry [148]. The manufactured preforms were subsequently infused using a peripheral infusion set-up and an aerospace grade resin (RTM6), infused following the suppliers recommendations [217]. The infusion of the steered laminates was identical and therefore laminates were directly comparable to the flat laminates. Samples of 10 x 25 mm were cut according to XX, then polished using a Buehler EcoMet 300 with and AutoMet 300 Power Head. The microscope used was an Observer Z1M and its complementary software AxioVision Rel. 4.8

(a) (b)

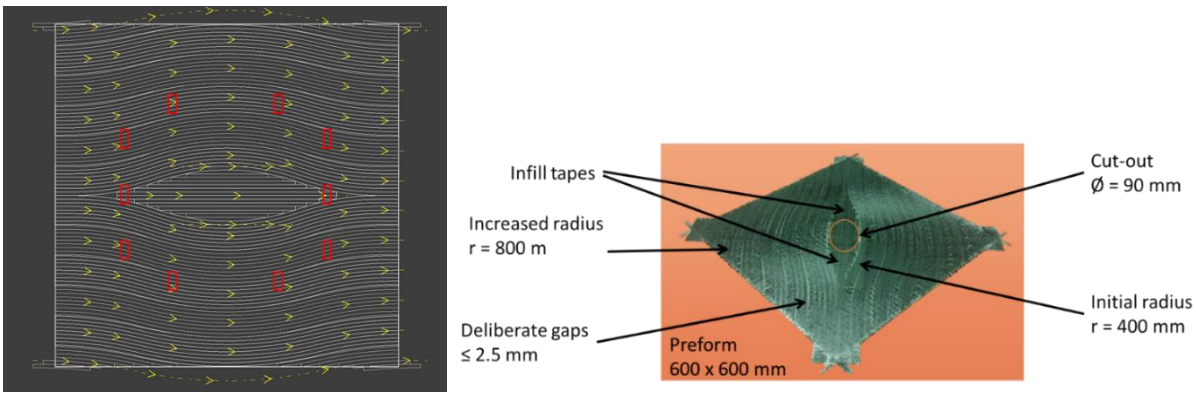

Figure 4-22: Fibre path plan of a 90° ply steering around a central, circular cut-out, where the red rectangles indicate the position of the microscopy samples (a); photo of deposited 45° ply (b); representative for all ply directions

The trials comprised of multiple plies on one single course were used to measure the influence of various AFP parameters. Multiple, individual strips were deposited on a metrology table, each time repeating the strip with the default setting three times to quantify repeatability. Flat, UD test strips using Material D made up of eight tapes and seven plies (50.8 mm wide course) with a radius of 400 mm as default, were deposited using different machine and process parameters (see exemplary test set up in Figure 4-23). The strips were laid up over a Nylon film vacuumed to the surface of a metrology table (Mitutoyo Graplate) with a coated nylon peel ply in between.

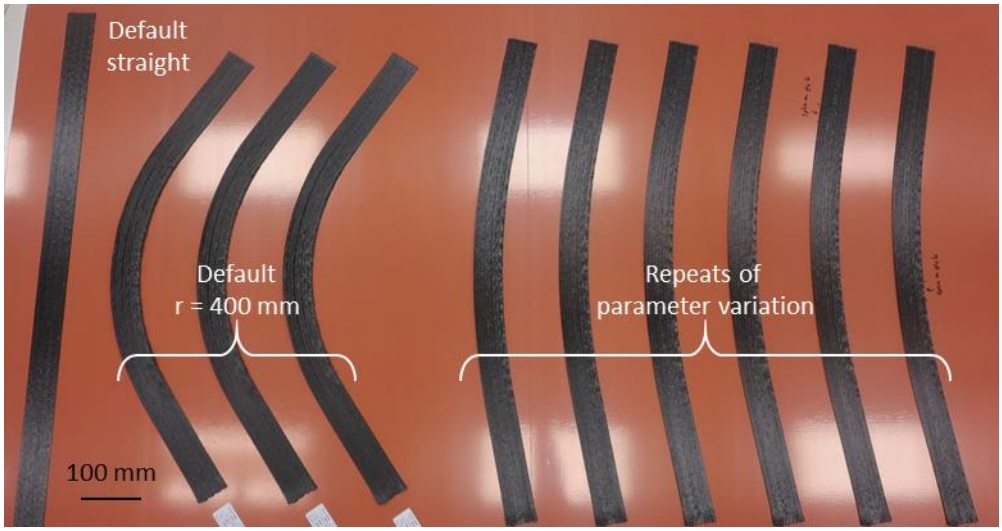

Figure 4-23: Top view of parameter comparison steering trials (default and parameter variation, as an example photograph with a radius variation of 1200 mm

The majority of the varied parameters were already investigated on straight fibre deposition (section 4.1). The hypothesis was that the influence of these parameters on the straight course preform V_f have a similar level of impact in the context of courses with a steered fibre path on the severity of

wrinkles. A high preform V_f and few and low out-of-plane wrinkles are both associated with high preform quality. The most influential AFP parameter in regards to preform V_f was laser power (see section 4.2.4) and was therefore assumed to have the highest impact on steering quality as well. The impact of compaction pressure and deposition speed was of secondary importance. The following manufacturing parameters were investigated by manufacturing the described multi-ply UD strips:

i. Laser power: As the speed of the robot during the steering path was not predefined, a power curve was used calculated for the default 230 °C, the variation was a power curve aimed at 200 °C (see Table 4-8).
ii. Compaction pressure: The default nominal compaction pressure was 0.47 N/mm^2 (achieved by a force of 449 N) achieved with the silicone roller. This was at the lower end of the range of the machine capability and its variation was 0.86 N/mm^2 (achieved by a force of 1017 N) at the higher end of the range that the machine can deliver. The foam roller, was used at the same two nominal forces, resulting in a lower (0.32 N/mm^2) and intermediate (0.53 N/mm^2) compaction pressure.
iii. Deposition speed: The default speed used was 200 mm/s, which was the highest speed that was possible at a radius of 400 mm at constant speed due to the constraints of the robotic movements, determined experimentally. The variation was 100 mm/s.
iv. Steering radius: The default radius used in these trials was 400 mm and 1200 mm as variation.
v. Steered length: The arc length of the steered radius was 471 mm at a 400 mm radius; the variation was reduced by 80% of that length, with a resulting arc length of 94 mm.

Table 4-8: Values of power curves used in steering trials for Material D

ID		***Pc1***	***Pc2***
Target temperature		**230°C**	**200°C**
Point	**Speed, m/s**	**Power, W**	**Power, W**
1	0.00	32	32
2	0.10	54	49
3	0.13	70	61
4	0.18	97	82
5	0.25	144	119
6	0.35	225	184
7	0.50	362	295
8	0.71	599	489
9	1.00	834	683
10	2.00	834	683

The two default configurations had the same manufacturing configuration, one of them was a straight strip (baseline representing straight UD strips, ideal case without a radius) and one had the default

radius of 400 mm (used as a comparison to the variable variation), see all tested variations in Table 4-9.

Table 4-9: Different tested configurations for parameter comparison trials (variation from default (italic) is underlined)

ID	Radius, mm	Speed, mm/s	Laser power, W	Arc length, mm	Pressure, N/mm² (2 SD)	Roller type
Default	∞	*200*	*Pc 1*	*471*	*0.47 ± 0.14*	*Silicone*
Default	*400*	*200*	*Pc 1*	*471*	*0.47 ± 0.14*	*Silicone*
Test 1	1200	200	Pc 1	471	0.47 ± 0.14	Silicone
Test 2	400	200	Pc 1	94	0.47 ± 0.14	Silicone
Test 3	400	100	Pc 1	471	0.47 ± 0.14	Silicone
Test 4	400	200	Pc 2	471	0.47 ± 0.14	Silicone
Test 5	400	200	Pc 1	471	0.32 ± 0.14	Foam
Test 6	400	200	Pc 1	471	0.53 ± 0.07	Foam
Test 7	400	200	Pc 1	471	0.86 ± 0.08	Silicone

Further tests investigated the material behaviour at a larger variety of radii. The test set-up was a combination of steered fibre path with different radii as a single ply deposition onto a substrate. Three straight biaxial plies serve as a substrate to avoid first ply adhesion influences. The fourth ply was comprised of steered fibre paths as shown in Figure 4-24.

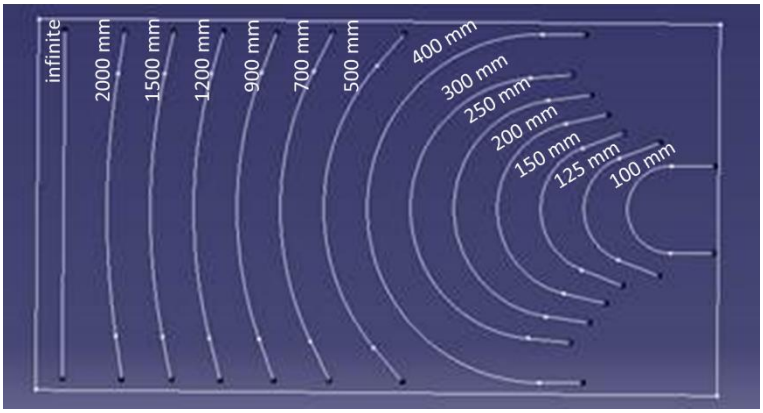

Figure 4-24: Test set up for multi-radii steering (centre line of each course displayed only)

Different radii were tested for Material D with one target temperature 230°C and Material A with a target temperature of 280°C. Both materials were deposited at a compaction pressure of 0.47 N/mm^2. The deposition speed was programmed to reach its machine capacity maximum; the speed variation was consistent across the different trials as the same machine program was used for all tests.

Table 4-10: Power curves for materials A and D including target temperatures (Power curve for Material D is identical with Pc1 from Table 4-8)

Material		***A***	***D***
Target temperature		**280°C**	**230°C**
Point	**Speed, m/s**	**Power, W**	**Power, W**
1	0.00	3	32
2	0.01	89	54
3	0.02	134	70
4	0.04	203	97
5	0.08	307	144
6	0.16	467	225
7	0.32	710	362
8	0.64	1081	599
9	1.00	1417	834
10	2.00	2160	834

Surface Measurement and Data Treatment

The surface of the as deposited preforms was captured using a laser line scanner to enable analysis of the thickness in a separate step. The preforms were scanned directly after deposition and the thickness was determined using the metrology software PolyWorks. The exported thickness data was used to calculate preform V_f using Equation 3-1. The measurement area for the steered panels was limited to a central circle with a diameter of 500 mm and a 90 mm cut out in the centre. The central, circular cut-out area only contains straight fibres and therefore no steering. For comparison, preforms with straight courses were measured on a central 500 x 500 mm area, all exemplary shown in Figure 4-25.

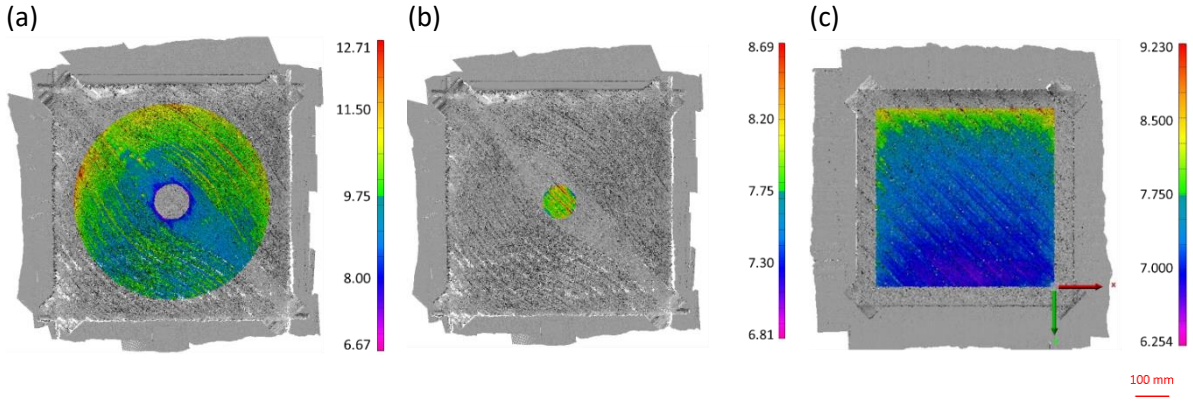

Figure 4-25: Steering panel with outer measurement area (Ø = 500 mm (a); steering panel with inner measurement area (Ø = 90 mm) (b); measurement area on panel with straight courses only (c)

The same data capture method was used for the single course trials (multiple and single ply), but the data was used in a different way. The data collected in the form of point clouds (x, y, z coordinates) was exported from PolyWorks after alignment for further processing.

There is a wide variety of 3D surface parameters available, which have been developed over the last ~ 40 years. The most common 3D surface parameters to assess 3D surfaces are described in ISO 4288, ISO 25178 and EUR 15178N [227], out of which the most frequently used parameters maximum height (Sz), maximum peak height (Sp) and maximum valley depth (Sv). These metrics are all dependent on the minima and maxima in the dataset. As this makes the calculation of these parameters highly dependent on a single value, outliers can alter the assessment significantly, and therefore these parameters were not suitable for the purpose of this work. Other frequently used parameters are average roughness (Sa, see Figure 4-26 (a)) and root mean square roughness (Sq). These parameters considered the entire dataset and were suitable to assess the steered paths; however, they do not capture either wrinkle heights or width. Kurtosis (Figure 4-26 (b)) and skewness (Figure 4-26 (c)) of the dataset can also be assessed, which may provide additional insights [238]–[240].

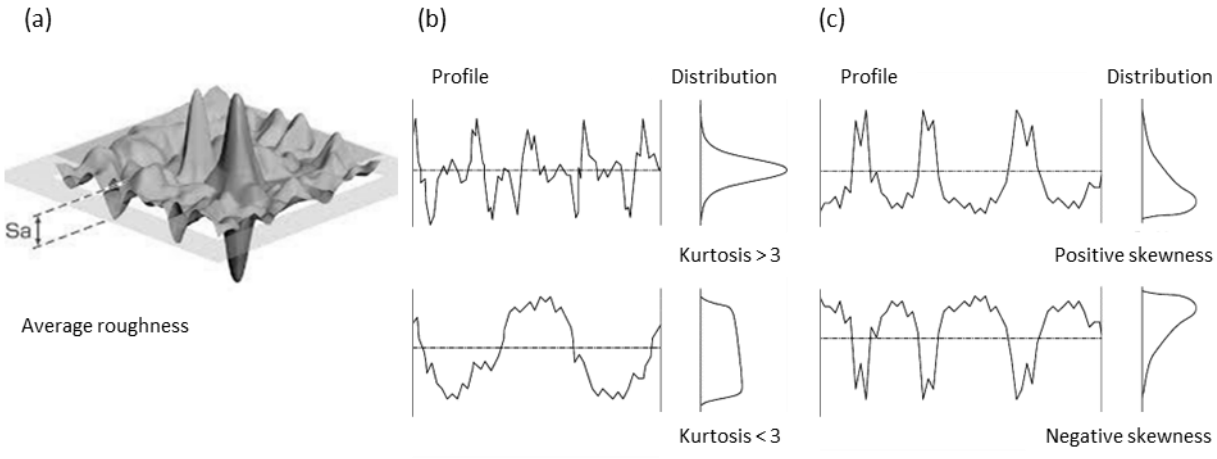

Figure 4-26: Graphical explanation of average roughness Sa (a) [241]*; kurtosis (b)* [238] *and skewness (c)* [238]

The different parameters shown in Figure 4-26 (a – c)can also be expressed using Equation 4-4, Equation 4-5 and Equation 4-6, where $\bar{f}$ is the height of the mean plane and L_1 and L_2 are the extent of the sample, $f(x,y)$ is the surface height at x,y [242].

$$S_a = \frac{1}{L_1 L_2} \int_0^{L_1} \int_0^{L_2} \left| f(x,y) - \bar{f} \right| dx\, dy \qquad \textit{Equation 4-4}$$

$$S_{sk} = \frac{1}{L_1 L_2 S_q^3} \int_0^{L_1} \int_0^{L_2} \left(f(x,y) - \bar{f} \right)^3 dx\, dy \qquad \text{Equation 4-5}$$

$$S_{ku} = \frac{1}{L_1 L_2 S_q^4} \int_0^{L_1} \int_0^{L_2} \left(f(x,y) - \bar{f} \right)^4 dx\, dy \qquad \text{Equation 4-6}$$

Functional parameters based on a digital surface representation which describes the surface in a more detailed way by assessing material and void volume in the peaks and valleys. This evaluation is in accordance with ISO 25178 Geometrical product specifications [230]. The calculations to determine Peak and Valley Volume (V_p and V_v) are carried out using an Abbott-Firestone curve (also called bearing curve), a two dimensional representation of the surface [239], [243]. This conversion of the data points was carried out with a Matlab routine. Within the code, the point cloud was transferred into a matrix compatible form by dividing the area of measurement into a grid (grid area 0.15 x 0.15 mm). The grid size was determined by convergence of the results to less than 1% change, a single grid area contains one or two data points on average. Illustrated in Figure 4-27, the gridded surface was assessed at the height of each data point, and the area of the intersection as a percentage of the total area was plotted against the height of the queried point. This was then displayed in a graph and the integration of these curves gives peak volume V_p and void volume V_v. The integration of the area under the curves (V_p for the peaks and V_v for the valleys) results in the cumulative volume of the peaks and valleys. For comparability, this volume was then converted to a volume per unit area (ml/mm^2). This Matlab routine was verified using a COTS software (provided by InfiniteFocus, Alicona, Austria), which works according to the same standard. The results showed good agreement.

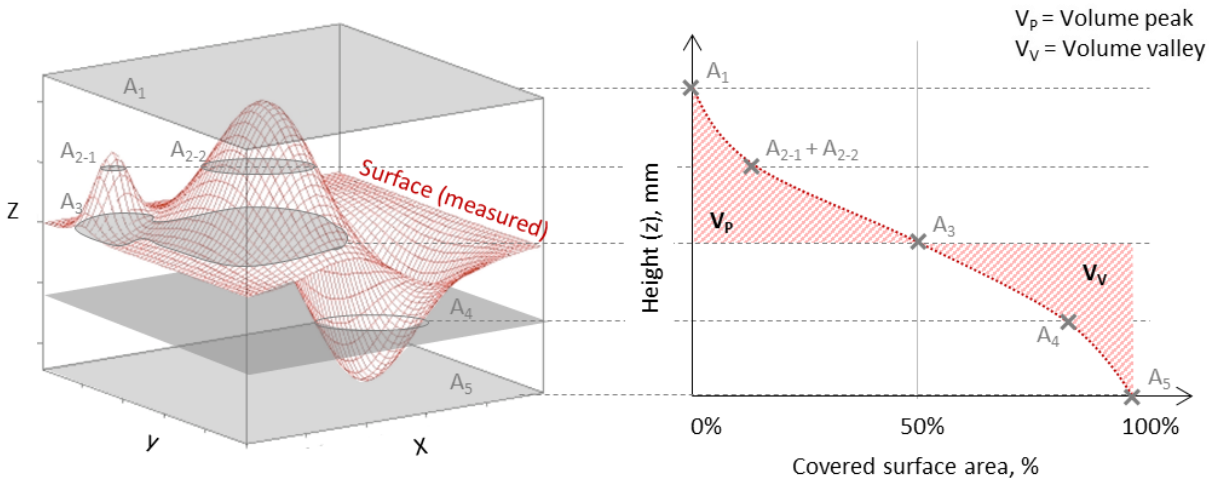

Figure 4-27: Schematic describing the derivation of the parameter peak volume V_p and valley volume V_v (left: measured surface; right: bearing curve and derived parameters)

Surface features (primary profile, roughness, waviness) were not filtered in this instance; the method was applied directly to the collected data under the assumption that there was no primary profile present due to the deposition on a nominally flat granite table. The output was the volume of the peaks (bulge of a wrinkle) and valleys (trough of a wrinkle), where the transition was at the mean value of minima and maxima. By using this metric, skewness and wrinkle severity of wrinkles were captured in one metric. Therefore, V_p and V_v were better suited for the analysis than the individual parameters Sa, Sq, Skewness and Kurtosis.

Prior to the implementation of the technique, a test was carried out to determine the impact of quantity of measurement points on the sum of V_p and V_v. Point clouds collected when scanning nominally flat panels (700 x750 mm, 26 plies) using Material A were used for the analysis. The dataset was randomly divided into smaller sub-sets to investigate the impact of point quantity per measurement. The data from one single panel was halved until each data set was split into 256 parts, resulting in a smaller area analysed at a time. Figure 4-28 shows the development of the error bars (minimum and maximum data point in respective data set). Furthermore, the repeatability and reproducibility of the measurement method was determined by following the same routine for a second scan of the same panel as well as a second panel that was nominally identical.

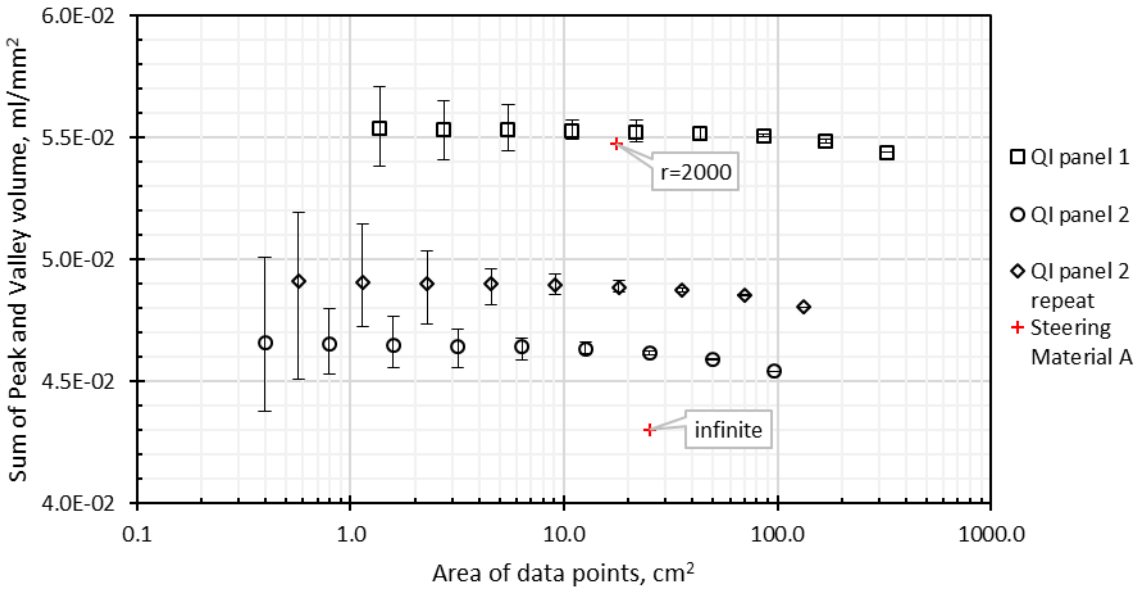

Figure 4-28: Assessment of measurement technique using 3D surface roughness using point clouds captured using a laser line scanner

The data shows that the repeated scan of the same preform twice (repeatability) results in an average discrepancy of 0.003 ml/mm^2. The discrepancy of the results of different preforms (reproducibility) was up to 0.009 ml/mm^2, which was the combined error of manufacturing and measurement including the set-up of the laser line scanner. To put this into perspective, the difference between a straight path and a steered path manufactured with the same material (r = 2000 mm) was 0.012 ml/mm^2. Consequently, unless the measurement method is improved, comparing datasets unless they were manufactured and scanned in one session may not give reliable results. For the purpose of this work, the reproducibility was excluded by determining a correction factor based on the straight default UD strip that was part of every test, manufactured with identical parameters. The factor required to adjust all measured default values to the maximum value measured determines the shift of the remaining data points, this calibration procedure was applied to all data sets.

The single course steering trials were additionally inspected using visual assessment for comparison. The criterion to pass visual inspection in this instance was the absence of fold on the outer side of a tape (refer to Table 2-4,.10).

4.4.2 Results and Discussion

Visual Assessment of Steering Trials

The multiple ply manufacturing was only partially successful. The paths were deposited directly onto the vacuum bag. The tension of the outer tapes in the steered paths lead to a separation of the tapes from the substrate, see Figure 4-29. In order to avoid the capture of such effects, only the inner 16 mm of the tape was taken into account for any further processing. All wrinkles were visibly amplified with every additional ply.

Figure 4-29: Partially unsuccessful manufacture of multiple radii trial carried out with Material D

The multiple radii manufacturing was successfully completed with the outlined parameters, exemplary shown in Figure 4-30, more details in Figure 4-31. A three ply, bi-axial substrate was used to ensure adhesion of the steered path. The visual assessment was used as an input for the design of the steered panels. Furthermore, the visual assessment will be compared to the approach of determining 3D surface roughness to check if the methodology can replace visual inspection.

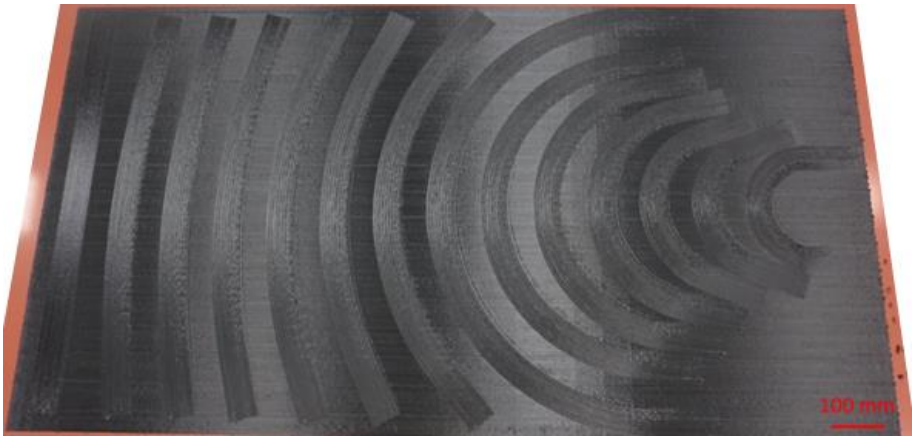

Figure 4-30: Successful manufacture of multiple radii trial, photo of Material D

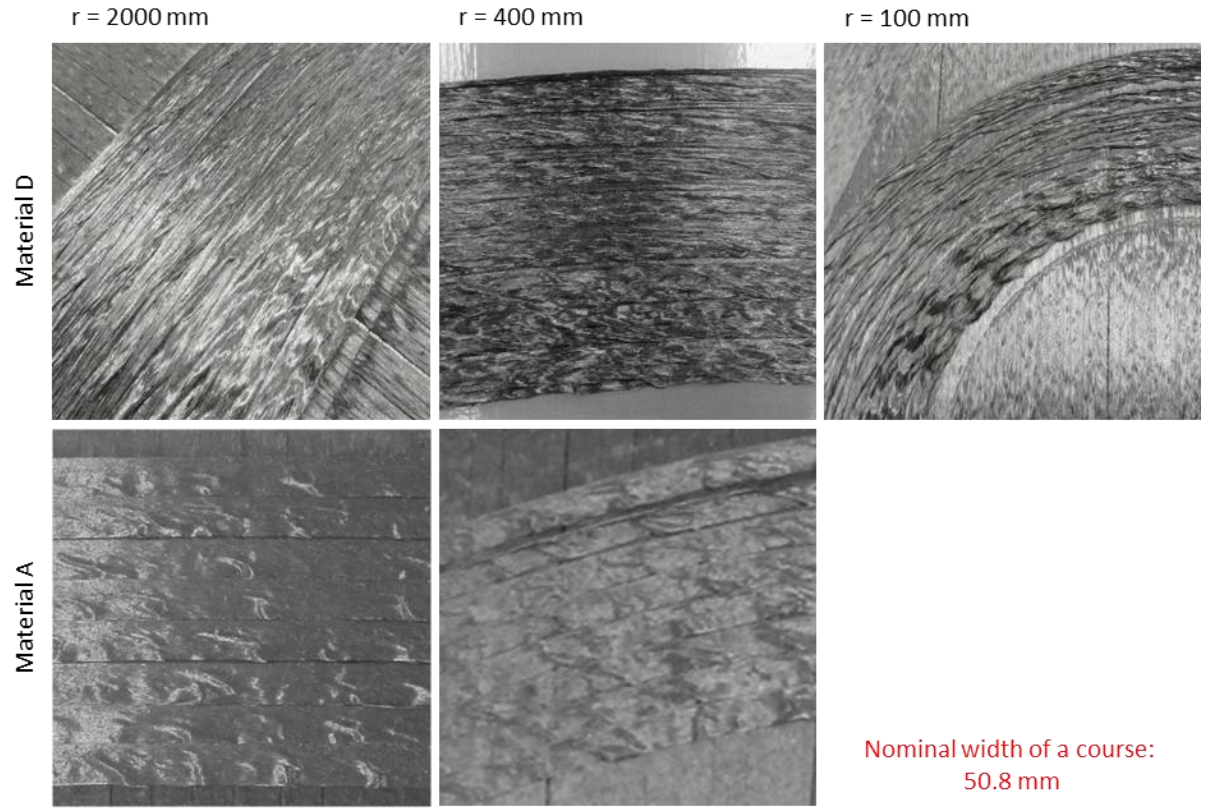

Figure 4-31: Detailed images of courses with different radii for Material A and D

Visually, the failure of steering radii at different deposition temperatures for Material A and D was assessed. Material D did not fail up to 100 mm according to the criterion (existence of a fold over, Table 2-4, 10), outlined (see Figure 4-31), wrinkling on the inner sides of the tapes were severe, but do not exhibit a fold over. A gradual increase of severity of the wrinkle heights was visually observable. Results for visual assessment of Material A was shown in Table 4-11, whereby the minimum radius possible to deposit was 700 mm at elevated temperatures. The use of 900 mm as minimum radius was advised for further trials based on the results.

Table 4-11: Results of visual assessment of Material A at different deposition temperatures

Radius, mm	**220 °C**	**240 °C**	**260 °C**	**280 °C**	**300 °C**	**320 °C**
straight	pass	pass	pass	pass	pass	pass
2000	fail	pass	pass	pass	pass	pass
1500	fail	pass	pass	pass	pass	pass
1200	fail	fail	pass	pass	pass	pass
900	fail	fail	pass	pass	pass	pass
700	fail	fail	fail	fail*	pass	pass
500	fail	fail	fail	fail	fail	fail

* Initially a pass, relaxation overnight caused fail

These visual observations informed the definition of the minimal steering radii for the manufacture of preforms with steered fibre paths.

Thickness and Fibre Volume Fraction of Steering Panels

The micrographs of laminates manufactured with Material D in straight and steered (r = 400 mm) fibre path configuration are shown in in Figure 4-32. It was clearly visible in the micrographs that the fibres were distorted throughout the laminate. The steered panel had numerus inconsistencies, folds, wrinkles and waviness; this shows that wrinkles induced in the preform will persist in the laminate.

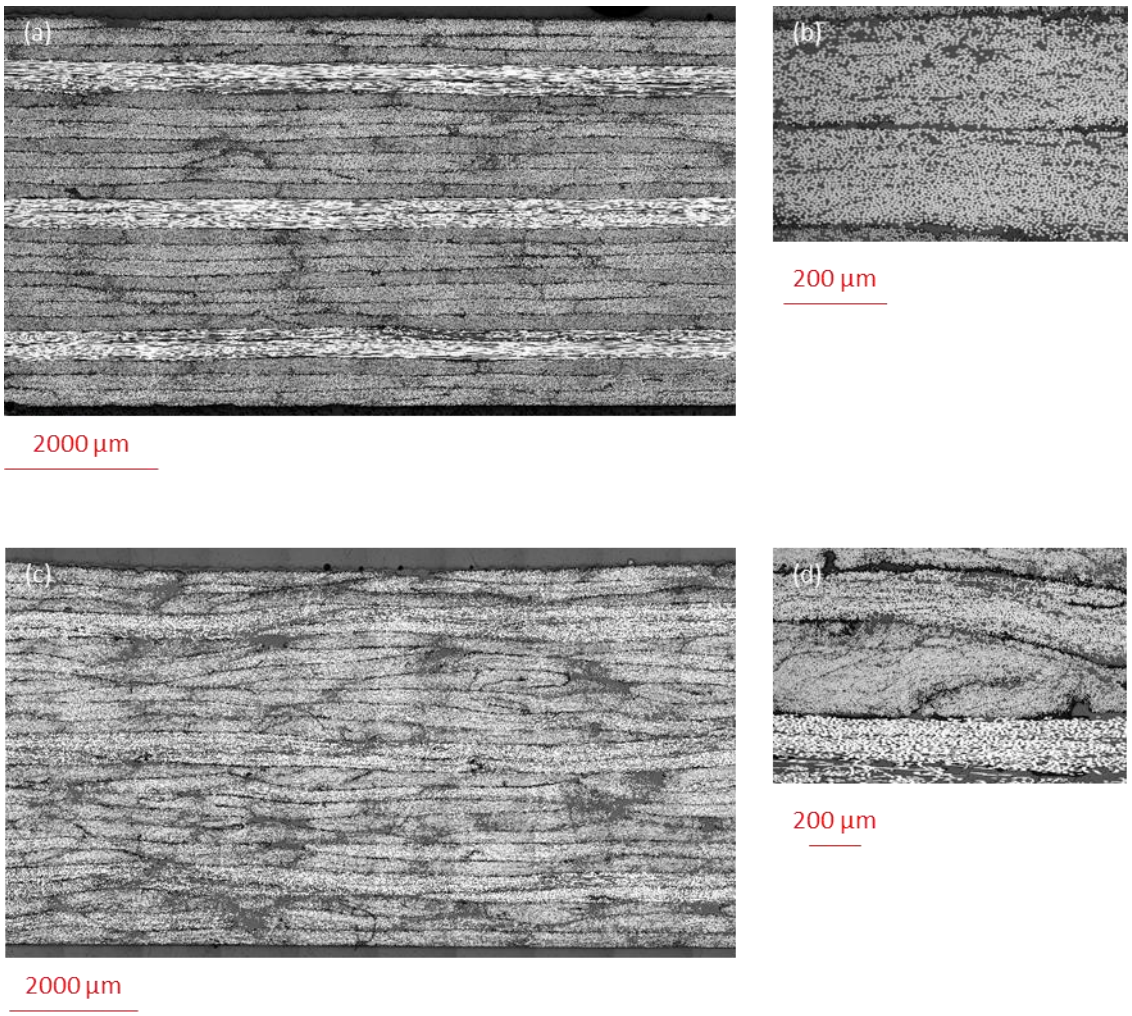

Figure 4-32: Micrographs of QI laminates manufactured using Material D with straight courses (a) and a close-up detail (b), and with steered courses (c) and a close-up detail (d)

The laminate V_f of the laminates were 55.5 ± 4.4 % (straight) and 51.1 ± 8.2 % (steered), determined by analysis of microscopic images. This was a very minor discrepancy to the laminate V_f determined by thickness (55.5 ± 2.1 % and 51.6 ± 5.2 %, respectively), which shows that these two measurement methods led to similar results. For comparability between preform and laminate V_f derived from thickness was plotted in Figure 4-33. It was not possible to deposit Material A to visually acceptable standards at the same radius as Material D, the low laminate V_f of 26.7 ± 6.3 % was indicative of the

poor result. This supports the result of the visual assessment. The test was repeated using a much larger radius of 900 mm, as determined by visual assessment of single course strips, and yielded an acceptable preform and laminate V_f.

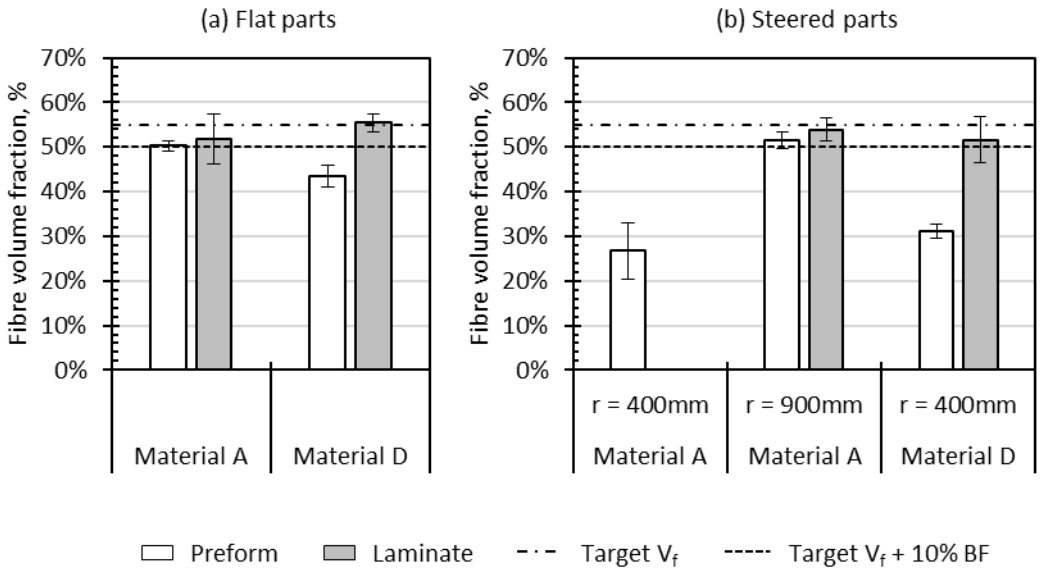

Figure 4-33: Comparison of flat (a) and steered (b) preforms and laminates of Material A and D as well as the baseline material (UD) where applicable; error bars indicate 2 SD

The plot shows that the infusion process was able to mitigate some of the loss in preform V_f observed in the preform, whereby the effect was much greater in Material D, consistent with trials on the L-shaped part. Therefore, the preform V_f of Material D was more susceptible to changes in the AFP process and in the infusion process. Furthermore, Material A was the more consistent material (i.e. smaller discrepancy between preform and laminate V_f) supporting previous results. The micrographs show that out of plane wrinkles in the preform also show in the laminate in form of significant distortions, supporting the opportunity for a wrinkle measurement during the preforming stage to indicate the fibre distortion within the laminate.

3D Surface Evaluation of Steering Trials

To improve the subjective visual inspection, a 3D surface roughness measurement method is applied to steered fibre path preform courses, determining the volume of the peaks and the valleys of the wrinkles. Resulting V_p and V_v of the analysis of the inner area of the seven ply thick steered paths are shown in Figure 4-34. The peaks were plotted positive while the valleys were plotted negative to highlight the skewness of some configurations.

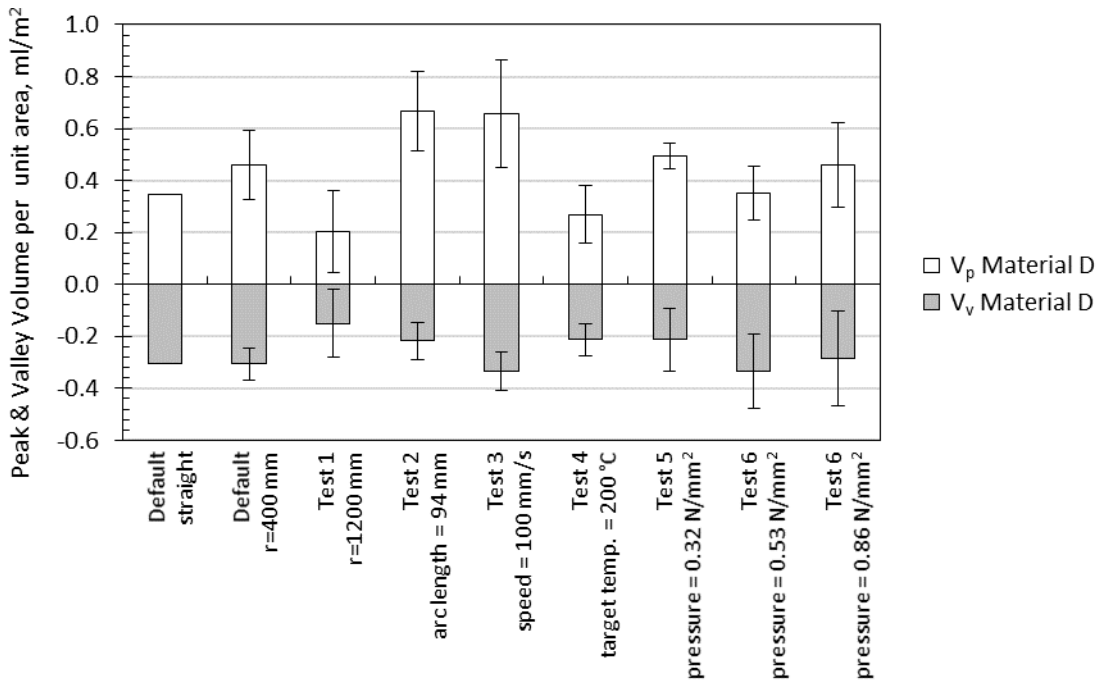

Figure 4-34: Peaks and valleys of different AFP configurations using Material D, data calibrated as described in section 4.4.1 (error bars indicate 2 SD)

These results indicated that the effect of parameter variation on preform V_f was different from the effect on V_p and V_v, which may lead to contradicting requirements of the process parameters when both are optimisation objectives in different areas of the same part. A summary of the difference in response behaviour can be found in Table 4-12.

Table 4-12: Summary of the effect of variable change on preform V_f and peak and valley volume ($\sum V_p$, V_v)

Variable change	**Effect on preform V_f**	**Effect on $\sum V_p$, V_v**
Increased speed	↑	↓
Increased nip-point temperature	↑	↓
Increased compaction pressure	↓	→

Different compaction pressure levels did not appear to have a significant impact on steering quality, which is inconsistent with previous findings. However, the higher compaction pressure exhibited a larger variation, which is consistent with previous trials. The decreased temperature appeared to be beneficial to V_p and V_v, contradicting the trend for preform V_f on straight paths. The heating area during the steering motion could change significantly; distorted tapes could lead to hot spots and an unevenly distributed heat. The results show that the deposition speed as well as arc length had a significant influence on the wrinkle formation. Counterintuitively, lower deposition speed does not improve the quality, which is inconsistent with the effect of speed on preform V_f of straight fibre paths.

During the deposition of multiple steered plies, the mechanical strain inflicted by the roller on the preform was significant. Extending the time, the material was subjected to this strain may cause the increased distortion, which outweighs the extended duration of exposure to heat observed in straight courses. The arc length was highly skewed towards V_p. V_v and V_p were lower for the 1200 mm steered path than the straight path, which could potentially be due to the slight tension flattening out the inherent wrinkles. Overall, there were a number of dissimilarities of process parameters beneficial for high quality deposition of steered and straight paths, which indicates that the mechanisms during the deposition were significantly different.

The investigation of different radii of the single ply deposition spans across seven different steering radii between 400 mm and 2000 mm for Material A and 14 different steering radii between 2000 mm and 100 mm for Material D as well as a straight path for comparison. Material A did not adhere to the substrate beyond 400 mm, as the pull-up was too severe. The sum of peaks and valleys, shown in Figure 4-35 show a positive correlation with decreasing steering radius for all materials. The respective peak and valley values show a skewness of all tests towards valleys, indicating a tendency for sharp, high peaks and less sharp and wider valleys. The sum of V_p and V_v show very similar behaviour of the different Materials A and D, showing the same tendency to increase consistently with a decreasing radius. Material A did not pass the visual assessment at radii below 900 mm while Material D visually passed all tested radii (i.e. no fibre pull-up occurred).

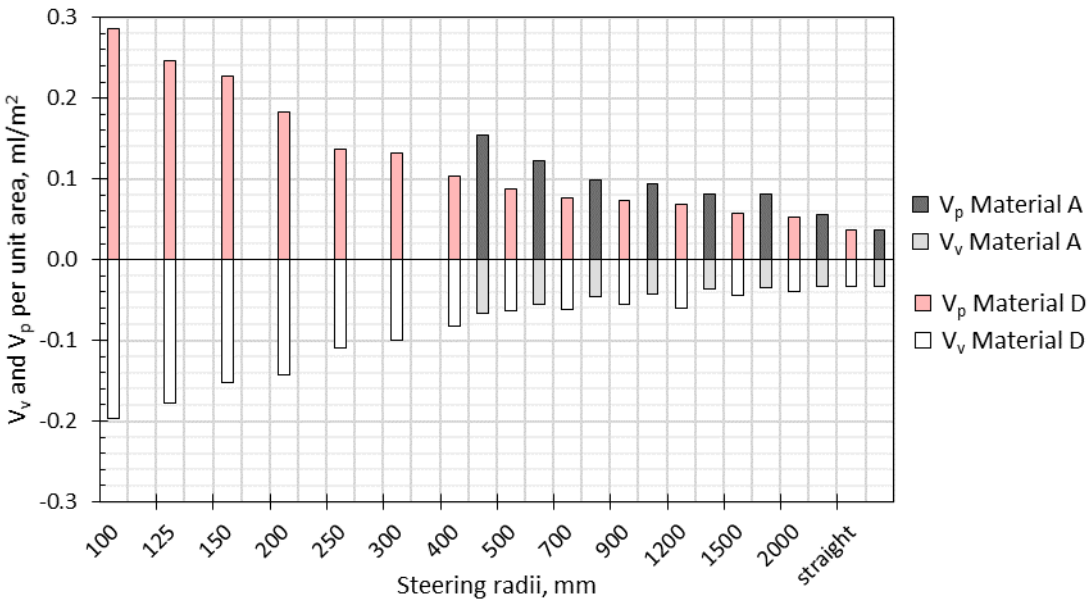

Figure 4-35: Measurement results of peak and valley volume (V_p and V_v, data calibrated as described in section 4.4.1)

The method quantifies out-of-plane wrinkles in terms of wrinkle volume well. The system was not capable of capturing in-plane waviness, and did not replicate visual, subjective observations, e.g. Material D passed and Material A failed the visual inspection at 0.14 ml/mm^2. Material A shows fold overs in the radii 400 and 500 mm, which appears to have a steeper increase than the larger radii. Overall, Material A increases in total volume faster than Material D, which was consistent with the observations during the trials that Material D was more conformable to steered fibre paths. This could indicate that Material D contains more in-plane waviness than Material A, as Material D is less rigid and potentially the inherent in-plane waviness increased before out-of-plane wrinkles emerge. The change from in-plane waviness into out-of-plane wrinkles has been shown for thermoset prepreg material [148]. Surface roughness measurements exclusively assess the surface, but a more detailed analysis e.g. an X-CT, capturing in plane-waviness could provide further insights. The surface regarded was one full course width (eight tapes), smearing the properties of one tape into the next one, possibly taking into account the valley between two adjacent tapes rather than exclusively the valleys of steering induced wrinkles. Regarding the individual tapes within a course could help to identify the differences across a course.

The values of V_p and V_v of the multiple radii trials were higher than the single ply trial, approximately fivefold in comparable datasets. The straight default of the multi-ply dataset had a V_p and V_v of 0.55 ml/mm^2 while the same trial as a single ply test in Figure 4-35 for Material D infinite only shows 0.07 ml/mm^2. This highlights a significant influence of the previous plies and the amplifying effect of depositing multiple steered courses on top of another.

In its current state, the method was used to understand the impact of different machine parameters on the steering quality without the need for impregnation and microscopy analysis, as a lower sum of V_p and V_v is indicative of higher quality and therefore more appropriate machine settings. Further work is needed to ensure that comparison across different data collection systems can be ensured, as currently an adjustment was carried out using an internal default. However, the development of a reliable tool to determine the minimum steering radius as an input to the design requires further work.

Even though the materials have a different visual appearance for the same radius, the excess material accommodated was the same, indicating that different mechanisms occur during the process. This was rooted in the material constituents; Material D does not contain binder within the tape may result in higher internal flexibility. Material A was comparably more rigid due to its internal binder distribution. This was an advantage for the preform and laminate V_f as presented in previous sections but appears to be a great disadvantage when conforming the tape to a non-geodesic path. The formation of wrinkles was based on geometry (length differential between inner and outer radii) and

the material type (Material A or D) or the material class (prepreg or dry fibre) only have an impact on how this length differential is distributed.

The sum of peak and valley volume ($\sum V_p$, V_v) follow a trend similar to the length differential calculated using Equation 4-3, as the peak and valley volume was directly linked to compensation of the additional length; see Figure 4-36. The offset in the large radii of $\sum V_p$, V_v was likely to be an attribute of the slight inherent wrinkling visible in Figure 4-36 (b). A steep increase of length difference and therefore an increase of material that has to be accommodated begins around the 500 mm radius.

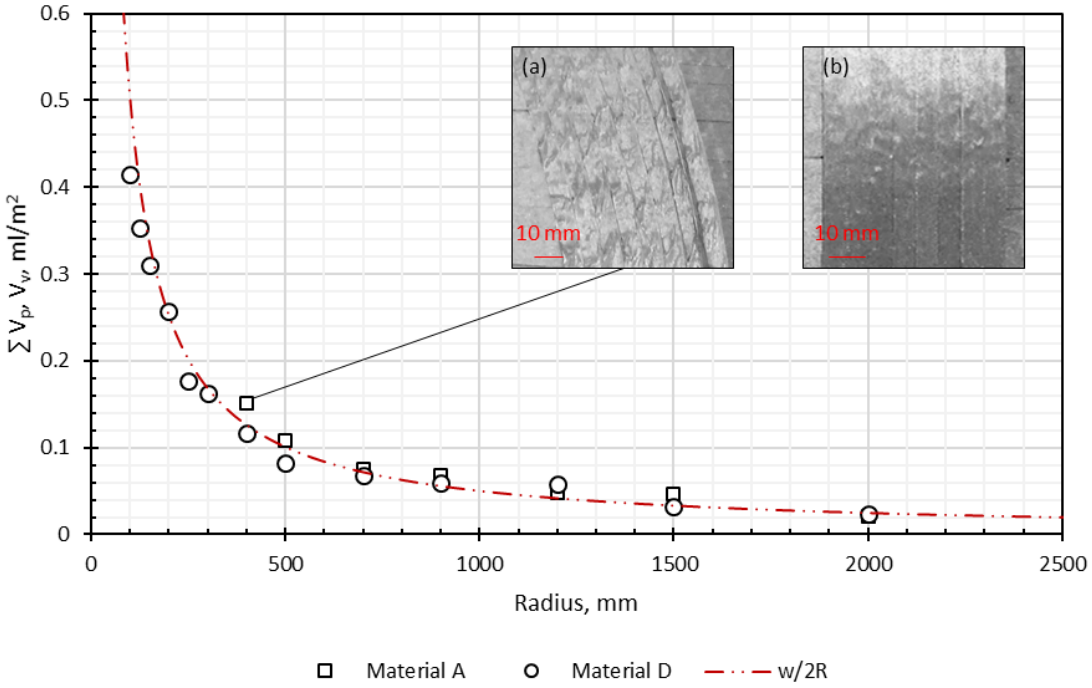

Figure 4-36: Trend of the percentage of additional length of the inner course edge compared to tape centre line and the trend of rising V_p and V_v for Material A and D, with photographs of the courses deposited using Material A with (a) 400 mm fibre path and (b) a straight fibre path without steering

Hörmann proposed the use of tension during the deposition of thermoset prepreg tapes, in order to reduce the out of plane wrinkles. As dry fibres are likely to be sheared more easily than thermoset prepreg, this could have a significant effect on reducing the out-of-plane wrinkles, but as this would require a machine modification was out of scope for this work.

4.4.3 Concluding Remarks

By manufacturing comparable quasi-isotropic panels, with straight or with steered fibre paths, it was proven that out-of-plane wrinkles emerging in the preforming stage have a significant impact on the fibre orientation in the laminate visible in micrographs. Some of the out-of-plane wrinkles were compressed into in-plane waviness, but a thickness increase of 10% from straight course to steered course laminate (Material D) showed that some out-of-plane wrinkles remained.

Reviewing methods to quantify dimensions of wrinkles has resulted in the identification of a methodology commonly used in surface roughness characterisation. This methodology quantifies the surface by measuring the volume under a peak and in a valley of the wrinkles in a dry fibre preform. Even when it was difficult to distinguish the difference in fibre wrinkling of different fibre path radii of the same material visually, the utilised method provided a quantitative measure. The AFP processing parameters contributing towards a high preform V_f were not consistent with the parameters contributing to fewer wrinkles. Low speed increased the wrinkles, while it increased preform V_f. Temperature had an insignificant effect in the steering trials, while it was a major contributor to preform V_f. Compaction pressure did not affect the wrinkle behaviour significantly, but also the effect on preform V_f was comparably small. In summary, the AFP parameter leading to low wrinkles contradict requirements for a high preform V_f, leading to conflicting requirements in selecting ADFP process parameters.

The difference between the materials (Material A and D) appears to be the mechanism of stress release of in-plane tape tension and compression, leading to different wrinkle formation in steered paths. Unless the impact of the shape of wrinkles and other distortions in the context of ADFP on a ply level is well understood, it is not possible to confirm improved geometrical complexity by using dry fibre materials as opposed to prepreg material.

4.5 Conclusion

The first section (4.2) of this chapter developed a promising methodology to define the process rapidly based on material efficient tests. This was useful to identify the most robust material for the manufacturing process, which has confirmed the material selection findings from Chapter 3. The first section also verified the validity of the results on thin preforms and a recommendation for suitable process parameters was made. The combination of process parameters optimised for a preform V_f of 50-55 % was then applied to a high preform thickness and a preform with a thickness change. The added challenge was the continued repetition of the robotic movement over the preform, which indicated that the process was not as well controlled and robust when utilising it repetitively, the material continually underwent the influence of temperature and pressure, potentially shearing forces or other mechanical strain. The applicability of the parameters was limited to similarity (different fibre orientations, QI, but thin and flat) between test samples and real component. This showed that the process is not yet understood well enough to enable an experimental design that provides a first-time-right process development for complex parts. However, the in-depth knowledge of the behaviour of materials under isolated processing conditions (temperature, speed, compaction pressure, heat zone length) allowed informed decisions on the adjustment of the process parameters to mitigate the effect

of repetitive deposition. Therefore, the established relationships between material and processing parameters were of value for thicker and more complex parts. A precise definition of the changes in the process when introducing complexity or regarding the feeding operation has to be investigated to improve the upfront process definition.

Steered paths that exhibited out-of-plane wrinkles in the preforming stage lead to a lower laminate V_f after the infusion process as well as significant fibre distortion, highlighting the importance of a high quality preform. A measurement method for the complex behaviour of the material in a course with a steered fibre path was developed. Derived from a commonly used 3D surface roughness metric, the method was implemented in the context of steering path quality assessment. The prior hypothesis that the same process parameters increase preform V_f also decrease wrinkles was not verified. A discrepancy in response to the processing parameters for the two metrics was shown, whereby higher speed and lower temperature reduced out-of-plane wrinkles, while they decreased preform V_f. This leads to conflicting requirements for the process definition of complex parts containing steered fibre paths.

In summary, this section has shown that it may not be possible to identify a universally applicable set of optimised process parameters for a material. This work established that different complex elements of a preform (i.e. thick preform or steered fibre paths) require different process parameter for optimal outcome. This work has provided a rapid and comprehensive process definition for multiple dry fibre materials based on economic small-scale trials, which has been validated to be transferable to geometrically simple parts. Additionally, challenges preventing the application of the process definition methods to complex were outlined.

Chapter 5

Infusion Characteristics and Laminate Assessment

This chapter shows an investigation into the influence of gaps and overlaps as well as the gap frequency within a preform on flow front progression. The results determine if utilising gap width and frequency can influence the infusion step and used as a Design for Manufacture feature. Furthermore, the results of the infusions of the various feature preforms manufactured as part of the work in previous chapters were discussed, in order to quantify the laminate quality and the influence of the infusion process on the parts.

5.1 Background and Aim

A high temperature infusion is needed to convert a preform into a laminate, aiming to enable an out-of-autoclave process and decrease the overall manufacturing cost. It is a common preconception in the industrial environment that the infusion process is directly transferable from conventional broad goods to ADFP preforms. Some prior work however proved that there are significant differences in the internal fibre architecture and influences on the infusion behaviour were documented [28], [45], [244]. This chapter is aiming to investigate aspects of the internal tape architecture as well as the infusion on various geometries on an industrially relevant level, which means using resin instead of test fluid where possible and considering reasonably large preforms instead of bespoke test rigs. In particular, this chapter aims to:

(1) Assess if the laminate design (gap width and gap frequency between courses) can be used as a Design for Manufacture tool to enhance resin flow (section 5.2).
(2) Determine the interaction of gaps within the preform and resin flow direction through their impact on the flow front progression as well as impact on the internal laminate structure (section 5.2).

(3) Verify the applicability of the standard practice in the infusion stage as an industrial process for different ADFP preforms (section 5.3).

(4) Assess the impact of the infusion on laminate V_f for two different dry fibre materials and different geometrical features in comparison to preform V_f (section 5.3).

5.2 Impact of Laminate Design on Infusion Behaviour

Design decisions, e.g. allowable gap width, are often made without considering the manufacturing process, even though these decisions can affect not only the deposition but also the infusion process. This section compares to the level of intervention that can be achieved through the infusion strategy, which can affect the resin flow direction. It is industrial practice to introduce gaps between adjacent tape courses in order to avoid an overlap of adjacent tapes. A default 1 mm gap is accounting for the variability of the robotic process, while any gap width can be programmed [28]. Unintentional gaps can be affected by the tape width variation as well as the complexity of the mould geometry [29]. Although such gaps can create a local permeability variation within the preform, the effect of gaps on the infusion characteristic has not yet been widely studied. Due to the lack of standardisation and reliability as outlined in section 2.3, comparison of the AFP acquired data with values from literature can only be indicative, but it is a rough point of reference.

5.2.1 Materials and Experimental Method

Preform manufacturing

Material A was chosen as material due to various advantages over other available materials rated against part specific criteria [245], partly due to its comparatively fast infusion. Preforms were manufactured with the four central or all eight 6.35 mm wide tapes were simultaneously deposited at the maximum achievable speed. Due to the machine kinematics and the size of the part, an acceleration and deceleration phase prevents the part to be manufactured at high speed continuously. The speed during the feeding operation was 200 mm/s and a maximum speed on diagonal paths 942 mm/s was achieved, the average speed was 297 mm/s, indicating a bias towards slower velocities. The laser was programmed to deliver a target temperature of 220 °C, suitable for thin flat parts [54]. Other parameters were kept in line with previously conducted trials: the tilt of the deposition end effector was set at a constant value of – 7° and a Shore 40A hardness silicone roller was used to deliver a nominal compaction pressure of 0.47 N/mm^2. The accuracy of gap width has already been assessed for the same machine as used in this work in combination with Material A by Matveev *et al.* The gap width was on average 20% lower than intended (0.8 mm instead of the nominal 1.0 mm) for flat laminates [28]. This finding is supported by Aziz *et al.* who also found 20% narrower gaps than intended in and a 27% reduction in the number of 0.2 mm gaps due to overlaps in one case, and a

300% increase of gaps for another case. These experiments were also conducted on a combination of a Coriolis machine and Material A [45].

Seven gap configurations were produced with the AFP machine, using the same QI ply book as previously described in section 3.2.5. As it is common practice, the program prescribes a regular shift of 3.5 tape widths relative to a previous layer of the same direction, in order to avoid accumulating gaps directly on top of each other [28]. The preform V_f was calculated using Equation 3-1 with the nominal areal weight (196 g/cm^2) of the material, the nominal fibre density (1.78 g/cm^3), the number of plies (26) and the preform thickness measured with a laser line scanner. The theoretical preform V_f for other gap configurations was calculated by linearly interpolating the areal weight assuming a rectangular gap in the preform. Even though Matveev *et al.* have not explored the discrepancy at other nominal gap widths [28], an offset of 0.2 mm for the calculation of the theoretical preform V_f was assumed across all gaps width tested. The preform V_f resulting from different laminate design configurations are shown in Figure 5-1, for simplicity the configurations were referred to by their nominal gap width within this work.

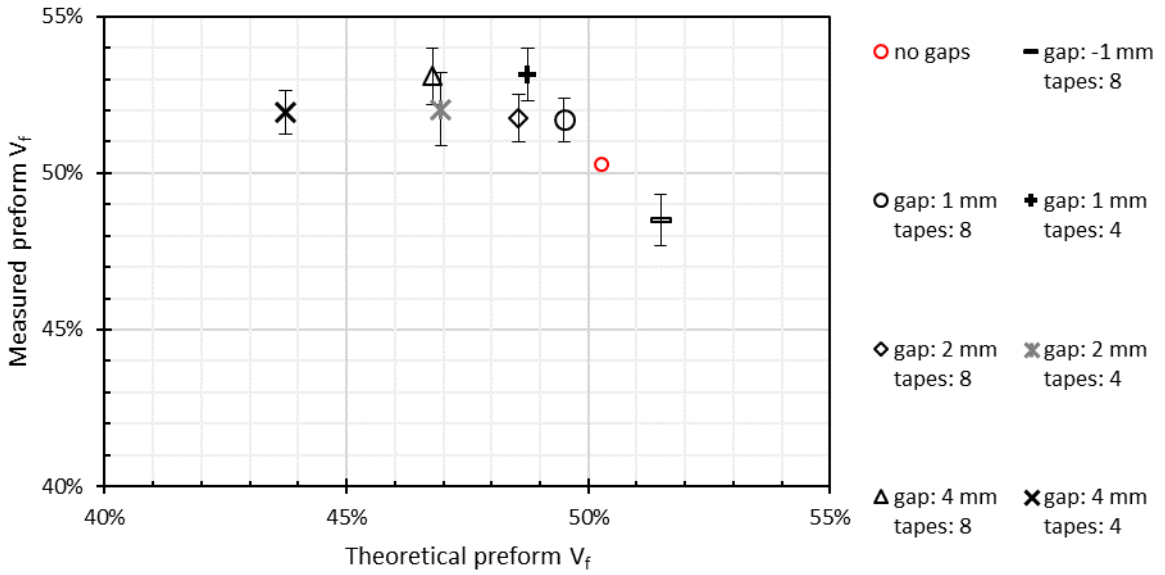

Figure 5-1: Sample set up for infusion trials and resulting theoretical and measured preform V_f (error bars indicate 2 SD). The data point 'no gaps' is only a theoretical value, no preform was manufactured

The measured values were mostly above the theoretical values, indicating a compression of the rectangular shape of the gaps. Two configurations should have the same preform V_f (1 mm gap every 8 tapes and 2 mm gap every 4 tapes as well as 2 mm gap every 8 tapes and 4 mm gap every 4 tapes), but due to the correction of gap width in the theoretical assessment they differ slightly. The exception was the preform with overlaps, where the measurement was below the estimate. As the theoretical

preform V_f assumes an equal distribution of the ply and does not take into account the thickness increase due to undulation of overlaps, it was overestimating the preform V_f.

For comparison, a carbon fibre UD weave with binder (HexForce® 48330 QB1200, HS12K carbon fabric, Hexcel Corporation, US)) was manually laid up, due to a different areal weight (343 g/m^2) with a stacking sequence for 16 plies $[+45/135/0/90]_{2s}$. The woven UD fabric only has a thin polymer thread in the weft direction, only carbon fibres in the warp direction and contains a binder. This closely matches a dry fibre material for ADFP even though it was a broad good. Prior to infusion, all preforms (AFP preforms and UD weave preform) were activated at 119 ± 9 °C (2 SD). The activation process takes 2 hours under vacuum to mimic the high temperature infusion process as closely as possible for the room temperature trials, where the preforms undergo an isothermal dwell at elevated temperature prior to infusion. Those panels were then cut into strips (nominally 650 mm long and 120 mm wide) that were infused individually, complying with a recommended thickness and minimal aspect ratio for infusion tests of this kind [122]. Each preform configuration was trialled twice.

Vacuum Assisted Infusion

Industrial production of an aerospace part with ADFP material requires infusion with a high temperature aerospace grade resin. The infusion tests were carried out with diluted sugar syrup at room temperature as well as a two-part aerospace grade epoxy resin (RTM6) at high temperature. This was necessary in order to test a larger number of variables and closely monitor the process. The transferability of the results was demonstrated through use of a high temperature curing resin for comparative tests. Taking the images of the flow front in the high temperature infusion tests was not possible due to the limitation of operation temperatures of the cameras. Instead of measuring the flow front over time at high temperature, the flow rate was monitored by measuring the weight change of the resin reservoir. To verify the applicability of the results obtained by the room temperate trials to high temperature trials the volumetric flow rate was compared. When comparing the volumetric flow rate of resin and diluted sugar syrup (high temperature vs. room temperature) against time for identical preforms a reasonable agreement between the volumetric flow rates was observed, as shown in Figure 5-2. The resin infusion had a slightly lower flow rate than the diluted syrup as time progresses, potentially due to the onset of the cure, as the decreasing viscosity with time at temperature cannot be replicated with diluted syrup. The visible steps in the recording of RTM6 were caused by the lower resolution of the scale used.

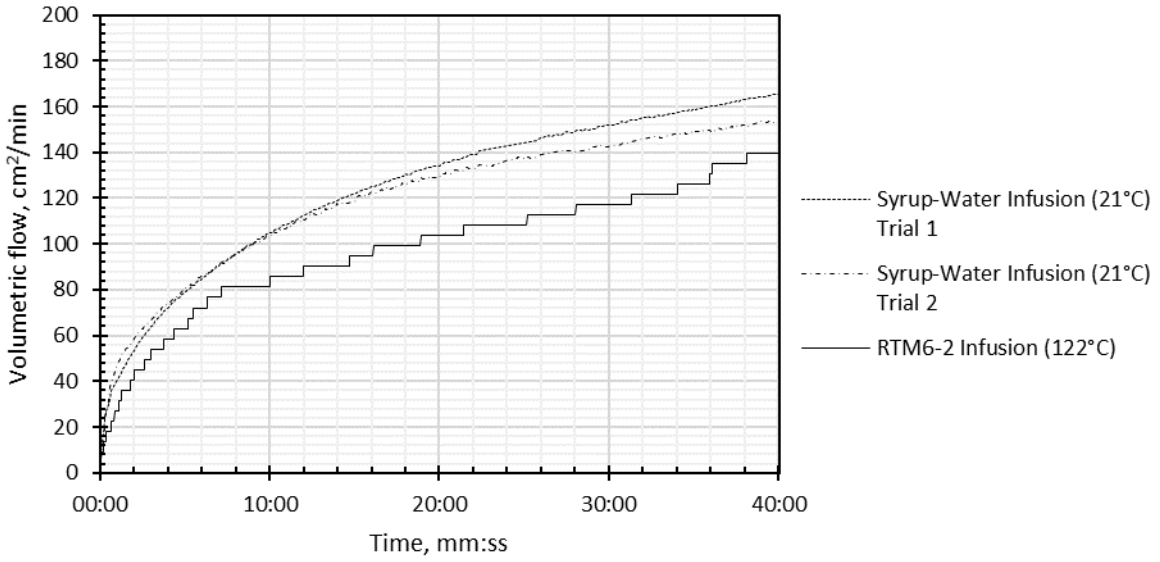

Figure 5-2: Comparison of volumetric flow rate of the infusion with flow mesh for RTM6 at 122 °C and two repeats of a water syrup mixtures at 21 °C for the samples with eight tapes and 1 mm gap

Therefore, the trials conducted with an alternative infusion fluid were representative of the infusions at elevated temperature. The verification using resin had the further advantage to enable microscopic images as the diluted sugar syrup does not cure and images could not be taken.

The room temperature infusion trials were conducted using a mixture of syrup (invert sugar syrup, 69 wt. %) and water (31 wt. %) with the same viscosity as the aerospace grade resin at infusion temperature. The viscosity of the diluted sugar syrup was determined to be 33.4 ± 2.5 mPa·s across all batches mixed. The viscosity measurement was conducted at 22 °C and a shear rate of 40 s^{-1} using a viscometer (Brookfield LVDV-I+, US) to match the viscosity of resin at infusion temperature (120 °C) of 30 mPa·s according to the manufacturer [217]. The room temperature during the infusion with diluted syrup was 20.8 ± 1.7 °C (2 SD) and the temperature of the diluted syrup was 20.8 ± 0.6 °C (2 SD). The temperature during the three high temperature infusions in an industrial oven was 121.5 ± 3.1 °C (2 SD) and the resin pot was kept at nominally 80°C and the heated hose at nominally 90 °C. The resin was degassed as per manufacturer's requirements prior to infusion.

The individual preform strips were bagged using a bagging scheme as depicted in Figure 5-3 (top view) and Figure 5-4 (side view). A second iteration of the infusion set-up included a flow mesh reaching over two thirds of the preform from the inlet. Bag sealant tape was used to seal the lengthwise edges and no race tracking was observed. For high temperature infusions, a layer of release film was added between preform and vacuum bag and a peel ply between the flow mesh and the preform, otherwise the set-up was identical. Only the set-up including flow mesh was used for the high temperature infusion tests.

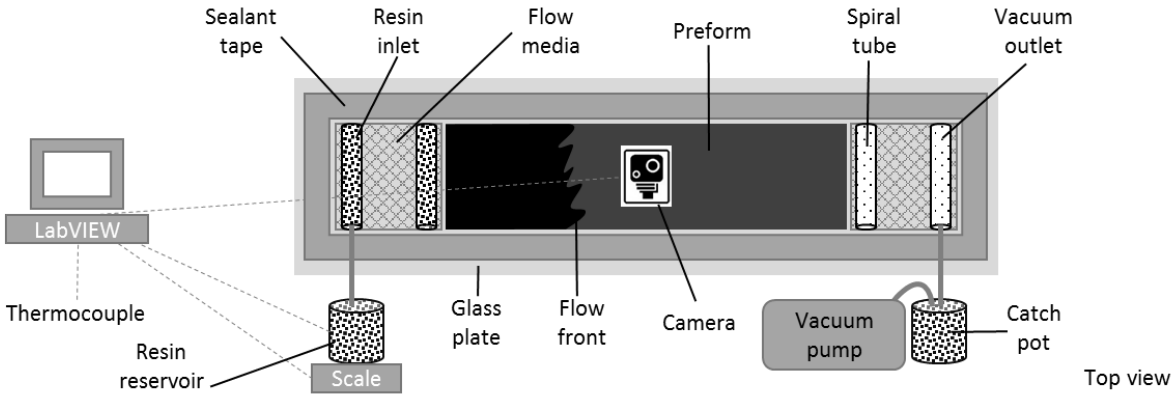

Figure 5-3: Schematic room temperature infusion set-up (top view), preform size 120 × 650 mm

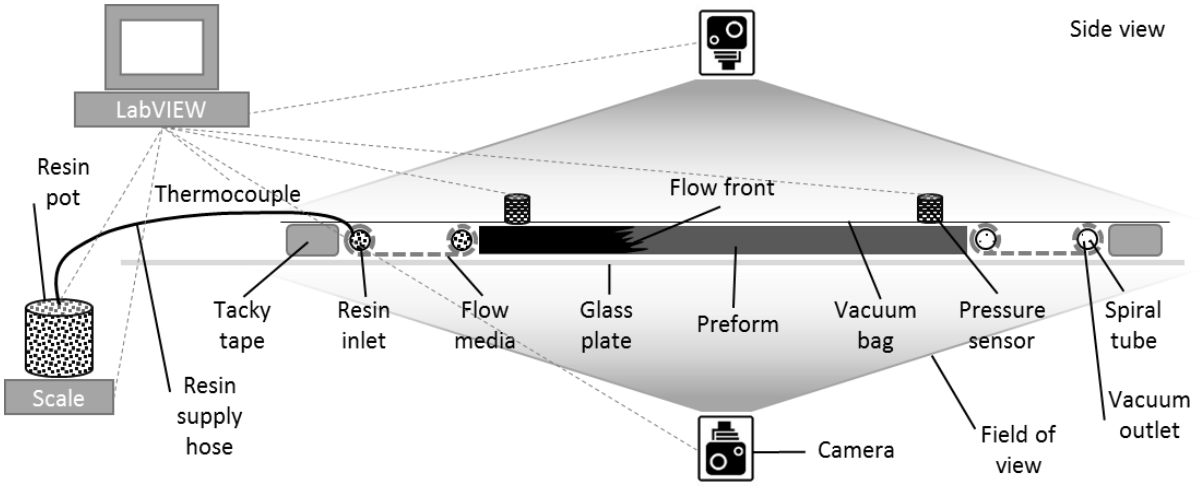

Figure 5-4: Schematic room temperature infusion set-up (side view)

Infusion Assessment Method

All measurements were logged using LabVIEW (National Instruments, US) to connect different measurement capabilities as required. Two thermocouples were used to record a temperature trace during infusion (room temperature and resin temperature, thermocouple wire type K, -75 to +250 °C, Ø = 0.2 mm). Cameras (Microsoft LifeCam Studio by Microsoft, 1080p HD sensor, 1920x1080 pixels, 96 dpi) capture the flow front progression during infusion and a scale (Benchtop Scale PCE-TB 15, up to 15 kg, accuracy 0.05 g) captures volumetric flow. These devices logged their respective data during the room temperature infusions, every second for the room temperature set-up including flow mesh, every 10 seconds for the room temperature set up without flow mesh and the high temperature infusions data was logged every 30 seconds. In a post processing step, the photos of the flow front taken throughout the room temperature trials underwent an image analysis using ImageJ for preparation (alignment, cropping and generating the correct file format) and a Matlab routine for the analysis for the image (flow front detection and measurement). The preform fill was determined as a ratio between wet and dry area, whereby the size of the preform was determined

by a ruler displayed in the images. The area covered by dark pixels in the wet area were then added up and are presented as a percentage of the initial full size of the dry area.

5.2.2 Results and Discussion

Effect of Gap Width and Frequency on Fill time

The flow front position at the same time (11 min 43 ± 5 sec) was investigated for all samples based on the images taken by the camera looking at the bottom surface through a glass plate on which the trial was set-up. This time was chosen, as it covers the full range of all samples across both set-ups. Two samples per configuration were tested. The fill time of the UD preform was an internal baseline, as the test was conducted with an identical set-up, overall similar fill positions to the ADFP preforms at the selected time. The results of the fill time of the set-up including the flow mesh, leading to a mixture of in-plane and through thickness flow are shown in Figure 5-5. Two repeats were carried out, the test with the smaller value is in the white column and the test with the higher value is indicated in grey.

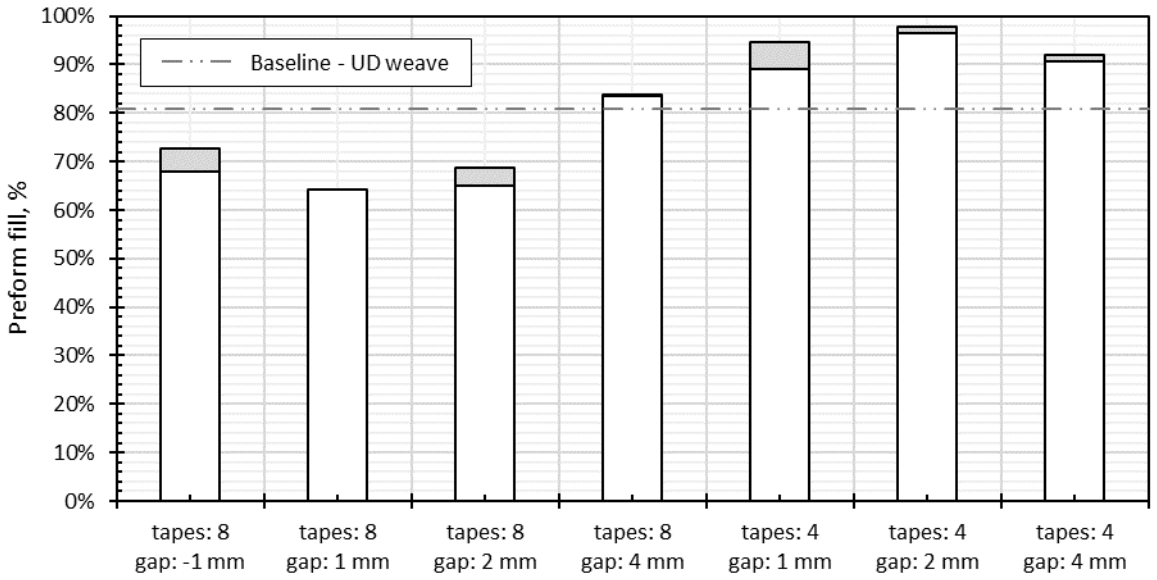

Figure 5-5: Preform fill at specific time for a variety of laminate designs in the infusion set-up with flow mesh (mixture of in-plane and out-of-plane flow)

A statistically significant trend towards faster fill of laminates manufactured with four tapes than with eight tapes time emerges. Even though a wider gap causes faster fill for eight tape preforms, this was not the case for the preforms with four tapes, so no consistent trend significant trend within gap width can be detected. A similar trend can be observed in the set-up without flow mesh, see Figure 5-6. There was no consistency regarding influence of the gap width, but the samples with only four tapes overall infuse faster than the eight-tape configuration. This would suggest that a higher gap frequency was beneficial for fast fill times, while less frequent gaps results in a slower preform fill. This is

consistent with findings on Material A by Aziz *et al.* who investigated through thickness flow. The tested frequency of 0.2 mm gaps between tapes by utilising variable tape width (6.35 and 12.7 mm), showed a 90% lower permeability in the preform with less frequent gaps [45].

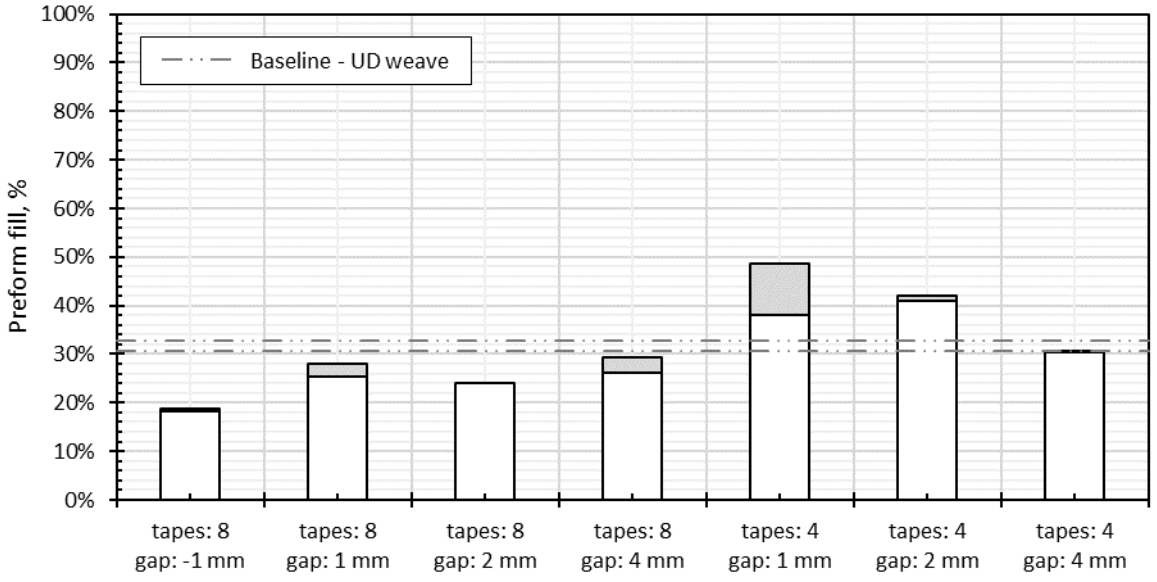

Figure 5-6: Preform fill at specific time for a variety of laminate designs in the infusion set-up without flow mesh (in-plane flow)

Gaps form a network of interconnected flow channels, which would lead to a higher number of interconnections in the configuration using four tapes only. Furthermore, this leads to a shorter distance from the flow channel to the centre of a tape. This shorter distance at a lower permeability within the tapes is a plausible reason for a higher fill rate. The decrease of preform fill with increasing gap width in the configuration with gaps every four tapes is counter intuitive, but the variation was likely to be within the variability of the test set-up. The variability can be relatively high, as in the sample with four tapes and 1 mm gap.

Effect of Infusion Set-up on Fill Time

The differences in gap width and frequency were not particularly strong, however a clear difference between the set-ups without flow mesh (pure in plane flow) and with flow mesh (a mixture of in-plane and through-thickness flow) was observed (see Figure 5-7). A two sample T-test confirmed that the two groups were different with 99% confidence. The flow front of the test with a mixture of in-plane and through-thickness flow was on average close to three times as fast as the in-plane flow front.

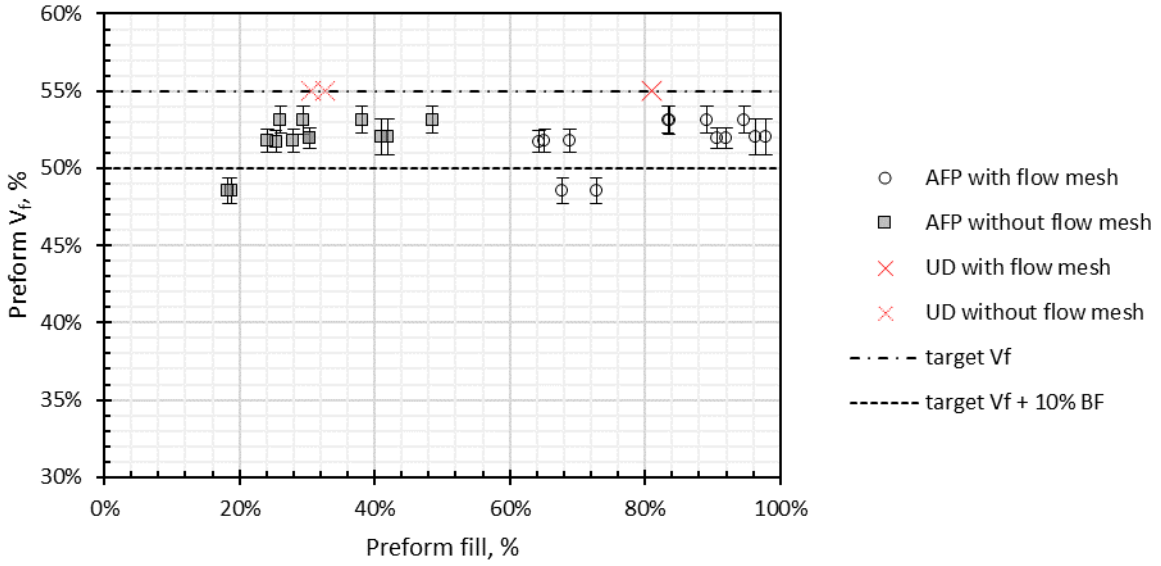

Figure 5-7: Flow front propagation at 11 min 43 sec for all set ups and preforms

Through-thickness flow has a much shorter distance to cross than in-plane flow, so this behaviour would be expected. These results show that the duration of the infusion was governed by the flow direction rather than the presence of flow channels in the form of gaps. Therefore, the use of gap width and frequency as a Design for Manufacture tool is not as promising as the optimisation of the infusion set-up, determining the resin flow direction.

Laminate Cross Sections

The cross sections of the preforms infused with an aerospace grade resin show, for a 1 mm gap every eight tapes, that the gap shape was close to being rectangular and was filled with resin (see Figure 5-8).

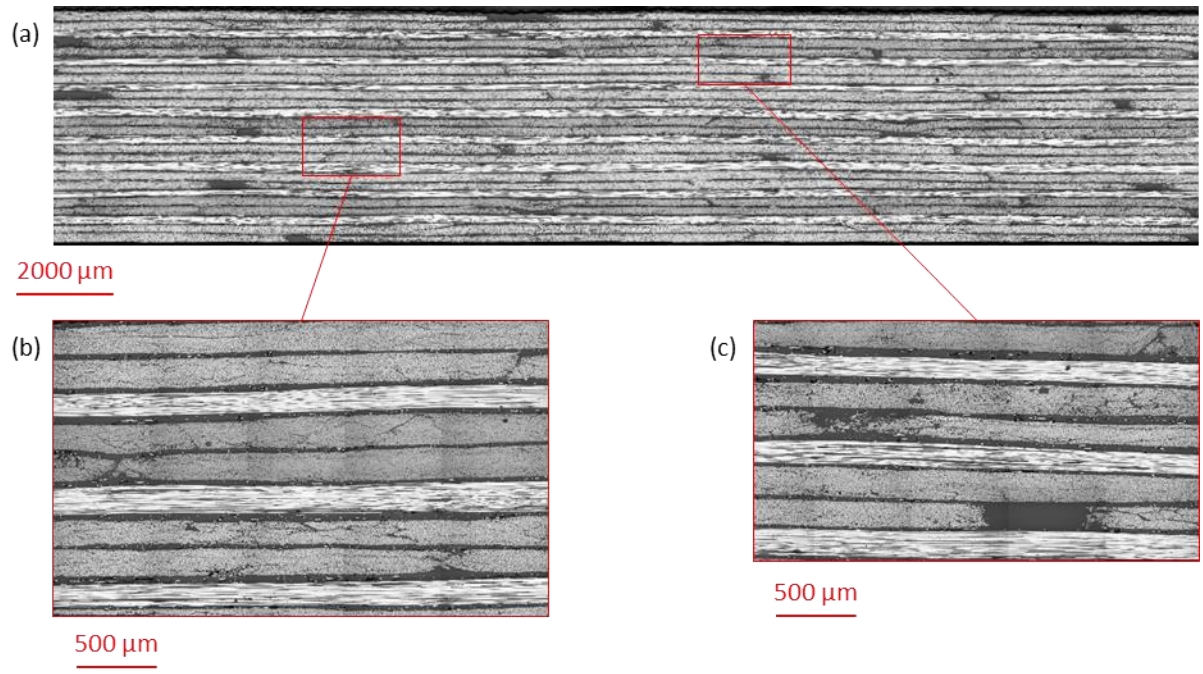

Figure 5-8: Cross section of sample with eight tapes and 1 mm gap (a) with details of an example of intentionally adjoined tapes without gap (b) and an example of a 1 mm intentional gap between courses (c)

With increasing gap width, in this instance to nominally 2 mm, the shape of the gap became distorted from the idealised rectangular shape (see Figure 5-9). For the 2 mm gap configuration, the tapes were slightly deformed into the cavity caused by gaps in the previous ply, this was consistent with observations in laminates manufactured using prepreg AFP [199], [246], [247]. The laminate exhibits some entrapped air, showing that the infusion had had an air leak and was not successful.

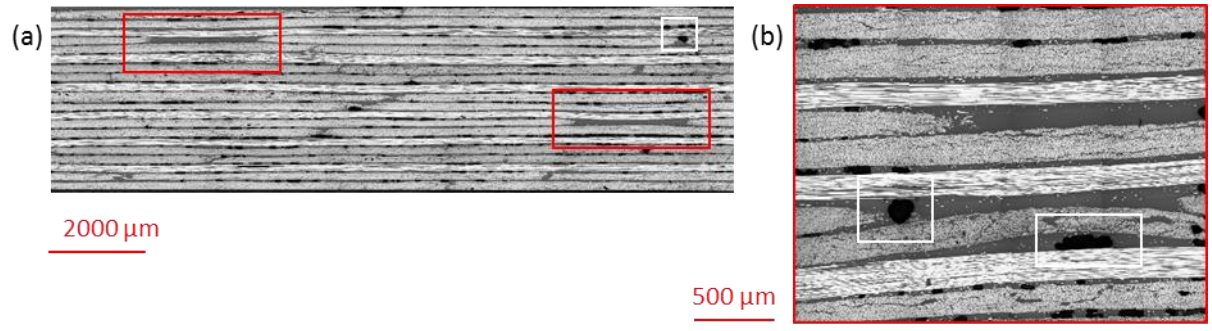

Figure 5-9: Cross section of sample with eight tapes and 2 mm gap with intentional gaps between courses (a) and a magnification of the partially deformed 2 mm gap (b). Red outlined areas highlight intentional gaps; white outlined areas highlight entrapped air bubbles

For the laminate with the 4 mm gaps (see Figure 5-10), the tapes fully comply with the cavity and were in contact with the previous ply. This shows that the volume of the flow channels created by the gaps within the preform does not increase proportionally with the increase of the gap width. The volume

of flow channels was similar across different gap configurations, which explained that the increase of gap width did not have a significant effect on the resin flow velocity. The results of the infusion trials were consistent with the observed change in flow channel cross section in preforms of varying width gaps. The through-thickness flow was likely to be affected less by the observed changes in flow channel cross section because overlapping gaps from adjacent plies continue to form a flow channel networks that promotes through-thickness flow across all configurations.

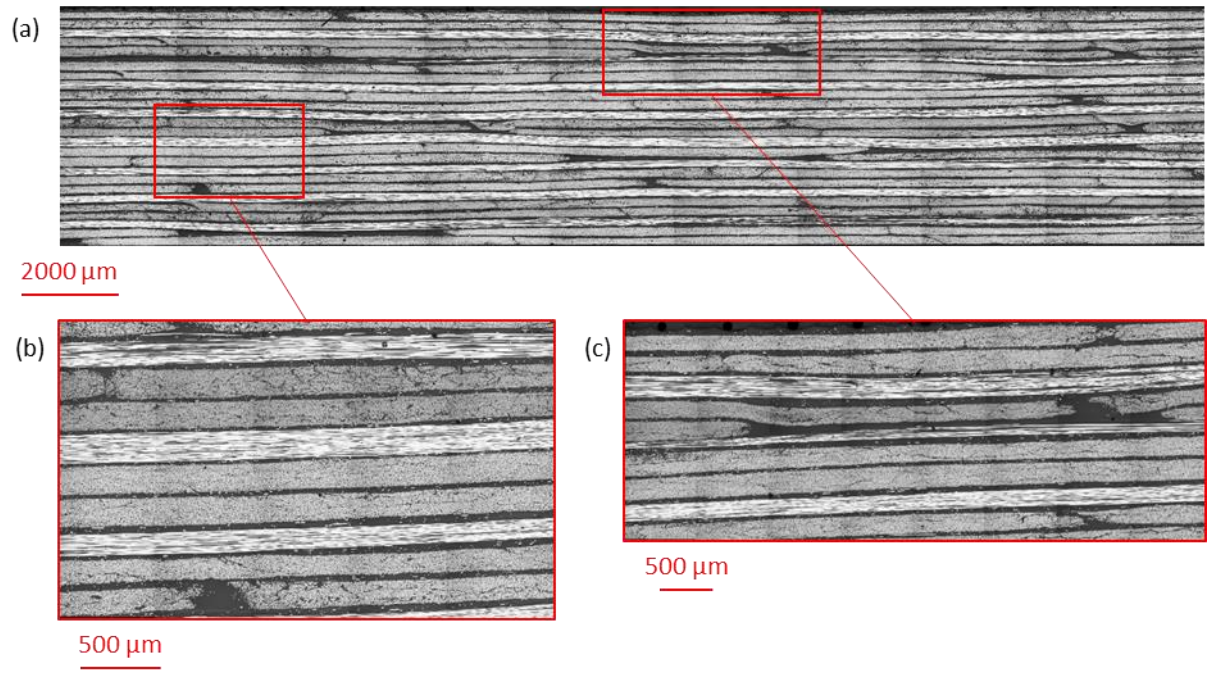

Figure 5-10: Cross section of sample with eight tapes and 4 mm gap (a) with details of an unintentional gap between tapes (b) and example of an intentional 4 mm gap between courses (c)

Flow Front Observations

The flow front of conventional broad goods was relatively straight, see the example in Figure 5-11 (a). The flow front shape of the ADFP preforms captured during the infusion was significantly different from that of any conventional material (Figure 5-11). This scattered flow front makes flow front progression measurements challenging. The flow front of all preforms was calculated using the wetted area divided by the measured specimen width resulting in average length, which does not take into account the scatter of the flow front. This method was a good approximation for a flow front in a woven material (a), but the high scatter in ADFP preform samples (b and c) were not well represented as a line. Especially the ADFP preforms infused with flow mesh exhibit a clear pattern of the gaps of subjacent plies (c). The flow mesh enhances the through-thickness resin flow by guiding the resin over to top of the preform quickly, leaving the through thickness flow as the only path forward for resin. The gaps form interconnected flow channels, which were connected through their crossing points. The configuration with four tapes contains more crossing points of gaps per area than the

configuration with eight tapes, but the number of crossover points only marginally changes with different gap widths. The denser interconnected network was likely to be the cause for the overall slightly higher flow front progression at higher gap frequency. The compaction of the subjacent plies into the flow channels causes a similar sized flow cavity, and therefore did not have a high impact.

Figure 5-11: Representative, binary images of flow front appearance seen from the bottom of UD-weave (a), ADFP preforms with 8 tapes, 4 mm gap and in-plane flow only, (b) and ADFP preforms with 8 tapes, 4 mm gap and in-plane and through thickness flow (c)

There were two fundamental differences between the two types of material (woven fabric and preforms manufactured by ADFP): reinforcement architecture as well as binder distribution. The more discrete fibre bundles of the carbon fibre weft was highlighted in Figure 5-12, the micrograph shows more frequent flow channels between the fibre bundles than the ADFP preform. These flow channels were well connected and provide a through thickness resin flow, the higher gap frequency was likely to contribute of a smaller scatter. The resin progresses faster in the flow channels than in the bundles and tapes and the through thickness permeability was highly dependent on the connection between gaps [45]. The subsequent permeation of the fibre bundles occurs faster in the case of the woven material than the permeation of the resin inside the tapes in the ADFP preform, indicating a significant difference of intra-tape permeability. The fibre bundles were more permeable and resin flow into the tapes occurs at the same time as lateral flow through the gaps, leading to a much smoother flow front. The flow of the resin into the centre of the ADFP tapes was likely to be inhibited by the presence of binder within the tape; however, the impact of binder location within an ADFP tape has not yet been investigated. This behaviour then leads to significant race tracking of the resin along the gaps in ADFP preforms, visible as scattered flow front.

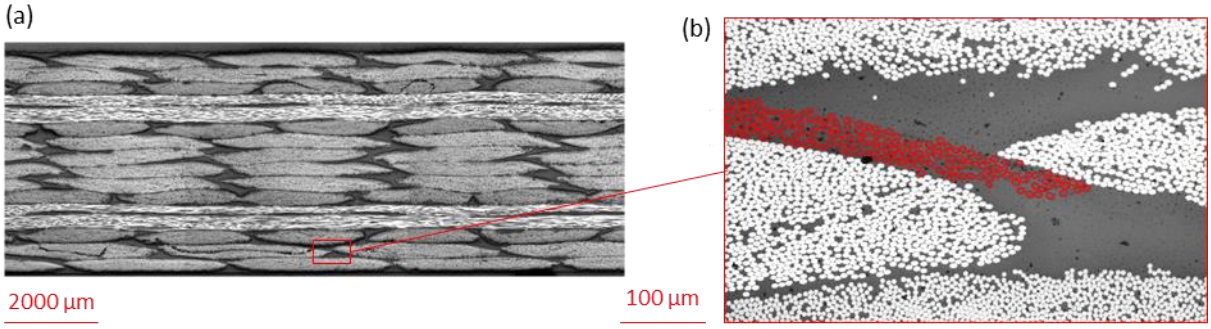

Figure 5-12: Microscopic image of cross section of UD woven material (a) overview and (b) detail of polymer warp thread (dark grey, highlighted in red) between the carbon fibre weft (white)

Such a severely scattered flow front may be more prone to dry spots and other faults than a more uniform flow front. Therefore, ADFP preforms infused with high temperature resin were at high risk of intra-tape dry spots.

5.2.3 Concluding Remarks

A relatively simple but representative test set-up gives a reasonable characterisation of the in-plane versus a mixture of in-plane and through-thickness flow front progression. The image analysis of the infusion shows that the impact of flow direction on the fill time was greater than the impact of gap width and frequency within the tested samples with gaps ≥ 1 mm. Therefore, the impact of a change in laminate design were far outweighed by the set up chosen during the infusion. This limited effect indicated that using internal gaps as a Design for Manufacture feature for infusion enhancement is not feasible for the investigated cases, but if used should increase the gap frequency rather than the gap width at the expense of a reduced laminate V_f.

The qualitative assessment of the microscopic images showed that gaps wider than 1 mm induce undulation of the tapes, as the ply conforms to the gap of the previous ply. This is likely the reason of low impact of gap width on flow front progression, the increased gap width does not increase the free porosity linearly. The gaps did however introduce undulation, which then led to more frequent and smaller flow channels, hence why gap frequency has a higher effect than gap width. The observations of the flow front during the infusion trials supported that gaps form interconnected flow channels within the preform during the infusion process. This scattered flow front can potentially lead to dry spots, as the resin can racetrack forward in the gaps, closing areas off and relying on capillary action to fill the entire preform.

A configuration in which very narrow gaps (< 1 mm) between individual tapes (e.g. by utilising tapes slightly narrower than 6.35 mm in a course) leads to a high frequency of gaps, potentially leading to faster infusion with a less scattered flow front. This approach would also circumvent the disadvantage of low productivity due to fewer tapes deposited at the same time and fibre undulation caused by tapes compacting into gaps. The role of intra-tape binder requires further research to understand the implications of its presence on the flow behaviour and permeability.

5.3 Feature Infusion and Laminate Comparison

The manufacture of different preforms was documented in previous chapters; however, the impact of the infusion stage on a part was not addressed. The optimisation of the infusion process itself was out of scope, neglecting the influence of different types of set-ups and auxiliary materials. Keeping the infusion set-up as consistent as possible, the fibre volume fraction between preform and laminate across a variety of geometries was compared.

5.3.1 Materials and Experimental Methods

ADFP Preform Manufacture

Various preforms were manufactured and used within a variety of different contexts within this work, an overview can be found in Table 5-1. The design, manufacturing and analysis of the respective preforms can be found in the section as indicated in the right column. The two different infusion set-ups as well as other differences will be described in the following section.

Table 5-1: Infusions conducted on various preforms (for infusion strategy set-up reference see Figure 5-13 and Figure 5-14), note: steering refers to in plane steering only

ID	Feature	Material	Resin	Infusion set-up	Repeats	Reference for preform manufacture
1	Flat	A	RTM6	Peripheral	1	4.2.3
3	Flat	D	RTM6	Peripheral	5	4.2.3
4	Flat	UD	RTM6	Peripheral	1	5.3.1
5	Steering	A	RTM6	Peripheral	1	4.4.2
6	Steering	D	RTM6	Peripheral	5	4.4.2
7	L-shape	A	RTM6	Edge-to-edge	1	3.3.3
8	L-shape	D	RTM6	Edge-to-edge	1	3.3.3
10	Ramp	A	EP2400	Edge-to-edge	1	4.3.2

As a baseline, where possible, the carbon fibre UD weave with binder was used with the same stacking sequence as described in section 5.3.1.

High Temperature Infusion Process

The infusion set-up for ADFP preforms follows the general principle that is used for conventional textile impregnation whereby a preform is placed onto the tool (or mould), flow media is added and an air-tight vacuum bag is placed over the stack to enable evacuation [48], [248], [249]. The flow media creates a combination of in-plane and through thickness flow. The details of the vacuum port and resin inlet placement, the exact location of the flow media and any further auxiliary consumables (VAP® membrane, bleeder, peel ply, or others) are often decided intuitively by skilled operators. The set-up was kept consistent across all infusions, but the transferability to large structures has not been verified.

For the work presented in this section, the resin system (RTM6) was used for preforms manufactured with different dry fibre materials to ensure a direct compatibility between the laminates. This resin system is conventionally used in conjunction with Material D commercially, while a different resin system is recommended for use with Material A (EP2400). Interactions between fibre, binder and resin

cannot be excluded to influence the infusion behaviour, however this was expected to affect predominantly mechanical properties, but they will not be tested as part of this work. Investigating the implications of the resin type and compatibility to the binder on the infusion process and laminate quality was out of scope. EP2400 only became available towards the end of this work, and it was therefore only used for the variable thickness part.

The preform was placed on a tool treated with release agent, covered with a layer of peel ply (60BR). A flow mesh was then placed over this, only partially covering the preform. The two different infusion set-ups used are shown in Figure 5-13 and Figure 5-14. On the edge-to-edge setup, the distance between the flow mesh and the preform edge was 50 mm either side and had an 85 mm distance to the edge opposite of the spiral coil providing the resin inlet. A satin weave glass fabric (style 7781) and flow mesh was serving as a spacer to enhance vacuum and resin flow. Two Nylon bagging film layers (Ipplon® DP1000 by Airtech International Inc., Huntington Beach, US) with an intermediate layer of breather fabric were used to prevent a bag failure during the infusion stage. For same purpose, multiple darts were placed in the setup to provide extra material if the bagging film shrinks at elevated temperature. Sealant tape (GS-213, Airtech International Inc., Huntington Beach, US) was ensuring an airtight seal of the bagging film to the tool.

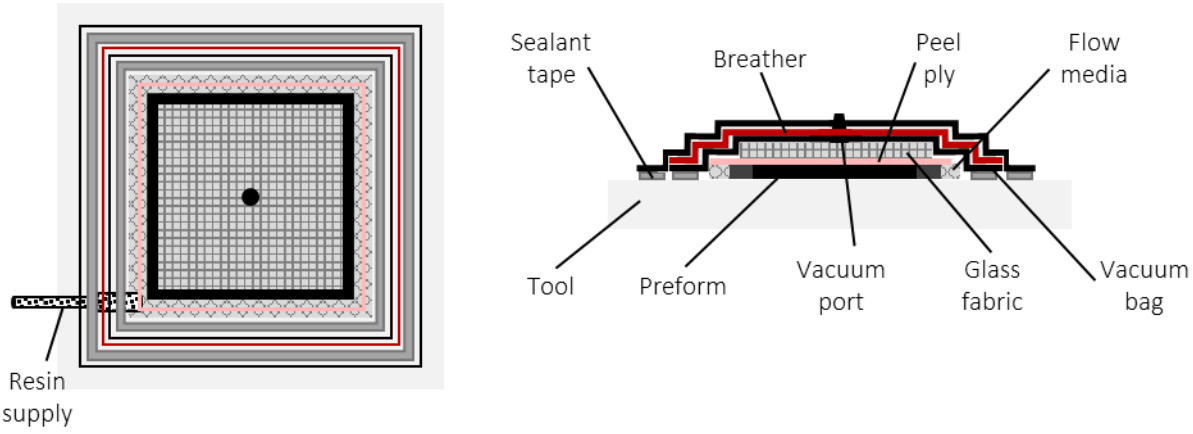

Figure 5-13: Peripheral high temperature infusion set-up

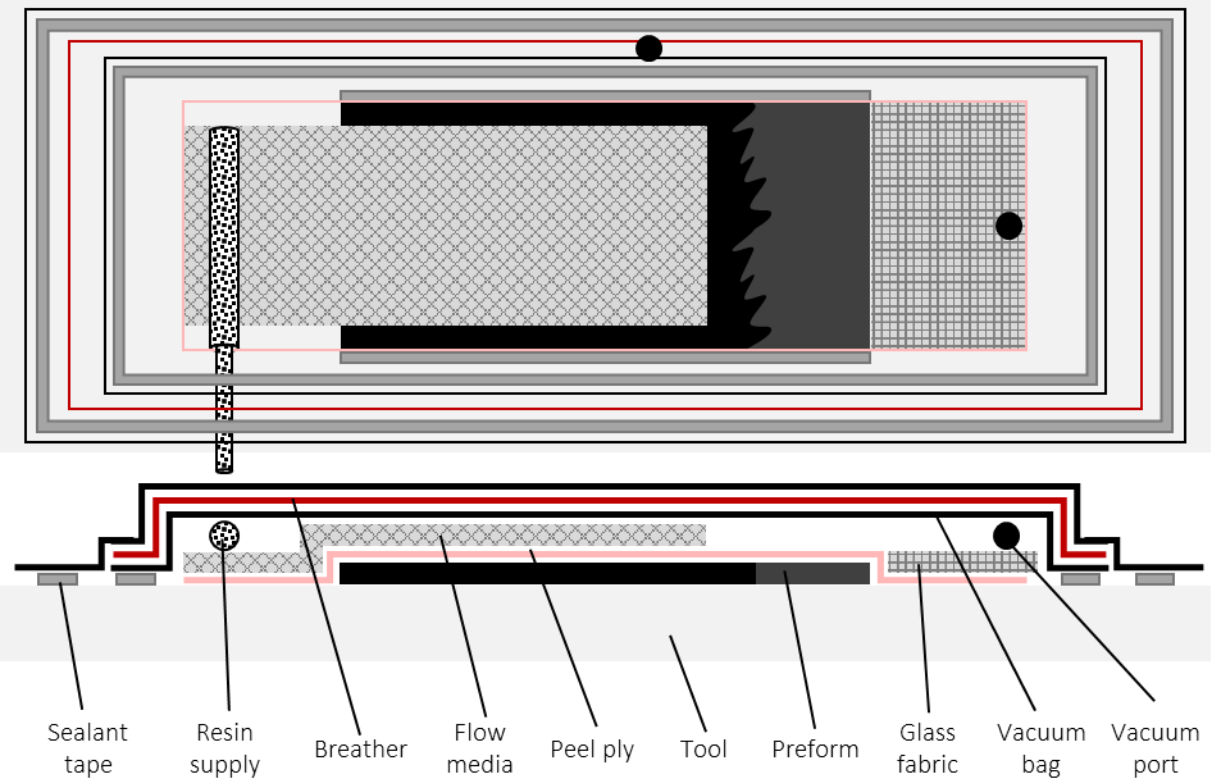

Figure 5-14: Edge-to-edge high temperature infusion set-up

After the preform was bagged up and placed into an oven, the set-up was heated up to the target infusion temperature [218]. An isothermal dwell ensures a uniform temperature throughout the entire preform and a complete air removal. The isothermal dwell also allows this preform relaxation to occur. Aziz *et al.* report a relaxation of the preform under pressure with time, indicating a slight re-arranging of the fibres [45]. The duration of the dwell depends on the thickness of the preform, but had a minimum duration of 2 h. Specific adjustments were made to the temperature cycle to suit each resin system, both heating cycles are shown in Figure 5-15. The resin was degassed and kept at its target temperature, then the valves were opened and the resin was drawn through the preform due to the vacuum applied, with an approximate pressure gradient of 0.9 - 1 bar between ambient pressure on the resin and the generated vacuum in the bag [250]. Even though this set-up is commonly used and recommended, it is not necessarily scalable to large structures, where placement of various resin supply and vacuum ports may be necessary.

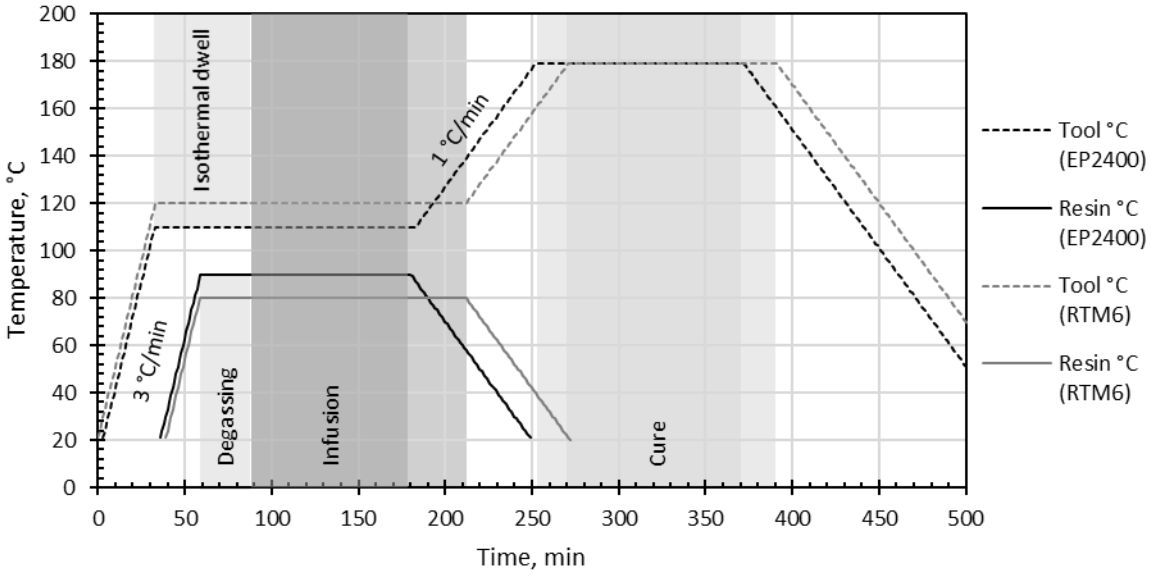

Figure 5-15: Temperature cycle used for the two resins EP2400 and RTM6

Resin infusion of all preforms was carried out using a Ciject 3 injection machine (Composite Integration, UK) and RTM6 or EP2400 aerospace grade epoxy resins. The resin was heated to 80°C and degassed within the equipment. A heated hose allows the resin to travel to the oven at temperature. An oven (16H025, QED Scientific, High Peak, UK) was used for all infusions, a large single doored oven that uses a temperature and process controller (Omron E5CC, Omron Corporation, Kyoto, Japan). Small adjustments to the set-up were made until the vacuum leak rate was no greater than 15 mb in 5 minutes (i.e. additional sealant tape to close air leaks). Once these criteria were met, the cure cycle as shown begins. Resin was heated to 90 ± 5 °C for EP2400 and to 80 ± 5 °C for RTM6 and degassed for minimum of 30 minutes. Tool and preform were heated to 110 ± 5 °C for EP2400 and 120 ± 5 °C for RTM6. The infusion was terminated when the resin was visible on the outlet pipe.

Both resin systems are aerospace-grade epoxy infusion system with a glass transition point (T_g) around 180 °C and were processed with identical equipment and similar processing parameters. EP2400 is a resin containing toughening agent to increase the damage tolerance [251]. However, the addition of toughening agents can increase the viscosity of the resin [252]. The datasheets provided by the manufactures exhibit a difference in viscosity, at t = 0 the viscosity of EP2400 is at ~70 mPa·s, while RTM6 has about half of this viscosity at ~35 mPa·s [217], [251], [253].

The increase of viscosity of the resins with time was measured at 110 and 120 °C to determine which temperature results in a viscosity comparable to RTM6. The tests were performed on *TA instruments discovery HR-1* and *TA instruments AR-G2* using 20 °C/min heating rate and 450 µm gap width between 40 mm diameter aluminium plates and compared to the nominal value of the datasheet

measured with a Brookefield Viscosimeter. The tests were performed at 110°C and 120°C with up to three repeats at each temperature, see Figure 5-16 and Figure 5-17, compared to values available from the supplier (Datasheet).

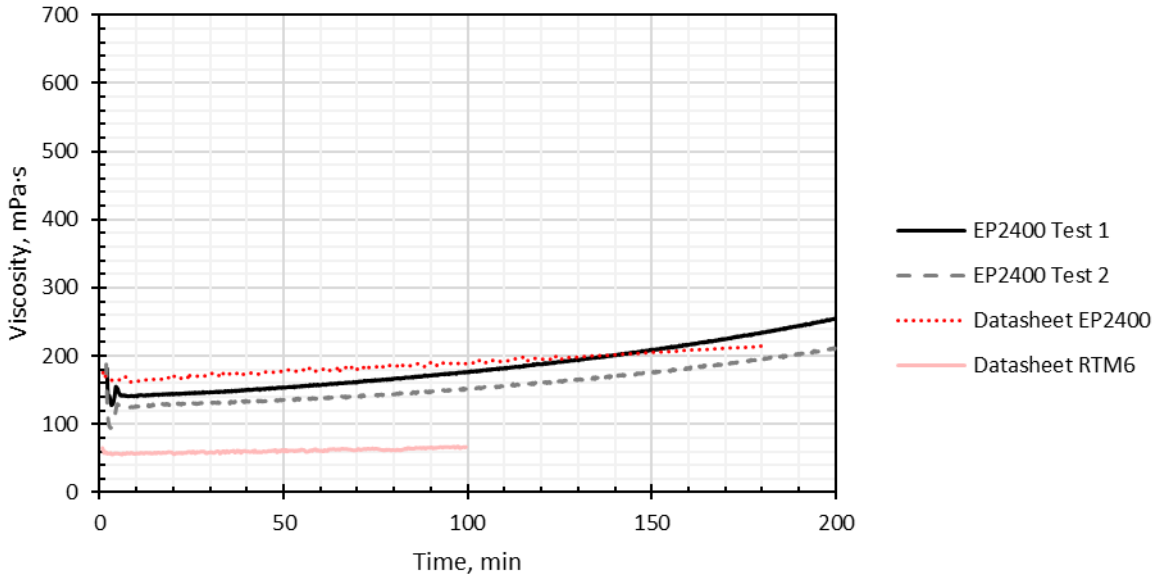

Figure 5-16: EP2400 viscosity measurement at 100 °C in comparison to values provided by data sheets

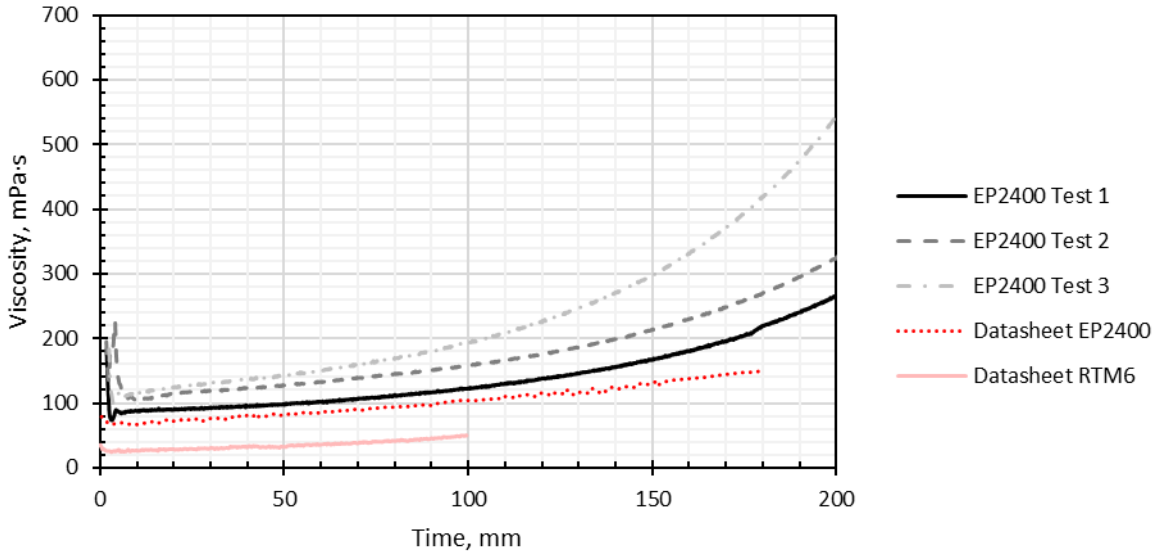

Figure 5-17: EP2400 viscosity measurement at 120 °C in comparison to values provided by data sheets

The results of the resin testing show that the resin used was around the values in the data sheet, and the viscosity of EP2400 was significantly higher than RTM6. In conclusion, the transferability between the two resin systems is challenging, the different viscosities may result in significantly different infusion behaviour, to minimise this, the use of 120 °C is recommended.

5.3.2 Laminate Assessment

Every laminate was checked using NDT, with the same methodology as described in section 3.2.5. NDT was carried out in accordance to ASTM 6-0011 class 1. The acceptable levels of back wall echo attenuation was 12 dB for laminates < 5 mm and 18 dB for ≥ 5mm [220]. The thickness was measured using a thickness gauge (C8100 by Kröplin, Germany) with a scale interval of 0.05 mm. A grid of 5 × 5 point was marked on the laminate, 50 mm from the edges and evenly distributed points. For laminates with a peripheral infusion strategy, the central measurement was disregarded due to the distortion of the surface by the vacuum port. The thickness of the manufactured laminate was also measured without contact using two different articulated measuring arms with 3D laser scanners. The arms used were:

i. ModelMaker MMDx 100 digital laser scanner and MCAx35+ Manual Coordinate measuring Arm, Nikon, Japan. Accuracy 76 microns (referred to as “Nikon arm”)
ii. ROMER Absolute Arm with Integrated scanner 7535 7-AXIS, Hexagon Manufacturing intelligence, Sweden. Accuracy 101 microns (referred to as “Romer arm”)

The two laser line scanners and the caliper was used for measurements on the same laminates at different times, the comparison can be found in Figure 5-18. Each cluster of points is one panel measured multiple times, all panels had a target thickness of 5.2 mm and vary slightly. Except the cluster in January 2016, which had a target thickness of 3.0 mm. The measurement with various methods overall shows a good agreement. The caliper measures discrete locations and can pick up peaks on the surface, while a laser line scanner was an average over an area on the panel, which is why the measurements of the caliper tends to indicate a thicker laminate.

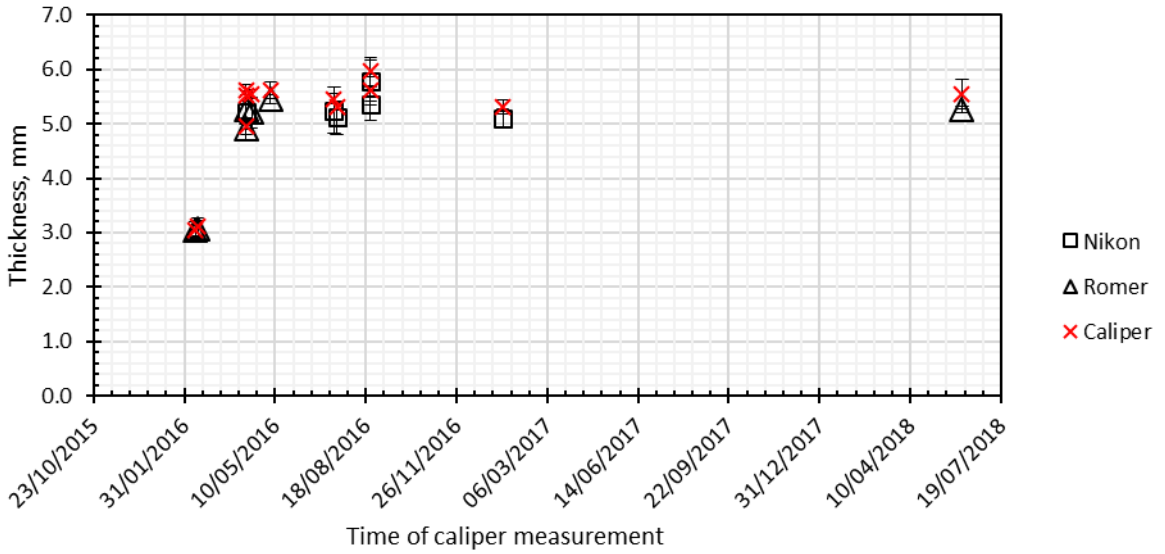

Figure 5-18: Measurements using different instruments on the same parts over time

The caliper was unsuitable for the measurement of L-shaped laminates because the caliper does not fit into the corner radius, so measurements of the L-shaped part were only carried out the laser line scanner.

To ensure the calculated laminate V_f based on laminate thickness was representative, microscopic images for Material D and the UD weave were analysed to determine laminate V_f as an independent comparison. The discrepancy between the two measurements was 1.1% as a maximum, showing that determining the laminate V_f by thickness was providing results in line with the more conventional microscopy.

5.3.3 Results and Discussion

The infused laminates passed the NDT test, and the measured laminate thicknesses of the various preforms are shown in Figure 5-19. The woven material infused significantly faster than the ADFP preforms at otherwise identical conditions, based on observations. The laminate V_f of Material A was slightly below the target in some instances, but never below 53.3 % in all cases. The baseline material achieved a higher laminate V_f than all ADFP laminates, apart from the corner of the L-shaped section manufactured with Material D. There was no statistically significance between the laminate V_f of Material A and D, however the range of the results of Material A was slightly smaller (53.3 – 57.2 %) than the range of Material D (51.9 – 58.9%) despite comprising a larger number of different geometries.

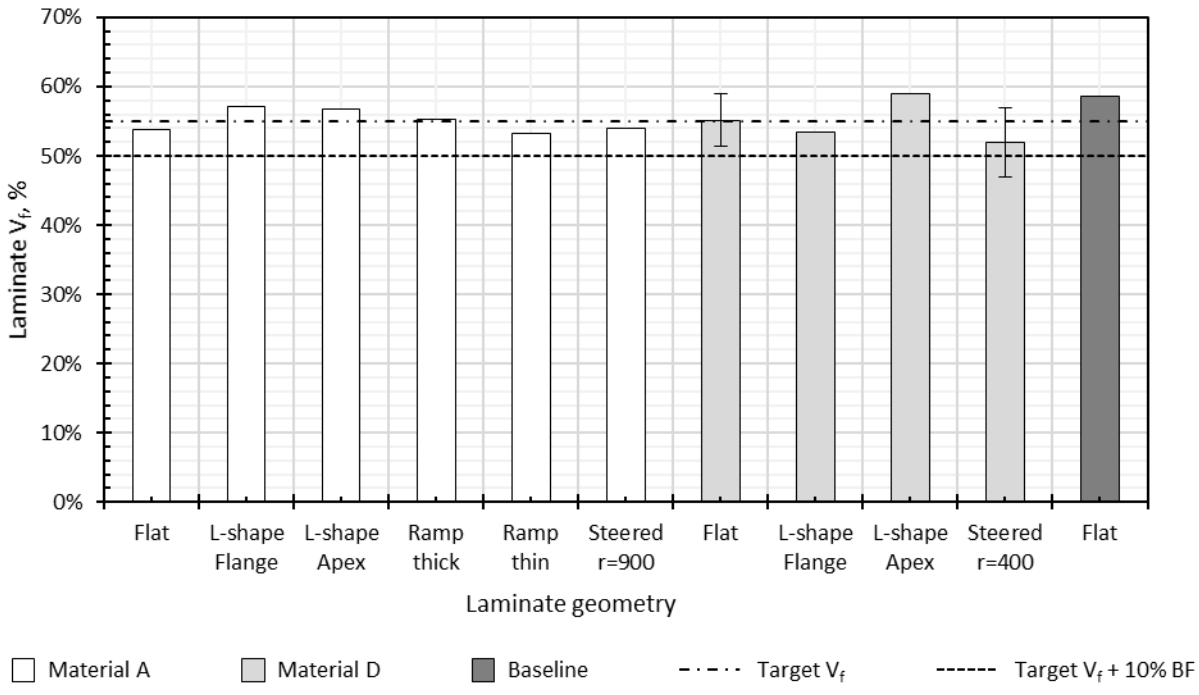

Figure 5-19: Laminate V_f comparison between various materials and geometries; error bars for Material D, flat and steered indicate 2 SD of five laminates

The variability within an L-shaped part was dependent on the geometrical feature, i.e. the corner consistently shows a higher preform and laminate V_f than the flat flanges. The infusion process mitigates the difference between the corner and the unconstrained flanges. It is likely that some movement occurs within the preform during the infusion. Even though the infusion had a positive effect on the laminate V_f, it would be more desirable to have as little change between the V_f of preform and laminate. The observed changes suggested some movement within the preform during the infusion process. Slight movements were possible within the presented L-shaped part, but for more constrained parts such as U-shapes this movement to mitigate differences between preform and laminate may not be possible to occur. Therefore, the closer the preform V_f is to the laminate V_f, the more predictable the outcome for complex geometries will be.

The preform V_f of the L-shaped section was very close to the laminate V_f of the L-shaped section, so only negligible change occurred during the infusion process. This absence of additional improvement could indicate that a maximum compaction level was reached. It could potentially constitute a new target preform V_f during the deposition process, whereby the assumption would be that at a preform V_f of 57% for Material A and 59% for Material D, the preform V_f equals the laminate V_f. Reaching this level of compaction however, was challenging on flat areas (refer to section 4.2.3).

5.3.4 Concluding Remarks

Infusions were completed successfully and with a laminate V_f close to the target of 55%. This was achieved on a variety of different geometric parts: simple flat panels with straight and steered fibre paths as well as for an L-shaped laminate for both Materials A and D and additionally on a laminate with a thickness change for Material A. The infusion process can mitigate some inconsistencies occurring in the ADFP deposition process when the preform is unconstrained in the case of an L-shaped part.

The consistency of laminate V_f across different individual geometrical features shows that a laminate V_f of 54.6 ± 4.4 % can be achieved for Material A and 54.9 ± 6.1 % can be achieved for Material D. Therefore, Material A and D exhibit a similar laminate V_f with a slightly higher variability for Material D, showing that the laminates manufactured with Material A were more consistent. This result was in line with the results of the material selection process in Chapter 3 and the preform assessment in Chapter 4, showing that the material constituents and the preforming process had a high impact on laminate quality.

5.4 Conclusion

The conventional high temperature vacuum infusion is a feasible method to convert ADFP preforms to laminates. This chapter confirmed that the oven based vacuum infusion of high temperature

aerospace resin is in principle a suitable technique to manufacture laminates from ADFP preforms manufactured using Material A and D. A uniform preform is more likely to result in a uniform laminate, but the infusion process was able to mitigate low preform V_f of unconstrained preforms and the laminate had a higher uniformity than the preform. This was the case for Material D with greater extent than for Material A.

In comparison to an infusion using a woven material as reinforcement, the laminate V_f of ADFP was slightly lower and the infusion took overall longer. The utilised setup is not transferable to large components, a larger number of inlet and outlet ports would be required to ensure complete preform fill. This shows, that further optimisation is required before deploying the process into an industrial environment. An optimisation of the infusion set-up and of variable parameters during infusion as well as cure will be necessary to yield improvements the future. This could potentially be an optimisation of dwell time and temperature to prevent or promote diffusion of the binder to alter the material permeability.

This work provided a baseline of laminate V_f achievable with ADFP preforms and a proof of concept for small components. Opportunities to improve laminate are not only in the infusion process, but in the material architecture. The first part of this chapter highlighted the significant impact of the internal architecture on the flow front progression. The material could be developed to have a less dense filament arrangement or an increased thickness of the veil. A different approach would be a slightly narrower material to create smaller, but more frequent gaps between the tapes. Overall, in order to transfer the use of high temperature vacuum infusion successfully into large structures, a better understanding of the process and opportunities for optimisation will be necessary.

Chapter 6

Process Scalability

A demonstrator representing industrial components is introduced as a case study. A complex geometry has the additional challenge of complex programming of fibre paths. As part of this chapter, the path planning procedure was assessed. Repeated demonstrator manufacture enables the industrial scale assessment of the preforms in terms of technical aspects such as process variability, but also economic aspects such as productivity. The infusion of the preforms enabled comparison of the laminates.

6.1 Background and Aim

Using an industrially relevant case study enables the critical assessment of previous findings in the context of an industrial application. Using Material A, this comparison showed manufacturing mechanisms that were not captured in the small-scale trials. Section 2.5 highlighted that previous work either researches isolated small-scale manufacturing issues in the form of journal publications (refer to sources listed in Table 2-1) or at large scale demonstrations in the form of collaborative projects [59], [120], [173]–[177]. The transfer between those two approaches is either not frequently pursued or not publicly available due to restrictions imposed by industrial collaborators. To close this gap, a demonstrator was designed as a representation of a partial aerospace structure by combining multiple basic geometrical features that were previously assessed individually into one structure. On the example of an aerospace spar and a tail cone, typical industrial challenges are highlighted in Figure 6-1.

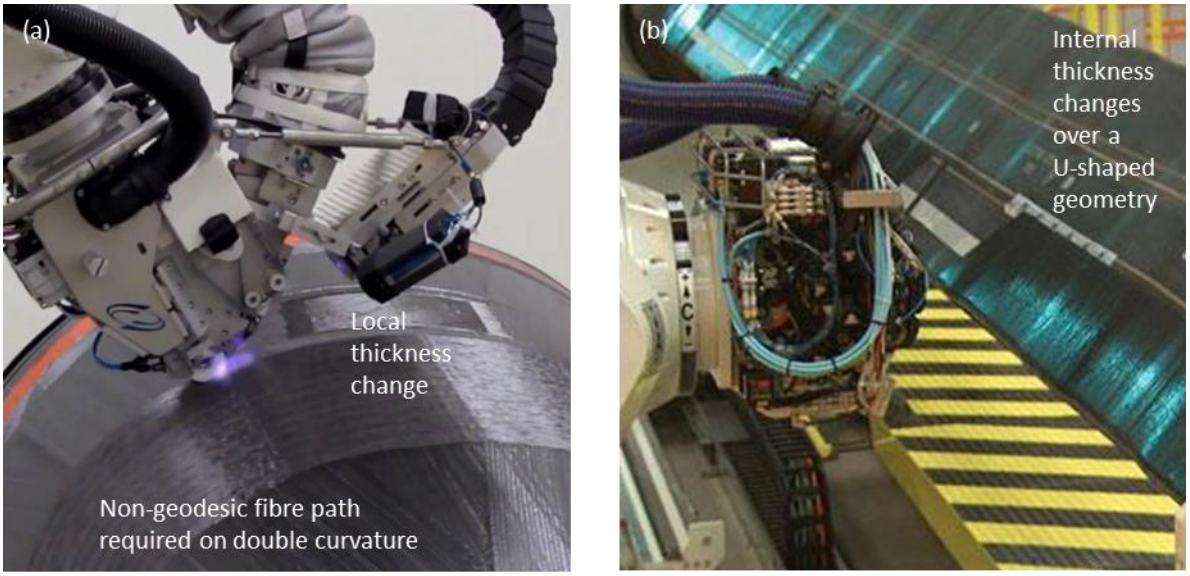

Figure 6-1: Different geometrical features occurring in industrial components highlighted on a tail cone, by ADVITAC and Coriolis (a) [175] *and a spar by GKN (b)* [254]

The individual geometrical features representing these challenges were discussed in previous sections of this work; thin flat parts (section 4.1), L-shape (section 3.2.5), thick preforms (section 4.3), thickness change (section 4.3) and fibre steering (section 4.4). The demonstrator combines these factors into a part that contains a thickness change on an L-shaped section, leading to a double curvature surface in the transition area from a conical corner to a cylindrical corner.

The required tool was designed based on these geometrical features and was used during deposition as well as for the infusion process. The tooling material best suited to endure both manufacturing steps was a composite tooling combing relatively low cost in tool manufacture and an adequate temperature expansion for the use of the tool. The tool had a radius difference of 20 mm on the corner of the L-shaped section requiring a 1:5 ramp over the tool surface. The resulting ramp was designed with a 25 mm fillet radius and continued on the flanges. The tooling manufacturing process as well as the dimensions are shown in Figure 6-2. The tool also comprises probing holes, used to align the tool with the machine program as well as the laser line measurements. The 20° tilt of the tool allows the robotic system to reach all areas while using a rigid and therefore lower cost mount on a table instead of the use of a movable horizontal positioner, such as the one used in the example shown in Figure 6-1 (b), at the expense of an additional degree of freedom.

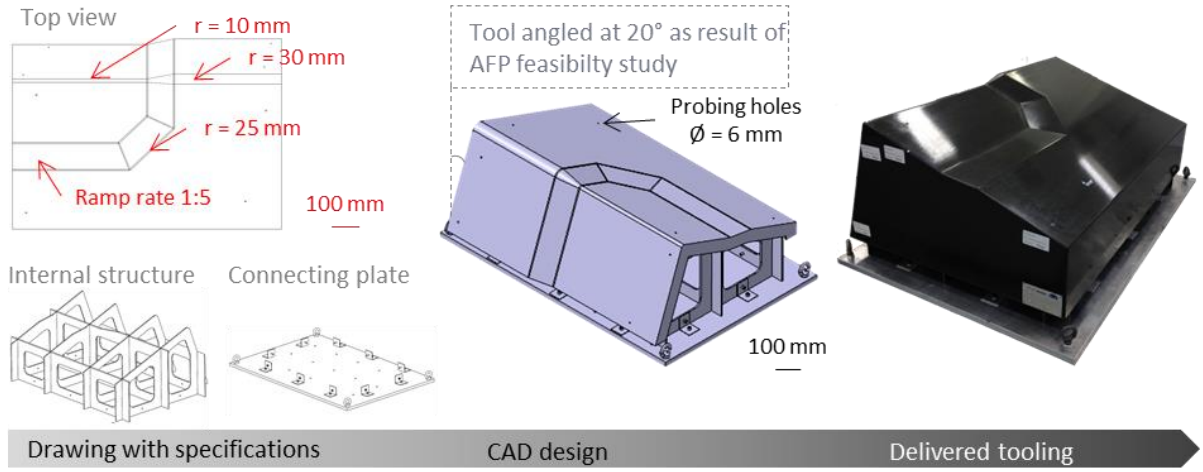

Figure 6-2: Tooling details of the demonstrator from drawing through to the manufactured tool

The ply book used is the same as previously outlined in Figure 4-15 applied to the demonstrator. The cross section of the internal structure at the ramp area to highlight the used layer structure can be seen in **Error! Reference source not found.**. Skin plies covered the entire part; the central continuous ply separates two distinct wedge pack stacks of 50 plies each. All plies were deposited by AFP, but only the two lower skin plies covered the double curved surface and therefore required complex programming. All other plies were programmed with an automated programming tool with geodesic fibre orientation; seven repeats of this demonstrator part were made.

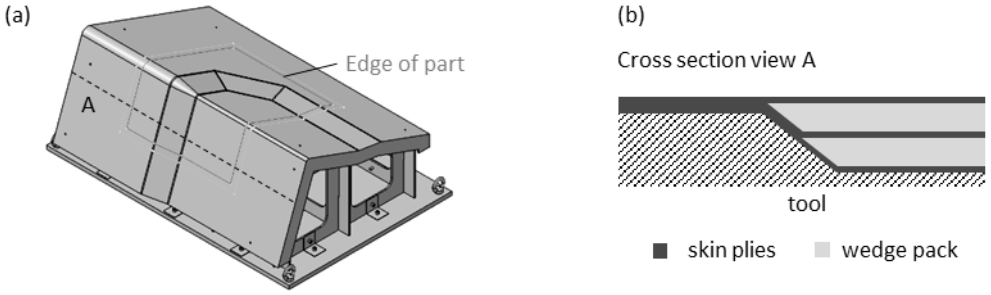

Figure 6-3: Laminate design of the demonstrator preform, tool with edge of part (a) and the cross section of the part showing the wedge pack design in cross section view A (b)

The challenge of the design in the programming stage for this demonstrator were non-geodesic fibre paths due to the thickness change over the corner. Programming complex structures is one of the significant up-front investments required to utilise the AFP process, bearing high cost and risk of failure. To move towards a scenario in which the initial phase is fully digitalised and is not reliant on significant experience, the COTS programming software was assessed to identify challenges that prevent to achieve this goal. The software used offers an integrated software tool to predict fibre path quality, which is commonly used by programmers to optimise fibre paths. However, it had not yet

been explored if the software tool provides a sufficiently accurate representation of the deposition quality in reality. Subsequently, the manufacture of seven demonstrators was used to verify the transferability of findings of the previous chapters and allows assessing the limitations of using small-scale trials for an industrial manufacturing process. Demonstrator preforms were manufactured and measured throughout the deposition and infusion stage. This part of the work provides realistic insights into the scalability of the process and allows investigating economic aspects such as productivity. In summary, this chapter aims to:

(1) Develop and apply a method to determine the predictability of preform quality based on the comparison between the geometric information provided by AFP programming software and the measured surface topography of the manufactured preform (section 6.2).
(2) Utilise the previously defined ADFP process and the infusion process to confirm their applicability by comparing preform V_f to laminate V_f and identify aspects that were not observed in small-scale trials (section 6.3).
(3) Assess the productivity and the time different activities take during the ADFP deposition stage, and compare the values to known values obtained during prepreg AFP manufacture (section 6.3).

6.2 Program-based Predictability of AFP Manufacturing

It is current industrial practice to optimise the fibre paths based on nominal outputs of the programming software, which provides a geometrical analysis of the target fibre paths. However, there is a lack of critical assessment of the program capability to predict preform quality. As determined in Chapter 2, due to the difficulties in analysing and quantifying the deposition accuracy and the accumulated error, there is little in-depth analysis available in literature [41]. This work will take the first step towards closing this gap by assessing the extent to which the programming software output can provide information about the deposition quality, and if its use as a tool to inform program optimisation is adequate.

6.2.1 Programming Challenges

The program of a complex part for AFP deposition had to consider multiple conflicting requirements. The main drivers for these constraints are imposed by requirements of mechanical behaviour of the laminate and productivity. Common constraints of the manufacturing process are:

(i) Minimum steering radius: 900 mm (experimentally determined in section 4.4)
(ii) Maximum allowable angle deviation of a course: 3° (industrial practice [145])
(iii) Maximum allowable gap width between courses: 1 mm (industrial practice [28], [124], [253])
(iv) Maximum cut tapes within a ply over a specified area: none (avoid internal defects)

(v) Minimum number of tapes per course: 8 tapes (highest machine dependent capability)

The preform acceptance criteria for most aerospace parts are very similar to these listed criteria but can vary based on part type (load bearing or not). For the purpose of this work, the outlined requirements were set based on industrial experience as well as findings of the previous work and the starting point for program optimisation.

Angle deviation describes the deviation of a programmed fibre path from the reference coordinate system. This deviation was set as a limit in the programming stage; it is usually based on mechanical performance requirements. However, if this deviation maximum is fully utilised in the programming stage, potential discrepancies in the manufacturing stage may exceed this limit. A mixture of machine inaccuracies, transfer of the software into a machine code and material behaviour during the deposition all may contribute to additional deviation from the planned deviation in the fibre path. The sum of these factors may potentially exceed the allowed value. It was out of the scope of this work to differentiate the contribution of these factors to the overall discrepancies, but this work will identify if further work was required to understand the origins of potential discrepancies, or if the current capability is adequate.

The number of cut tapes was avoided to prevent any negative influence of overlaps or resin rich areas. Avoiding discontinuous tapes i.e. not allowing cut tapes within the ply was treated as a non-negotiable requirement throughout the work. The number of tapes per course has a significant impact on productivity, as it determines the number of robotic motions, and therefore duration required to deposit the material. The minimum number of tapes per course should be as high as possible to maximise the productivity. The number of tapes may need to be reduced significantly to deposit tapes along a corner radius. A reduction to two tapes on the 10 mm radius and four tapes on the 25 mm radius is necessary when depositing directly along the corner on the L-shaped section, as reported by Di Francesco [202].

6.2.2 AFP programming and Assessment Methods

The software tool has a significant limitation in taking the characteristics of the tape materials into account. Therefore, the predictive capability was assessed using a series of deposition trials to compare the prediction with the real outcome. The manufacturing quality of these paths was assessed immediately after the deposition. This work proposes methods for single ply inspection by more objective means than solely relying on simple visual inspection producing highly subjective results. In particular, this work focuses on two aspects of potential discrepancies by analysing the difference between the programmed target fibre paths and the actual courses (angle deviation) as well as out-of-plane fibre wrinkles on the manufactured preform induced by fibre steering.

Programming Procedure

The programming process requires several different proprietary and often machine specific software. This work focused only on the software package provided by the machine manufacturer of the used machine. Initially, a composites design software package embedded in CATIA® (Composite Part Design, Dassault Systemes, France) was used, exporting the laminate sequence to CATFiber® (Coriolis Composites). On a ply level, the part contours were defined and guide curves were generated. This can be a partially automated process in the case of simple geometries using in-built programming tools, and a manual time-consuming process for complex geometries such as the presented demonstrator (custom curves). The individual tapes were generated using CADFiber® (Coriolis Composites). At the end of the programming process, the software shows geometry-based information such as steering radius, roller contact based on a non-conforming roller, angle deviation from a reference rosette and gap width between courses as a graphical output. This information is based only on the created program and is frequently used for optimisation. Therefore, it was important to understand the reliability of the information provided by the software. When the optimisation cycle is completed, the entire laminate sequence is simulated in the virtual cell, where robotic movements are specified and clashes between the end effector and the tool were detected. The heating system required is dependent on material type, but material behaviour was not considered. A post processor then compiles the program into a file format that is transferred to the machine, where the program can be run. This step can potentially add some inaccuracies, because discrete points are transferred, and spline interpolations are generated by the post-processor. Further design iterations and other improvements e.g. of the robotic movements take place based on the visual assessment of the deposited tapes and observations.

Some automatic path planning options are available, but generally optimise one single objective, e.g. a geodesic fibre path can be programmed automatically and avoids all steering but is likely to violate the angle deviation rule. The result of an initial feasibility study of the ply directions 45° and 135° showed that automated programming tools were not sufficient to meet the design guidelines. The multitude of requirements and a lack of optimisation algorithms leads to manual optimisation of the program during the design process. The demonstrator was only a partial structure and therefore relatively small in comparison to parts that would normally be manufactured using AFP. This requires often rather abrupt directional changes, making the geometry more challenging than most industrial components in terms of programming. Most initial constraints had to be relaxed in order to ensure manufacturability as it was not feasible within the time and budget constraints to satisfy all requirements. The angle deviation was extended up to 17° locally, however only the discrepancy between the planned fibre path and the actual course was assessed as part of this work, so the impact

of this change had a minimal effect on the presented work. The number of tapes was reduced to increase the gap frequency, which has the positive impact of decreasing the need for wide gaps. This had a negative effect on the productivity, but it was not the focus of the work to enhance the productivity and was therefore acceptable. As a 1 mm gap with was highly restricting to the programming process, and a maximum gap width of 2.5 mm was allowed.

The small dimensions of the demonstrator do not allow small radii to transition into larger radii over long distances, leading to relatively abrupt radius changes. Therefore, compromises on the requirement steering radii were made, as a preliminary feasibility study showed that the low radii paths (as low as 20 mm) with a short transition length can be manufactured without tape pull-ups. The very low radii in the resulting fibre paths often occur only over a very short distance (~10-30 mm). Even though the previous results in section 4.4 indicated that a reduced arc length has a negative effect on wrinkle formation on a flat surface, this was not replicated on the demonstrator.

Experimental procedure

Tapes were deposited on a complex geometry with the previously defined and adjusted parameters and the actual deposition quality was correlated with the result of the programming software tool. Due to the complexity of the tool, the vacuum bag used was Stretchlon® 200 (Airtech International Inc., Huntington Beach, US). The actual path quality was measured utilising the surface topography of the preform captured by a laser line scanner. The CAD drawing of the tool was imported into the metrology software and aligned to the scanned data by probing the real ply prior to scanning it. Probing holes were used to match the physical locations of the reference mould surface and the scan results using a 2 mm diameter probe attached to the articulated arm of the laser line scanner. The holes in the CAD model were not the nominal holes as drawn but corrected by measurements using a GOM system (Atos Triple Scan, GOM, Germany) during the tooling acceptance procedure. The surface topography of a single ply onto the tool was converted into a colour plot, taking the measured height from the tool, using the previously described inbuilt functionality of the software.

Steering Path Quality Comparison

Every machine program was exported highlighting the steering radii resulting from the fibre paths. This was an output plot generated through the software, based on the geometry of the fibre paths. These plots were then compared to the experimental outcome, by overlaying the two images. This provided an assessment on how accurately the CADFiber® plot can identify the areas with fibre steering induced wrinkles.

The metrology software has an in-built colour-plotting tool, which uses the height information of the gathered data against a reference, in this instance the probed tool. The shortest distance of the

individual points against the CAD tool was represented by colour. The colour plot was dependent on the probing quality, and the accuracy of the absolute numbers was not verified. Therefore, the absolute numbers of the height information should be regarded as indication and not as measurements. Nevertheless, the height difference between the collected data points was not reliant on the probing quality and provided valuable insight. This data was then compared directly with the quality prediction of the analysis tool provided by the AFP machine manufacturer and determined if the geometry-based quality prediction is a credible tool for programming optimisation.

Compaction pressure

Compaction pressure can be analysed by the AFP programming software using the nominal distance of a virtual rigid roller (not conformed to the geometry) to the tool, as shown in Figure 6-4. The areas where the distance between the roller and the tool was > 0 mm is only an indication of potential loss of contact, as the roller conforms in reality. The proposed integration of a roller compaction simulation by Giddings and Di Francesco has not yet been integrated into the AFP software to improve the accuracy of the prediction [73].

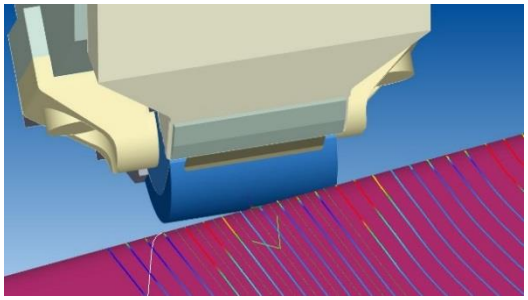

Figure 6-4: Detailed view showing the behaviour of the digital roller and the resulting compaction prediction in CADFibre®

Experimental Assessment of Angle Deviation

To assess the angle deviation of a ply against the programmed paths, the point cloud collected using a laser line scanner was meshed using an inbuilt function of the metrology software (PolyWorks Inspector). The mesh was then imported into a second software package of the same metrology software (PolyWorks Modeler), where a feature detection tool was used to isolate the centre line in the gaps between courses. The coordinates of these detected gap centre lines were exported and used for further processing in a Matlab routine, see Figure 6-5. The coordinates describing the centre lines of the tapes adjacent to each gap also provide an input to the Matlab routine, which were exported from the AFP programming software. A spline interpolation for all datasets ensured equal point density across the dataset. The coordinates of the gap centre line were paired up with the matching tape centre coordinates that were located left and right of the gap (Figure 6-5 (b)). The

nearest neighbours of the individual data points between the three data sets by Euclidean distance were determined for all three datasets.

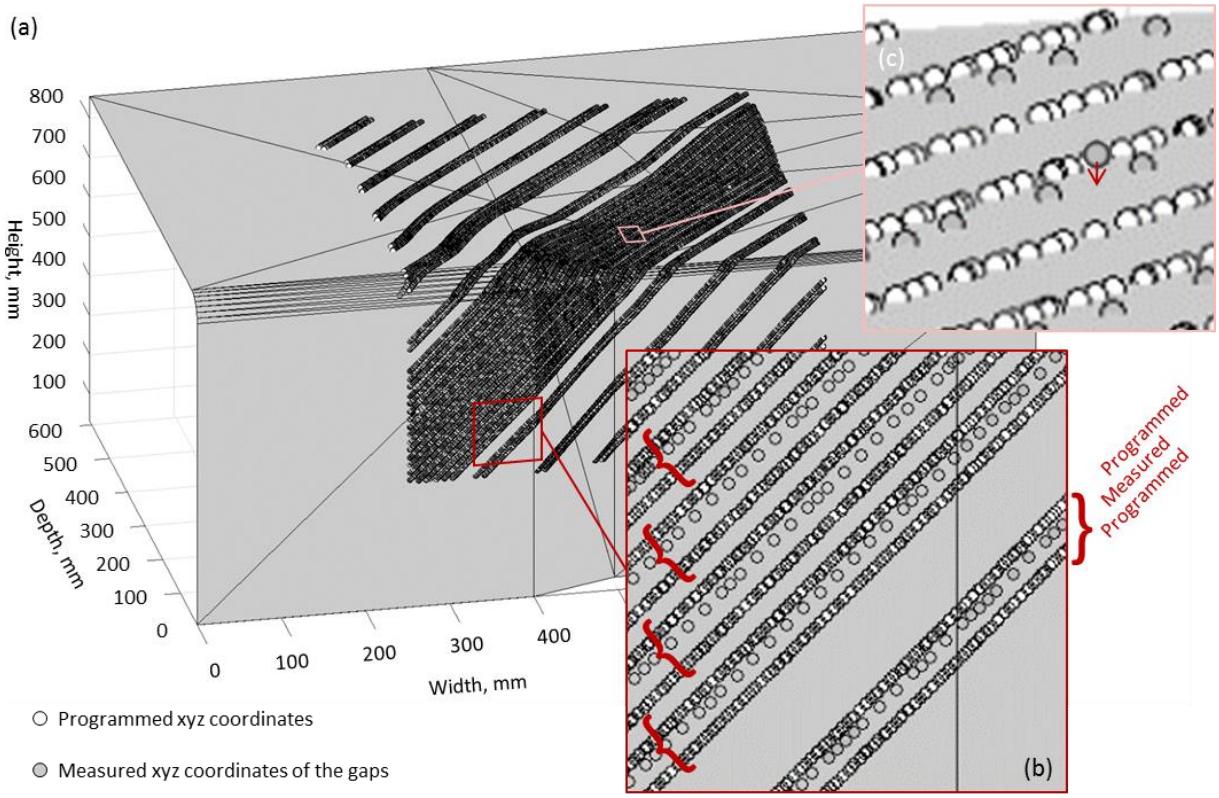

Figure 6-5: Input data used in Matlab routine exemplary overview of 135° ply (a), detail of triplet datasets used for comparison (two tape centre lines exported from the program and one measured data set of the gap centre line per triplet, indicated by curly bracket) (b), and an illustration of data point projection (c)

The Matlab routine was coded to create and compare vectors between each point and produce a plot indicating the angle deviation of the vectors of the experimentally determined paths to the programmed paths. Two subsequent points of each line were used to define a vector, see Figure 6-6 (a). The two nearest neighbouring vectors of the programmed path were paired up with the nearest neighbour gap centre line vector. Even though the three vectors should all be on the same plane locally, experimental data can exhibit a slight offset. To avoid the measurement of out of plane angle deviation, the data points of the gap centre line was projected onto the created plane of their closest neighbours; see Figure 6-5 (c). The sum of the vectors that describe the two tape centre lines calculated a vector representing the gap centre line from the programmed fibre paths, Figure 6-6 (b). The resulting vector provided a direct comparison to the data of the measured gap centre line within the same plane. The inverse cosine was used to determine the angle Θ between the two vectors.

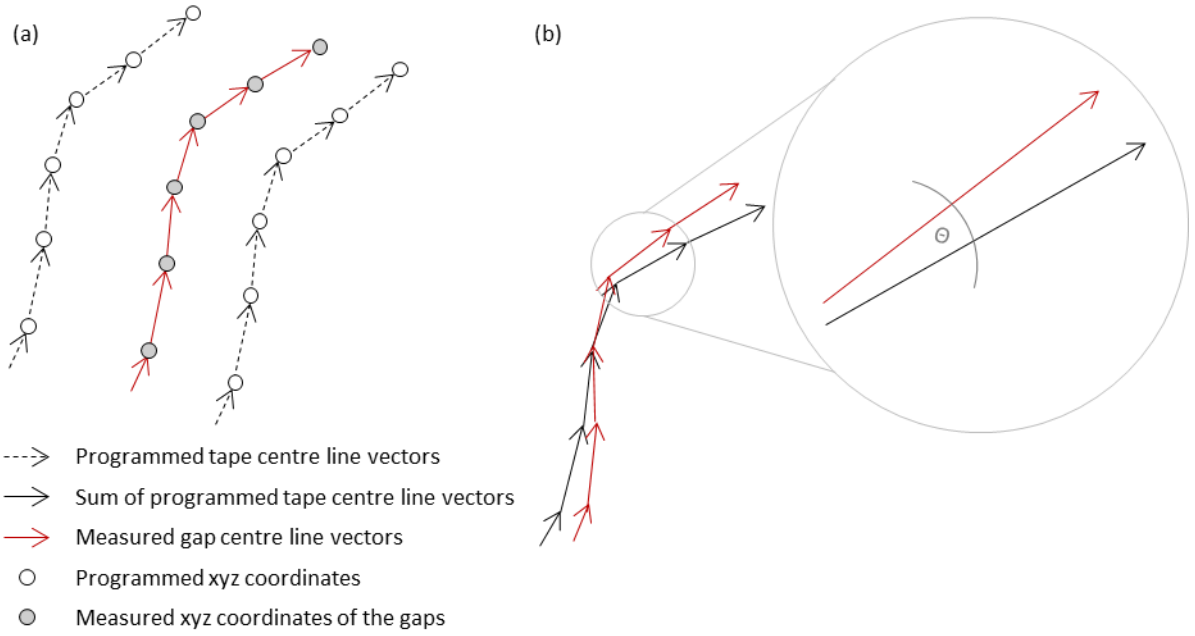

Figure 6-6: Vector representation of the data (a) converted from measured program data, (b) comparison to obtain angel deviation Θ between the sum of programmed vector and measured vector

The determined angle was plotted using the coordinates of the measured gap centre line with the angle as a fourth dimension represented as a colour plot as an output of the Matlab routine.

6.2.3 Results and Discussion

Effect of Steered Fibre Path on Preform

The use of the data collected with a laser line scanner to visualise the deposition quality was a valuable tool as the colour-plotting tool facilitates the interpretation of the results. Figure 6-7 exemplary shows the steering analysis of a 45° ply with seven manually generated curves with only four tapes per course. In Figure 6-7 (a) the numbers in the triangles represent the number of tapes used in the courses, with a four indicate the manually created guide curves, six and eight tape courses were automatically generated. The direction of the arrows indicates the direction of the deposition.

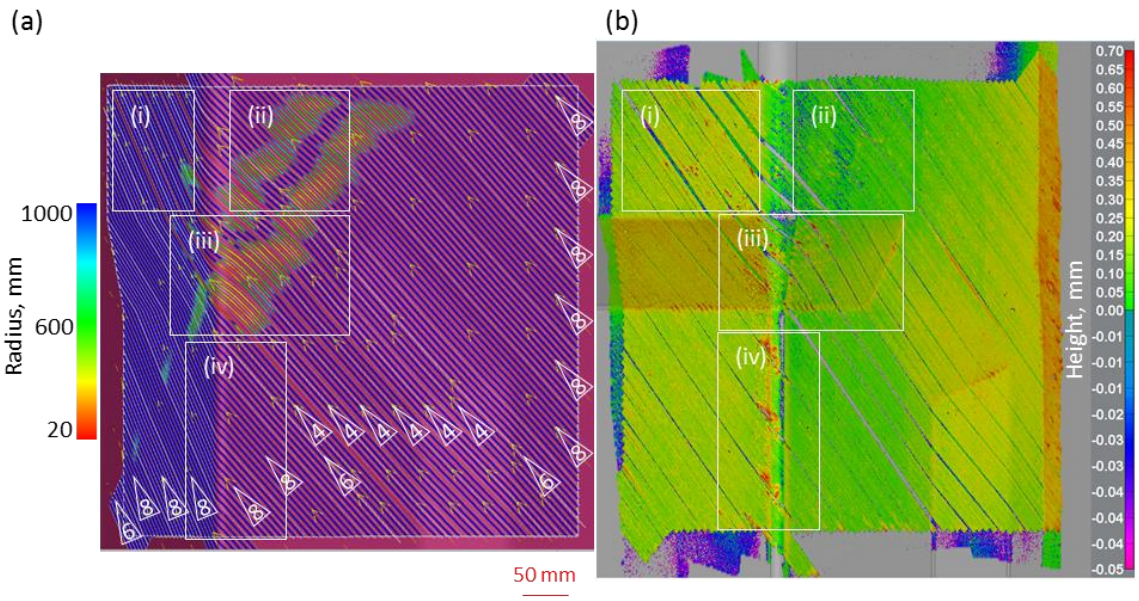

Figure 6-7: Steering analysis on 45° ply from AFP programming software (a), thickness colour plot of measured data (b) with (i) area of nominally no steering; (ii) area of medium steering radii 600 - 1000 mm); (iii) area of low steering radii (20 – 600 mm); (iv) area with out of plane wrinkles but no steered fibre path

The three rectangular areas marked in Figure 6-7 show different scenarios. Area (i) shows an area that exhibits some wrinkles in the scanned data even though the steering analysis does not indicate a steered fibre path on the flange of the demonstrator. Area (ii) shows relatively few peaks in an area that had two distinct areas that contain a radius of 600 - 900 mm according to the program. A delay between the predicted radius and the occurrence of wrinkles in the direction of deposition can also be seen in area (ii). Area (iii) shows an area where some wrinkles were predicted by the software appear in the preform, but only tapes near the inner radius of the course were affected. Area (iv) indicated out-of-plane distortion near the corner with the 10 mm radius fillet, which was not an area including steering. However, these areas were visible in the compaction analysis shown in Figure 6-8.

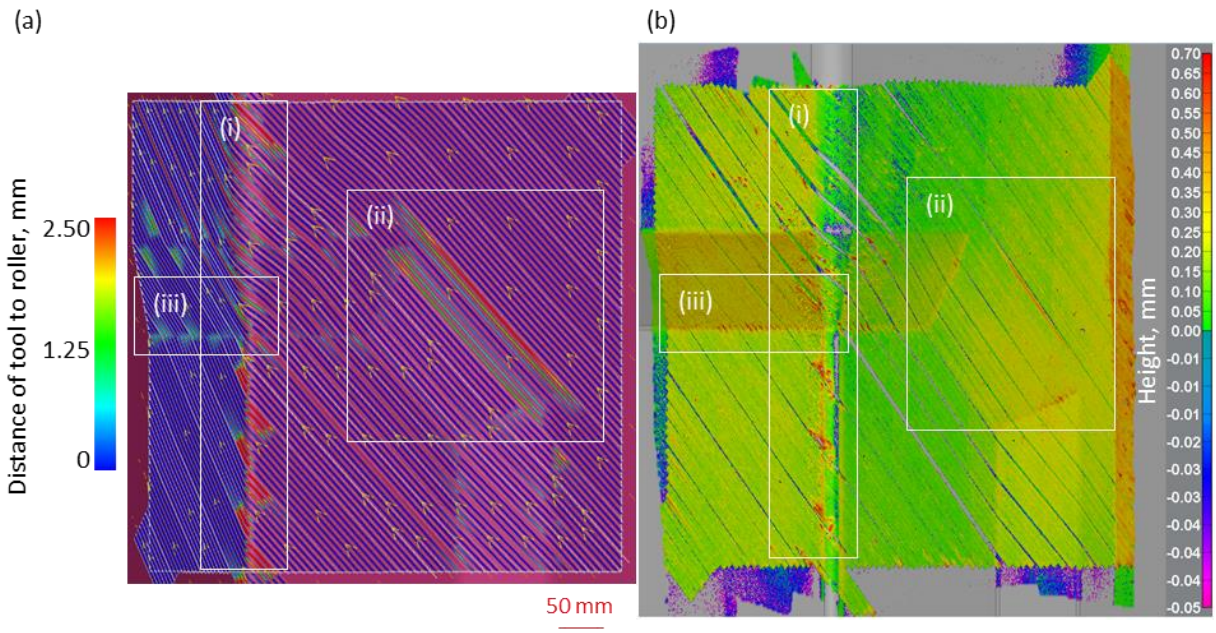

Figure 6-8: Compaction analysis on 45° ply from AFP programming software (a), thickness colour plot of measured data (b) with (i) corner area with only partial roller contact; (ii) area of partial loss of roller contact; (iii) area of minor loss of roller contact

Figure 6-8 (a) shows the resulting compaction analysis, with significant loss in roller contact in area (i). This does not prevent deposition of the tapes in reality, but the loss of contact might cause out-of-plane distortion visible in Figure 6-8 (b). The loss of contact not only results in a lack of compacting pressure, it also changes the heated area significantly. This change in heating area can prevent sufficient exposure of the binder to the heat source and the binder may not be fully activated in these areas of the geometry. Only the fibre tension caused the tapes to lay on the tool where the courses were tacked on either side of the corner on the flanges of the L-shaped section. This could potentially cause a slip between tape material and roller or tape material and tool. Area (ii) was an example for the over-prediction of loss of compaction due to the stiff roller. In reality, the roller conforms to the shape of the ramp and only the red areas show that the tape was not fully adhered to the substrate. It is difficult to establish a threshold for the loss of contact. While area (ii) suggests a threshold of 2.5 mm distance between roller and the surface, area (iii) exhibits out of plane distortion in an area with a 1 mm distance. The colour plot of the preform exhibited some fibre bridging due to a lack of compaction. The appropriate threshold is highly dependent on the ability of the roller to conform to a specific geometry and therefore its conformability and the applied force.

For comparison, some photographs of the same ply are shown in Figure 6-9, where the distortions highlighted by the metrology software were barely visible. This shows that the commonly used practice of visual inspection fails to detect patterns that were clearly visible and enhanced in the colour plot.

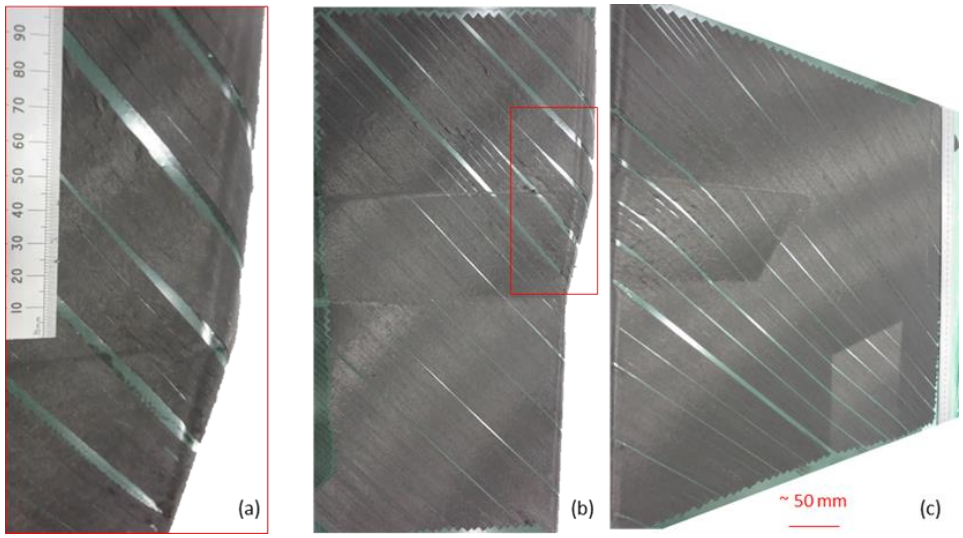

Figure 6-9: Photographs for comparison of the ply shown in Figure 6-8, (a) detail of corner, (b) shorter flange, (c) flange with ramps (due to the distortion in the photographs, only an approximate scale is provided in the larger images)

There was a delay between the start of fibre steering indicated by the software and the formation of wrinkles. This effect was more pronounced on a 135° ply than on a 45° ply, shown in Figure 6-10. In both rectangular areas (i) and (ii), the predicted fibre steering is visible before the actual wrinkles started to occur in deposition direction. Furthermore, area (ii) in Figure 6-10 (a) shows a gradual change from a relatively low radius at the lower ply edge to an extremely low radius towards the corner. However, the height plot in Figure 6-10 (b) does not show such a gradual change; the severity of the wrinkles appears relatively uniform within the area of predicted fibre steering in area (ii).

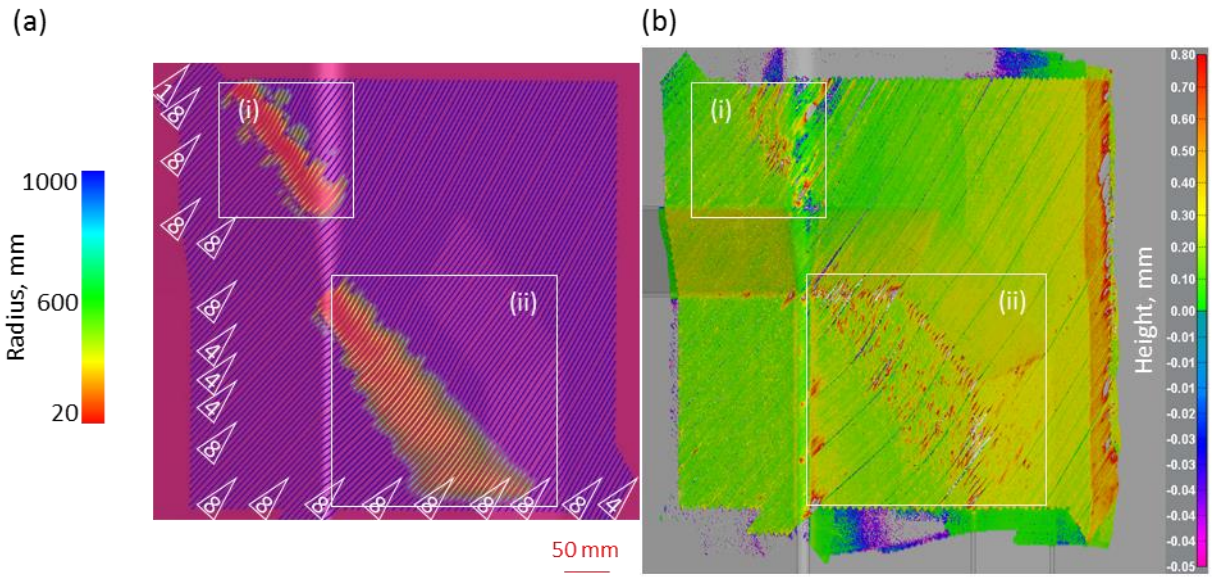

Figure 6-10: Steering analysis on 135° ply from AFP programming software (a), thickness colour plot of measured data (b): (i) area of significant steering with radii as low as 20 mm; (ii) area of variable steering radius

Steered areas in the measurement appear to occur further ahead in the deposition direction than the prediction, an observation that was made on the majority of tested plies. To investigate this phenomenon further, the individual images of Figure 6-7 and Figure 6-10 were combined into overlays as shown in Figure 6-11. The coloured areas were from the metrology data colour plot, the light and dark overlay was the radii prediction from the AFP path planning software. In Figure 6-11 (a), the area of lower steering radii, lighter than the remaining ply, shows clearly that the wrinkling begins to occur approximately in the middle of the steered area. This delay can be up to 50 mm along the length of the path with a radius, but this distance can be shorter, as shown in Figure 6-11 (b).

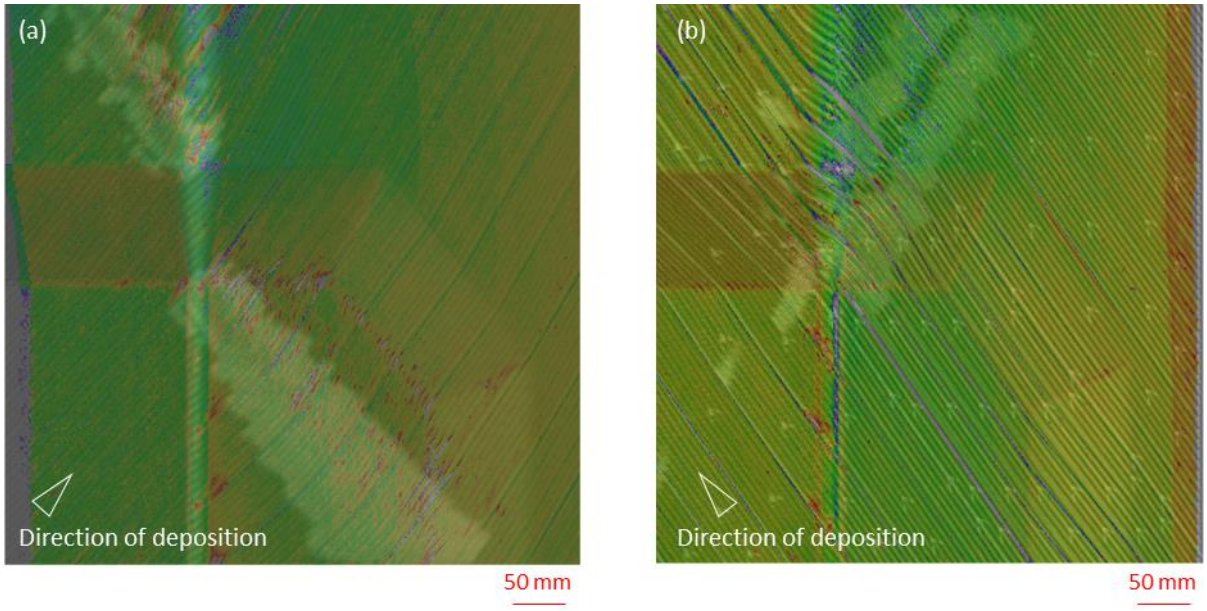

Figure 6-11: Overlay of height plot (coloured) and AFP program output (light shading fibre path steering; dark shading: straight fibre path) exemplary for (a) 135° ply with geodesic central area and (b) 45° ply with central custom curves

The overlay plots show a clear discrepancy between the predictive capability of the software and the actual quality of the deposited tapes. Due to restrictions of the COTS programming software, the data underlying the predictive colour plot cannot be exported. This means that a quantitative comparison cannot be made within this work, but some qualitative insights into the causes were made.

The causes for the observed delay could lay in inaccuracies of the machine, the material behaviour or a mixture of the two. It was not possible to compare the planned machine movements with the actual machine movements, which could potentially cause part of this observed discrepancy. The machine programme is approximated by the machine using discrete points and a spline interpolation to connect these points, the density of the points fed into the post processor generating the G-code could introduce some error in accurate delivery. It would be unlikely, that such an error could cause the entire delay of steering a fibre path by as much length as observed. A further potential contributing

factor was the ability of the tape to absorb small length discrepancies through internal imperfections such as waviness of the fibres present in the material, refer back to Figure 4-36 (b). The tape releases the stress inflicted by the length differential during the steering motion in the form of wrinkles (compression on the inside of the tape) and tape pull up (tension on the outside of the tape). However, in the initial phase with a large steering radius, the internal structure may be able to absorb the length differential resulting in straightening of internal wrinkles and an increase of predominantly in-plane wrinkles. A possible explanation for the delay in the appearance of wrinkles could be that the tape absorbs the induced stress through internal shifts within the tape, a behaviour observed in woven fabric and NCF [255]. A delay in wrinkle formation can also be attributed to the transition from straight to the final fibre path radius to create a smooth transition between straight and steered fibre paths. This caused a decrease of the fibre path radius to a critical point where the length differential increases significantly leading to stress release as out-of-plane wrinkles. This would lead to the initial phase in the steered path to appear unaffected, as the effect is either not an out-of-plane effect or small enough not to be captured with the laser line scanner.

The previously described method of defining a minimum steering radius based on a single radius fibre path was not a reliable input for the complex programs for dry fibre material. The area highlighted in Figure 6-11 only shows the steered state (light shading) and the non-steered state (dark shading), without differentiating the radii. Referencing back to Figure 6-10 (a), the incremental change was visible. The radii decrease incrementally along the length of the course (later to increase after the steered area) within the demonstrator component. The resulting mixture of different radii present within the steered area on a component was significantly different to single radii tests. A single radius test was not representative, and the results can therefore not be used to determine a minimal steering radius.

Other contributing factors could include material slip on roller and tool and the change in the pressure field under the roller due to roller compliance to geometrical features. Furthermore, the influence of lack of binder activation in some areas due to a change of the heating area over geometrical features could play a role in the preform appearance.

In summary, the mechanisms behind steered deposition have not yet been fully understood and it appears that various mechanisms coincide. Process parameter variation, machine inaccuracy and material behaviour were all likely to contribute to the difference of the predicted fibre path and the actual steered course. This work showed that the small-scale tests with single radii on a flat tool only provide very limited information that was not easily transferable, as too many variables were not represented. The steering radius limit determined by previous trials of 900 mm based on the

observation of tow pull-ups was not applicable to the complex geometry, at radii as low as 20 mm, tape pull ups did not occur.

This work proved that the limitation of the AFP programming software tool to account for material behaviour affects the accuracy in predicting of the preform quality. The presented method provides a way to capture the out-of-plane features occurring with a specific material, machine program, deposition parameters and tool geometry, which is an improvement to visual observation only. This means that captured data could be collated in a manufacturing feature library, which could provide useful guidance for similar cases. Once the mechanisms of a steered path are understood better, predictive capability of a path planning software could be enhanced by material models representing the actual behaviour as part of the software.

Accuracy of Fibre Angles Predicted by AFP Software

Angle deviation was a suitable metric to quantify the accuracy of the individual courses following their planned fibre paths. By comparing the deposited course with the fibre path program, a cumulative error of machine program and material influence can be assessed. The majority of deviations occurring were very small, indicating that the prediction made by the software was relatively close to reality. Much of the detected disparity was below 0.3 ° across all trials for the 45 ° plies (69-75 % of all calculated angles across five repeats). Similarly, for the other direction tested (135 °), the majority of all detected deviations were below 0.7 ° (75% of all calculated angles, two repeats).

Even though these results show that the deposition process follows the prescribed fibre paths in general, the deviations that were detected accumulate mostly in the corner of the L-section, as seen in Figure 6-12 and Figure 6-13. Deviations of > 3 ° across all five repeats occur consistently at the upper and lower end of the chamfered ramp where the tool exhibits double curvature, particularly isolated on the 45 ° plies. For the 135 ° plies, the fibre angles deviated more over the entire corner of the L-shaped section. The areas of the flat flanges show a relatively low angle deviation, even in areas where the course follows in-plane steering paths.

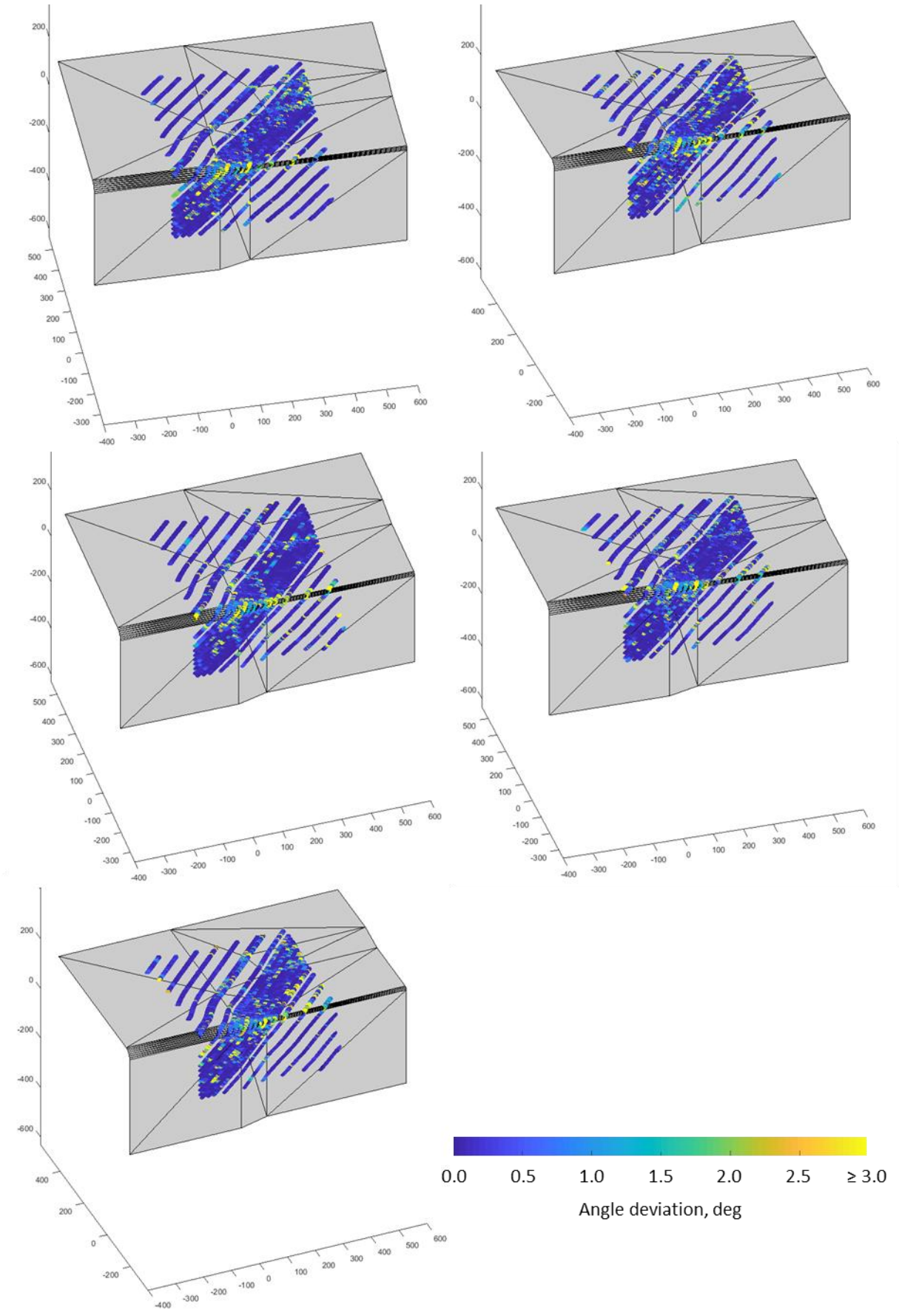

Figure 6-12: Results of five first ply deposition trials with the same fibre path program (45°)

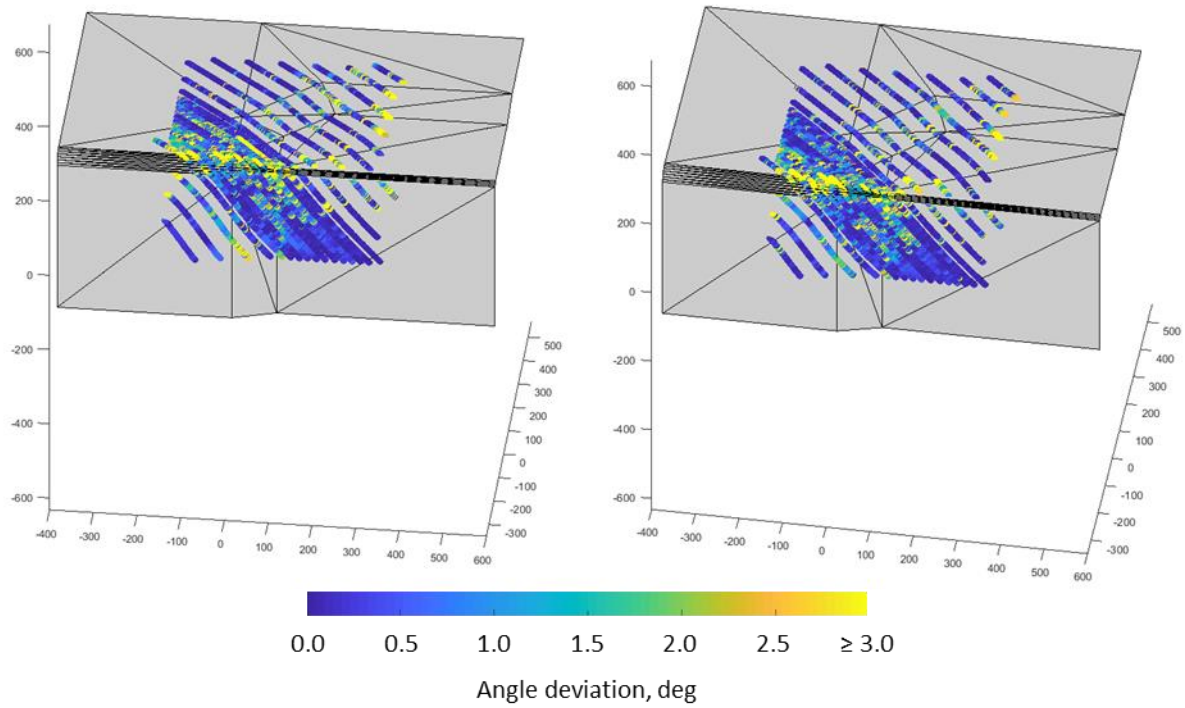

Figure 6-13: Results of two first ply deposition trials with the same fibre path program (135°)

The presented results show that the predictive capability of the fibre path planning software for angle deviation was good on geometrically simple areas. However, the results also highlight the need for more accurate path planning predictions for complex structures, and potentially a margin accounting for the manufacturability variability. As this proof of concept tested on a highly complex structure, it would be beneficial to reduce the geometrical complexity for the analysis and assess discrepancies on isolated geometrical features first, and then build up the complexity to isolate the type of geometrical features that had the highest impact on the loss of accuracy in the predictability.

6.2.4 Concluding Remarks

This section assessed the predictive capability of AFP path planning software by comparing the software outputs with manufactured plies. A method was developed using standard tools such as the AFP programming software, a metrology software and a Matlab routine. Neglecting material characteristics, program conversion and robotic accuracy when predicting preform quality had a significantly negative effect on the prediction accuracy of wrinkles. Neither position nor severity of wrinkles were well represented by the programming software. The programming software was able to indicate areas where inconsistencies occur but was not suitable to predict wrinkled areas accurately and therefore was not a reliable tool for path planning optimisation. In order to use the software output as optimisation tool, the prediction capabilities require further development to incorporate material behaviour to become a more accurate representation of reality.

The use of a minimum radius derived from visual observation of in-plane steering was not suitable to recommend a minimum steering radius suitable for a complex geometry to manufacture ADFP preforms. Aspects introduced by steered fibre paths over a geometry were not captured in the simple coupon sized tests, such as variable compaction pressure and changes in the heated area at the nip-point. A more extensive test campaign would be required to capture the material behaviour fully.

The prediction of angle deviation was relatively accurate on flat areas, but deviations from the fibre path were observed in the corner region of an L-section. Part of the margin for angle deviation that determines the program (for example 3 °) should partially take into account manufacturing variability (up to 0.7 ° in the tested configuration).

This work proposed assessment methods to track the impact of the path planning strategy on a particular aspect of the program enables fine-tuning the paths more efficiently to minimise the risk of defects. Such a measurement can aid to reduce the trial and error approach in the process of programming a complex part in the future. Due to the current trial and error approach towards programming complex parts, the learning process is constraint to individuals who carry out the task of optimisation. Deposited plies are not captured quantitively and visual inspection often drives design iterations. The proposed method to collect and analyse data of deposition quality could eventually be used as a database within the software, for example to flag up warnings or integrated into a training and knowledge management system.

6.3 Demonstrator Manufacturing

Once the program paths for the complex plies were finalised, the full demonstrator was programmed. The manufacture of multiple demonstrators enabled two key aspects; quality assessment in an environment close to an industrial application as well as some insights into productivity. For a suitable comparison of productivity, the time log data from an additional project was used.

6.3.1 Material and Experimental Method

Preform manufacture

The final stage of this work was programming and deposition of the full demonstrators.

The AFP machine was setup with the parameters for the trials conducted as outlined in Table 6-1 as a result of previous assessments. Predictions based on previous trials (thick part and variable thickness part) estimate an expected preform V_f of at least 51 %.

Table 6-1: Machine parameters used for demonstrator manufacture

AFP machine parameter	Settings
Roller type	Shore 40A silicone roller
Laser optics	8 mm x 57 mm spot size
Optics target	Nip point (30%/70%)
Target temperature	280 °C
Compaction pressure	0.47 ± 0.14 N/mm^2

The heating law used had a target temperature of 280°C at the visible nip-point. The piecewise linear approximation of the power law adjusting the laser power can be found in Table 6-2, as previously determined and modified in Chapter 4.

Table 6-2: Piecewise linear approximation of the power law adjusting the laser power for a target temperature of 280 °C and the processing parameters as outlined in Table 6-1

Target temperature		**280°C**
Point	**Speed, m/s**	**Power, W**
1	0.00	3
2	0.01	89
3	0.02	134
4	0.04	203
5	0.08	307
6	0.16	467
7	0.32	710
8	0.64	1081
9	1.00	1417
10	2.00	2160

High Temperature Infusion

The infusion was set up in the same way as the infusion process described in section 5.3. The resin system used for the work within this section was EP2400 as opposed to the previously used RTM6. Initially the majority of the infusions were conducted using the system RTM6 with the advantage of comparability, but the disadvantage was that this resin system is only recommended for use with Material D. To achieve a closer representation of the industrial manufacturing process, a change of resin systems to EP2400 was carried out for the infusions of the demonstrator. An exemplary infusion process of a demonstrator can be seen in Figure 6-14.

(a) (b)

Figure 6-14: Photograph of the infusion set up in the oven before (a) and during the test through the glass door of the oven (b)

6.3.2 Process Assessment Methods

Fibre Volume Fraction and Spring-In

The thickness of the manufactured preforms was measured with a laser line scanner in the same manner as previously described for single ply trials (section 6.2.2). The preform V_f was calculated using Equation 3-1. The analyses of the thickness measurements were carried out in the metrology software, where only the relevant areas were regarded, e.g. edges were not captured, the four flat areas considered are shown in see Figure 6-15. All areas were at least 10 mm from a geometrical change (e.g. beginning of a ramp) or the outer edge.

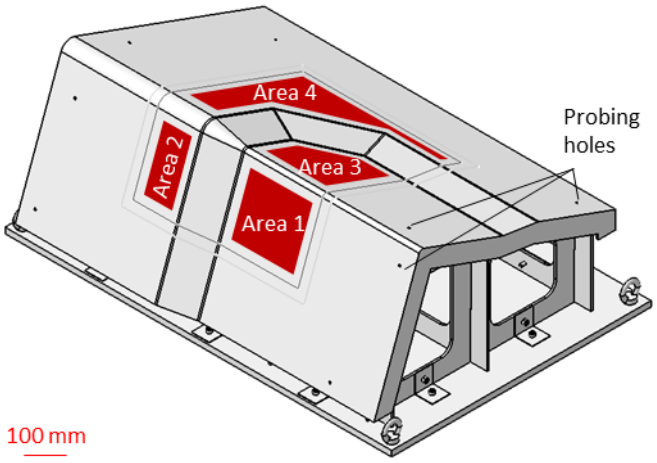

Figure 6-15: Measurement area sketches of the demonstrator projected to the tooling surface

The thickness of the manufactured laminate was measured without contact using articulated measuring arms with 3D laser scanners (refer to section 5.3.2 for details). The side of the laminates facing the vacuum film and the tool during infusion were scanned separately to allow each side to act

as a reference when inspecting different regions. All areas were identical to the preform assessment areas for comparability. The areas selected for measurement can be seen in Figure 6-16.

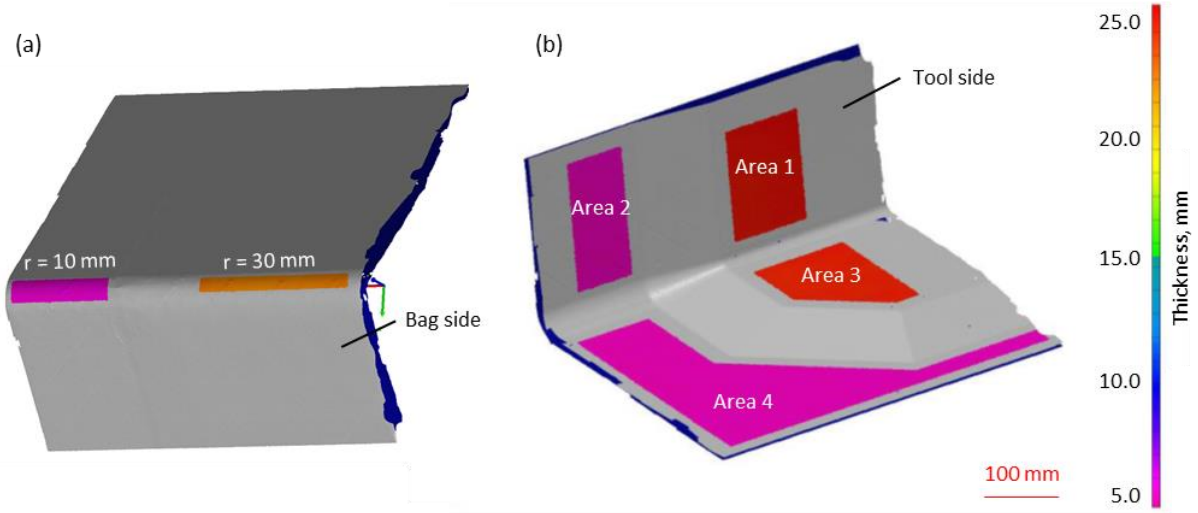

Figure 6-16: Measured areas of the demonstrator, corner regions on demonstrator laminates on the bag facing side (a) and flat regions on demonstrator laminates on the tool facing side (b)

The corner sections were examined in the thin and the thick regions separately. A Cartesian coordinate system was created such that the Z-axis was normal to the apex of the corner. The areas were selected on the bag side of the part normal to the corner apex as seen in Figure 6-16 (a).

In addition to the laminate thickness, spring-in of the L-shaped section was measured. Spring-in of composite materials is a widely researched topic, as the unintended difference of geometry causes challenges in production environments. Mechanisms that are major contributors to generate stresses and distortion during the manufacturing process are thermos-elastic spring-in, cure shrinkage and tool - part interaction, but other contributors can be stacking sequence, thickness and auxiliary materials [256], [257]. Spring-in angles reported in literature are around 1° - 2°, depending on a variety of factors [256], [258], [259]. The flange angles of the demonstrator were measured between the flat areas Area 1 and 3 as well as Area 1 and 4 on the tool side and the entire flat areas of the bag side, see Figure 6-17.

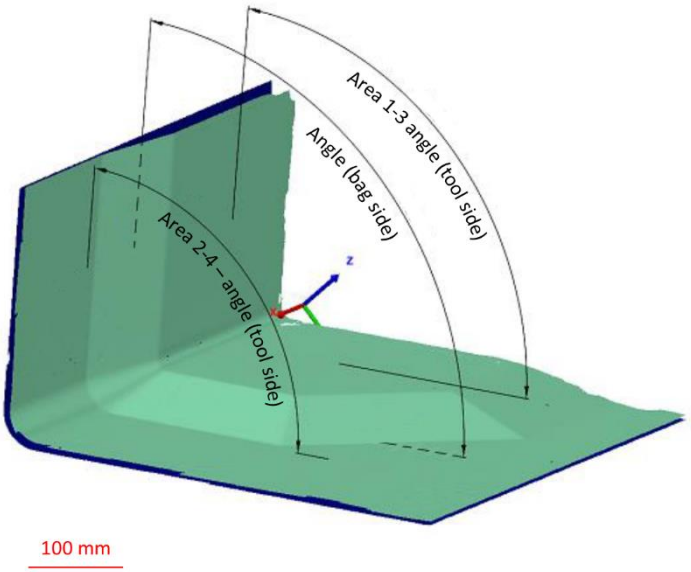

Figure 6-17: Different angles between the flanges of the demonstrator investigated on demonstrator laminate (green: tool side; blue: bag side)

Production Rate and Manufacturing Time Split

In order to assess the productivity when manufacturing ADFP preforms, time of manufacturing was recorded. Similar to the findings in literature, four activity groups were defined: setup, deposition, non-process breaks and process breaks. These were furthermore categorised into value added and non-value added, as outlined in Table 6-3. The times logged during various trials were converted into a percentage of the overall manufacturing time for comparability.

Table 6-3: Four activities defined for the manufacturing process

Activity	**Category**	**Example activities**
Setup	Non-Value adding	Probing, tool preparation for next preform, dry running.
Deposition	Value adding	Fibre deposition
Non-Process Breaks	Non-Value adding	Technician breaks, visits, machine breakdown, and other job request
Process Breaks	Non-Value adding	Material change, head clean, inspection, rework

The manufacturing time was recorded for three types of preform; simple flat QI preforms, a mildly doubly curved preforms (650 × 900 mm) as well as the demonstrator preforms. At least three repeats per type of preform were recorded. The duration needed to carry out these various activities were categorised and recorded on a sheet during the manufacturing process by the technician, which means that the recordings were subject to human error. As the set-up of the machine was not

representative in comparison to industrial manufacturing processes, it was excluded from the assessment. The difference was for example that the laser optics was mounted and removed as part of a set-up time, whereas this would not occur in a production facility. The use of a single tool means that the preform was removed and stored elsewhere. Therefore, a tool change was not part of the set-up between parts, which is an activity that would be part of an industrial manufacturing site. In addition, the tool was comparably small and could be lifted manually; the time taken to do a tool change would not be representative. Comparable values of deposition time quoted in literature are 27% and 23%, respectively [171], [172].

To complement the time split assessment outlined, the overall deposition rate was measured. However, the hourly deposition rate ($^{kg}/_{h}$), even though often used, is a debatable metric to determine productivity. Different numbers were published over the years, the reported deposition rates for prepreg materials are between 1.9 to 13.6 $^{kg}/_{h}$ [17]–[20]. Under the assumption of a laminate V_f of 55%, these values would equate to 1.05 $^{kg}/_{h}$ to 7.5 $^{kg}/_{h}$ for dry fibre material. These numbers are often reported without referencing the type of part, material or type of machine used.

6.3.3 Results and Discussion

Demonstrator Preform Quality

The thickness measurements of the seven demonstrators were converted into preform V_f and achieve an average of 50.8 ± 3.5% (2 SD), the individual measurements of the demonstrators can be seen in Figure 6-18. The corner of the L-shaped preform showed on average a 9.1 % higher preform V_f than the flange sections across all seven demonstrators, which was slightly higher than the difference observed in the simple, thinner L-shaped section (6.3% difference in preform V_f). This shows that the results obtained in a simple L-shaped geometry were showing the same trend but were not directly representative of a more complex structure. All results of the flat areas were within the target preform V_f of 50-55%, the corner was slightly over-compacted than expected with 57.8 - 61.2%.

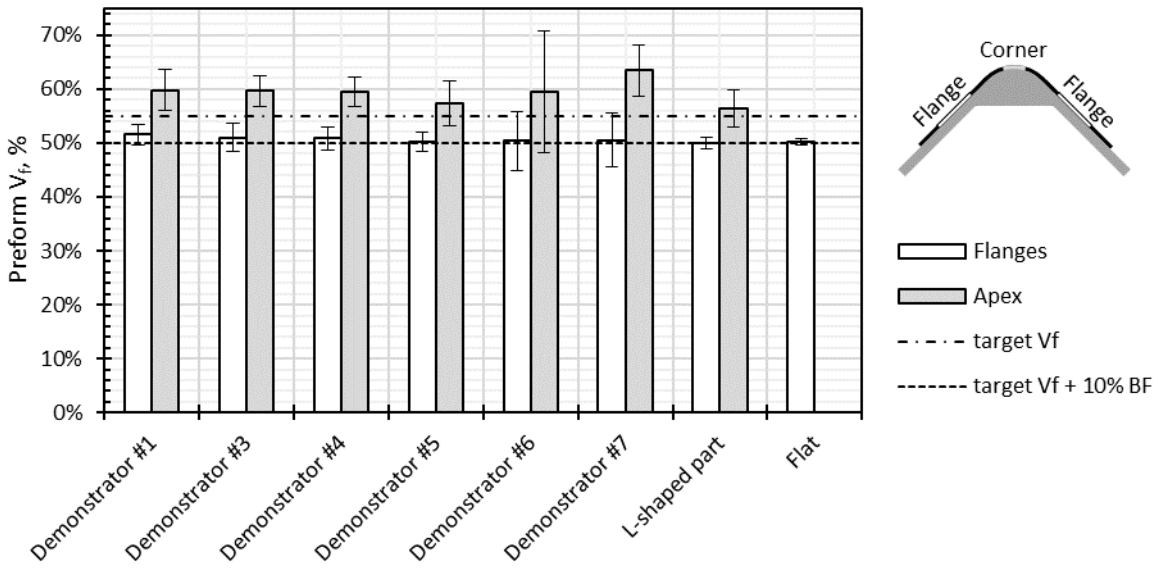

Figure 6-18: Comparison of the preform V_f of corner and flange section of the demonstrators and the L-shaped geometry

The higher deviation in demonstrator #6 and #7 can be attributed to a refurbishment of the machine. The complex geometry of the demonstrator caused a slightly higher variability in comparison to the L-shaped preform, but overall the results are similar. This section was able to prove that a systematic approach to determine the processing parameters enables a first-time right demonstrator manufacture.

Demonstrator Laminate Quality

The laminate V_f was derived from the thickness measurement using Equation 2-2. As the calculation was based on thickness only, voids were not captured, and the assumption was that the laminates do not contain voids. Across all demonstrators, a laminate V_f of 55.0 ± 3.3 % (2 SD) was achieved. Figure 6-19 shows feature preform V_f plotted against laminate V_f of the different features as well as the demonstrator. The total variability of all laminate geometries calculated by sum in quadrature for uncertainty results in 6.3 % (2 SD) for the laminate V_f, which is well above the measured variability in demonstrator #4 with 3.1 % (2 SD). This means that the combination of the features does not cause as much variability as the individual features suggest.

The preform V_f is much wider spread than the laminate V_f, showing the positive impact of the infusion step on the variability of laminates, the effect is greatest on the steered part. The variability of the demonstrator as well as the flat part with thickness change was greatest, the commonality is the high repeat of mechanical strain during deposition in thick preforms.

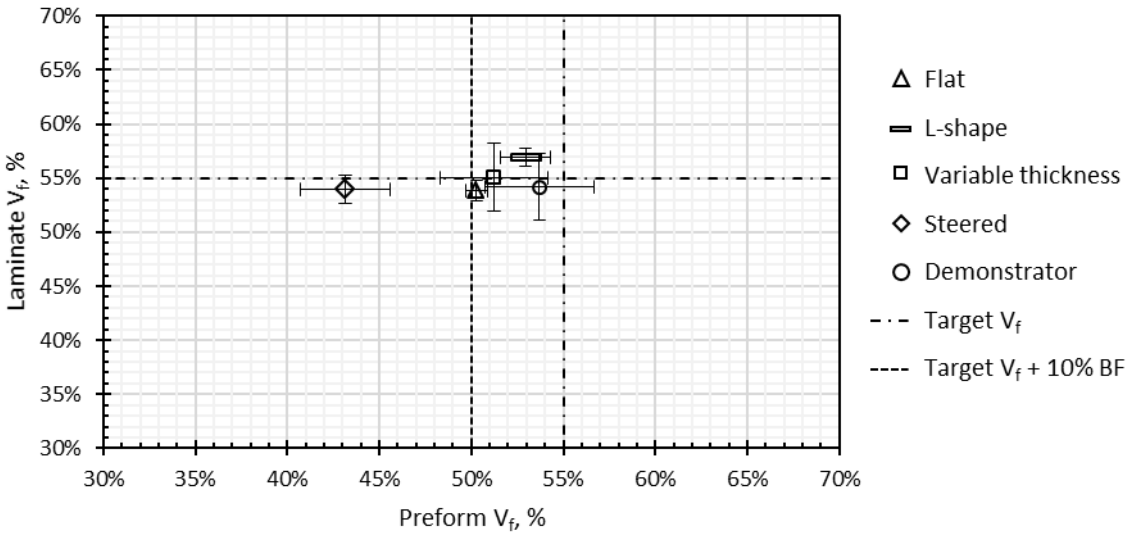

Figure 6-19: Preform V_f and laminate V_f of various parts manufactured with Material A (error bars indicate 2 SD within a part, demonstrator #5 shown)

This shows the current state of the art of process control, whether or not this is sufficient highly relies on the requirements of the application. Thick sections (nominally 24 mm tested) is introducing the greatest source of error, so using ADFP for thick parts is currently limited to a relatively high variability.

The flange angle was measured in three configurations, the angle between the thin flat areas (Area 2 and 4) and the thick flat areas (Area 1 and 3) on the tool side and the angle between the two flat areas of the bag side. The angle of the tool was determined as part of the tool acceptance procedure and is very close to a right angle with a measured 89.97°. Therefore, the measured spring in can be attributed to the laminate entirely. The resulting angle between the flanges across all seven demonstrators was 88.2 ± 0.3°, resulting in a spring-in angle similar to values reported in literature. The preforms consistently showed a spring-back of the flange (> 90 °) when removing them from the tool, exhibiting the opposite behaviour from the laminate spring in (< 90 °). The spring-in occurred similar to laminate manufactured with other composite processes but the underlying mechanisms were not investigated as part of this work. As the majority of the cited reasons for spring-in are related to the infusion stage, such as thermo-elastic spring-in, cure shrinkage and tool to part interaction, it is likely that the same mechanisms apply to the laminate manufactured by ADFP and high temperature infusion.

A typical photograph of one of the seven manufactured demonstrator laminates and the key achievements are shown in Figure 6-20.

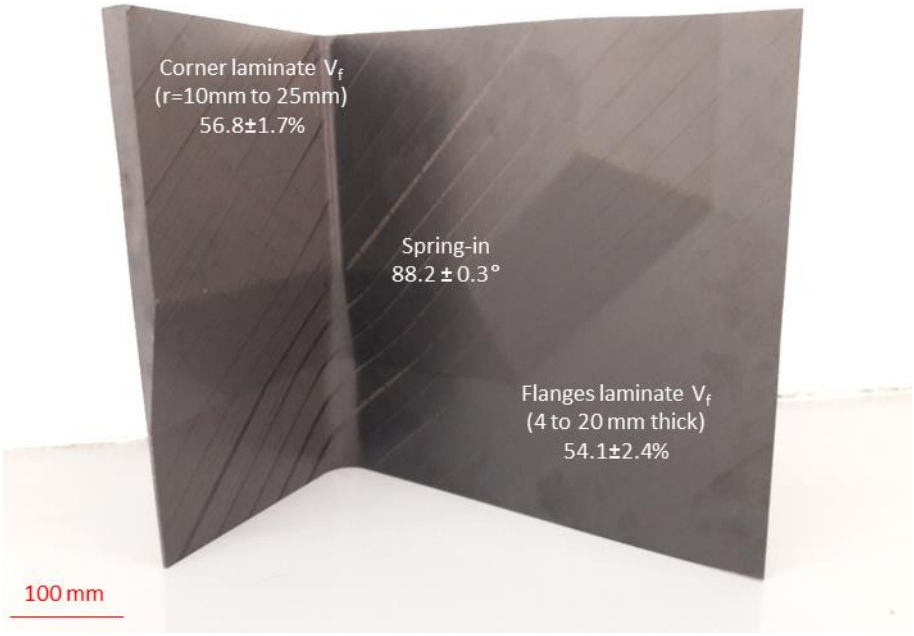

Figure 6-20: Photograph of an infused demonstrator including some key measurement results as average of all seven demonstrators (2 SD)

The manufacturing process was relatively consistent and repeatable, the target laminate V_f was achieved. This confirmed the success of the approach of building up a knowledge base by scaling up the complexity slowly and adjusting the parameters as needed, but also showed that simple trials do not fully capture all aspects of the manufacturing process.

Activity Split and Productivity

During manufacturing trials of different sized and shaped preforms, the activities carried out by the technician was self-reported. Even though some activities may vary from a production environment, the average time spend on deposition was similar to literature values, see Figure 6-21.

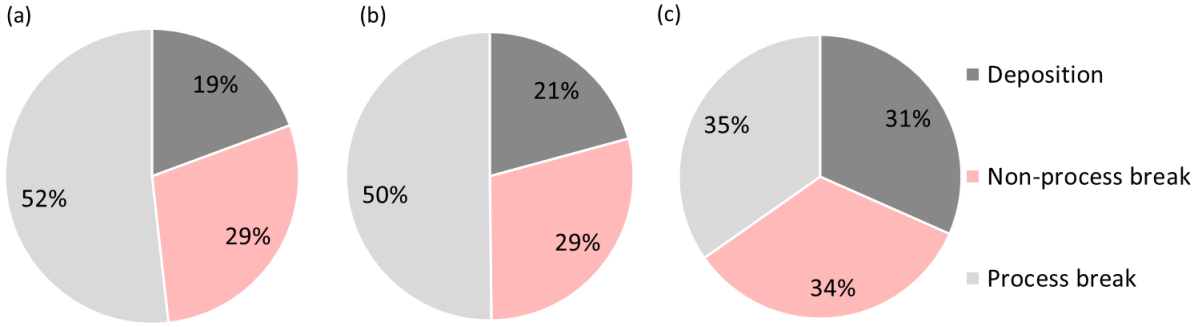

Figure 6-21: Distribution of time spend in ADFP manufacturing for different preforms split by activity without set-up for flat preforms (a), double curvature preforms (b) and demonstrators (c)

This figure suggests that the manufacturing technology may not yield significant advantages during the deposition stage in comparison to conventional AFP processes. The activities carried out do not differ significantly.

The minimum deposition rate achieved was 0.35 $^{kg}/_{h}$ which was the first demonstrator made without any prior experience and the maximum achieved value was 1.5 $^{kg}/_{h}$ which was the third part made of the larger double curvature preforms, see Figure 6-22. It is notable that the deposition rate of the flat preform was almost double the deposition rate of the demonstrator in spite of a similar size. The demonstrator had a significantly higher complexity and internal ply drop, causing a slower deposition speed due to more robotic repositioning movements. Even though the doubly curvature part had a more complex geometry than the flat part, a higher deposition rate was possible due to its larger size. The double curvature was mild enough to allow high acceleration, hence increased the deposition rate.

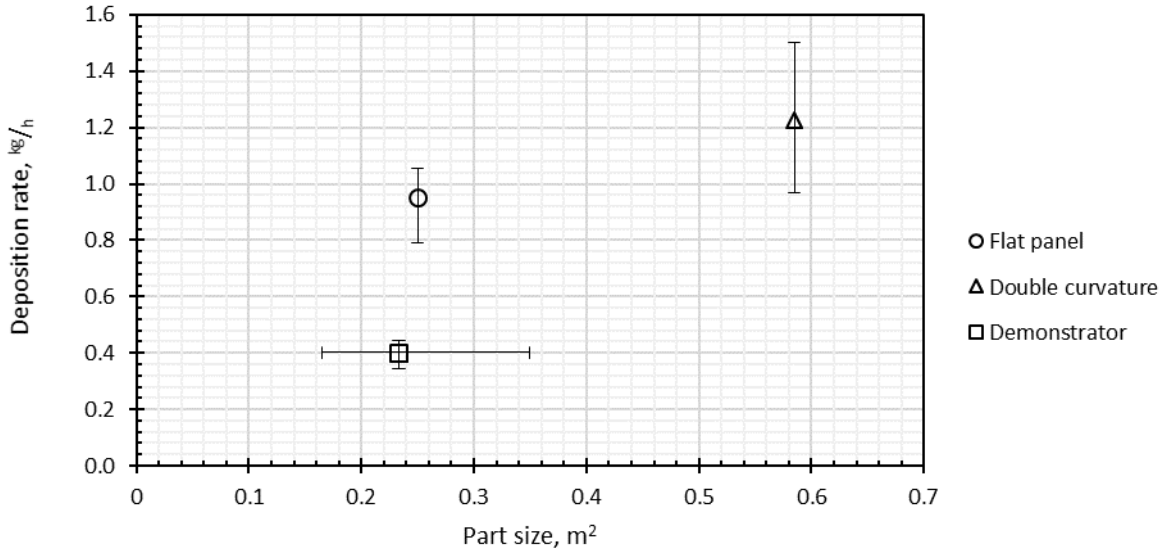

Figure 6-22: Hourly rate of production for different preform plotted against size of preform (error bar X-axis indicates variation of ply size; error bar of Y axis indicates min and max values of different parts)

This highlights that both complexity of the part as well as size should be taken into consideration for an estimation of deposition rate. The deposition rates of the largest part were similar to the literature values. The demonstrator deposition rate was significantly lower than the values found in literature, but the parts were relatively small and complex and were therefore unlikely to be suitable for a direct comparison. Due to the relatively small number of repeats, the reported time split and deposition rates should only be an indication and require further repeats.

6.3.4 Concluding Remarks

The ADFP process parameters were applied to the manufacture of a complex preform, which was subsequently infused using the same method as in the previous chapter. Across all demonstrators, a preform V_f of 50.8 ± 3.5% was achieved, which was within the target of 50-55% and laminate V_f of 55.0 ± 3.3 % above the target 55% was achieved. The mitigation of the variability in the preform by the infusion process was relatively small in the case of the demonstrator in comparison to the simpler geometries tested in the previous chapter. The variable thickness L-shaped geometry of the demonstrator increased the variability in comparison to a thin continuous thickness L-shaped part from 0.8% to 3.3% (2 SD). This shows the impact of increased complexity of the geometry on the laminate uniformity, and highlights that the process was not controlled well enough to produce consistent laminates across a range of geometries. The flange angle of the laminate was 88.2 ± 0.3° (2 SD) across all angle measurements on all demonstrators, a value consistent with laminates measured in literature.

6.4 Conclusion

The use of a highly complex demonstrator provided an industrially relevant challenge and exhibited some manufacturing aspects in addition to those found within the individual geometrical features. The predictive capability of the AFP software for steered areas as well as angle deviation were critically assessed. The placement of individual courses was relatively accurate in terms of their angle deviation against the nominal fibre path, but discrepancies appeared to accumulate on the corner region of the L-shaped section, as the AFP software does not take into account material specific influences during the deposition process. The steering radii as an output of the programming software were unsuitable to predict location or magnitude of wrinkles. Steering areas were roughly predicted; however, the level of detail was insufficient as a basis for fibre path optimisation. The severity of the wrinkles did not appear to be directly linked with the steering radius indicated by the software, and the wrinkled areas tended to be further along the deposition direction than indicated. The minimum steering radius determined using a flat tool for testing is not applicable, as it does not capture the gradual increase and decrease of the radii as well as influences from a 3D tool. A delay between the start of the programmed steered fibre path and wrinkle generation was observed. In order to achieve a fully digitalised development tool that reflects reality to enable fibre path optimisation for manufacturability, future work is needed to integrate a database of prior experience or modelling of specific scenarios into COTS software packages. This would reduce the barrier to entry and would be a step towards the commoditisation of the technology.

The repeated manufacture of the demonstrator was an opportunity to assess the productivity of the AFP system using dry fibre materials. The deposition rate had a high dependency on part size and component complexity, while an activity time split similar to literature values was achieved. As the ADFP manufacturing performed similarly to the manufacture of prepreg in terms of time spend and its split, little gain of productivity within the deposition process was achieved. This means that other aspects within the process must provide the economic advantage over the conventional process.

Chapter 7

Conclusions

In this final chapter, an overarching conclusion of the work is drawn and the achievements against the initial aims of the work are assessed. Contributions of the work to academia as well as to industry are summarised and discussed, followed by proposals for future work to fulfil industrial requirements.

7.1 Final Remarks

ADFP is a relatively new process introduced to the aerospace industry due to its high potential by combining the advantages of the prepreg AFP process and the vacuum infusion progress of broad goods. The process provides an out-of-autoclave solution for composite manufacture and the frozen storage of tapes was not necessary, simplifying the logistics of material out-life management. A further anticipated advantage of this novel material format is higher geometrical flexibility of the deposition process by better conformity of the tapes to a radius in steered fibre path.

However, the industry is facing challenges in accessing the potential of the ADFP process. Previous research has often regarded specific aspects of the process in isolation, but the different process steps are closely linked. Because of this complexity, the technology has a high barrier to entry, significant upfront investment is required to plan and optimise the manufacturing process in the digital space and to define the process required for a successful deposition. Additionally, measurement methods for some of these aspects are not yet readily available.

This work aimed to address these challenges by considering the process chain from raw material up to the manufactured laminate in a number of ways. A small series of tests was proposed to define the material selection based on minimal material usage. Measurement methods or metrics were developed where needed, for example to quantify the outcome of steered fibre paths. Predictive

capabilities of the AFP programming software were assessed to clarify the feasibility of a digital manufacturing process. Finally, preforms and laminates were compared to determine the impact of the individual processes and establish requirements for the different processes.

The combination of industrial scale and academic approaches proved to be beneficial to increase the understanding of this technology comprehensively. In this research, a clear link between the materials constituents and their performance throughout the deposition and infusion process was established. It is industrial practice to develop a process based on specific parts, which is then repeated for a new part. This approach was improved by proposing to gather knowledge that is not part specific but transferable, build up from a small scale to a component scale and tested for transferability at each increment. The scalability exercise showed which elements of the manufacturing process were captured in small-scale testing and what aspects of the process were not yet captured. The process is not yet controlled well enough to extrapolate a test result on a coupon level to a complex component directly, but some suggestions of potential improvements to capture the process fully with small-scale test methods were made.

Some of the drawbacks of the infusion process are not eliminated by infusion ADFP preforms. Even though the primary objective of creating an out-of-autoclave process was achieved, the process still relies heavily on manual labour and large quantities of disposable consumables. What became evident within this work was that a large number of factors throughout the ADFP manufacturing process contribute to the laminate quality, high levels of interaction between various material and different processes were shown but are only partially understood so far.

In summary, the manufacturing process is unlikely to provide a step change needed for the high manufacturing rate anticipated by the aerospace industry. The automated deposition phase of the ADFP process alone does not bring the significant advantages needed, dry fibre or prepreg AFP are likely to yield similar results in terms of productivity. Therefore, the advantage should lie in other aspects of the process chain, such as initial investments, raw material cost or subsequent manufacturing processes.

7.2 Results and Discussion

The aim of this work was to determine the effect of various materials on the manufacturing process as well as the resulting quality and to a lesser extent economic aspects. The results of this work were enablers to avoid costly trial and error approaches for process development and optimisation through a better understanding of the relationship between material and processes. Measurement methods were developed where necessary because even though the ADFP technology is based on mature

technologies, some aspects have such different requirements that COTS methods were not applicable or suitable.

7.2.1 Contribution to Academia

Currently isolated activities to understand the ADFP process are predominant in literature, leading to a fragmented picture of the process. This work aims to provide the necessary context for more detailed investigations, and addresses some of the gaps in publicly available knowledge that were assessed in Chapter 2.

The initial material selection process is commonly based on prior knowledge such as material characterisation data, but that is only the case for a well-known and well-characterised manufacturing process. To enable an evidence-based material selection, a multi-criteria decision-making tool was used in Chapter 3. A series of criteria were captured, based on knowledge and experience in related fields only. As verified in subsequent chapters, the chosen criteria were sufficiently representing the process. Some suggestions on improving the criteria were made to capture aspects of the manufacturing process relevant for complex parts.

In Chapter 4, the response behaviour of dry fibre materials to the AFP parameters (nip-point temperature, residence time and compaction pressure) was quantified across a range of commercial materials by using preform V_f as metric. This enabled the definition of optimised manufacturing parameters for component manufacture using dry fibre materials. The effect of the processing parameters was captured for various materials and linked to the materials constituents such as binder type and location, which had a high influence on the preform V_f. Small scale testing enabled a rapid process definition methodology, resulting in a set of manufacturing parameters optimised for each material for application on larger preform components. Some of these process parameters can require additional adjustment when applying to a larger scale (e.g. thick or complex parts), showing that the process is not yet controlled well enough for significant extrapolation.

Aligning the fibre paths to loading directions within the preform more easily was one of the potential advantages of the technology in comparison to prepreg. This alignment requires fibre steering, which means that the fibres are placed along non-geodesic paths. Steering in prepreg AFP is well known to cause wrinkles, which is why AFP programming software requires a constraint based on the lowest steering radius possible to achieve the desired quality. However, a significant gap in the existing research was a methodology to quantify wrinkles rapidly and objectively. This has led to the acceptance of a rather subjective quality assessment of steered tapes, resulting in neither comparable nor reproducible results. By proposing a measurement methodology for out-of-plane wrinkles that is independent of the instrument, machine and material, this gap was closed. The proposed

measurement only requires a digital point cloud representing the preform surface, which was a simple way of making steered fibre paths comparable. An objective comparison was enabled by a standardised 3D surface roughness parameter. This metric makes it possible to determine the ADFP parameters required for high quality steered courses, by linking the input parameters to an output quality metric. The optimum machine parameters can be conflicting with the parameter settings leading to a high quality in straight path preforms. This opens up the need for multi-objective optimisation if a part requires both straight and steered fibre paths. The anticipated increase of flexibility in the form of steering could not be verified. Wrinkle severity and distribution change with radius, but the impact of the distribution between in-and out-of-plane wrinkles within a ply on the laminate properties has not yet been studied sufficiently to confirm an improvement.

Chapter 6 explored fibre steering on a complex geometry and showed that the steering trials on a flat surface do not fully capture what occurs within an industrially relevant part. Many aspects of the process are interacting during the deposition of complex parts, variable compaction pressure distribution, changes of the heating area, different deposition speeds and variable steering radii. The in-depth knowledge of these interactions would greatly improve the ADFP process to allow high quality deposition on highly complex structures.

Vacuum infusion is a widely and successfully used process for composite manufacture from broad goods to convert the preform into a laminate, however the resin flow of ADFP preforms differs significantly and the pre-existent knowledge was only partially applicable. A significant scatter in the flow front was observed. This and the large repeating pattern of the preform may make traditional assessment methods challenging to apply, requiring a very large number of repeats or probabilistic models. As a result, the bespoke test set-up used only allows comparison within the tested samples. Nevertheless, the results provided valuable insights: the flow direction (either in-plane or a combination of in-plane and out-of-plane flow) had a high impact on preform fill time, and gap frequency had a higher impact on preform fill time than gap variations wider than 1 mm. Microscopic images show that plies tend to collapse into wider gaps, obscuring the flow path, leading to a similar infusion velocity across different gap width. The flow in ADFP preforms is highly dependent on the inner structure of the preform.

A direct comparison between preform and laminate quality showed the importance of a high quality preform for a high-quality laminate, consistently across a variety of geometrical features such as a flat part with significant thickness change and an L-shaped section. Even though the infusion process can mitigate some imperfections of the ADFP process, it became clear that a more homogenous preform leads to a more even laminate. This emphasises the need to optimise the ADFP deposition process.

Overall, this work provided additional background knowledge for academic research on ADFP and highlighted the needs for further, in-depth research to understand the underlying principles that prevent direct application of laboratory scale work to an industrial context.

7.2.2 Contribution to Industry

This work was funded by industry to assess if the ADFP manufacturing route including an out-of-autoclave or oven-based infusion process is a viable technology. The motivation of the industrial sponsors was to raise the technology maturity level to enable industrial implementation. To raise the maturity, it was important to quantify the technology capability in terms of part-to-part variability. Furthermore, the contribution of variability can now be linked to either the ADFP or the vacuum infusion process, allowing for targeted process optimisation in the future. This work will underpin the decision making with technical insights when a change in manufacturing process or the set-up of a new production line is needed. This is supported by the technical aspects, as well as some economic elements, such as productivity, included in Chapter 6. Within the constraints of the small number of manufactured parts, the productivity of the ADFP was comparable to the more conventional prepreg AFP process. Therefore, the effectivity of the infusion process is of great importance to ensure that the ADFP process brings an economic advantage over prepreg AFP.

Chapter 3 and Chapter 4 showed that the use of relatively simple trials enable a successful and rapid manufacturability based material selection and ADFP process definition. One major barrier to entry for many businesses to adopt automated technologies is the high upfront capital investment, which comprises the machinery, software and space, but also the initial development work needed to manufacture a product successfully. The first type of investment is often committed early on, and any hardware and software adjustments at a later stage come at a high price. The latter type of investment is often at high-risk to incur higher cost than anticipated, as it is difficult to estimate costs for development requirements accurately. The proposed tests already enabled a significantly shorter time in process development for some of the project sponsors.

Digital manufacturing can help to further decrease this risk and therefore the barrier to entry by assessing the manufacturing process digitally prior to any hardware investment and can reduce and define the development need. Chapter 6 investigated the predictive capability of the AFP programming software as it is currently used as part of a drive towards digital manufacturing support. The current industrial practice of using machine-programming output as optimisation input was unsuitable in the instance of depositing steered fibre paths. Significant further work is needed to incorporate material specific deposition behaviour into AFP programming software, but some preliminary methods for the assessment of deposition accuracy was proposed on an industrial scale.

Chapter 5 and Chapter 6 showed the successful infusion of various preform geometries, including repeated manufacture of a highly complex part. The successful manufacture of geometrical features was a significant step towards higher maturity of the manufacturing process in many industrial assessments. In addition, the laminate assessment allowed linking the impact of the preform quality to the laminate quality. These preliminary results suggest that a minimum quality threshold for the preform thickness can be established to determine when to terminate production or when to continue with a high probability of high laminate quality.

7.3 Further Work

A drawback of the ADFP process is its complexity and therefore need for high upfront investment in the development stage. However, as it is an automated process, outcomes are much easier to predict than with manual processes due to the higher level of process control. The exploitation of digital manufacturing tools has the potential to reduce the development time significantly in the longer term and need to be developed further. Pre-production activities such as fibre path planning and process definition could benefit from more accurate process prediction and a higher level of digitalisation. This could help to assess the feasibility of the manufacturing process for a particular application and drive the technology towards commoditisation, i.e. a significant simplification for operation to rely less on experience and intuition. This work showed that the current prediction capability of AFP programming software does not take into account material specific aspects, which means programmers take many decisions without evidence during the path planning stage. As a result, long and iterative processes are utilised for machine programming. Further work should aim to integrate process definition and preform quality predictions into the programming software, so these aspects can be assed prior to any experimental work. This could result in a process fully defined and optimised, bespoke to a specific material, with all process variables defined when transferred to the AFP system.

Similarly, the vacuum infusion process still heavily depends on skilled craftsmanship often rooted in operators experience and engineering judgement rather than scientific evidence. A validated flow simulation could support the optimisation of the infusion step by exploring a wide range of options regarding the infusion set up (e.g. valve placement etc.) and the internal structure (e.g. intra tape gaps), instead of resorting to a costly trial-and-error approach. As only COTS materials were taken into consideration, the opportunity to investigate the contribution of the material constituents was limited. However, previous research as well as findings within this work support that the exact makeup of the material has a significant impact on the infusion process, in particular the composition and location of the binder within the tape. The assessment of the available materials against criteria showed that every material scored highest in at least one category, which means that there is room

for improvement within every commercially available material. Combining the successful features of the different materials can lead to a superior product.

The advantages of ADFP in comparison to alternative manufacturing processes were relatively incremental. Potential novel concepts to innovate the infusion stage could involve eliminating it. Examples could include application of resin during the deposition process as film or employing an on-line prepreg manufacture within the AFP system. This could also potentially involve an in-situ curing step for epoxy-based materials to eliminate the curing stage. Another approach would be the automation of the infusion process at a large scale, both in terms of the bagging operation and in-process adjustments. Furthermore, the deposition stage could be improved in terms of productivity by combining broad fabrics with wide and narrow tapes depending on the geometry to achieve the highest possible production rate.

Laminate assessment in terms of mechanical testing was excluded from this work; the primary focus was on manufacturability. Nevertheless, mechanical performance of the laminates is of vital importance for industrial use. Variables within the manufacturing process, for example deposition temperature, are likely have an impact on mechanical properties of laminates. Therefore, requirements of the manufacturing process imposed by the effect on laminate quality should be considered in the future. This could potentially add further conflicting requirements to the definition of the manufacturing process.

Due to the complexity of the production chain, only a comprehensive cost model could show which aspects of the manufacturing process is the highest contributor to manufacturing cost and duration and could guide further research. Due to the outlined, relatively minor differences between the manufacturing processes, a careful process selection is necessary for a particular application, the ADFP process does not provide such a significant advantage that the choice of manufacturing process becomes obvious. Insight into economic drivers should be taken into account as valuable guidance for future research topics.

Bibliography

[1] Airbus, “Growing Horizons 2017/2036,” 2017.

[2] N/a, “Mapping Demand,” *Airbus Mark. Forecast*.

[3] M. Fendt, Martin; Stone, Rod; Dubon, Justin; Duvelleroy, “Airbus achieves new commercial aircraft delivery record in 2018,” *Press release*, no. January, Toulouse, p. 2, 09-Jan-2019.

[4] T. Hepher, B. Felix, and A. Croft, “Airbus confirms plans to raise A320 output to 63 a month | Reuters,” *Reuters Business News*, Paris, 2018.

[5] R. Bogue, “The growing use of robots by the aerospace industry,” *Ind. Robot An Int. J.*, p. IR-08-2018-0160, Oct. 2018.

[6] A. Crosky, C. Grant, D. Kelly, X. Legrand, and G. Pearce, “Fibre placement processes for composites manufacture,” in *Advances in composites manufacturing and process design*, P. Boisse, Ed. Cambridge: Woodhead Publishing Limited, 2015, pp. 79–92.

[7] C. G. Grant, “Fiber Placement Process Utilization within the Worldwide Aerospace Industry,” in *Bridging the Centuries with Sampe’s Materials and Processes Technology*, 2000, vol. 45.

[8] C. Grant, “Automated processes for composite aircraft structure,” *Ind. Robot An Int. J.*, vol. 33, no. 2, pp. 117–121, 2006.

[9] M. P. Wiehn and R. D. Hale, “Low cost robotic fabrication methods for tow placement,” in *47th International Sampe Symposium and Exhibition*, 2002, vol. 47, pp. 1842–1852.

[10] O. Constant, “Coriolis change de dimension,” *Entreprises et marches*, Nantes, FR, p. 32, Apr-2017.

[11] M. Motilva, “Dry fiber in automated composites lamination,” in *SAMPE Conference 18 Southampton*, 2018.

[12] J. C. de Kruijk, “Automated composite manufacturing using robotics lowers cost, lead- time and scrap rate,” in *Future of Manufacturing for Military Applications*, 2018, pp. 1–14.

[13] E. Hardesty, W. Goldsworthy, and H. Karlson, “Geodesic path length compensator for composite-tape placement head,” US3810805A, 14-Apr-1972.

[14] D. H.-J. A. Lukaszewicz, C. Ward, and K. D. Potter, “The engineering aspects of automated prepreg layup: History, present and future,” *Compos. Part B Eng.*, vol. 43, no. 3, pp. 997–1009, Apr. 2012.

[15] “Fiber Reinforced Polymer Composite Manufacturing Workshop: Summary Report,” Arlington, VA, 2014.

[16] J. Frketic, T. Dickens, and S. Ramakrishnan, “Automated manufacturing and processing of fiber-reinforced polymer (FRP) composites: An additive review of contemporary and modern techniques for advanced materials manufacturing,” *Addit. Manuf.*, vol. 14, pp. 69–86, Mar. 2017.

[17] B. Domke, “Boeing 787 Lessons Learnt.” Airbus, 2008.

[18] U. P. Breuer, *Commercial aircraft composite technology*, 2nd ed. Kaiserslautern: Springer, 2016.

[19] S. Van Hoa, “Automated composites manufacturing,” in *Advanced Materials International Forum*, 2014.

[20] D. E. Bullock, “Automated prepreg tow placement for composite structures,” in *35th International SAMPE symposium*, 1990.

[21] K. Croft, L. Lessard, D. Pasini, M. Hojjati, J. Chen, and A. Yousefpour, “Experimental study of the effect of automated fiber placement induced defects on performance of composite laminates,” *Compos. Part A Appl. Sci. Manuf.*, vol. 42, no. 5, pp. 484–491, May 2011.

[22] F. C. Campbell, *Manufacturing processes for advanced composites*. Kidlington, UK: Elsevier Advanced Technology, 2003.

[23] A. Mcllhagger, E. Archer, and R. Mcllhagger, “Manufacturing processes for composite materials and components for aerospace applications,” in *Polymer composites in the aerospace industry*,

E. Irving and C. Soutis, Eds. Cambridge: Woodhead Publishing Limited, 2014, pp. 53–76.
[24] C. Soutis, “Introduction: engineering requirements for aerospace composite materials,” in *Polymer composites in the aerospace industry*, E. Irving and C. Soutis, Eds. Cambridge: Woodhead Publishing Limited, 2015, pp. 1–17.
[25] A. Jacob, “BMW counts on carbon fibre for its Megacity Vehicle,” *Reinf. Plast.*, vol. 54, no. 5, pp. 38–41, Sep. 2010.
[26] G. Gardiner, “The evolution of infusion,” *CompositesWorld*, Aug-2012.
[27] C. D. Rudd, “Processing of thermoset matrix composites,” in *Composites for automotive applications*, 11th ed., S. Ward, Ed. Shawbury, UK: Rapra Technology Ltd, 2000, p. 12.
[28] M. Matveev, F. Ball, I. Jones, A. Long, P. Schubel, and M. Tretyakov, “Uncertainty in geometry of fibre preforms manufactured with Automated Dry Fibre Placement and its effects on permeability,” *J. Compos. Mater.*, pp. 1–15, 2017.
[29] M. Belhaj *et al.*, “Dry fiber automated placement of carbon fibrous preforms,” *Compos. Part B Eng.*, vol. 50, pp. 107–111, Jul. 2013.
[30] G. Dell’Anno *et al.*, “Automated manufacture of 3D reinforced aerospace composite structures,” *Int. J. Struct. Integr.*, vol. 3, no. 1, p. 19, 2012.
[31] S. Toms and Q. Zhang, “Marks & Spencer and the Decline of the British Textile Industry, 1950–2000,” *Bus. Hist. Rev.*, vol. 90, no. 01, pp. 3–30, Mar. 2016.
[32] P. Mandelson, “The UK Composites Strategy,” London, 2009.
[33] K. Kozaczuk, “Automated Fiber Placement Systems Overview,” *Trans. Inst. Aviat.*, vol. 4, no. 245, pp. 52–59, 2016.
[34] “Aerospace - Coriolis Composites,” *Coriolis Composites*, 2018. [Online]. Available: https://www.coriolis-composites.com/sector-solutions/aerospace.html. [Accessed: 30-Aug-2018].
[35] “AFP I – Accudyne Systems, Inc,” *Accudyne Systems, Inc*, 2016. [Online]. Available: https://www.accudyne.com/composites-automation/automated-fiber-placement-afp/afp-i/. [Accessed: 30-Aug-2018].
[36] D. Dawson, “Automation: Robots taking off in commercial aircraft,” *CompositesWorld*, 2016.
[37] G. Marsh, “Automating aerospace composites production with fibre placement,” *Reinf. Plast.*, vol. 55, no. 3, pp. 32–37, 2011.
[38] P. Ribeiro, H. Akhavan, A. Teter, and J. Warmiński, “A review on the mechanical behaviour of curvilinear fibre composite laminated panels,” *J. Compos. Mater.*, vol. 48, no. 22, pp. 2761–2777, Sep. 2014.
[39] G. G. Lozano, A. Tiwari, and C. Turner, “A design algorithm to model fibre paths for manufacturing of structurally optimised composite laminates,” *Compos. Struct.*, Jul. 2018.
[40] G. Rousseau, R. Wehbe, J. Halbritter, and R. Harik, “Automated Fiber Placement Path Planning: A state-of-the-art review,” *Comput. Des. Appl.*, vol. 16, no. 2, pp. 172–203, 2019.
[41] G. G. Lozano, A. Tiwari, C. Turner, and S. Astwood, “A review on design for manufacture of variable stiffness composite laminates,” *Proc. Inst. Mech. Eng. Part B J. Eng. Manuf.*, vol. 230, no. 6, pp. 981–992, Jun. 2016.
[42] P. Debout, H. Chanal, and E. Duc, “Tool path smoothing of a redundant machine: Application to Automated Fiber Placement,” *Comput. Des.*, vol. 43, no. 2, pp. 122–132, Feb. 2011.
[43] W.-P. Tang, B. Johnson, and D. E. Gonsor, “Optimizing non-productive part motion in an automated tape laydown machine,” US7720561B2, 21-Sep-2007.
[44] D. Maass, “Progress in automated ply inspection of AFP layups,” *Reinf. Plast.*, vol. 59, no. 5, pp. 242–245, 2015.
[45] A. R. R. Aziz, M. A. A. Ali, X. Zeng, R. Umer, P. Schubel, and W. J. J. Cantwell, “Transverse permeability of dry fiber preforms manufactured by automated fiber placement,” *Compos. Sci. Technol.*, vol. 152, no. August, pp. 57–67, Sep. 2017.
[46] R. Umer, S. Rao, J. Zhou, Z. Guan, and W. J. Cantwell, “The Low Velocity Impact Response of Nano Modified Composites Manufactured Using Automated Dry Fibre Placement,” *Polym.*

Polym. Compos., vol. 24, no. 4, pp. 233–240, 2016.

[47] M. Y. M. Matveev, P. J. P. Schubel, A. A. C. Long, and I. A. I. Jones, "Understanding the buckling behaviour of steered tows in Automated Dry Fibre Placement (ADFP)," *Compos. Part A Appl. Sci. Manuf.*, vol. 90, pp. 451–456, Nov. 2016.

[48] N. Gharabegi, S. V. Hoa, and M. Hojjati, "Composite Laminates Made by Automated Fiber Placement of Dry Fibers and Vacuum Assisted Resin Transfer Molding," in *3rd International Symposium on Automated Composites Manufacturing*, 2017.

[49] R. K. Boer, "AUTOW Automated Preform Fabrication by Dry Tow Placement," 2008.

[50] R. Agogue, N. Chebil, M. Deleglise-Lagardere, P. Beauchene, and C. H. Park, "Efficient Permeability Measurement and Numerical Simulation of the Resin Flow in Low Permeability Preform Fabricated by Automated Dry Fiber Placement," *Appl. Compos. Mater.*, pp. 1–14, Oct. 2017.

[51] O. Rimmel, D. Becker, and P. Mitschang, "Maximizing the out-of-plane-permeability of preforms manufactured by dry fiber placement," *Adv. Manuf. Polym. Compos. Sci.*, vol. 2, no. 3–4, pp. 93–102, Oct. 2016.

[52] A. Mills, "Automation of carbon fibre preform manufacture for affordable aerospace applications," *Compos. - Part A Appl. Sci. Manuf.*, vol. 32, no. 7, pp. 955–962, 2001.

[53] M. Y. Matveev, A. C. Long, I. A. Jones, and P. J. Schubel, "Variability of permeability in fibre preforms manufactured with automated fibre placement (AFP)," in *20th International Conference on Composite Materials*, 2015, pp. 19–24.

[54] M. Di Francesco, L. Veldenz, G. Dell'Anno, and K. Potter, "Heater power control for multi-material, variable speed Automated Fibre Placement," *Compos. Part A Appl. Sci. Manuf.*, vol. 101, pp. 408–421, Oct. 2017.

[55] M. Turner, "Tow Placement Studies for Liquid Composite Moulding," University of Nottingham, 1998.

[56] K. J. Ahn, L. Peterson, J. C. Seferis, D. Nowacki, and H. G. Zachmann, "Prepreg aging in relation to tack," *J. Appl. Polym. Sci.*, vol. 45, no. 3, pp. 399–406, 1992.

[57] R. Calawa and J. Nancarrow, "Medium Wave Infrared Heater for High-Speed Fiber Placement," in *SAE Aerofast*, 2007.

[58] D. H.-J. A. Lukaszewicz, "Optimisation of high-speed automated layup of thermoset carbon-fibre preimpregnates," University of Bristol, 2011.

[59] C. Krombholz, F. Kruse, and M. Wiedemann, "GroFi: Large-scale fiber placement research facility," *J. large-scale Res. Facil.*, vol. 2, no. A58, pp. 1–4, Mar. 2016.

[60] C. M. Stokes-Griffin and P. Compston, "The effect of processing temperature and placement rate on the short beam strength of carbon fibre–PEEK manufactured using a laser tape placement process," *Compos. Part A Appl. Sci. Manuf.*, vol. 78, pp. 274–283, Nov. 2015.

[61] R. F. X. Lichtinger, "Thermo-Mechanical Coupled Simulation of the Thermoset Automated Fibre Placement Process," Technical University of Munich, 2015.

[62] D. Williams and M. Brown, "Xenon Flashlamp Heating for Automated Fibre Placement," in *The Third International Symposium on Automated Composites Manufacturing*, 2017.

[63] Y. Grohmann, "CoRe HeaT – A new heating method for faster fibre placement," in *ICMAC 2018 - 11th International Conference on Manufacturing of Advanced Composites*, 2018, pp. 1–2.

[64] F. Helber, A. Amann, S. Carosella, and P. Middendorf, "Intrinsic fibre heating: a novel approach for automated dry fibre placement," in *13th International Conference on Textile Composites (TEXCOMP-13)*, 2018.

[65] B. Denkena, C. Schmidt, and P. Weber, "Automated Fiber Placement Head for Manufacturing of Innovative Aerospace Stiffening Structures," *Procedia Manuf.*, vol. 6, pp. 96–104, 2016.

[66] C. M. Stokes-Griffin and P. Compston, "A combined optical-thermal model for near-infrared laser heating of thermoplastic composites in an automated tape placement process," *Compos. Part A Appl. Sci. Manuf.*, vol. 75, pp. 104–115, Aug. 2015.

[67] K. Yassin and M. Hojjati, "Processing of thermoplastic matrix composites through automated

fiber placement and tape laying methods: A review," *Thermoplast. Compos. Mater.*, pp. 1–50, 2017.

[68] L. Ma, R. A. Peck, I. Herszberg, and S. John, "Air-jet compaction system for draping and consolidation in the automated manufacture of composite components," in *Eleventh International Conference on Composite Materials*, 1997, pp. 474–481.

[69] Z. Han, S. Sun, W. Li, Y. Zhao, and Z. Shao, "Experimental Study of the Effect of Internal Defects on Stress Waves during Automated Fiber Placement," *Polymers (Basel).*, vol. 10, no. 4, p. 413, Apr. 2018.

[70] M. Deleglise and C. Binetruy, "Towards the on-line qualification of carbon preforms produced by AFP," *JEC Compos. Mag.*, vol. 57, no. May, pp. 50–52, 2010.

[71] R. Lichtinger, J. Lacelle, R. Hinterhoelzl, U. Beier, and K. Drechsler, "Simulation and experimental validation of gaps and bridging in the automated fiber placement process," *Sci. Eng. Compos. Mater.*, vol. 22, no. 2, pp. 131–148, Jan. 2015.

[72] A. B. Hulcher, J. M. Marchello, J. A. Hinkley, N. J. Johnston, and M. A. Lamontia, "Dry Ribbon for Heated Head Automated Fiber Placement," *Sci. Adv. Mater. Process Eng. Ser.*, vol. 44, pp. 146–155, 1999.

[73] P. Giddings and M. Di Francesco, "Reducing cost and risk in layup of convex corners using Automated Fibre Placement : A simulation led approach," in *The Second International Symposium on Automated Composites Manufacturing*, 2015, no. April, p. 16.

[74] R. Pitchumani, J. W. Gillespie, and M. A. Lamontia, "Design and Optimization of a Thermoplastic Tow-Placement Process with In-Situ Consolidation," *J. Compos. Mater.*, vol. 31, no. 3, pp. 244–275, 1997.

[75] J. J. Gangloff, P. Simacek, S. Sinha, and S. G. Advani, "A process model for the compaction and saturation of partially impregnated thermoset prepreg tapes," *Compos. Part A Appl. Sci. Manuf.*, vol. 64, pp. 234–244, 2014.

[76] J. P.-H. Belnoue, O. J. Nixon-Pearson, D. Ivanov, and S. R. Hallett, "A novel hyper-viscoelastic model for consolidation of toughened prepregs under processing conditions," *Mech. Mater.*, vol. 97, pp. 118–134, Jun. 2016.

[77] M. Matsudaira and H. Qin, "Features and Mechanical Parameters of a Fabric's Compressional Property Features and Mechanical Parameters ofa Fabric's Compressional Property," *J. Text. Inst.*, vol. 86, no. 3, pp. 476–486, 1995.

[78] Z. Yousaf, P. Potluri, and P. J. Withers, "Influence of Tow Architecture on Compaction and Nesting in Textile Preforms," *Appl. Compos. Mater.*, vol. 24, no. 2, pp. 337–350, Apr. 2017.

[79] S. Aranda, F. Klunker, and G. Ziegmann, "Influence of the Binding System on the Compaction Behaviour of Ncf Carbon Fibre," in *18th International Conference on Composite Materials*, 2011, pp. 1–6.

[80] F. Robitaille and R. Gauvin, "Compaction of textile reinforcements for composites manufacturing. I: Review of experimental results," *Polym. Compos.*, vol. 19, no. 2, pp. 198–216, 1998.

[81] C. Zhao, J. Xiao, W. Huang, X. Huang, and S. Gu, "Layup quality evaluation of fiber trajectory based on prepreg tow deformability for automated fiber placement," *Reinf. Plast. Compos.*, vol. 35, no. 21, pp. 1576–1585, 2016.

[82] C. Schmidt, B. Denkena, K. Völtzer, and T. Hocke, "Thermal Image-based Monitoring for the Automated Fiber Placement Process," *Procedia CIRP*, vol. 62, pp. 27–32, Jan. 2017.

[83] S. Van Hoa, M. D. Hoang, and J. Simpson, "Manufacturing procedure to make flat thermoplastic composite laminates by automated fibre placement and their mechanical properties," *J. Thermoplast. Compos. Mater.*, vol. 30, no. 12, pp. 1693–1712, 2017.

[84] M. A. Lamontia and M. B. Gruber, "Remaining developments required for commercializing in situ thermoplastic ATP," in *International SAMPE Symposium and Exhibition*, 2007.

[85] S. Astwood, K. Krishnamurthy, and A. Tiwari, "A strategy to analyse composite designs to improve automated production speeds," *J. Eng. Manuf.*, vol. 232, no. 1, pp. 32–39, 2018.

[86] M. K. Hagnell and M. Åkermo, “A composite cost model for the aeronautical industry: Methodology and case study,” *Compos. Part B Eng.*, vol. 79, pp. 254–261, Sep. 2015.

[87] P. J. J. Schubel, “Cost modelling in polymer composite applications: Case study - Analysis of existing and automated manufacturing processes for a large wind turbine blade,” *Compos. Part B Eng.*, vol. 43, no. 3, pp. 953–960, 2012.

[88] Y. Bauswein, L. Veldenz, and C. Ward, “Developing a cost comparison technique for hand lay-up versus automated fibre placement and infusion versus out-of-autoclave,” in *SAMPE EUROPE 2017*, 2017, pp. 1–8.

[89] B. T. Astrom, *Manufacturing of Polymer Composites*, 2nd ed. Cheltenham: Nelson Thornes Ltd, 2002.

[90] L. Veldenz, M. Di Francesco, S. Astwood, G. Dell’Anno, B. C. Kim, and K. Potter, “Characteristics and Processability of Bindered Dry Fibre Material for Automated Fibre Placement,” in *17th European Conference on Composite Materials*, 2016.

[91] C. . Rudd, M. . Turner, A. . Long, and V. Middleton, “Tow placement studies for liquid composite moulding,” *Compos. Part A Appl. Sci. Manuf.*, vol. 30, no. 9, pp. 1105–1121, Sep. 1999.

[92] Y. Grohmann, N. Stoffers, A. Kühn, and T. Mahrholz, “Development of the direct roving placement technology (DRP),” in *17th European Conference on Composite Materials*, 2016.

[93] Y. Grohmann, N. Stoffers, A. Kühn, T. Mahrholz, S. Schmidt, and F. Kruse, “Reducing manufacturing costs by direct roving placement,” in *20th European Conference on Composite Materials*, 2015.

[94] J. Allen, T. Tepp, K. Vaiente, and C. Michel, “Cytec Providing Composite Products for the MS-21 Program,” *Cytec Solvay Press Release*, 2014. [Online]. Available: https://www.solvay.com/en/press-release/cytec-providing-composite-products-ms-21-program. [Accessed: 26-Jul-2018].

[95] M. Ponsolle, Dominique; Restuccia, Carmelo Luca; Joacobs, William; Blackburn, Robert; Lofaro, Carmelo; Price, Richard; Doyle, Marc; Smith, Mitchell; Roman, “Dry fibrous material for subsequent resin infusion,” WO2013096377 A2, 27-Jun-2013.

[96] D. Pratte, James F.; Rogers, Scott A.; Ponsolle, “Thermoplastic composites and methods of making and using same,” US20120160399A1, 2012.

[97] D. Ponsolle *et al.*, “A binder composition for forming a dry fibrous material for subsequent resin infusion,” WO 2013/096377, 04-Apr-2018.

[98] R. G. Kline, “JEC Europe 2014 Review,” *High-performance Composites*, Cincinnati, OH, pp. 30–35, May-2014.

[99] J. Solano, “Oak Aerocomposit chooses innovative solutions to build the MS-21 composite wing,” *JEC Composites Magazine*, vol. 72, no. May, pp. 44–46, May-2012.

[100] “HiTape® advanced reinforcements for OOA-processed aircraft primary structures | JEC Group,” *JEC Group*, 2013. [Online]. Available: http://www.jeccomposites.com/knowledge/international-composites-news/hitape®-advanced-reinforcements-ooa-processed-aircraft. [Accessed: 31-Jul-2018].

[101] M. Schneider, B. Wohlmann, and T. Fibers, “Carbon Fibre Sewing Yarn and Binder Yarn for Preform Applications,” no. April, pp. 1–6, 2005.

[102] B. Schneider, Markus; Stusgen, Silke; Witzel, Silke; Wohlmann, “Flexible reinforcement fiber yarn pre-impregnated with resin,” CA2843488 A1, 07-Feb-2013.

[103] “Creating structures in three dimensions - Unlimited solutions,” *Porcher Industries*. [Online]. Available: http://weavalu.com/uploads/files/D3sign2013_web.pdf. [Accessed: 26-Jul-2018].

[104] T. Groene and F. Michl, “cevoTape - Tailored to your automated fiber placement processes,” *Cevotec*, 2018. [Online]. Available: https://www.cevotec.com/en/cevotape/. [Accessed: 27-Jul-2018].

[105] F. Michl, “Spread Tow Tape - Lessons on production and quality,” Taufkirchen bei München, 2018.

[106] “MTorres launches for the very first time its dry carbon fibre material for AFP,” *torres*

newsletter, 2018.
[107] O. Rimmel, J. Mack, D. Becker, and P. Mitschang, “Automated Direct Fibre Placement with Online Binder Application,” *lightweight.design*, vol. 10, no. 2, pp. 48–53, Feb. 2017.
[108] M. Tanoglu, S. Robert, D. Heider, S. H. McKnight, V. Brachos, and J. W. Gillespie, “Effects of thermoplastic preforming binder on the properties of S2-glass fabric reinforced epoxy composites,” *Int. J. Adhes. Adhes.*, vol. 21, no. 3, pp. 187–195, 2001.
[109] M. Tanoglu and S. A. Tugrul, “Investigating the effects of a polyester preforming binder on the mechanical and ballistic performance of E-glass fiber reinforced polyester composites,” *Int. J. Adhes. Adhes.*, vol. 23, pp. 1–8, 2003.
[110] C.-H. Shih and L. J. Lee, “Tackification of Textile Fiber Preforms in Resin Transfer Molding,” *J. Compos. Mater.*, vol. 35, no. 21, pp. 1954–1981, 2001.
[111] V. Rohatgi, L. J. Lee, and J. L. Lee, “Moldability of tackified fiber preforms in liquid composite molding,” *J. Compos. Mater.*, vol. 31, no. 7, pp. 720–744, 1997.
[112] M. Dickert, D. C. Berg, and G. Ziegmann, “Influence of binder activation and fabric design on the permeability of non-crimp carbon fabrics,” in *Flow Processes in Composite Materials FPCM-11*, 2012, p. 18.
[113] F. Weyrauch, A. Hohmann, and B. Mesow, “Prozesskette zur Ressourceneffizienten Composite Herstellung fuer die E-Mobilitaet,” *Universtität Stuttgart Website*, 2015. [Online]. Available: http://tuxweb.ifb.uni-stuttgart.de/presche/index.php?seite=kontakt.htm. [Accessed: 27-Nov-2018].
[114] G. Estrada, C. Vieux-Pernon, and S. G. Advani, “Experimental Characterization of the Influence of Tackifier Material on Preform Permeability,” *J. Compos. Mater.*, vol. 36, no. 19, pp. 2297–2310, 2002.
[115] D. Tilbrook, D. Blair, M. Boyle, and P. MacKenzie, “Composite materials with blend of thermoplastic particles,” US7754322B2, 17-Apr-2007.
[116] T. K. Tsotsis, “Interlayer Toughening of Composite Materials,” *Polym. Compos.*, vol. 30, no. 1, pp. 70–86, 2009.
[117] A. Rodriguez, S. Hill, and R. Blackburn, “A robust UD dry tape product for Automated Manufacturing of Composites,” in *SC Aerospace Conference & Expo 2016 ACE’16 Technical Symposium Proceedings*, 2016.
[118] N. Odagiri, H. Kishi, and M. Yamashita, “Development of TORAYCA prepreg P2302 carbon fiber reinforced plastic for aircraft primary structural materials,” *Adv. Compos. Mater.*, vol. 5, no. 2, pp. 249–252, 1996.
[119] J. Ellis and J.-M. Beraud, “Improvements in or relating to fibre reinforced materials,” WO2013093053A2, 21-Dec-2012.
[120] R. K. De Boer, “Development of Automated Dry Fiber Placement Material, Process and Design Technology,” 2011.
[121] J. F. Wlodarski and L. E. Robertson, “Effect of fabrication process on composite material properties,” in *38th Structures, Structural Dynamics and Materials Conference*, 1997.
[122] N. Vernet *et al.*, “Experimental determination of the permeability of engineering textiles: Benchmark II,” *Compos. Part A Appl. Sci. Manuf.*, vol. 61, pp. 172–184, 2014.
[123] S. Aranda, F. Klunker, and G. Ziegmann, “Compaction response of fibre reinforcements depending on processing temperature,” in *17th International Conference on Composite Materials*, 2009, pp. 1–6.
[124] R. Graupner, “Adaption of dry fiber placement lay-up strategies for optimized off-plane impregnation,” in *Symposium on the occasion of the 5 th anniversary of the Institute for Carbon Composites*, 2014, vol. 49, no. 0.
[125] S. Zambal, C. Eitzinger, M. Clarke, J. Klintworth, and P. Mechin, “A digital twin for composite parts manufacturing - Effects of defects analysis based on manufacturing data,” *IEEE Int. Conf. Ind. Informatics*, pp. 803–808, 2018.
[126] D. H.-J. A. Lukaszewicz and K. D. Potter, “The internal structure and conformation of prepreg

with respect to reliable automated processing," *Compos. Part A Appl. Sci. Manuf.*, vol. 42, no. 3, pp. 283–292, Mar. 2011.

[127] M. Lan, D. Cartié, P. Davies, and C. Baley, "Influence of embedded gap and overlap fiber placement defects on the microstructure and shear and compression properties of carbon–epoxy laminates," *Compos. Part A Appl. Sci. Manuf.*, vol. 82, pp. 198–207, Mar. 2016.

[128] J. P.-H. Belnoue *et al.*, "Understanding and predicting defect formation in automated fibre placement pre-preg laminates," *Compos. Part A Appl. Sci. Manuf.*, vol. 102, pp. 196–206, Nov. 2017.

[129] T. D. Dang, S. R. Hallet, B. C. Kim, Y. Le Cahain, R. Butler, and W. Liu, "Modelling of as manufactured geometry for prediction of impact and compression after impact behaviour of variable angle tow laminates," *J. Compos. Mater.*, vol. 49, no. 12, pp. 1423–1438, May 2015.

[130] S. Mukhopadhyay, M. I. Jones, and S. R. Hallett, "Tensile failure of laminates containing an embedded wrinkle; numerical and experimental study," *Compos. Part A Appl. Sci. Manuf.*, vol. 77, pp. 219–228, Oct. 2015.

[131] K. Potter, B. Khan, M. Wisnom, T. Bell, and J. Stevens, "Variability, fibre waviness and misalignment in the determination of the properties of composite materials and structures," *Compos. Part A Appl. Sci. Manuf.*, vol. 39, no. 9, pp. 1343–1354, Sep. 2008.

[132] N. Bakhshi and M. Hojjati, "An experimental and simulative study on the defects appeared during tow steering in automated fiber placement," *Compos. Part A Appl. Sci. Manuf.*, vol. 113, pp. 122–131, Oct. 2018.

[133] R. Harik, C. Saidy, S. J. Williams, Z. Gurdal, and B. Grimsley, "Automated fiber placement defect identity cards: cause, anticipation, existence, significance, and progression," in *SAMPE Conference Proceedings*, 2018.

[134] L. Veldenz, M. Di Francesco, S. Astwood, P. Giddings, B. C. Kim, and K. D. Potter, "Assessment of Steering Capability of Automated Dry Fibre Placement through a Quantitative Methodology," in *The Third International Symposium on Automated Composites Manufacturing*, 2017.

[135] R. Wehbe, "Modeling Of Tow Wrinkling In Automated Fiber Placement Based On Geometrical Considerations," South Carolina, 2017.

[136] G. Clancy, D. Peeters, V. Oliveri, R. O'higgins, D. Jones, and P. M. Weaver, "Steering of Carbon Fiber/Thermoplastic Pre-preg Tapes using Laser-Assisted Tape Placement," in *AIAA/ASCE/AHS/ASC Structures, Structural Dynamics, and Materials Conference*, 2018.

[137] B. Denkena, C. Schmidt, K. Völtzer, and T. Hocke, "Thermographic online monitoring system for Automated Fiber Placement processes," *Compos. Part B Eng.*, vol. 97, pp. 239–243, Jul. 2016.

[138] K. D. Potter, "Understanding the origins of defects and variability in composites manufacture," *17 th Int. Conf. Compos. Mater.*, pp. 27–31, 2009.

[139] E. Oromiehie, B. G. Prusty, P. Compston, and G. Rajan, "Characterization of process-induced defects in automated fiber placement manufacturing of composites using fiber Bragg grating sensors," *Struct. Heal. Monit.*, p. 147592171668593, Feb. 2017.

[140] M. Arian Nik, K. Fayazbakhsh, D. Pasini, and L. Lessard, "Optimization of variable stiffness composites with embedded defects induced by Automated Fiber Placement," *Compos. Struct.*, vol. 107, pp. 160–166, Jan. 2014.

[141] K. Fayazbakhsh, M. Arian Nik, D. Pasini, and L. Lessard, "Defect layer method to capture effect of gaps and overlaps in variable stiffness laminates made by Automated Fiber Placement," *Compos. Struct.*, vol. 97, pp. 245–251, Mar. 2013.

[142] T. R. Brooks and J. R. R. A. Martins, "On manufacturing constraints for tow-steered composite design optimization," *Compos. Struct.*, vol. 204, pp. 548–559, Nov. 2018.

[143] "Unidirektionalgelege -prepreg aus Kohlenstoffasern und Epoxidharz DIN29971." p. 16, 2007.

[144] S. Rao, R. Umer, and W. J. Cantwell, "An Evaluation of the Compression Response of High-Performance Prepregs for AFP Applications," *Polym. Polym. Compos.*, vol. 23, no. 6, pp. 389–398, 2015.

[145] R. R. Smith, Z. Qureshi, R. Scaife, and H. El-Dessouky, “Limitations of processing carbon fibre reinforced plastic/polymer material using automated fibre placement technology,” *J. Reinf. Plast. Compos.*, vol. 35, no. 21, p. 0731684416659544, Jul. 2016.

[146] M. Belhaj and M. Hojjati, “Wrinkle formation during steering in automated fiber placement: Modeling and experimental verification,” *J. Reinf. Plast. Compos.*, pp. 1–14, Jan. 2018.

[147] A. Blom, “Fibre-placed, variable-stiffness composite: the future of aerospace structures?,” *JEC Magazine #58*, 2010.

[148] P. Hörmann, “Thermoset automated fibre placement - on steering effects and their prediction,” Technical University Munich, 2016.

[149] A. Beakou, M. Cano, J.-B. Le Cam, and V. Verney, “Modelling slit tape buckling during automated prepreg manufacturing: A local approach,” *Compos. Struct.*, vol. 93, no. 10, pp. 2628–2635, Sep. 2011.

[150] R. S. Moon, C. C. Johnson, and R. D. Hale, “Nondestructive Evaluation And Mechanical Testing Of Steered Fiber Composites,” in *47th International Sampe Symposium and Exhibition*, 2002, vol. 47, p. 14.

[151] R. Flory and E. Benardon, “Effect of Steering and Conformance Requirements of Automated Material Deposition Equipment,” in *39th International SAMPE Symposium*, 1994, pp. 2593–2603.

[152] S. Nagendra, S. Kodiyalam, J. E. Davis, and V. N. Parthasarathy, “Optimization of tow fiber paths for composite design,” in *36th Structures, Structural Dynamics and Materials Conference*, 1995.

[153] J. Chen, T. Chen-Keat, M. Hojjati, A. A. J. Vallee, M.-A. Octeau, and A. Yousefpour, “Impact of layup rate on the quality of fiber steering/cut-restart in automated fiber placement processes,” *Sci. Eng. Compos. Mater.*, vol. 22, no. 2, pp. 165–173, 2015.

[154] G. Clancy, D. Peeters, V. Oliveri, D. Jones, R. M. O’Higgins, and P. M. Weaver, “A study of the influence of processing parameters on steering of carbon Fibre/PEEK tapes using laser-assisted tape placement,” *Compos. Part B Eng.*, Nov. 2018.

[155] B. Cornelissen, B. Rietman, and R. Akkerman, “Frictional behaviour of high performance fibrous tows: Friction experiments,” 2013.

[156] B. Zhu, T. X. Yu, J. Teng, and X. M. Tao, “Theoretical Modeling of Large Shear Deformation and Wrinkling of Plain Woven Composite,” *J. Compos. Mater.*, vol. 43, no. 2, pp. 125–138, Nov. 2008.

[157] S. E. Arnold, M. P. F. Sutcliffe, and W. L. A. Oram, “Experimental measurement of wrinkle formation during draping of non-crimp fabric,” *Compos. Part A Appl. Sci. Manuf.*, vol. 82, pp. 159–169, Mar. 2016.

[158] G. Bardl *et al.*, “Automated detection of yarn orientation in 3D-draped carbon fiber fabrics and preforms from eddy current data,” *Compos. Part B Eng.*, vol. 96, pp. 312–324, Jul. 2016.

[159] C. Liu, “New Method of Fabric Wrinkle Measurement Based on Image Processing,” *FIBRES Text. East. Eur.*, vol. 22, no. 1103, pp. 51–55, 2014.

[160] P. J. Joyce, D. Kugler, and T. J. Moon, “A Technique for Characterizing Process-Induced Fiber Waviness in Unidirectional Composite Laminates-Using Optical Microscopy,” *J. Compos. Mater.*, vol. 31, no. 17, pp. 1694–1727, Sep. 1997.

[161] S. W. Yurgartis, “Measurement of small angle fiber misalignments in continuous fiber composites,” *Compos. Sci. Technol.*, vol. 30, no. 4, pp. 279–293, Jan. 1987.

[162] S. Rajan *et al.*, “Experimental investigation of prepreg slit tape wrinkling during automated fiber placement process using StereoDIC,” *Compos. Part B Eng.*, Dec. 2018.

[163] R. A. Smith, N. Xie, L. J. Nelson, and S. R. Hallett, “Use of 3D non-destructive characterisation for modelling the mechanical properties of as-manufactured composite components,” in *NDT 2014 - 53rd Annual Conference of the British Institute of Non-Destructive Testing*, 2014.

[164] R. A. Smith, G. Roldo, S. Mukhopadhyay, A. Lawrie, and S. R. Hallett, “3D characterisation of fibre orientation and resulting material properties,” in *52nd Annual Conference of the British Institute of Non-Destructive Testing 2013, NDT 2013*, 2013, pp. 198–209.

[165] B. S. Hayes and L. M. Gammon, *Optical microscopy of fiber reinforced composites*, 1st ed. ASM International, 2010.
[166] ASTM E1131-08(2014), "Standard Test Method for Compositional Analysis by Thermogravimetry." 2014.
[167] T. B. Åström, *Manufacturing of polymer composites*, 1st ed. Stockholm, Sweden: Chapman & Hall, 1997.
[168] A. Fahr, *Aeronautical applications of non-destructive testing*. Lancaster, PA: DEStecj Publications, Inc., 2014.
[169] B. Carreira and B. Trudell, *Lean Six Sigma that works: a powerful action plan for dramatically improving quality, increasing speed, and reducing waste*. New York, US: American Management Association, 2006.
[170] D. J. Winter, "A socio-technical approach for enhancing rate ramp-up in high value, low volume manufacturing: From New Product Introduction to Steady State Manufacture," University of Bristol, 2016.
[171] T. Rudberg, J. Nielson, M. Henscheid, and J. Cemenska, "Improving AFP Cell Performance," *SAE Int. J. Aerosp.*, vol. 7, no. 2, pp. 2014-01–2272, 2014.
[172] A. Halbritter and R. Harper, "Big Parts Demand Big Changes to the Fiber Placement Status Quo," *SME Compos. Manuf. Conf.*, 2012.
[173] F. Weiland and F. Dorn, "PRECARBI (Materials, Process and CAE Tools Developments for Pre-impregnated Carbon Binder Yarn Preform Composites)," Eschborn, DE, 2011.
[174] F. Weiland *et al.*, "Manufacture of a Rotor Blade Pitch Horn Using Novel Binder Yarn Fabrics," *Int. Conf. Compos. Mater.*, p. 11, 2009.
[175] D. A. SAS, "ADVITAC (ADVanced Integrated composite TailCone)." European Commission, Saint Julien de Chedon, FR, 2014.
[176] M. Abel *et al.*, *Prozesskette zur ressourceneffizienten Composite-Herstellung für die E-Mobilität - PRESCHE* -. Augsburg, DE: VDI Verlag, 2015.
[177] T. Wille, "ECOMISE (Enabling Next Generation Composite Manufacturing by In-Situ Structural Evaluation and Process Adjustment)," Braunschweig, DE, 2017.
[178] A. Jahan, M. Y. Ismail, S. M. Sapuan, and F. Mustapha, "Material screening and choosing methods – A review," *Mater. Des.*, vol. 31, no. 2010, pp. 696–705, 2009.
[179] E. Triantaphyllou and S. H. Mann, "Using the Analytic Hierarchy Process for Decision Making in Engineering Applications: Some Challenges," *Int. J. Ind. Eng. Appl. Pract.*, vol. 2, no. 1, pp. 35–44, 1995.
[180] E. Triantaphyllou and S. H. Mann, "An examination of the effectiveness of multi-dimensional decision-making methods: A decision-making paradox," *Decis. Support Syst.*, vol. 5, no. 3, pp. 303–312, 1989.
[181] G.-H. Tzeng and J.-J. Huang, *Multiple Attribute Decision Making - Methods and Applications*. Boac Raton, FL: CRC Press Taylor & Francis Group, 2011.
[182] E. O'Loughlin, *An introduction to business systems analysis: problem solving techniques and strategies*. Liffey Press, 2009.
[183] G. Locatelli and M. Mancini, "A framework for the selection of the right nuclear power plant," *Int. J. Prod. Res.*, vol. 50, no. 17, pp. 4753–4766, Sep. 2012.
[184] T. L. Saaty, "Decision making with the analytic hierarchy process," *Int. J. Serv. Sci.*, vol. 1, no. 1, pp. 83–98, 2008.
[185] T. L. Saaty, "A scaling method for priorities in hierarchical structures," *J. Math. Psychol.*, vol. 15, no. 3, pp. 234–281, 1977.
[186] P. R. Adhikari and R. Mirshams, "Study of Knowledge-Based System (KBS) and Decision Making Methodologies in Materials Selection for Lightweight Aircraft Metallic Structures," *J. Appl. Sci. Eng. Technol.*, vol. 5, no. 1, pp. 1–19, 2017.
[187] F. T. S. Chan, "Interactive selection model for supplier selection process: an analytical hierarchy process approach," *Int. J. Prod. Res.*, vol. 41, no. 15, pp. 3549–3579, Jan. 2003.

[188] A. Hambali, S. M. Sapuan, N. Ismail, and Y. Nukman, “Application of Analytical Hierarchy Process in the design concept selection of automotive composite bumper beam during the conceptual design stage,” *Sci. Res. Essay*, vol. 4, no. 4, pp. 198–211, 2009.

[189] M. R. Mansor, S. M. Sapuan, E. S. Zainudin, A. A. Nuraini, and A. Hambali, “Hybrid natural and glass fibers reinforced polymer composites material selection using Analytical Hierarchy Process for automotive brake lever design,” *Mater. Des.*, vol. 51, pp. 484–492, 2013.

[190] M. . Rosli *et al.*, “Analytical Hierarchy Process for Natural Fiber Composites Automotive Armrest Thermoset Matrix Selection,” *MATEC Web Conf.*, vol. 97, p. 01039, Feb. 2017.

[191] M. Luqman, M. U. Rosli, C. Y. Khor, S. Zambree, and H. Jahidi, “Manufacturing Process Selection of Composite Bicycle’s Crank Arm using Analytical Hierarchy Process (AHP),” *IOP Conf. Ser. Mater. Sci. Eng.*, vol. 318, pp. 1–8, 2018.

[192] U. Khaleeq uz Zaman, M. Rivette, A. Siadat, and S. M. Mousavi, “Integrated product-process design: Material and manufacturing process selection for additive manufacturing using multi-criteria decision making,” *Robot. Comput. Integr. Manuf.*, vol. 51, pp. 169–180, Jun. 2018.

[193] A. Mayyas *et al.*, “Using Quality Function Deployment and Analytical Hierarchy Process for material selection of Body-In-White,” *Mater. Des.*, vol. 32, no. 5, pp. 2771–2782, 2011.

[194] M. Ipek, I. H. Selvi, F. Findik, O. Torkul, and I. H. Cedimoglu, “An expert system based material selection approach to manufacturing,” *Mater. Des.*, vol. 47, pp. 331–340, 2013.

[195] P. Wang, H. Lei, X. Zhu, H. Chen, C. Wang, and D. Fang, “Effect of manufacturing defect on mechanical performance of plain weave carbon/epoxy composite based on 3D geometrical reconstruction,” *Compos. Struct.*, vol. 199, pp. 38–52, Sep. 2018.

[196] X.-Y. Zhou and P. D. Gosling, “Influence of stochastic variations in manufacturing defects on the mechanical performance of textile composites,” *Compos. Struct.*, vol. 194, pp. 226–239, Jun. 2018.

[197] P. Davidson and A. M. Waas, “The effects of defects on the compressive response of thick carbon composites: An experimental and computational study,” *Compos. Struct.*, vol. 176, pp. 582–596, Sep. 2017.

[198] R. Protz, N. Kosmann, M. Gude, W. Hufenbach, K. Schulte, and B. Fiedler, “Voids and their effect on the strain rate dependent material properties and fatigue behaviour of non-crimp fabric composites materials,” *Compos. Part B Eng.*, vol. 83, pp. 346–351, Dec. 2015.

[199] W. Woigk, S. R. Hallett, M. I. Jones, M. Kuhtz, A. Hornig, and M. Gude, “Experimental investigation of the effect of defects in Automated Fibre Placement produced composite laminates,” *Compos. Struct.*, vol. 20, pp. 1004–1017, Oct. 2018.

[200] C. Baley, M. Lan, P. Davies, and D. Cartie, “Porosity in Ocean Racing Yacht Composites: a Review,” *Appl. Compos. Mater.*, vol. 22, no. 1, pp. 13–28, 2014.

[201] K. Potter, *Introduction to composite products: design, development and manufacture*, 1st ed. London: Chapman & Hall, 1997.

[202] M. Di Francesco, “Laser-Assisted Automated Fibre Placement Process Development,” University of Bristol, 2017.

[203] P. Monnot, D. Williams, and M. Di Francesco, “Power Control of a Flashlamp-Based Heating Solution,” in *18th European Conference on Composite Materials*, 2018, no. June, pp. 24–28.

[204] D. Purslow, “On the optical assessment of the void content in composite materials,” *Composites*, vol. 15, no. 3, pp. 207–210, Jul. 1984.

[205] S.-B. Shim and J. C. Seferis, “Thermal and air permeation properties of a carbon fiber/toughened epoxy based prepreg system,” *J. Appl. Polym. Sci.*, vol. 65, no. 1, pp. 5–16, Jul. 1997.

[206] “MIL-Hdbk-17-3F Chapter 2: Materials and Processes - the Effects of Variability on Composite Properties,” 2002.

[207] A. J. Comer *et al.*, “Mechanical characterisation of carbon fibre–PEEK manufactured by laser-assisted automated-tape-placement and autoclave,” *Compos. Part A Appl. Sci. Manuf.*, vol. 69, pp. 10–20, Feb. 2015.

[208] T. Kok, “On the consolidation quality in laser assisted fibre placement,” Universiteit Twente, 2018.
[209] Y. M. Elsherbini and S. V. Hoa, “Fatigue threshold-stress determination in AFP laminates containing gaps using IR thermography,” *Compos. Sci. Technol.*, vol. 146, pp. 49–58, Jul. 2017.
[210] T. J. J. Dodwell, R. Butler, and G. W. W. Hunt, “Out-of-plane ply wrinkling defects during consolidation over an external radius,” *Compos. Sci. Technol.*, vol. 105, no. October, pp. 151–159, Dec. 2014.
[211] S. M. Lee, *Dictionary of composite materials technology*. Technomic Publishing Company, 1989.
[212] D. Chen, K. Arakawa, and C. Zu, “Reduction of Void Content of Vacuum-Assisted Resin Transfer Molded Composites by Infusion Pressure Control,” *Polym. Polym. Compos.*, vol. 36, no. 9, pp. 1629–1637, 2015.
[213] M. G. Abdallah *et al.*, *Test methods and design allowables for fibrous composites*, 2nd ed. Philadelphia, PA: ASTM, 1989.
[214] N. C. Judd and W. W. Wright, “Voids and their effects on the mechanical properties of composites- an appraisal,” *Sampe J.*, vol. 14, pp. 10–14, 1978.
[215] S. T. Peters, *Handbook of Composites*, 2nd ed. Springer-Science+Business Media, B.V., 1998.
[216] S. Sihn, R. Y. Kim, K. Kawabe, and S. W. Tsai, “Experimental studies of thin-ply laminated composites,” *Compos. Sci. Technol.*, vol. 67, no. 6, pp. 996–1008, 2006.
[217] “HexFlow ® RTM6-2 Product Data 180°C bi-component epoxy system for Resin Transfer Moulding and Infusion technologies.” Hexcel Corporation, p. 4.
[218] Hexcel Corporation, “HiTape Reinforcements,” *Hexcel Corporation*, 2018. [Online]. Available: http://www.hexcel.com/Products/Fabrics-Reinforcements/HiTape. [Accessed: 25-Jan-2018].
[219] “Standard Guide for Nondestructive Testing of Polymer Matrix Composites Used in Aerospace Applications.” ASTM, US, 2017.
[220] D. Roach, P. Walkington, and K. Rackow, “Pulse-Echo Ultrasonic Inspection System for In-Situ Nondestructive Inspection of Space Shuttle RCC Heat Shields,” Albuquerque, NM, 2005.
[221] G. T. Smith, *Industrial Metrology : Surfaces and Roundness*, First edition. Springer London, 2002.
[222] M. Di Francesco, L. Veldenz, A. Koutsomitopoulou, G. Dell’Anno, and K. Potter, “On the development of multi-material Automated Fibre Placement technology,” *Int. Conf. Manuf. Adv. Compos.*, p. 2, 2015.
[223] H. Sarrazin and G. S. Springer, “Thermochemical and Mechanical Aspects of Composite Tape Laying,” *J. Compos. Mater.*, vol. 29, no. 14, pp. 1908–1943, Sep. 1995.
[224] B. Hasenjaeger, “AFP/ATL Glossary of Terms : CompositesWorld,” *Composites World Knowledge Center*. [Online]. Available: http://www.compositesworld.com/knowledgecenter/AFP-ATL-Software/glossary-of-terms. [Accessed: 01-Dec-2016].
[225] D. C. Jegley, B. F. Tatting, and Z. Gürdal, “Tow-Steered Panels with Holes Subjected to Compression or Shear Loading,” in *Structures, Structural Dynamics and Materials Conference*, 2005.
[226] K. Nemoto *et al.*, “Development of a roughness measurement standard with irregular surface topography for improving 3D surface texture measurement,” *Meas. Sci. Technol.*, vol. 20, no. 8, p. 084023, Aug. 2009.
[227] R. Deltombe, K. J. Kubiak, and M. Bigerelle, “How to select the most relevant 3D roughness parameters of a surface,” *Scanning*, vol. 36, no. 1, pp. 150–160, Jan. 2014.
[228] I. N. Bobrovskij, “How to Select the most Relevant Roughness Parameters of a Surface: Methodology Research Strategy,” *IOP Conf. Ser. Mater. Sci. Eng.*, vol. 302, no. 1, pp. 1–6, Jan. 2018.
[229] A. Townsend *et al.*, “An interlaboratory comparison of X-ray computed tomography measurement for texture and dimensional characterisation of additively manufactured parts,” *Addit. Manuf.*, vol. 23, pp. 422–432, Oct. 2018.

[230] L. A. Franco and A. Sinatora, “3D surface parameters (ISO 25178-2): Actual meaning of S pk and its relationship to V mp,” *Precis. Eng.*, vol. 40, pp. 106–111, 2015.
[231] “BS EN ISO 25178-2 2012 Geometrical product specificaitons (GPS) - surface texture.pdf.” .
[232] K. Potter, C. Langer, B. Hodgkiss, and S. Lamb, “Sources of variability in uncured aerospace grade unidirectional carbon fibre epoxy preimpregnate,” *Compos. Part A Appl. Sci. Manuf.*, vol. 38, no. 3, pp. 905–916, 2007.
[233] M. Y. Matveev *et al.*, “A numerical study of variability in the manufacturing process of thick composite parts,” *Compos. Struct.*, Sep. 2018.
[234] L. D. Bloom, J. Wang, and K. D. Potter, “Damage progression and defect sensitivity: An experimental study of representative wrinkles in tension,” *Compos. Part B Eng.*, vol. 45, no. 1, pp. 449–458, 2013.
[235] B. Khan, K. D. Potter, and M. R. Wisnom, “Simulation of process induced defects in resin transfer moulded woven carbon fibre laminates and their effect on mechanical behaviour,” no. July, pp. 261–270, 2006.
[236] C. Zhao, B. Wang, and J. Xiao, “Macroscopic characterization of fiber micro-buckling and its influence on composites tensile performance,” *J. Reinf. Plast. Compos.*, vol. 36, no. 3, pp. 196–205, Nov. 2016.
[237] Y. Mahadik and S. R. Hallett, “Effect of fabric compaction and yarn waviness on 3D woven composite compressive properties,” *Compos. Part A Appl. Sci. Manuf.*, vol. 42, no. 11, pp. 1592–1600, Nov. 2011.
[238] E. S. Gadelmawla, M. M. Koura, T. M. A. Maksoud, I. M. Elewa, and H. H. Soliman, “Roughness parameters,” *J. Mater. Process. Technol.*, vol. 123, pp. 133–145, Apr. 2002.
[239] W. P. Dong, P. J. Sullivan, and K. J. Stout, “Comprehensive study of parameters for characterising three- dimensional surface topography III: Parameters for characterising amplitude and some functional properties,” *Wear*, vol. 178, pp. 29–43, 1994.
[240] E. C. Teague, F. E. Scire, and S. M. Baker, “Three-dimensional stylus profilometry,” *Wear*, vol. 83, pp. 1–12, 1982.
[241] n/a, “Roughness (3D) parameter,” *Knowledge, Olympus*. [Online]. Available: https://www.olympus-ims.com/en/knowledge/metrology/roughness/3d_parameter/. [Accessed: 20-Nov-2018].
[242] D. J. Whitehouse, *Handbook of Surface and Nanometrology*, 2nd ed. Coventry, UK: CRC Press Taylor & Francis Group, 2010.
[243] K. K. Manesh, B. Ramamoorthy, and M. Singaperumal, “Numerical generation of anisotropic 3D non-Gaussian engineering surfaces with specified 3D surface roughness parameters,” *Wear*, vol. 268, no. 11–12, pp. 1371–1379, 2010.
[244] L. Veldenz, S. Astwood, P. Giddings, B. C. Kim, and K. Potter, “Infusion characteristics of preforms manufactured by automated dry fibre placement,” in *SAMPE Europe Conference 2017 Stuttgart*, 2017, no. C, pp. 1–8.
[245] L. Veldenz, M. Di Francesco, P. Giddings, B. C. Kim, and K. D. Potter, “Material Selection for Automated Dry Fibre Placement using the Analytical Hierarchy Process,” *Adv. Manuf. Polym. Compos. Sci.*, 2018.
[246] W. E. Guin, J. R. Jackson, and C. M. Bosley, “Effects of tow-to-tow gaps in composite laminates fabricated via automated fiber placement,” *Compos. Part A Appl. Sci. Manuf.*, vol. 115, no. July, pp. 66–75, 2018.
[247] X. Li, S. R. Hallett, and M. R. Wisnom, “Modelling the effect of Gaps and Overlaps in Automated Fibre Placement (AFP) manufactured laminates,” *Sci. Eng. Compos. Mater.*, vol. 22, no. 2, pp. 115–129, 2015.
[248] H. Girardy, “Dry reinforcements for Aerospace OOA technologies NCF & HiTape ®,” in *CFK-Valley Stade Convention*, 2014, pp. 1–17.
[249] A. B. Strong, *Fundamentals of Composites Manufacturing, Second Edition: Materials, Methods*. Society of Manufacturing Engineers, 2008.

[250] G. Francucci, E. S. Rodríguez, and A. Vázquez, “Study of saturated and unsaturated permeability in natural fiber fabrics,” *Compos. Part A Appl. Sci. Manuf.*, vol. 41, no. 1, pp. 16–21, 2010.

[251] “Technical Data Sheet PRISM EP2400 Resin for Infusion,” *Solvay Composite Materials*, 2018. [Online]. Available: http://catalogservice.solvay.com/downloadDocument?fileId=MDkwMTY2OWM4MDRlNjdkMg==&fileName=PRISM EP2400_CM_EN.pdf&base=FAST. [Accessed: 06-Dec-2018].

[252] N. Nash, “Improving the Performance of Out-of-Autoclave Composite Laminates Using an Interlaminar Toughening Technique,” University of Limerick, 2016.

[253] N. Gharabegi, “Composite Laminates Made by Automated Fiber Placement of Dry Fibers and Vacuum Assisted Resin Transfer Molding,” Concordia University, 2018.

[254] B. Griffiths, “GKN A350 spar program update,” *CompositesWorld*, Jan-2011.

[255] F. J. Schirmaier, K. A. Weidenmann, L. Kärger, and F. Henning, “Characterisation of the draping behaviour of unidirectional non-crimp fabrics (UD-NCF),” *Compos. Part A Appl. Sci. Manuf.*, vol. 80, pp. 28–38, Jan. 2016.

[256] K. Çinar and N. Ersoy, “Effect of fibre wrinkling to the spring-in behaviour of L-shaped composite materials,” *Compos. Part A Appl. Sci. Manuf.*, vol. 69, pp. 105–114, 2015.

[257] M. R. Wisnom, M. Gigliotti, N. Ersoy, M. Campbell, and K. D. Potter, “Mechanisms generating residual stresses and distortion during manufacture of polymer–matrix composite structures,” *Compos. Part A Appl. Sci. Manuf.*, vol. 37, no. 4, pp. 522–529, Apr. 2006.

[258] T. Grankäll, P. Hallander, and M. Åkermo, “Geometric compensation of convex forming tools for successful final processing in concave cure tools - an experimental study,” *Compos. Part A Appl. Sci. Manuf.*, Oct. 2018.

[259] C. Albert and G. Fernlund, “Spring-in and warpage of angled composite laminates,” *Compos. Sci. Technol.*, vol. 62, no. 14, pp. 1895–1912, Nov. 2002.

[260] A. Rangone, “An analytical hierarchy process framework for comparing the overall performance of manufacturing departments,” *Int. J. Oper. Prod. Manag.*, vol. 16, no. 3, pp. 104–119, 1990.